D 2019

U.PORTO

FEUP FACULDADE DE ENGENHARIA
UNIVERSIDADE DO PORTO

IMPACT OF NANOPARTICLES IN FRESHWATER AQUATIC SYSTEMS: PHYSICO-CHEMICAL CHARACTERISTICS *VERSUS* ECOTOXICOLOGICAL EFFECTS

CÁTIA FILIPA ASSUNÇÃO DE SOUSA

TESE DE DOUTORAMENTO APRESENTADA
À FACULDADE DE ENGENHARIA DA UNIVERSIDADE DO PORTO EM
ENGENHARIA DO AMBIENTE

Impact of nanoparticles in freshwater aquatic systems: physico-chemical characteristics *versus* ecotoxicological effects

Cátia Filipa Assunção de Sousa

A dissertation submitted in a partial fulfilment of
the requirements for the degree of
Doctor in
Environmental Engineering

Supervised by Doctor Helena Maria Vieira Monteiro Soares
Co-supervised by Doctor Eduardo Jorge Valente Soares

Faculty of Engineering, University of Porto,
Department of Chemical Engineering

Junho 2019

“Never give up on what you really want to do.
The person with big dreams is more powerful
that the one with all the facts.”
Albert Einstein

ABSTRACT

Over the last decade, concerns have been raised regarding the potential health and environmental effects associated with the release of oxide nanoparticles (NPs) into ecosystems. This thesis aims to access the toxicity of six oxide NPs (Al_2O_3, In_2O_3, Mn_3O_4, NiO, SiO_2 and SnO_2) using as cell models the yeast *Saccharomyces cerevisiae* and the freshwater alga *Pseudokirchneriella subcapitata*.

The yeast *S. cerevisiae* exposed for 6 h to 100 mg/L NiO NPs presented reduced metabolic activity and enhanced accumulation of reactive oxygen species (ROS). NiO NPs induced the loss of cell viability in a dose-dependent manner. Study of the dissolution of NiO NPs in aqueous media with the toxicological data suggests that the nickel released by the NPs cannot explain all the toxic effects observed in yeast caused by the NPs. Transmission electron microscopy (TEM) observations revealed that NiO NPs were adsorbed onto cell surface but did not enter into yeast cells. Isogenic mutants (*cwp1*Δ and *cwp2*Δ) with increased cell wall porosity did not display enhanced susceptibility to NiO NPs compared to the wild type strain. Our results suggest that NiO NPs exert their toxic effect by an indirect mechanism. Yeast cells exposed to NiO NPs accumulated superoxide anions and hydrogen peroxide, which are intracellularly generated. Yeast cells co-exposed to NiO NPs and antioxidants showed quenching of ROS and increased resistance to NiO NPs, indicating that the loss of cell viability was associated with ROS accumulation. Mutants lacking mitochondrial DNA (ρ^0) displayed reduced levels of ROS and increased resistance to NiO NPs, suggesting the involvement of the mitochondrial respiratory chain in ROS production. Yeast cells exposed to NiO NPs presented decreased levels of reduced glutathione (GSH). Mutants deficient in *GSH1* (*gsh1*Δ) or *GSH2* (*gsh2*Δ) genes displayed increased levels of ROS and increased sensitivity to NiO NPs. Also, cells exposed to NiO NPs exhibited typical hallmarks of regulated by apoptosis (loss of cell proliferation capacity, exposure of phosphatidylserine at the outer cytoplasmic membrane leaflet, nuclear chromatin condensation and DNA damage) in a process which required *de novo* protein synthesis. The execution of yeast cell death induced by NiO NPs is Yca1p metacaspase-dependent, also inducing the reduction of the mitochondrial membrane potential and the increasing of the frequency of respiratory deficient mutants. Cells deficient in the apoptosis-inducing factor (*aif1Δ*) displayed higher tolerance to NiO NPs, which reinforces the involvement of mitochondria in the RCD by apoptosis.

The Al_2O_3, In_2O_3, Mn_3O_4, SiO_2 and SnO_2 NPs displayed a negative charge, agglomeration, insolubility (dissolution <8 %) and did not generate detectable amounts of ROS under abiotic conditions. The comparative analysis of the loss of cell viability induced by the NPs with the ions released by NPs, suggested that SiO_2 toxicity was mainly caused by the NPs, Al_2O_3 and SnO_2 toxic effects could be

attributed to both the NPs and the respective released ions and Mn_3O_4 harmfulness could be mainly due to the released ions. MOx NPs induced the loss of metabolic activity and the generation of intracellular ROS without permeabilization of plasma membrane. The co-incubation of yeast cells with MOx NPs and ascorbic acid quenched intracellular ROS and significantly restored cell viability and metabolic activity, indicating that the loss of cell viability was associated with ROS accumulation.

P. subcapitata exposed to NiO NPs presented a 72 h-EC_{50} of 1.6 mg/L, which allowed this NP to be classified as toxic. NiO NPs caused the loss of esterase activity, the bleaching of photosynthetic pigments and the intracellular accumulation of ROS in the absence of the disruption of plasma membrane integrity, disturbing the photosynthetic process. A reduction in Φ_{PSII} accompanied by a decrease in the flow rate of electrons through the photosynthetic chain was also observed. The exposure to NiO NPs led to the arrest of the cell cycle prior to the first cell division, an increase in cell volume. With other five oxide NPs, using the algal growth inhibition assay and taking into account the respective 72h-EC_{50} values, it was possible to categorize the NPs as: toxic (Al_2O_3 and SnO_2); harmful (Mn_3O_4 and SiO_2) and non-toxic (In_2O_3). The toxic effects were mainly due to the NPs, except for SnO_2 NPs, which toxicity can be mainly attributed to the dissolved Sn ions. It was observed that Al_2O_3, Mn_3O_4 and SiO_2 induced an algistatic effect most likely as a consequence of the cumulative effect of adverse outcomes: i) reduction of Φ_{PSII}; ii) intracellular ROS accumulation and iii) loss of metabolic activity. SnO_2 NPs also provoked an algistatic effect probably as a consequence of the reduction of Φ_{PSII} since no modification of intracellular ROS levels and metabolic activity were observed.

The evaluation of the impact of pH, water hardness and natural organic matter (humic acids, HA), on Al_2O_3, NiO and SnO_2 NPs ecotoxicity and physico-chemical properties in a freshwater was done. A reduction of the dissolved metals from the NPs was observed with the increase of pH. HA reduced the dissolved metals and induced the dispersion of algal-Al_2O_3 NPs hetero-agglomerates. Additionally, 10 mg/L HA abrogate completely the Al_2O_3, NiO and SnO_2 NPs toxic effects studied. The water hardness did not inhibit the dispersive effect of HA or impaired the protective effect of HA against NPs toxicity.

Altogether, the results here presented allowed to categorize the toxicity of the six oxide NPs and shed light on the mechanisms behind NPs toxicity in the yeast and the alga and the importance of organic matter (HA) on the modulation of MOx NPs toxicity.

Key-words: abiotic factors; ecotoxicity; freshwater; metal(loid) oxide nanoparticles characterization; oxidative stress; yeasts and algae physiology

RESUMO

Durante a última década, têm aumentado as preocupações relativas aos potenciais efeitos tóxicos, associadas à libertação de nanopartículas (NPs) de óxido de metal(lóide) (MOx) nos ecossistemas. Esta tese tem como objetivo avaliar a toxicidade de seis MOx NPs (Al_2O_3, In_2O_3, Mn_3O_4, NiO, SiO_2 e SnO_2) utilizando como modelos celulares a levedura *Saccharomyces cerevisiae* e a alga de água doce *Pseudokirchneriella subcapitata*.

A levedura *S. cerevisiae*, exposta durante 6 h a 100 mg/L NiO NPs, apresentou uma redução da atividade metabólica e um aumento da acumulação de espécies reativas de oxigénio (ROS). NiO NPs induziram à perda da viabilidade celular de uma maneira dependente da sua concentração. O estudo da dissolução das NPs em meio aquoso e dos resultados toxicológicos sugerem que o Ni^{2+} dissolvido não explica todos os efeitos tóxicos observados na levedura causados pelas NiO NPs. Por microscopia eletrónica de transmissão (TEM), foi possível observar que as NPs ficam adsorvidas na superfície celular, não entrando nas células. Os mutantes isogénicos (*cwp1*Δ e *cwp2*Δ), que têm a porosidade da parede celular aumentada, não apresentaram uma maior suscetibilidade às NiO NPs quando comparado com a estirpe selvagem. Os resultados sugerem que as NiO NPs exercem toxicidade por um mecanismo indireto. A levedura exposta às NiO NPs acumulou intracelularmente aniões superóxido e peróxido de hidrogénio. Nas células de levedura co-expostas às NiO NPs e a antioxidantes ocorreu a eliminação de ROS e um aumento da sua resistência às NiO NPs, indicando que a perda de viabilidade celular está associada à acumulação de ROS. Os mutantes que não possuem ADN mitocondrial (ρ^0) apresentaram níveis reduzidos de ROS e um aumento da resistência às NiO NPs, o que sugere o envolvimento da cadeia respiratória mitocondrial na produção de ROS. As células de levedura expostas às NiO NPs apresentaram uma diminuição da glutationa reduzida. Os mutantes deficientes nos genes GSH1 (*gsh1*Δ) ou GSH2 (*gsh2*Δ) apresentaram níveis de ROS superiores e maior sensibilidade às NiO NPs. Além disso, células expostas às NiO NPs exibiram marcadores típicos da regulação da morte celular por apoptose (perda de capacidade de proliferação celular, exposição da fosfatidilserina na membrana citoplasmática externa, condensação da cromatina nuclear e danos no ADN) num processo que exigiu a síntese da proteína *novo*. A execução da morte celular pelas leveduras, induzida pelas NiO NPs, é dependente da metacaspase Yca1p, induzindo também à redução do potencial de membrana mitocondrial e ao aumento de mutantes deficientes respiratórios. As células deficientes no fator indutor de apoptose (*aif1*Δ) apresentaram maior tolerância às NiO NPs, o que reforça o envolvimento das mitocôndrias na morte celular por apoptose. As Al_2O_3, In_2O_3, Mn_3O_4, SiO_2 e SnO_2 NPs apresentaram carga negativa, aglomeração, insolubilidade

(dissolução <8%) e não geraram quantidades detetáveis de ROS, em condições abióticas. A análise comparativa da perda de viabilidade celular induzida pelas NPs e dos iões dissolvido sugeriu que a toxicidade das SiO_2 foi causada principalmente pelos efeitos tóxicos das NPs, Al_2O_3 e SnO_2 pode ser atribuída tanto às NPs quanto aos respetivos iões e Mn_3O_4 pode ser principalmente devido ao ião dissolvido. As MOx NPs induziram à perda de atividade metabólica e à geração intracelular de ROS, sem permeabilização da membrana plasmática. A co-incubação da levedura com as MOx NPs e ácido ascórbico eliminou o ROS intracelular, restaurou a viabilidade celular e a atividade metabólica, indicando que a perda de viabilidade celular está associada à acumulação de ROS. A alga *P. subcapitata* exposta às NiO NPs apresentou um 72h-EC_{50} de 1.6 mg/L o que permitiu que a NP fosse classificada como tóxica. As NiO NPs causaram a perda da atividade esterásica, a redução dos pigmentos fotossintéticos e a acumulação de ROS intracelular, na ausência da rutura da integridade da membrana plasmática, perturbando o processo fotossintético. Foi também observada uma redução no Φ_{PSII} acompanhada por uma diminuição na taxa de fluxo de eletrões através da cadeia fotossintética. A exposição às NiO NPs levou à interrupção do ciclo celular na primeira divisão celular e a um aumento no volume celular. As outras cinco MOx NPs, com o ensaio da inibição do crescimento das algas e os valores do 72h-EC_{50} obtidos, foram categorizadas como: tóxicas (Al_2O_3 e SnO_2); nocivas (Mn_3O_4 e SiO_2) e não tóxica (In_2O_3). Os efeitos tóxicos foram devidos às NPs, exceto nas SnO_2 NPs, cuja toxicidade pode ser atribuída principalmente aos iões Sn dissolvidos. Al_2O_3, Mn_3O_4 e SiO_2 induziram um efeito algistático, provavelmente como consequência dos efeitos cumulativos adversos: i) redução de Φ_{PSII}; ii) acumulação intracelular de ROS e iii) perda de atividade metabólica. As SnO_2 NPs também provocaram um efeito algistático provavelmente como consequência da redução de Φ_{PSII}, uma vez que não foram observadas alterações na acumulação de ROS e na atividade metabólica. A avaliação do impacto do pH, dureza da água e matéria orgânica natural (ácidos húmicos, AH) na ecotoxicidade e nas propriedades físico-químicas das NPs de Al_2O_3, NiO e SnO_2 em água doce foi realizada. Com o aumento do pH e dos AH foi observada uma redução do metal dissolvido das NPs. Os AH induziram à dispersão dos hetero-aglomerados. Os 10 mg/L de AH anularam os efeitos tóxicos de Al_2O_3, NiO e SnO_2 NPs. A dureza da água não inibiu o efeito dispersivo dos AH nem prejudicou o seu efeito protetor contra a toxicidade das NPs. Tendo em conta os resultados aqui apresentados, foi possível classificar a toxicidade das seis MOx NPs, mostrar os seus possíveis mecanismos da toxicidade na levedura e na alga e a importância dos AH na sua toxicidade.

Palavras-chave: Água doce; caraterização das nanopartículas de óxido de metal(lóide); ecotoxicidade; fatores abióticos; fisiologia da levedura e da alga; *stress* oxidativo

ACKNOWLEDGEMENTS

First of all, I want to thank to my supervisor Professor Helena Soares and my co-supervisor Professor Eduardo Soares for all the support, friendship and advices during these four years.

Secondly, I want to thank to Fundação para a Ciência e Tecnologia (FCT), for the PhD scholarship with the reference SFRH/BD/101452/2014 and to Faculty of Engineering of University of Porto (Department of Chemical Engineering), Rede de Química e Tecnologia (REQUIMTE), Centre of Biological Engineering (CEB) of University of Minho and Bioengineering Laboratory-CIETI of Polytechnic Institute of Porto for the facilities and equipment.

I also want to thank to my lab colleagues and friends, Maryam and Carlos (for all the adventures during four years), Manuela, Diana (my favorite cheese lover), Isabel Neto (for all your friendship and patience with me), Ângela, João Jesus, Bruno and João. Also, I cannot forget my "Erasmus" friend Guillaume. And the others Erasmus students: Frederick, Nele, Mike and Tanguy, thank you all for the good mood and the good moments.

To my family, my mother, father and brother for all the love, help, support and presence in every moment of my life, especially the most difficult. Also, I want to thank to my godmother for all the help and friendship during these years.

Finally, especially, I want to thank to Ricardo for the love, friendship, presence, understanding and encouragement during these years.

Cátia

TABLE OF CONTENTS

LIST OF FIGURES

LIST OF TABLES

ABBREVIATIONS

AA	L-ascorbic acid
Al_2O_3	Aluminium oxide
AAS-FA	Atomic absorption spectroscopy with flame atomization
AAS-EA	Atomic absorption spectroscopy with electrothermal atomization
CAPSO	3-(cyclohexylamino)-2-hydroxy-1-propanesulfonic acid
Can	Canavanine
CFU	Colony forming units
Cyh	Cycloheximide
DHE	Dihydroethidium
DHR123	Dihydrorhodamine 123
$DiOC_6(3)$	3,3'dihexyloxacarbocyanine iodide
DNA	Deoxyribonucleic acid
DOM	Dissolved organic matter
FDA	Fluorescein diacetate
FUN-1	2-chloro-4-(2,3-dihydro-3-methyl-(benzo-1,3-thiazol-2-yl)-methylidene)-1-phenylquinolinium iodide
GSH	Reduce glutathione
HA	Humic acids
H_2DCFDA	2′,7′-dichlorodihydrofluorescein diacetate
H_2DCF	2′,7′-dichlorodihydrofluorescein
HEPES	4-(2-hydroxyethyl)-1piperazineethanesulfonic acid
H_2O_2	Hydrogen peroxide
In_2O_3	Indium oxide
Mn_3O_4	Manganese oxide
MES	2-(N-morpholino) ethanesulfonic acid
mBCl	Monochlorobimane
MOx	Metal(loid) oxide
NiO	Nickel oxide
NOM	Natural organic matter
NPs	Nanoparticles
$O_2^{\cdot-}$	Superoxide anion radical
OD_{600}	Optical density at 600 nm
OS	Oxidative stress
OXO	Oxonol, bis 1,3-dibutylbarbituric acid trimethine oxonol ($DiBAC_4(3)$)
PBN	*N-tert*-butyl-α-phenylnitrone
PBS	Phosphate buffered saline solution
PI	Propidium iodide
PS	Phosphatidylserine
RCD	Regulated cell death
RFU	Relative fluorescence units
ROS	Reactive oxygen species
SiO_2	Silicon dioxide
SnO_2	Tin oxide (IV)
TEM	Transmission electron microscopy
YEP	Yeast extract-peptone-dextrose

Chapter 1 - Introduction

1.1. Relevance and aims

The industrial development and the increase of consumption are increasing the demand of cost-effective and easy-to-handle materials, such as nanoparticles (NPs). Metal(loid) oxide (MOx) NPs due to their easy manipulation and synthesis are increasing their usage, presenting a small size (< 100 nm) and distinct physico-chemical characteristics (Andreescu et al., 2012; Fernández-García and Rodriguez, 2007). The extensive usage of MOx NPs is increasing concerns in scientific community and regulatory agencies about the impact in humans and the release in the environment, such as aquatic environments, which emphasizes the importance of evaluation of NPs potential hazard.

The aim of the present thesis was the evaluation of the physico-chemical properties of six MOx NPs (Al_2O_3, In_2O_3, Mn_3O_4, NiO, SiO_2 and SnO_2) and the impact using the yeast *Saccharomyces cerevisiae* as a eukaryotic cell model and the alga *Pseudokirchneriella subcapitata* as ecologically relevant model organism.

1.2. Outline

This thesis is organized in ten Chapters. Chapter 2 includes a bibliographic review about the subjects addressed in this thesis. From Chapters 3 to 9, the experimental work is described and the results are presented and discussed. Chapter 3 assessed the physico-chemical properties of NiO NPs in media and the potential hazards of NiO NPs using the yeast *S. cerevisiae* as a cell model, analyzing the proliferation capacity, metabolic activity and the intracellular reactive oxygen species (ROS) production. Chapter 4 aimed to elucidate whether the toxic effects of NiO NPs on the yeast were associated with oxidative stress (OS) and what mechanisms may contribute to this OS. The Chapter 5 evaluated the involvement of caspase- and mitochondria-dependent apoptosis in yeast caused by NiO NPs. Chapter 6 analyzed the physico-chemical properties of five MOx NPs (Al_2O_3, In_2O_3, Mn_3O_4, SiO_2 and SnO_2), the possible toxic impacts and the respective modes of action using the yeast as a cell model. At Chapter 7, the potential hazards of NiO NPs were investigated using the ecologically relevant freshwater alga *P. subcapitata* and NiO NPs were characterized according to: agglomeration, surface charge, stability and abiotic ROS production. Chapter 8 presented the physico-chemical properties of five oxide NPs (Al_2O_3, In_2O_3, Mn_3O_4, SiO_2 and SnO_2) and the toxicity caused in the freshwater alga *P. subcapitata*. At Chapter 9, the influence of surface water parameters (pH, organic matter and water hardness) in the toxicity of three MOx NPs in *P. subcapitata* were studied. Chapter 10 contained a global conclusion and possible work that can be considered in the future.

References

Andreescu, S., Ornatska, M., Erlichman, J.S., Estevez, A., Leiter, J.C., 2012. Biomedical applications of metal oxide nanoparticles, in: Matijević, E. (Ed.), Fine particles in medicine and pharmacy. Springer, Boston, MA, pp. 57-100.

Fernández-García, M., Rodriguez, J.A., 2007. Metal oxide nanoparticles Nanomaterials: inorganic and bioinorganic perspectives. Brookhaven Science Associates, LLC New York, USA.

Chapter 2 – State of the art

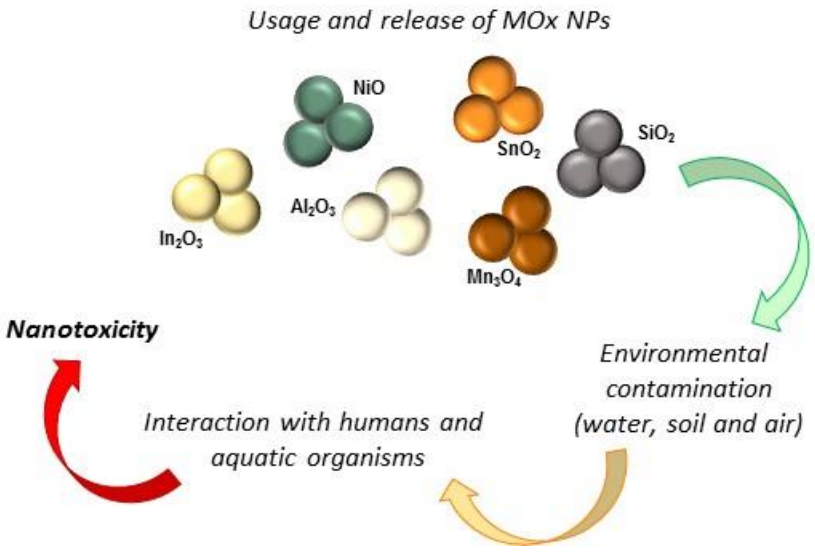

2.1. Introduction

According to the Environmental European Commission, nanoparticle (also named nanomaterial) is a material with a size range between 1 and 100 nm, which can be formed naturally or manufactured (EEC, 2011). In general, all international organizations are in agreement with this description, without distinction among nanoparticles and nanomaterials. However, for example, Scientific Committee on Consumer Products (SCCP) and British Standards Institution (BSI) described nanoparticles as a particle with at least one side in the nanoscale range and nanomaterials as a material with at least one side or internal structure in the nanoscale size (Horikoshi and Serpone, 2013).

Due to their specific and diverse characteristics, nanoparticles (NPs) can be divided in different groups, taking into account their morphology, size and chemicals properties (Khan et al., 2017). The most common groups of NPs are: carbon-based, metal(loid) oxide (MOx), semiconductor (such as quantum dots), zerovalent metals (like iron or gold) and polymeric (Khan et al., 2017; Klaine et al., 2013).

Carbon-based NPs (CBN) are widely used in industry due to their properties, such as macromolecular structure, electrical conductivity and optical characteristics (Cha et al., 2013; Klaine et al., 2013). Carbon nanotubes (CNT) are the most common and used CBN, synthetized by graphite using arc discharge or chemical vapor deposition (Cha et al., 2013). Oxide NPs are very common because of their easy synthesis; they present a large range of technological applications, such as in medicine, telecommunications, catalysis, energy storage and sensing (Corr, 2012). Semiconductor NPs, such as quantum dots, have properties of metals and non-metals, with a reactive core that controls their optical properties (Klaine et al., 2013). They can be used in photocatalysis, photo optics and medical imaging (Sun et al., 2000). In case of nano zerovalent metals, their properties can be changed by varying the reductant type and the synthesis conditions (Klaine et al., 2013). They can be used mainly to degrade contaminants in the environment but also in medicine (Roberts et al., 1996). Polymeric NPs are normally organic and present a shape of nanospheres or nanocapsular (Khan et al., 2017). Due to their multifunctional capability, they can be used in biology, material sciences and catalysis (Klaine et al., 2013). The examples presented above demonstrate the versatility of NPs, not only because of their different properties but also due to their easy adaptation to be used in a variety of fields.

NPs in the environment can contaminate soils, water (such as surface water) and, consequently, interact with organisms. Taking into account that NPs are considered an important emerging contaminant, potentially high-risk (Wilkinson, 2013), the knowledge of their toxicity and behavior in the environment is an important issue. The toxicity caused by MOx NPs and their physico-chemical

properties are not very well studied and understood. In this chapter, it was reviewed the most common physico-chemical properties of six oxide NPs (Al_2O_3, In_2O_3, Mn_3O_4, NiO, SiO_2 and SnO_2) and their implications in toxicity, as well as the main mechanisms of MOx NPs toxicity, using microorganisms as cell models.

2.2. Metal(loid) Oxide Nanoparticles

MOx NPs have been widely used in different fields (Klaine et al., 2013). Due to their different geometries with an electronic structure, uncommon redox and catalytic properties, high surface area and good mechanical stability, MOx NPs can have a metallic, semiconductor or insulator characteristics (Andreescu et al., 2012; Fernández-García and Rodriguez, 2007). The applications of MOx NPs in technological fields can be in microelectronic circuits, sensors, fuel cells and catalysis (Fernández-García and Rodriguez, 2007). However, the use of MOx NPs in biomedical applications are becoming very common and in the recent years it has increased, such as in medical implants, cancer diagnosis, therapy and bio-imaging (Andreescu et al., 2012). These vast usage and applications of MOx NPs transport concerns about the impact in organisms and their toxicity, as well as their mechanisms of action in different organisms.

2.2.1. Physico-chemical properties

The exponential rise of NPs use is due, in part, to a particular property: small size (Sajid et al., 2015). NPs have a high superficial area *per* weight, which increases exponentially by decreasing the particles size, becoming these particles more reactive and toxic (Sajid et al., 2015; Shin et al., 2015). Therefore, it is important to study and understand the most important and common physico-chemical properties of NPs, such as: size, surface area and surface charge (Fig 2.1).

2.2.1.1 Size

Particle size can be described as the diameter of a spherical particle. However, nanoparticles are rarely spherical. Therefore, their size can be presented as volume diameter or hydrodynamic diameter (Powers et al., 2006). Particle size can have an impact of MOx NPs toxicity in organisms because (i) size controls the type of interactions between NPs and organisms; (ii) size determines how the NPs enter into the organism; (iii) size can empower the mechanisms of NPs toxicity (inducing mutagenicity, apoptosis or necrosis), and (iv) size influences the surface area, changing NPs reactivity and toxicity (Powers et al., 2007). Particle size can be modified by pH, ionic strength, surface tension and

conductivity, once these parameters can interfere with NPs agglomeration or dissolution (Abyadeh et al., 2017; Jiang et al., 2009).

The most common methods for size characterization are dynamic light scattering (DLS), transmission electron microscopy (TEM), scanning electron microscope (SEM), atomic force microscopy (ATM) and nanoparticle-tracking analysis (NTA) (Love et al., 2012). In the present thesis, the NPs size characterization was carried out using DLS and TEM (please see Chapters 3, 6, 7 and 8).

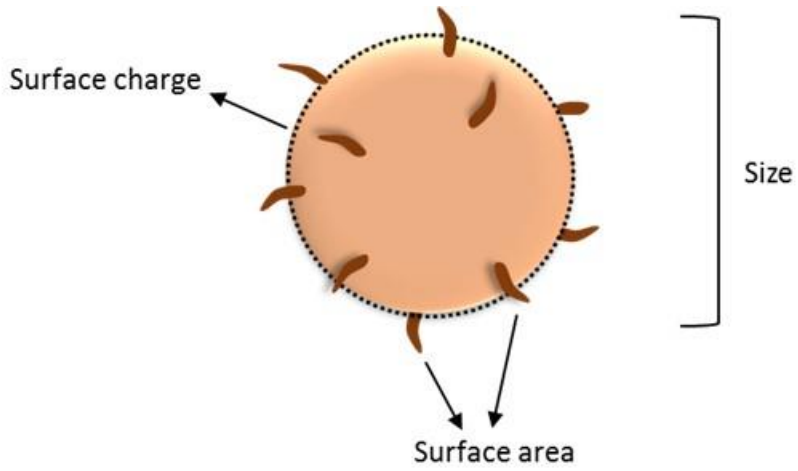

Figure 2.1. Surface charge, size and surface area of a nanoparticle. NPs presents high superficial area (internal area) with small particle sizes (< 100 nm), which make these particles more reactive and toxic. Surface charge is the particle dispersion properties in suspension.

2.2.1.2 Surface charge

The importance of to study the surface charge is related to the understanding of the particle dispersion properties in a medium, the influence of surface charge in the adsorption of ions or biomolecules and reaction with organisms (Powers et al., 2006). The surface charge of MOx NPs can be measured through the zeta potential. The zeta potential can be described as the electrical potential in the interfacial double layer of a particle disperse in medium (Fig 2.2) (Lu and Gao, 2010). A nanoparticle, when suspended in a medium, will form two regions: an inner region and an outer region. In the first one, ions (with an opposite charge compared with the nanoparticle surface) are strongly bound into the nanoparticle surface (Stern layer) (Fig 2.2) (Lin et al., 2014). In the outer region, ions are not strongly attached and form an electrical double layer (Fig 2.2) (Lin et al., 2014). The potential formed in the outer region is called zeta potential (Fig 2.2). The factors that can alter the zeta potential are: pH, ionic strength, others particles concentration and temperature (Lu and Gao, 2010). The MOx NPs zeta potential indicates their stability in suspensions: at lower zeta potential

values (positive or negative values), MOx NPs become instable in suspension and tend to agglomerate (Lin et al., 2014).

The measurement of zeta potential is usually made by electrophoretic light scattering (ELS) and nanoparticle-tracking analysis (NTA) (Love et al., 2012). In the present thesis, the zeta potential of the NPs was determined using ELS (please see Chapters 3, 6, 7 and 8).

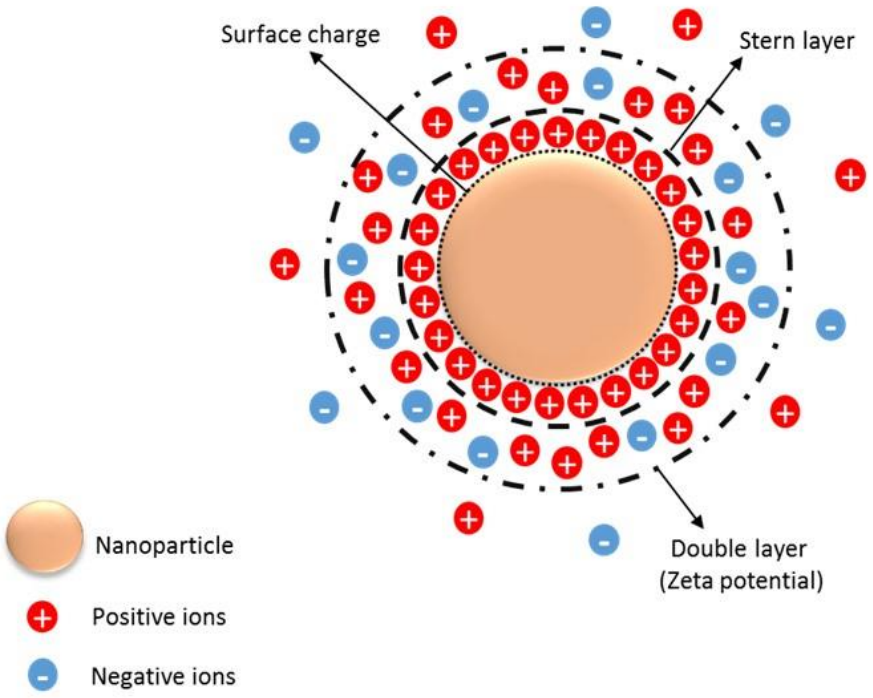

Figure 2.2. Zeta potential of a nanoparticle disperse in a medium. A suspended NP presents two regions: an inner region (Stern layer) and an outer region formed by an electrical double layer (zeta potential).

2.2.1.3 Surface area

Surface area is the interfacial area, external (geometric surface area) or internal (if the nanoparticle is porous), of a nanoparticle (Powers et al., 2006). Such as particle size, surface area defines the interactions between nanoparticles and organisms or environment, as well as their distribution and elimination (Gatoo et al., 2014). This property is important in MOx NPs toxicity once, increasing the surface area, the NPs reactivity and toxicity can also increase. The surface area can be modified due to biomolecules adsorption or agglomeration (Powers et al., 2006).

The technique usually employed to determine NPs surface area is through gas adsorption using the BET (Brunauer – Emmett – Teller) method; however, surface titrations (wet chemical) and aerosol diffusion chargers can also be used (Love et al., 2012; Powers et al., 2006).

2.2.1.4 Behavior of NPs suspensions

Nanoparticles behavior determines their fate and bioavailability in organisms and environment (Labille and Brant, 2010). This property depends of the NPs, size and concentration (Sajid et al., 2015). There are also a range of conditions that can interfere with NPs agglomeration or dissolution in suspensions, some of them were already discussed previously. Briefly, NPs agglomeration or dissolution can be influenced through intrinsic properties, like surface, solution characteristics (such as ionic strength, ionic composition and pH) and macromolecules adsorption into NPs surface (Labille and Brant, 2010).

The NPs agglomeration can be determined using DLS, AFM, UV-visible spectroscopy (by sedimentation assay), TEM, nanoparticle tracking analysis (NTA), fluorescence correlation spectroscopy (FCS) and flow field fractionation (FFFF) (Agarwal et al., 2013; Love et al., 2012). In this thesis, the agglomeration was evaluated by DLS, UV-visible spectroscopy (by sedimentation assay) and TEM (please see, chapters 3, 6 and 7). The NPs dissolution can be determined by atomic absorption spectroscopy with flame atomization or with electrothermal atomization (AAS-EA) or by inductively coupled plasma – optical emission spectrometry (ICP-OES), as it was used in this thesis (please see Chapters 3, 6, 7 and 8).

2.2.2. General mechanisms of nanoparticles toxicity in microorganisms

The general mechanisms of action of MOx NPs can be divided into 3 major groups: i) direct or indirect toxicity mechanism; ii) reactive oxygen species (ROS)-mediated toxicity and iii) non-ROS-mediated toxicity.

The toxicity mechanisms of MOx NPs can be induced in an intracellular or extracellular way. In the first one, direct mechanism, NPs pass through cell membrane, for example, by endocytosis, and once inside the cell, NPs cause toxicity (Miao et al., 2010). In an extracellular toxicity, MOx NPs are in contact with cell (adsorbed into cell wall or membrane, depending on the cell type), never passing inside the cell, exercising an indirect toxicity (Bao et al., 2015; Kasemets et al., 2013; Lok et al., 2007). This indirect mechanism consists in the release of metal ions from NPs, when they are adsorbed into the cell wall or membrane, increasing the amount of metal ions inside the cell and, consequently, triggering the toxic effects (Bao et al., 2015; Kasemets et al., 2013; Lok et al., 2007).

The ROS-mediated toxicity mechanism consists in the production of extracellular or intracellular ROS (such as $O_2^{\cdot -}$, $OH^{\cdot}$ and H_2O_2), causing oxidative stress in the cells and inducing lipid peroxidation, decrease of cell viability, depolarization of cell membrane and loss of cell membrane integrity (Avery,

2011; Manke et al. 2013; Wang et al., 2017). Consequently, this mechanism can cause cells death (Wang et al., 2017a).

Intracellular ROS production seems to be the principal responsible for MOx NPs toxicity (Aruoja et al. 2015). The ROS-mediated toxicity can also interfere with the molecular mechanisms. The production of ROS can cause damage of DNA, permeabilization of mitochondrial membrane, activation of caspase and reduction of levels of antioxidants (such as GSH) or metabolic activity (by esterase activity for example) (Manke et al., 2013; Sabella et al., 2014). Being the production of intracellular ROS the principal cause of MOx NPs toxicity, it is also important to know their major production sources, such as mitochondrial respiratory chain, as was done in Chapter 4. The toxicity mechanisms associated with MOx NPs exposure were studied, at different levels, in Chapters 4, 5, 6, 7 and 8.

The non-ROS-mediated toxicity is related with the suspension turbidity, cellular sequestration, diffusional limitations and metal dissolution (without causing extracellular ROS production) (Aruoja et al., 2015; Rogers et al., 2010; Wang et al., 2017b). The turbidity of MOx NPs, in a suspension, can provoke a shadow effect, which is particularly important for photosynthetic organisms, since their growth can be affected due to light reduction (Rogers et al., 2010). The cellular sequestration, due to the hetero-agglomeration between organisms and MOx NPs, can also inhibit the ions exchange (isolating the cells from nutrients), disturb the exocytosis process and, consequently, induce cell death (Wang et al., 2017a). The ions exchange can also be disturbed due to accumulation of MOx NPs into the cell surface (Wang et al., 2017a). The dissolution of MOx NPs in suspensions can be the mechanism of toxicity, once the dissolved metal can be enough to cause the damage of organisms due to their inherent toxic properties (Aruoja et al., 2015).

The MOx NPs mechanisms of action can be studied using *in-vivo* or *in-vitro* experiments. The *in-vivo* tests are cell-based experiments, they are defaulters, expensive and involve ethical concerns. The *in-vitro* assays, such as membrane integrity and metabolic activity, are faster, economical and without ethical concerns (Fard et al., 2015).

2.3. Models used in the evaluation of NPs toxicity

The evaluation of MOx NPs toxicity can be made using different models. Depending on the study type, different cells or organisms can be used to determine the mechanisms of action of MOx NPs. Thus, NPs toxicity can be usually tested in animal models, cell-lines and microorganisms.

2.3.1. Use of animals and cell lines

The main animal models used are mice, rats, zebrafish, rabbits and the nematode *Caenorhabditis elegans* (*in-vivo* tests) (Yang et al., 2017). The toxicity is evaluated by exposing the animals (through ingestion or inhalation) to NPs and evaluate the possible cytotoxic impacts over kidney, lung or brain, for example (Yang et al., 2017). These *in-vivo* studies allow to relate the effects caused in animals with possible effects in humans, during MOx NPs exposure.

In humans, the health effects reported are in lungs, intestines and skin, by inhalation, ingestion or infiltration (Agarwal et al., 2013). However, human cells can be tested *in-vitro* using MOx NPs to perceive the mechanism of action, such as human bronchial epithelial cells (Duan et al., 2015). Due to recent cancer therapy, MOx NPs are also being used to induce toxicity only in cancer cells, such as ZnO or SiO_2 NPs. This toxicity is exerted by ROS production, apoptosis or necrosis (Vinardell and Mitjans, 2015).

2.3.2. Use of microorganisms

All over the world, the use of animals for research or development in medical technology has increased. *In-vivo* tests permit to understand effects of treatments as well as toxicological effects of a variety of toxicants (Saraf and Kumaraswamy, 2013). The use of animals in toxicological experiments have been discussed for years, because these experiments cause pain, distress and death in animals, becoming an ethical issue. It is necessary to use alternatives to animals, such as *in-vitro* studies without any ethical issues (Doke and Dhawale, 2015). An important and common option used for toxicological experiments is the use of microorganisms as models, such as bacteria, yeast or algae. These experiments using microorganisms allow to study metabolic alterations, genetic modifications, neurodegenerative diseases pathways (such as Parkinson's and Alzheimer's disease), cell death or pollution in the environment (Doke and Dhawale, 2015), without ethical constraints.

2.3.2.1 Yeast as cell model

Yeasts had become a useful eukaryotic cell model, commonly used in biology (Botstein et al., 1997). *Saccharomyces cerevisiae* is the most common and important yeast used as a cell model for toxicological examination of organic and inorganic chemicals (dos Santos and Sa-Correia, 2015). Its use is due to the similarity between *S. cerevisiae* cellular organization and animal cells. *S. cerevisiae* is a non-pathogenic microorganism, is easy to manipulate and is the first yeast with the DNA sequence complete (Goffeau et al., 1996). *S. cerevisiae* can be used as a cell model for studying pathologies that

can occur in human cells (Karathia et al., 2011). The advantage of using this yeast as a cell model for toxicological evaluation of different toxicants, such as MOx NPs, is the usage of yeast as a first screening tool because it limits the use of animal models. (dos Santos et al., 2012).

2.3.2.2 Algae as cell model

Algae are the center of aquatic ecosystem once they produce biomass (being the base for nutrition of food chain) and contribute to the cleansing of polluted water (Ji et al., 2011). If any significant alteration occur in this trophic level, the higher levels can suffer a strong influence, changing the entire food chain (Geis et al., 2000).

International agencies, such as Environmental Protection Agency (EPA), described algae as a model for toxic evaluation in aquatic systems, due to their ecological relevance, universal distribution and sensitivity to a variety of toxicants (Geis et al., 2000), like nanoparticles (Aruoja et al., 2015). The most common algae used in toxicological studies are *Pseudokirchneriella subcapitata*, *Chlorella kesslerii* and *Chlamydomonas reinhardtii* (De Schamphelaere et al., 2014).

2.3.3. Toxic impact of metal(loid) oxide nanoparticles on microorganisms

During the last years, many authors described the toxicological effects of MOx NPs in a variety of microorganisms, such as yeast, algae or bacteria. Six oxide NPs, aluminium oxide (Al_2O_3), indium oxide (In_2O_3), manganese oxide (Mn_3O_4), nickel oxide (NiO), silicon dioxide (SiO_2) and tin oxide (IV) (SnO_2), are not very well studied or their mechanism understood, using different microorganisms as models.

Al_2O_3 NPs caused growth inhibition in *Pseudomonas putida* (Doskocz et al., 2017), *Candida albicans* (Sikora et al., 2018), *Pseudokirchneriella subcapitata* (Aruoja et al., 2015), *Chlorella* and *Scenedesmus* species (Sadiq et al., 2011), *Porphyridium aerugineum* Geitler (KarunaKaran et al., 2015) and in protozoa *Paramecium multimicronucleatum* (Mortimer et al., 2010). The presence of this NP caused reduction of biofilm biomass in *P. aeruginosa*, *Staphylococcus aureus* and *Escherichia coli* (Sikora et al., 2018) and an impact in soil bacterial and fungal community (Chai et al., 2015; McGee et al., 2017).

In_2O_3 NPs were not very toxic to the yeast *Saccharomyces cerevisiae* or even toxic for *E. coli* and *P. subcapitata* (Braydich-stolle et al., 2012).

Mn_3O_4 NPs caused growth inhibition or bioluminescence reduction in *Vibrio fischeri*, *E. coli, S. aureus*, *P. subcapitata* and *Tetrahymena thermophile* (Aruoja et al., 2015).

Different authors described that NiO NPs decreased the bioluminescence of *Photobacterium phosphoreum* (Wang et al., 2016), caused mutagenicity in *Salmonella typhimurium* (Ko and Kong,

2014) and reduced cell viability in the bacteria *E. coli*, *Bacillus subtilis* and *S. aureus* (Baek et al., 2011) and in the yeast *S. cerevisiae* with ROS production (Bao et al., 2015; Kasemets et al., 2013; Zhang et al., 2016). NiO NPs also caused growth inhibition in *Chlorella vulgaris* (Gong e al., 2011), *P. subcapitata* (Nogueira et al., 2015; Li et al., 2017; Oukarroum et al., 2017) and inhibition of cell division, deterioration of the photosynthetic apparatus (chlorophyll synthesis and photochemical reactions of photosynthesis), disorder in thylakoid lamella, plasmolysis, disruption of plasma membrane and intracellular ROS production in *C. vulgaris* (Gong et al., 2011; Li et al., 2017; Oukarroum et al., 2017).
SiO_2 caused growth inhibition in *P. subcapitata* (Aruoja et al., 2015), *Dunaliella tertiolecta* (Manzo et al., 2013; 2015) and *P. aerugineum* Geitler (KarunaKaran et al., 2015); impact in soil bacterial and fungal community (Chai et al., 2015; McGee et al., 2017) and reduction of chlorophyll and protein content in *P. aerugineum* Geitler (KarunaKaran et al., 2015).

2.4. Metal(loid) oxide nanoparticles and environment

The increase of MOx NPs synthesis and consumption inevitably rises the amount of MOx NPs discharge into the environment. Besides natural sources, the usage of MOx NPs in industry and commercial products also increases their release in atmosphere, soil and water (Srivastava et al., 2015). Between 2016 and 2021, it is expected an increase in a global market of NPs, from $1.6 billion to $5.3 billion, which represents an annual growth rate of 26.7% (Research, 2017). Due to the actual and future extensive use of MOx NPs, it is important to perceive their release mechanisms and fate in the environment.

2.4.1 Release of NPs in the environment

The releases of NPs in the environment can occur naturally, intended or unintended manner (also called engineered NPs) (EEC, 2011).
The natural source of NPs (specially constituted by metal ions, such as Al or Fe) are volcanic eruptions, forest fires, deserts surfaces and cosmic dust coming from the solar system. The last source of NPs is due to the constant chemical transformations or reactions with major components of the atmosphere (such as oxygen or carbon dioxide) (Strambeanu et al., 2015).
The unintended and indirect releases of NPs occur due to the gas, liquid and solid emissions from production in industries (such as paints or cosmetics industries). On the other hand, direct and intended releases are connected to the use of NPs, like zerovalent iron in soils remediation. The NPs releases in the environment, for example by painting and cosmetic, are proportional to their

production or usage (Klaine et al., 2013). Taking into account the different groups of NPs, the CBN-NPs can have an incidental (Fig 2.3) or a manufactured source, once these NPs only enter in the environment after their industrial production through industrial discharges in wastewater or soil and gas emissions (Stern and McNeil, 2008). The presence of MOx NPs in the environment can be due to natural (Fig 2.3), incidental or manufactured sources, as described before (Strambeanu et al., 2015). The semiconductor and polymeric NPs can only be found in the environment by a manufactured source (Fig 2.3). The nano zerovalent metals can be produced naturally or in a manufactured manner (Keane, 2009).

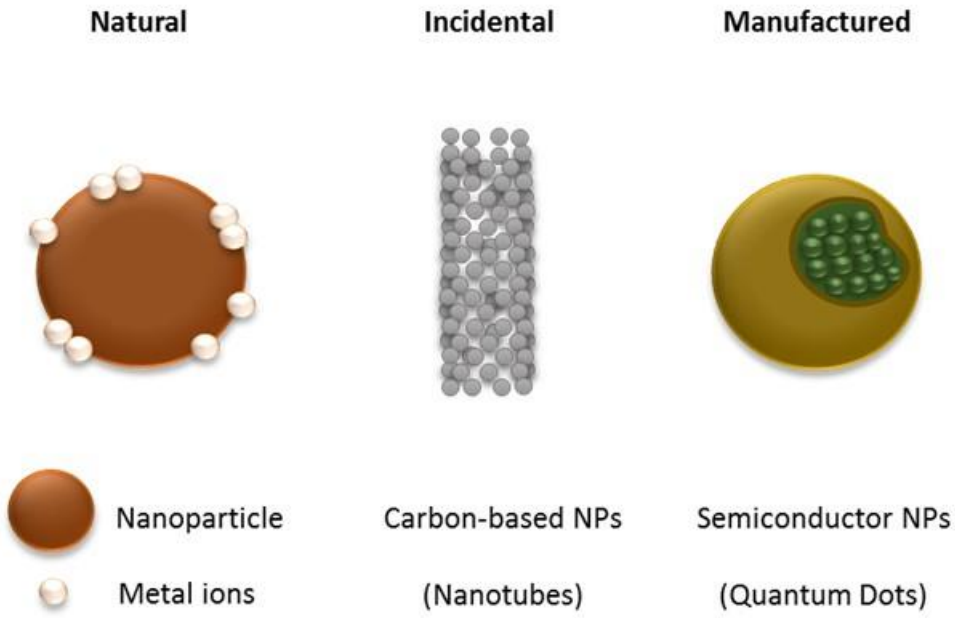

Figure 2.3. Example of NPs groups and their common release into the environment. The MOx NPs can enter in the environment by natural (such as volcanic eruptions or forest fires), incidental or manufactured sources. The carbon-based NPs can have an incidental source (by industrial discharges in wastewater or soil and gas emissions) and semiconductor NPs present a manufactured source.

2.4.2 Environmental cycle

The release of MOx NPs in the environment can be due to natural sources or as consequence of the manufacturing of NPs (Fig 2.4, black and blue arrows). After their release into the environment, MOx NPs can contact with atmosphere, water and soil (Fig 2.4, two-way black arrow) (Sajid et al., 2015). The industrial manufacture, as well as the natural production of NPs can lead to air and water contamination, through gas emission or discharge of wastewaters; soils can also be contaminated due to waste discharge in landfills (Viswanath and Kim, 2016). Also through air pollution, particles can

react with other components present in the atmosphere and being precipitated under MOx NPs form (Strambeanu et al., 2015), contaminating freshwaters and soils.

Once in the environment, MOx NPs can interact with humans, microorganisms, animals and plants, causing toxicity (Fig 2.4, red dashed-arrow). A direct contact between humans and MOx NPs, for example, is through the use of cosmetic products, additives in food or contaminated water (Srivastava et al., 2015). Soil and, consequently, waters contamination by MOx NPs may put in contact MOx NPs with plants (by internalization), microorganisms and other animals (through the food chain) (Srivastava et al., 2015; Klaine et al., 2013). After the MOx NPs internalization through organisms, a small amount will be eliminated (by excretion through urine, for example) (Fig 2.4, yellow arrow) being released, again, into the environment (Sajid et al., 2015). A few portion of MOx NPs will be introduced again in the environment and the process returns again like a cycle (Fig 2.4, green dashed-arrow).

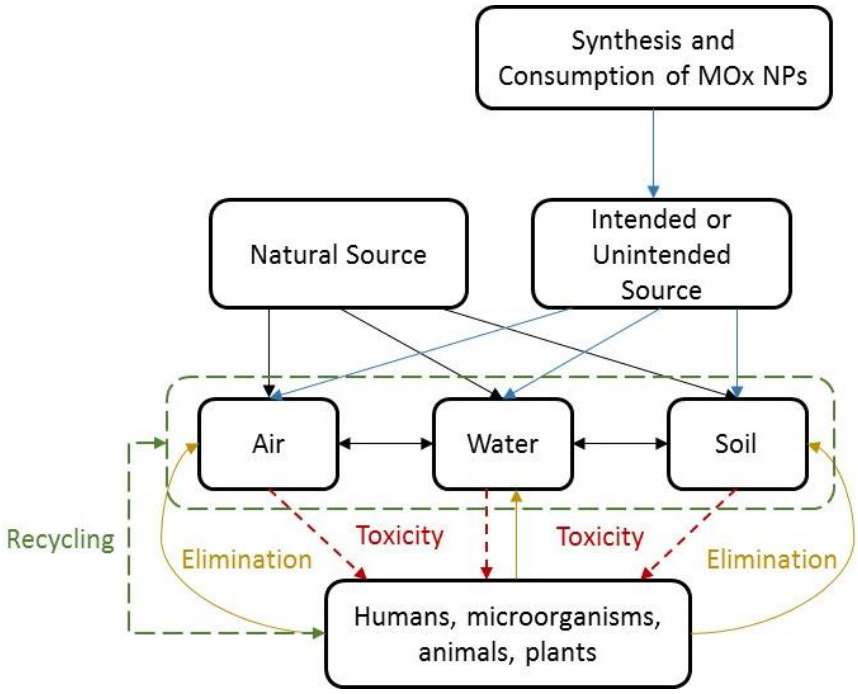

Figure 2.4. Cycle of MOx NPs in the environment. MOx NPs can enter in the environment through natural or manufactured sources (black and blue arrows). MOx NPs can contact with atmosphere, water and soil (two-way black arrow). Once in the environment, MOx NPs can interact with humans, microorganisms, animals and plants, causing toxicity (red dashed-arrow). A minor amount will be eliminated by organisms (yellow arrow) and return again into the environment (green dashed-arrow).

2.4.3 Influence of environmental factors

Different environmental factors can change the physico-chemical characteristics of MOx NPs and, consequently, their mobility and bioavailability (Keller et al., 2010). These environmental factors can modify agglomeration, dissolution or stabilization into the environment, changing MOx NPs toxicity (Chambers et al., 2014; Fang et al., 2015).

Particle concentration, pH, ionic strength, temperature, ionic composition and presence of natural organic matter (NOM) are examples of factors that can alter the MOx NPs properties in the environment (Oukarroum et al., 2014; Yung et al., 2017). MOx NPs may not react in the same manner to environmental variations, depending on their characteristics. For example, pH and ionic strength variations may modify the surface charge of MOx NPs, causing variations in MOx NPs agglomeration and dissolution (Guzman et al., 2006). The increase of temperature reduce the MOx NPs solubility and, consequently, MOx NPs tend to agglomerate. However, at higher ionic strength values, the temperature do not cause any change on MOx NPs properties (Majedi et al., 2014). The presence of NOM can modify MOx NPs agglomeration as it can be adsorbed onto MOx NPs; as consequence, MOx NPs can be more stabilized and their toxicity modified (Keller et al., 2010; Yu et al., 2018). The environmental factors, together or separately, can interfere with agglomeration or dissolution of MOx NPs, in the environment, altering their fate in air, water or soil and their toxicity when the interaction between MOx NPs and organisms occur.

References

Abyadeh, M., Karimi Zarchi, A.A., Faramarzi, M.A., Amani, A., 2017. Evaluation of factors affecting size and size distribution of chitosan-electrosprayed nanoparticles. Avicenna J. Med. Biotechnol. 9, 126-132.

Agarwal, M., Murugan, M.S., Sharma, A., Rai, R., Kamboj, A., Sharma, H., Roy, S.K., 2013. Nanoparticles and its toxic effects: a review. Int. J. Curr. Microbiol. App. Sci. 2, 76-82.

Andreescu, S., Ornatska, M., Erlichman, J.S., Estevez, A., Leiter, J.C., 2012. Biomedical applications of metal oxide nanoparticles, in: Matijević, E. (Ed.), Fine particles in medicine and pharmacy. Springer, Boston, MA, pp. 57-100.

Aruoja, V., Pokhrel, S., Sihtmae, M., Mortimer, M., Madler, L., Kahru, A., 2015. Toxicity of 12 metal-based nanoparticles to algae, bacteria and protozoa. Environ. Sci. Nano 2, 630-644.

Avery, S.V., 2011. Molecular targets of oxidative stress. Biochem. J. 434, 201-210.

Baek, Y.W., An, Y.J., 2011. Microbial toxicity of metal oxide nanoparticles (CuO, NiO, ZnO, and Sb2O3) to *Escherichia coli*, *Bacillus subtilis*, and *Streptococcus aureus*. Sci. Total Environ. 409, 1603-1608.

Bao, S.P., Lu, Q.C., Fang, T., Dai, H.P., Zhang, C., 2015. Assessment of the toxicity of CuO nanoparticles by using *Saccharomyces cerevisiae* mutants with multiple genes deleted. Appl. Environ. Microbiol. 81, 8098-8107.

Botstein, D., Chervitz, S.A., Cherry, J.M., 1997. Genetics - yeast as a model organism. Science 277, 1259-1260.

Cha, C., Shin, S.R., Annabi, N., Dokmeci, M.R., Khademhosseini, A., 2013. Carbon-based nanomaterials: multi-functional materials for Biomedical Engineering. ACS Nano 7, 2891–2897.

Chai, H.K., Yao, J., Sun, J.J., Zhang, C., Liu, W.J., Zhu, M.J., Ceccanti, B., 2015. The effect of metal oxide nanoparticles on functional bacteria and metabolic profiles in agricultural soil. Bull. Environ. Contam. Toxicol. 94, 490-495.

Chambers, B.A., Afrooz, A., Bae, S., Aich, N., Katz, L., Saleh, N.B., Kirisits, M.J., 2014. Effects of chloride and ionic strength on physical morphology, dissolution, and bacterial toxicity of silver nanoparticles. Environ. Sci. Technol. 48, 761-769.

Corr, S.A., 2012. Metal oxide nanoparticles, in: O'Brien, P. (Ed.), Nanoscience: Volume 1: nanostructures through chemistry. The Royal Society of Chemistry London, UK, pp. 180-207.

De Schamphelaere, K.A.C., Nys, C., Janssen, C.R., 2014. Toxicity of lead (Pb) to freshwater green algae: development and validation of a bioavailability model and inter-species sensitivity comparison. Aquat.Toxicol. 155, 348-359.

Doke, S.K., Dhawale, S.C., 2015. Alternatives to animal testing: a review. Saudi Pharm. J. 23, 223-229.

dos Santos, S.C., Sa-Correia, I., 2015. Yeast toxicogenomics: lessons from a eukaryotic cell model and cell factory. Curr. Opin. Biotech. 33, 183-191.

dos Santos, S.C., Teixeira, M.C., Cabrito, T.R., Sa-Correia, I., 2012. Yeast toxicogenomics: genome-wide responses to chemical stresses with impact in environmental health, pharmacology, and biotechnology. Front. Genet. 3, 1-17.

Duan, W.X., He, M.D., Mao, L., Qian, F.H., Li, Y.M., Pi, H.F., Liu, C., Chen, C.H., Lu, Y.H., Cao, Z.W., Zhang, L., Yu, Z.P., Zhou, Z., 2015. NiO nanoparticles induce apoptosis through repressing SIRT1 in human bronchial epithelial cells. Toxicol. Appl. Pharmacol. 286, 80-91.

EEC, 2011. Definition of a nanomaterial. Environmental European Commission, http://ec.europa.eu/environment/chemicals/nanotech/faq/definition_en.htm (7 December 2017).

Fang, T., Yu, L.P., Zhang, W.C., Bao, S.P., 2015. Effects of humic acid and ionic strength on TiO2 nanoparticles sublethal toxicity to zebrafish. Ecotoxicology 24, 2054-2066.

Fard, J.K., Jafari, S., Eghbal, M.A., 2015. A review of molecular mechanisms involved in toxicity of nanoparticles. Adv. Pharm. Bull. 5, 447-454.

Fernández-García, M., Rodriguez, J.A., 2007. Metal oxide nanoparticles Nanomaterials: inorganic and bioinorganic perspectives. Brookhaven Science Associates, LLC New York, USA.

Gatoo, M.A., Naseem, S., Arfat, M.Y., Dar, A.M., Qasim, K., Zubair, S., 2014. Physicochemical properties of nanomaterials: implication in associated toxic manifestations. Biomed Res. Int.

Geis, S.W., Fleming, K.L., Korthals, E.T., Searle, G., Reynolds, L., Karner, D.A., 2000. Modifications to the algal growth inhibition test for use as a regulatory assay. Environ. Toxicol. Chem. 19, 36-41.

Goffeau, A., Barrell, B.G., Bussey, H., Davis, R.W., Dujon, B., Feldmann, H., Galibert, F., Hoheisel, J.D., Jacq, C., Johnston, M., Louis, E.J., Mewes, H.W., Murakami, Y., Philippsen, P., Tettelin, H., Oliver, S.G., 1996. Life with 6000 genes. Science 274, 546-567.

Gong, N., Shao, K.S., Feng, W., Lin, Z.Z., Liang, C.H., Sun, Y.Q., 2011. Biotoxicity of nickel oxide nanoparticles and bio-remediation by microalgae *Chlorella vulgaris*. Chemosphere 83, 510-516.

Guzman, K.A.D., Finnegan, M.P., Banfield, J.F., 2006. Influence of surface potential on aggregation and transport of titania nanoparticles. Environ. Sci. Technol. 40, 7688-7693.

Horikoshi, S., Serpone, N., 2013. Introduction to nanoparticles in: Horikoshi, S., Serpone, N. (Eds.), Microwaves in nanoparticle synthesis, First ed. Wiley-VCH Verlag GmbH & Co. KGaA, Weinheim, Germany, pp. 1-24.

Ji, J., Long, Z.F., Lin, D.H., 2011. Toxicity of oxide nanoparticles to the green algae *Chlorella sp.* Chem. Eng. J. 170, 525-530.

Jiang, J., Oberdorster, G., Biswas, P., 2009. Characterization of size, surface charge, and agglomeration state of nanoparticle dispersions for toxicological studies. J. Nanopart. Res. 11, 77-89.

Karathia, H., Vilaprinyo, E., Sorribas, A., Alves, R., 2011. *Saccharomyces cerevisiae* as a model organism: a comparative study. PLoS One 6, 1-10.

Karunakaran, G., Suriyaprabha, R., Rajendran, V., Kannan, N., 2015. Toxicity evaluation based on particle size, contact angle and zeta potential of SiO_2 and Al_2O_3 on the growth of green algae. Adv. Nano Res. 3, 243-255.

Kasemets, K., Suppi, S., Kunnis-Beres, K., Kahru, A., 2013. Toxicity of CuO nanoparticles to yeast *Saccharomyces cerevisiae* BY4741 wild-type and its nine isogenic single-gene deletion mutants. Chem. Res. Toxicol. 26, 356-367.

Keane, E., 2009. Fate, transport, and toxicity of nanoscale zero-valent iron (nZVI) used during superfund remediation Environmental Protection Agency USA, pp. 1-38.

Keller, A.A., Wang, H.T., Zhou, D.X., Lenihan, H.S., Cherr, G., Cardinale, B.J., Miller, R., Ji, Z.X., 2010. Stability and aggregation of metal oxide nanoparticles in natural aqueous matrices. Environ. Sci. Technol. 44, 1962-1967.

Khan, I., Saeed, K., Khan, I., 2017. Nanoparticles: properties, applications and toxicities. Arab. J. Chem. Article in Press.

Klaine, S.J., Edgington, A., Seda, B., 2013. Nanomaterials in the Environment, in: Férard, J.-F., Blaise, C. (Eds.), Encyclopedia of Aquatic Ecotoxicology. Springer Publishers, Dordrecht, pp. 767-779.

Ko, K.S., Kong, I.C., 2014. Toxic effects of nanoparticles on bioluminescence activity, seed germination, and gene mutation. Appl. Microbiol. Biotechnol. 98, 3295-3303.

Labille, J., Brant, J., 2010. Stability of nanoparticles in water. Nanomedicine 5, 985-998.

Li, Y.Q., Xiao, R., Liu, Z.L., Liang, X.J., Feng, W., 2017. Cytotoxicity of NiO nanoparticles and its conversion inside *Chlorella vulgaris*. Chem. Res. Chinese U. 33, 107-111.

Lin, P.-C., Lin, S., Wang, P.C., Sridhar, R., 2014. Techniques for physicochemical characterization of nanomaterials. Biotechnol. Adv. 32, 711–726.

Lok, C.N., Ho, C.M., Chen, R., He, Q.Y., Yu, W.Y., Sun, H., Tam, P.K.H., Chiu, J.F., Che, C.M., 2007. Silver nanoparticles: partial oxidation and antibacterial activities. J. Biol. Inorg. Chem. 12, 527-534.

Love, S.A., Maurer-Jones, M.A., Thompson, J.W., Lin, Y.-S., Haynes, C.L., 2012. Assessing nanoparticle toxicity. Annu. Rev. Anal. Chem. 5, 181-205.

Lu, G.W., Gao, P., 2010. Emulsions and microemulsions for topical and transdermal drug delivery, in: Kulkarni, V.S. (Ed.), Handbook of non-invasive drug delivery systems. William Andrew, USA, pp. 59-94.

Majedi, S.M., Kelly, B.C., Lee, H.K., 2014. Combined effects of water temperature and chemistry on the environmental fate and behavior of nanosized zinc oxide. Sci.Total Environ. 496, 585-593.

Manke, A., Wang, L.Y., Rojanasakul, Y., 2013. Mechanisms of nanoparticle-induced oxidative stress and toxicity. Biomed Res. Int.

Manzo, S., Buono, S., Rametta, G., Miglietta, M., Schiavo, S., Di Francia, G., 2015. The diverse toxic effect of SiO_2 and TiO_2 nanoparticles toward the marine microalgae *Dunaliella tertiolecta*. Environ. Sci. Pollut. Res. 22, 15941-15951.

Manzo, S., Miglietta, M.L., Rametta, G., Buono, S., Di Francia, G., 2013. Toxic effects of ZnO nanoparticles towards marine algae *Dunaliella tertiolecta*. Sci. Total Environ. 445, 371-376.

McGee, C.F., Storey, S., Clipson, N., Doyle, E., 2017. Soil microbial community responses to contamination with silver, aluminium oxide and silicon dioxide nanoparticles. Ecotoxicology 26, 449-458.

Miao, A.J., Luo, Z.P., Chen, C.S., Chin, W.C., Santschi, P.H., Quigg, A., 2010. Intracellular uptake: a possible mechanism for silver engineered nanoparticle toxicity to a freshwater alga *Ochromonas danica*. PloS One 5.

Mortimer, M., Kasemets, K., Kahru, A., 2010. Toxicity of ZnO and CuO nanoparticles to ciliated protozoa *Tetrahymena thermophila*. Toxicology 269, 182-189.

Nogueira, V., Lopes, I., Rocha-Santos, T.A.P., Rasteiro, M.G., Abrantes, N., Goncalves, F., Soares, A., Duarte, A.C., Pereira, R., 2015. Assessing the ecotoxicity of metal nano-oxides with potential for wastewater treatment. Environ. Sci Pollut. Res. 22, 13212-13224.

Oukarroum, A., Samadani, M., Dewez, D., 2014. Influence of pH on the Toxicity of Silver Nanoparticles in the Green Alga Chlamydomonas acidophila. Water Air Soil Pollut. 225.

Oukarroum, A., Zaidi, W., Samadani, M., Dewez, D., 2017. Toxicity of nickel oxide nanoparticles on a freshwater green algal strain of *Chlorella vulgaris*. Biomed Res. Int. 2017, 1-9.

Powers, K.W., Brown, S.C., Krishna, V.B., Wasdo, S.C., Moudgil, B.M., Roberts, S.M., 2006. Research strategies for safety evaluation of nanomaterials. Part VI. Characterization of nanoscale particles for toxicological evaluation. Toxicol. Sci. 90, 296-303.

Powers, K.W., Palazuelos, M., Moudgil, B.M., Roberts, S.M., 2007. Characterization of the size, shape, and state of dispersion of nanoparticles for toxicological studies. Nanotoxicology 1, 42-51.

Research, 2017. Research B. global markets for nanocomposites, nanoparticles, nanoclays, and nanotubes, http://www.bccresearch.com/market-research/nanotechnology/nanocomposites-nanoparticles-nantubes-market-report-nan021g.html (accessed 23 January 2017).

Roberts, A.L., Totten, L.A., Arnold, W.A., Burris, D.R., Campbell, T.J., 1996. Reductive elimination of chlorinated ethylenes by zero valent metals. Environ. Sci. Technol. 30, 2654-2659.

Sadiq, I.M., Pakrashi, S., Chandrasekaran, N., Mukherjee, A., 2011. Studies on toxicity of aluminum oxide (Al_2O_3) nanoparticles to microalgae species: *Scenedesmus* sp. and *Chlorella* sp. J. Nanopart. Res. 13, 3287-3299.

Sajid, M., Ilyas, M., Basheer, C., Tariq, M., Daud, M., Baig, N., Shehzad, F., 2015. Impact of nanoparticles on human and environment: review of toxicity factors, exposures, control strategies, and future prospects. Environ. Sci. Pollut. Res. 22, 4122-4143.

Saraf, S.K., Kumaraswamy, V., 2013. Basic research: issues with animal experimentations. Indian J. Orthop. 47, 6-9.

Shin, S.W., Song, I.H., Um, S.H., 2015. Role of physicochemical properties in nanoparticle toxicity. Nanomaterials 5, 1351-1365.

Srivastava, V., Gusain, D., Sharma, Y.C., 2015. Critical review on the toxicity of some widely used engineered nanoparticles. Ind. Eng. Chem. Res. 54, 6209-6233.

Stern, S.T., McNeil, S.E., 2008. Nanotechnology safety concerns revisited. Toxicol. Sci. 101, 4-21.

Strambeanu, N., Demetrovici, L., Dragos, D., Lungu, M., 2015. Nanoparticles: definition, classification and general physical properties, in: Lungu, M., Neculae, A., M., B., Biris, C. (Eds.), Nanoparticles' promises and risks. Springer International Publishing Switzerland, pp. 3-19.

Sun, S.H., Murray, C.B., Weller, D., Folks, L., Moser, A., 2000. Monodisperse FePt nanoparticles and ferromagnetic FePt nanocrystal superlattices. Science 287, 1989-1992.

Vinardell, M.P., Mitjans, M., 2015. Antitumor activities of metal oxide nanoparticles. Nanomaterials 5, 1004-1021.

Viswanath, B., Kim, S., 2016. Influence of nanotoxicity on human health and environment: the alternative strategies, in: de Voogt, P. (Ed.), Reviews of Environmental Contamination and Toxicology. Springer International Publishing, Switzerland, pp. 62-104.

Wang, D., Lin, Z., Wang, T., Yao, Z., Qin, M., Zheng, S., Lu, W., 2016. Where does the toxicity of metal oxide nanoparticles come from: The nanoparticles, the ions, or a combination of both? Journal of Hazardous Materials 308, 328-334.

Wang, Y.L., Ding, L., Yao, C.J., Li, C.C., Xing, X.J., Huang, Y.A., Gu, T.J., Wu, M.H., 2017. Toxic effects of metal oxide nanoparticles and their underlying mechanisms. Sci. China Math. 60, 93-108.

Wilkinson, K.J., 2013. Emerging issues in ecotoxicology: characterization of (metallic) nanoparticles in aqueous media, in: Férard, J.-F., Blaise, C. (Eds.), Encyclopedia of Aquatic Ecotoxicology. Springer Publishers, Dordrecht, pp. 767-779.

Yang, Y., Qina, Z., Zeng, W., Yang, T., Cao, Y.B., Mei, C.R., Kuang, Y., 2017. Toxicity assessment of nanoparticles in various systems and organs. Nanotechnol. Rev. 6, 279-289.

Yung, M.M.N., Kwok, K.W.H., Djurisic, A.B., Giesy, J.P., Leung, K.M.Y., 2017. Influences of temperature and salinity on physicochemical properties and toxicity of zinc oxide nanoparticles to the marine diatom Thalassiosira pseudonana. Sci. Rep. 7.

Zhang, W.C., Bao, S.P., Fang, T., 2016. The neglected nano-specific toxicity of ZnO nanoparticles in the yeast *Saccharomyces cerevisiae*. Sci. Rep. 6.

Chapter 3 - Nickel oxide (NiO) nanoparticles disturb physiology of the yeast *Saccharomyces cerevisiae**

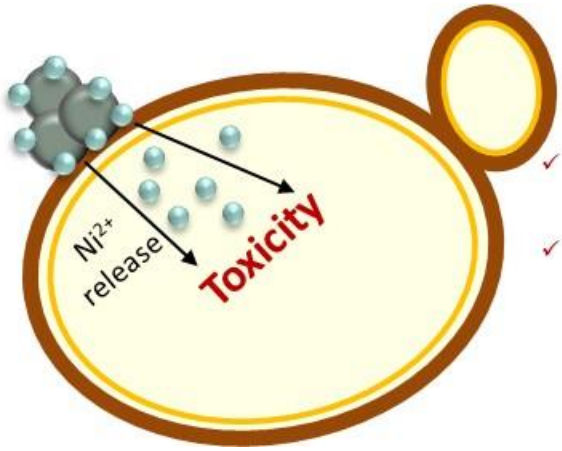

- ✓ *NiO NPs exert their toxic effect, in yeast cells, by an indirect mechanism.*
- ✓ *NiO NPs toxicity, in yeast cells, is characterized by:*
  - *Loss of cell viability in a dose-dependent manner;*
  - *Reduction of metabolic activity.*

*Published in Applied Microbiology and Biotechnology (2018) 102: 2827-2838

3.1. Introduction

Nanomaterials, including metal oxides such as nickel oxide (NiO) nanoparticles (NPs), have received special attention because they present a wide variety of applications and are easily synthetized (Klaine et al., 2013). Their properties are directly related to their size, chemical composition, shape and surface charge, allowing for an extensive range of applications (Oukarroum et al., 2015).

The physical form and chemical reactivity that make nano-sized metal oxides distinctive also provide them with potential to interfere with biological processes and produce toxic effects (Klaine et al., 2013). It was reported that NiO NPs showed typical dose-dependent toxicity in human broncho-alveolar carcinoma-derived cells (Chusuei et al., 2013; Latvala et al., 2016) and had inflammatory effects on mouse lungs (Gillespie et al., 2010).

Various microorganisms have been used to evaluate NiO NP toxicity. Hence, inhibition of the growth of the bacteria *Escherichia coli, Bacillus subtilis* and *Streptococcus aureus* on agar medium containing NiO NPs was described (Baek and An, 2011). A negative impact of NiO NPs on different aquatic organisms such as a bacterium (*Vibrio fischeri)*, unicellular algae (*Pseudokirchneriella subcapitata* and *Chlorella vulgaris)*, a freshwater aquatic plant *(Lemna minor),* crustaceans (*Artemia salina* and *Daphnia magna)*, a rotifer (*Brachionus plicatilis*) and fish (*Danio rerio*) was also reported (Ates et al., 2016; Gong et al., 2011; Lin et al., 2013; Nogueira et al., 2015).

Saccharomyces cerevisiae is a highly relevant experimental model in toxicological evaluations of organic and inorganic chemicals (dos Santos and Sa-Correia, 2015). The use of the yeast *S. cerevisiae* as a cell model for the toxicological assessment of environmental pollutants seems to be very advantageous as a first screening tool because it limits the use of animal models (dos Santos et al., 2012).

Notwithstanding the recognized importance of the use of *S. cerevisiae* as cell model, as far as we know, this is the first study that uses this yeast in the assessment of NiO NPs toxicity. For this purpose, the potential hazardous impacts of NiO NPs on the yeast *S. cerevisiae,* at different levels, were examined: cell metabolism (evaluation of esterase activity, FUN-1 dye processing and intracellular accumulation of reactive oxygen species) and cell population (inhibition of cell growth in liquid and solid media). In addition, to better understand how NiO NPs exerts its toxicity in this model organism, it was examined: the agglomeration of NPs in different media, the release of nickel by the NPs, the toxic effects exerted by Ni^{2+} and the possible internalization of NPs in yeast cells. The results obtained indicate that NiO NPs exerts the toxic action over *S. cerevisiae* by an indirect mechanism. This Chapter

contributes to the assessment of the potential hazards of NiO NPs and to better understand the related mechanisms of toxicity.

3.2. Materials and Methods

3.2.1. Preparation of NiO nanoparticles (NPs) stock suspensions and characterization of suspensions

Nickel oxide (NiO) with a particle size <50 nm and a purity of 99.8 % (trace metal basis) was purchased from Sigma-Aldrich. According to the literature, the analysis made by Brunauer–Emmett–Teller (BET) technique revealed that these NPs present a total specific surface area of 61.19 m^2/g (Capasso et al., 2014).

NiO NPs stock suspensions were prepared in deionized water at a concentration of 0.5 g/L. The NPs suspensions were shaken, sonicated for 1 hour in a 80-160 W ultrasonic bath (Bandelin, Sonorex RK 100) and sterilized under an ultraviolet lamp for 30 min. The stock suspensions of NiO NPs were stored in the dark at 4ºC. Before each experiment, stock suspensions were shaken and sonicated for 1 hour. NiO NPs were characterized in different media: deionized water, yeast extract-peptone-dextrose (YEP) broth (pH adjusted to 6.0) and 10 mmol/L 2-(N-morpholino) ethanesulfonic acid (MES) buffer (Sigma-Aldrich), pH 6.0, with 20 g/L glucose.

To check the agglomeration of NiO NPs in different media, the hydrodynamic size distribution of NPs was monitored by dynamic light scattering (DLS), using a Zetasizer Nano ZS (Malvern Instruments) coupled with Zetasizer Software, version 7.11. Samples were analysed in a polystyrene cuvette (DTS0012).

Zeta potential of the NPs in the different media was determined using Zetasizer Nano ZS. NPs suspensions were carefully placed in a disposable folded capillary cell (DTS1070).

For DLS and zeta potential studies, NPs were previously placed in the different media and incubated in the same conditions (temperature and agitation) used for the toxicity tests (see below, exposure of yeast cells to NiO NPs). Hydrodynamic size distribution and zeta potential were determined at 30 ºC.

The size and morphology of NiO NPs suspended in MES buffer were analysed by transmission electron microscopy (TEM). For comparative purposes, dried NiO NPs were also observed. NiO NPs in powder or in aqueous suspension (10 µL) were placed onto a nickel grid; aqueous suspensions were dried at room temperature. Samples were examined under JEOL JEM 1400 TEM. Images were digitally recorded using a CCD digital camera Orius 1100W at the HEMS/I3S of the University of Porto.

The NiO NPs stability was assessed by quantifying the nickel released from the NPs (NPs dissolution). To determine the Ni^{2+} released, the NPs were suspended in the correspondent medium at a final concentration of 50 or 100 mg/L and incubated at 30ºC. As a control, NiO NPs were also suspended in deionized water (pH adjusted to 6.0) at 100 mg/L. At different times, samples were taken and centrifuged at 20.000x*g* for 30 min at 25ºC. Clear supernatants were carefully collected and nickel was determined by atomic absorption spectroscopy with flame atomization (AAS-FA) in a Perkin Elmer AAnalyst 400 spectrometer. In order to check if the centrifugation conditions described above were adequate to remove the non-soluble fraction of the NPs, the NPs were alternatively removed through a centrifugal ultrafiltration using a membrane with a nominal molecular weight limit of 3 kDa (Merck Millipore, Amicon Ultra-15 3K). For this purpose, NiO NPs suspensions were transferred to ultrafiltration tubes and centrifuged at 3.200*xg* for 20 min at 25ºC. Nickel concentration in the filtrate was determined by AAS-FA, as described above.

Total nickel concentration present in the NPs was determined by total digestion of the NiO NPs suspensions with aqua regia (a mixture of nitric and hydrochloric acids, in a volume ratio 1:3, respectively) during 1 hour. Then, the solutions were filtered through a 0.45-µm-pore-size filter and nickel was determined by AAS-FA, after appropriate dilution of the samples.

3.2.2. Strains, media and growth conditions

The wild type (WT) yeast *S. cerevisiae* BY4741 and the isogenic mutants *cwp1*Δ (Y04945) and *cwp2*Δ (Y07026) were purchased from the European *Saccharomyces cerevisiae* archive for functional analysis (EUROSCARF) collection (Frankfurt, Germany). All strains were maintained at 4ºC on YEP agar slants [5 g/L yeast extract (Difco-BD), 5 g/L peptone (Difco-BD), 10 g/L glucose (Merck) and 15 g/L agar (Merck)].

The pre–cultures were prepared in 10 mL of YEP broth (pH adjusted to 6.0) in 100 mL Erlenmeyer flasks and were incubated at 30ºC, on an orbital shaker at 150 rpm, for 8 hours. The cultures, in exponential phase of growth, were obtained by inoculating 40 mL of YEP broth, pH 6.0, with an appropriate volume of the pre–culture and then incubating overnight to an OD_{600} of ~1.0 under the same conditions as the pre-cultures. After growth, cells were harvested by centrifugation (2.500x*g*, 5 min), washed twice and re-suspended in sterile deionized water.

3.2.3. Exposure of yeast cells to NiO NPs or Ni^{2+}

Yeast cells were exposed to NiO NPs or Ni^{2+} in two media: YEP broth, which is a rich medium optimal for yeast growth, or 10 mmol/L MES buffer with glucose. MES buffer is appropriate for toxicity assays with yeast cells since it does not disturb yeast physiology (Soares et al., 2000) and does not complex Ni^{2+}. The highest concentration of NiO NPs tested (100 mg/L) was selected taking into account the maximum limit of concentration, advised by OECD, for testing toxicity (OECD, 2011). Toxicity studies were carried out by cultivating or incubating the strains without (control) or with the toxicants in YEP broth (growth inhibition assay) or in MES buffer (cell viability assay).

Growth inhibition assay was carried out in test tubes containing 1.0 mL of double-strength YEP broth. NiO NPs (from the stock suspension described above) or Ni^{2+} (from a 1000 mg/L $NiCl_2$ stock solution, Merck) was added to the medium (final concentration: 6.25-100 mg/L) and inoculated with yeast cells at a final concentration of $1x10^6$ cells/mL. As a control, yeast cells were inoculated in YEP broth without NiO NPs or Ni^{2+}. The total volume of each assay (2.0 mL) was adjusted with sterile deionized water. Due to the turbidity of the NiO NPs suspensions, abiotic controls, without yeast cells, were performed for the different NPs concentrations. Cultures and controls were incubated for 24 h at 30ºC. The yeast growth was monitored spectrophotometrically (Unicam, Helios γ) at 600 nm and the absorbance was corrected considering the respective abiotic control. In this assay, as toxicity end point, the difference of yeast growth, after 24h, in the presence of toxicants and in its absence (control) was compared.

Cell viability assay was performed in MES buffer. NiO NPs or Ni^{2+} were used at final concentrations of 50-100 mg/L or 6.25-100 mg/L, respectively. Yeast cells were suspended at a final concentration of $1x10^7$ cells/mL. The assay was carried out in 100 mL Erlenmeyer flasks with a final volume of 20 mL. As a control, yeast cells were placed in MES buffer without NiO NPs or Ni^{2+}. Cell suspensions were incubated at 150 rpm, for 6 h, at 30ºC. Samples were taken (two replicates), serially diluted with sterile deionized water and plated (in duplicate for each replica) on YEP agar from the convenient dilution. The plates were incubated for 3 – 5 days at 30ºC. Colony forming units (CFU) per mL were determined. After this period of incubation, no further CFUs appeared. In this assay, as toxicity end point, the cell viability was determined considering the number of CFUs/mL at zero time as reference (100%).

In kinetic studies, samples were taken at defined times indicated in the figures; the cell viability and the metabolic activity of yeast cells (evaluated as described below) were analysed. The effect concentration (EC) values, ie, EC_{10}, EC_{25}, EC_{50}, EC_{75}, and EC_{90} represent the concentration of Ni^{2+}, which inhibited the growth of yeast cells in YEP broth (growth inhibition assay) or reduced the cell viability

(cell viability assay) by 10, 25, 50, 75 or 90%, respectively. The EC values were calculated using linear interpolation method (Tidepool Scientific Software, TOXCALC version 5.0.32).

The toxic effect of NPs supernatants was also evaluated. Suspensions of 100 mg/L NiO NPs, in MES buffer, had been shaken with yeast cells for 6 h and then centrifuged at 20.000x*g* for 30 min at 25ºC. Clear supernatants were carefully collected and re-inoculated with yeast cells at $1x10^7$ cells/mL. Cell viability and intracellular accumulation of reactive oxygen species (ROS) (see below, fluorescent staining procedures) were determined.

3.2.4. Fluorescent staining procedures

The metabolic activity was measured using fluorescein diacetate (FDA, Sigma-Aldrich) or with 2-chloro-4-(2,3-dihydro-3-methyl-(benzo-1,3-thiazol-2-yl)-methylidene)-1-phenylquinolinium iodide (FUN-1) (Molecular Probes-Invitrogen). FDA diffuses freely into yeast cells being hydrolysed by the action of esterases in metabolically active cells (Breeuwer et al., 1995). The probe FUN-1 is processed in the cytosol of yeast cells by an enzyme-mediated process; subsequently, the dye (biochemically modified) is transported and sequestered in the vacuole as a cylindrical intravacuolar structure (CIVS) (Millard et al., 1997).

Cells suspensions, treated with NiO NPs or Ni^{2+}, were collected, at defined times indicated in the figures, harvested by centrifugation and then re-suspended in one of the following buffers according to each determination: (i) 10 mmol/L PBS buffer solution, pH 7.0, for FDA staining; (ii) 10 mmol/L 4-(2-hydroxyethyl)-1-piperazineethanesulfonic acid (HEPES) buffer (Sigma-Aldrich), pH 7.2, with 20 g/L glucose for FUN-1 staining. Cells were incubated in the dark with 4.2 µg/mL FDA, for 20 minutes at 25 ºC and, subsequently, for 10 minutes at 4ºC. In FUN-1 staining, yeast cells were incubated with 0.2 mmol/L FUN-1, for 30 minutes, in the dark, at 25°C. Cells were counted (at least 200 cells, in duplicate, for each experiment) using an epifluorescence microscope (Leica Microsystems) equipped with an HBO 100 mercury lamp and the I3 filter set from Leica. The images were acquired with a Leica DC 300 F camera (Leica Microsystems) and processed using Leica IM 50 - Image manager software. To obtain FDA and FUN-1 negative cells, healthy cells (in exponential growth-phase) suspended in deionized water were placed in a glass tube and heat-treated (at 65ºC for 1h) in a water bath. Subsequently, cells were cooled to room temperature and stained as described above.

For the assessing of the esterase activity, $1x10^7$ cells/mL not exposed (control) or exposed to NiO NPs or Ni^{2+}, for 6 h, were stained with 4.2 µg/mL FDA, placed in quadruplicate in a 96-well flat microplate (Orange Scientific) and incubated in the dark for 40 minutes at 25ºC. Fluorescence (in relative

fluorescent units, RFU) was measured in a microplate reader (PerkinElmer, Victor3) at a fluorescence excitation wavelength of 485/14 nm and an emission of 535/25 nm.

Intracellular ROS accumulation was monitored with 2′,7′-dichlorodihydrofluorescein diacetate (H_2DCFDA, Sigma-Aldrich). Cells were suspended in MES buffer with glucose, pH 6.0, at a final concentration of $1x10^7$ cells/mL and incubated with 20 µmol/L H_2DCFDA at 25ºC for 10 minutes. Then, cells were exposed to NiO NPs or Ni^{2+} and placed in quadruplicate in a 96-well flat microplate. Fluorescence was determined as described above for FDA (esterase activity). Cells were also observed using an epifluorescence microscope; images were obtained as described above.

3.2.5. TEM observation of yeast cells

Yeast cells incubated for 6h in MES buffer without (control) or with 100 mg/L NiO NPs were examined by TEM. In brief, cells were fixed with 2.5% glutaraldehyde (Electron Microscopy Sciences) and 2% paraformaldehyde (Merck) in 0.1 mol/L cacodylate buffer (pH 7.4), dehydrated and embedded in Epon resin (TAAB). Ultrathin sections (40-60 nm thickness) were prepared on an ultramicrotome (RMC-Boeckeler Instruments, PowerTome) using diamond knives (DDK). The sections were mounted on Formvar/carbon film-coated 300 mesh nickel grids (Electron Microscopy Sciences), stained with uranyl acetate and lead citrate and examined under TEM. Images were digitally recorded as described above ["Preparation of NiO nanoparticles (NPs) stock suspensions and characterization of suspensions"].

3.2.6. Statistical analysis

Statistical differences between control and treated cells were tested using unpaired *t* test. Alternatively, the mean values were subject to one-way ANOVA followed by Tukey-Kramer multiple comparison method. In all experiments, *P* values <0.05 were considered statistically significant.

3.3. Results

3.3.1. Characterization of nickel oxide (NiO) nanoparticles (NPs)

The characterization of NiO NPs in powder (namely NPs size and shape), suspended in deionized water and in aqueous media (YEP and MES buffer), namely NPs agglomerations properties, surface charge and dissolution of the NPs were carried out.

During the incubation of yeast cells in YEP broth or MES buffer, the pH of the medium was modified. This alteration can be mostly attributed to the metabolism of the cells since the dispersion of NPs did not modify the pH value in either medium (Table 3.1). In YEP, due to the growth of yeast cells, the pH

of the medium varied from 6.00 to 4.76. In MES buffer, no appreciable growth occurred, and the pH only decreased 0.2 units (Table 3.1).

Table 3.1. Measurement of the pH in different media.

Medium	[NiO] (mg/L)	Time (h)	pH
YEP	0	24	4.76 ± 0.05
	50		4.70 ± 0.07
	100		4.76 ± 0.06
MES	0	6	5.80 ± 0.04
	50		5.80 ± 0.07
	100		5.79 ± 0.03

The data reported are the mean values ± standard deviation at least three independent experiments performed in duplicate ($n \geq 6$).

According to the manufacturer, the NiO NP size in powder is <50 nm. Observation by TEM confirmed the NiO NP size; most of the particles have a polyhedral morphology (Fig 3.1A). It was also possible to observe that, in aqueous suspension, NiO NPs have the tendency to agglomerate (Fig 3.1B).

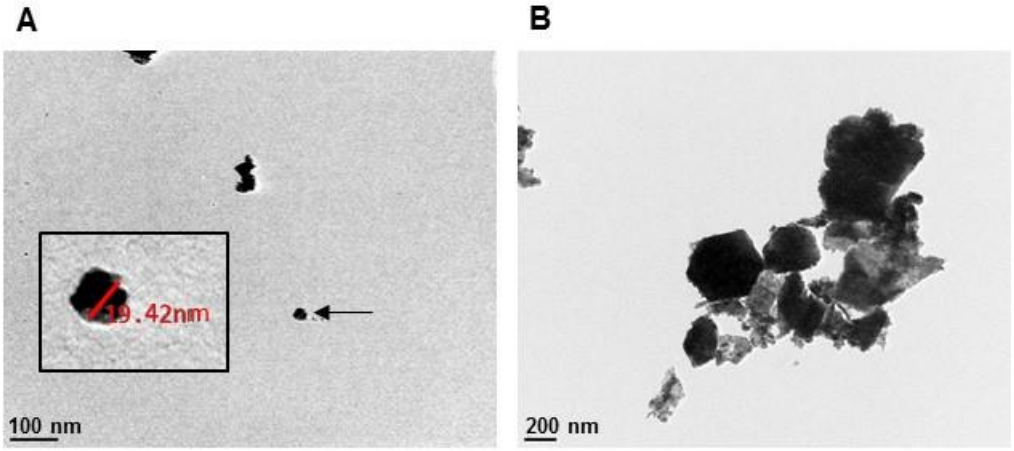

Figure 3.1. Characterization of nickel oxide (NiO) nanoparticles (NPs). A and B – Representative transmission electron microscopy (TEM) images of NiO NPs in powder or suspended in MES buffer, respectively. A – Insert: high magnification image of the NiO NPs marked with an arrow in left panel, limited by the black-box.

In YEP broth, the mean hydrodynamic size of the NiO NPs at 0 h (after the preparation of NiO suspension) was (344±30) nm, which is similar to the hydrodynamic size observed in deionized water (324±53) nm (Table 3.2); an increase of NP agglomeration after 24 h (1105±218) nm was observed

(Table 3.2). In MES buffer, at time zero, for both concentrations of NiO NPs tested, a Z-average diameter of ~1200 nm was determined, which revealed an immediate enhancement of NiO NP agglomeration (Table 3.2); in this medium, the agglomeration of the NPs was higher than in YEP and increased over time, as can be observed by the increase of hydrodynamic size after 6 h (~5000 nm). Also in MES buffer, the polydispersity index was higher than 0.7, which indicates that the sample had a very broad size distribution (Table 3.2).

The zeta potential is an indicator of the stability of the NPs in the suspension (Hanaor et al., 2012). The suspension of NiO NPs displayed a negative value in deionized water, YEP medium and MES buffer (Table 3.2). The zeta potential values of the NiO NPs were more negative in YEP medium comparatively to MES buffer (Table 3.2).

Table 3.2. Characterization of NiO NPs in different media.

Medium	Concentration (mg/L)	Time (h)	Z-average diameter (nm)	Polydispersity index	Zeta potential (mV)
Deionized Water	100	0	324 ± 53	0.34 ± 0.07	-6.4 ± 0.3
YEP	100	0	344 ± 30	0.4 ± 0.2	-21 ± 2
		3	395 ± 49	0.55 ± 0.07	-20.5 ± 0.5
		24	1105 ± 218	0.5 ± 0.1	-16.8 ± 0.4
MES	50	0	1015 ± 230	0.7 ± 0.2	-5.6 ± 0.4
		1	2117 ± 151	0.96 ± 0.05	-6.0 ± 0.7
		3	2415 ± 373	0.96 ± 0.05	-7.6 ± 0.4
		6	4279 ± 391	0.97 ± 0.04	-7.4 ± 0.6
	100	0	1262 ± 130	0.73 ± 0.06	-5.1 ± 0.6
		1	2530 ± 217	1.000 ± 0.001	-4.4 ± 0.4
		3	2728 ± 386	1.0 ± 0.1	-7.6 ± 0.3
		6	5076 ± 624	1.000 ± 0.001	-7.8 ± 0.9

It has been described that the pH of the medium can have an important impact on the dissolution of metal oxide NPs (Bao et al., 2015; Studer et al., 2010). Therefore, the influence of the contact of yeast cells with NiO NPs, particularly due to the effect of the pH decreasing (Table 3.1), on the characteristics of the NP suspensions was evaluated. The dissolution of the NiO NPs into their component ions was evaluated by quantifying the dissolved nickel in different media; as control, NPs dissolution was evaluated in deionized water (Fig 3.2). The dissolved nickel in deionized water after 6 and 24 h, for 100 mg/L NiO NPs, was 4.3±0.5 and 4.9±0.2 mg/L, which corresponds to a dissolution of 5.5 and 6.3%, respectively. For 100 mg/L NiO NPs, the concentration of dissolved nickel in YEP remained

approximately constant over 24 h and was 3.0±0.1 mg/L (a dissolution of NPs of 2.6 %) (Fig 3.2A). For 100 mg/L NiO NPs, in MES buffer, after 6 h, the nickel released was 5.1±0.2 mg/L (Fig 3.2A), which corresponds to a dissolution of 6.6%; this value is similar to the observed in deionized water after 6h and it is independent of the technique used to remove (Fig 3.2B). Also, the concentration corresponds to the dissolved nickel in the MES buffer when yeast cells were incubated for 6 h with 100 mg/L NiO NPs was 5.2±0.2 mg/L (Fig 3.2B). In resume, the dissolution of NiO NPs was low (<7%) for all the media and NPs concentration tested.

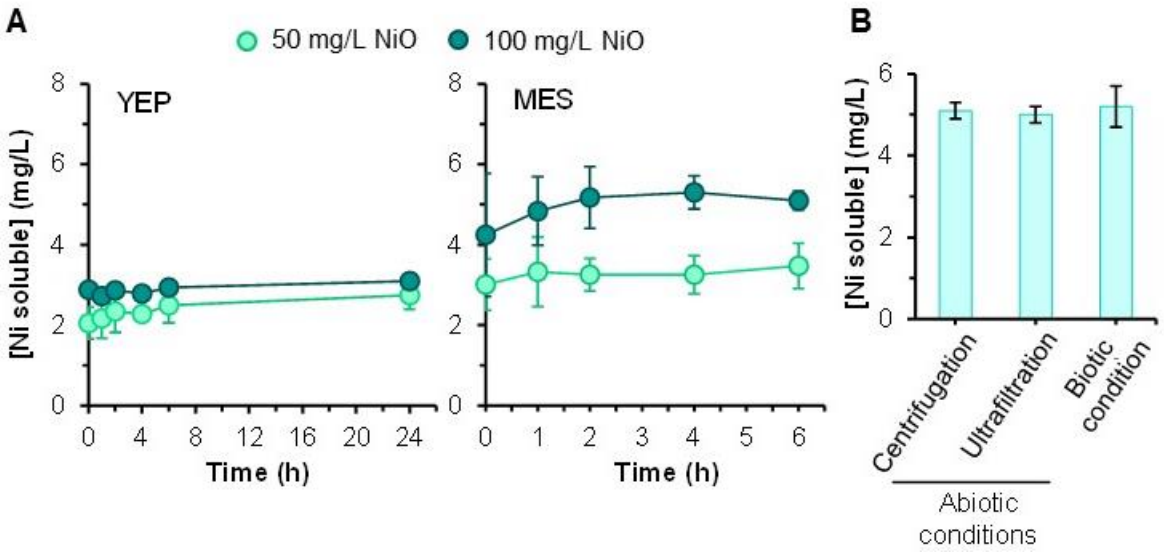

Figure 3.2. Dissolved nickel from NiO NPs, in YEP broth and MES buffer. A – The nickel dissolved from NiO NPs in YEP broth or MES buffer, for 50 and 100 mg/L NiO. Each point represents the mean of at least three independent experiments performed in duplicate ($n \geq 6$). B – Dissolved nickel in MES buffer using different techniques (abiotic conditions) and nickel dissolution in the presence of yeast cells (biotic condition), after 6 h. Standard deviations (SD) are presented (vertical error bars); where no error bars are shown, SD are within the points.

3.3.2. Loss of cell viability induced by NiO NPs and Ni^{2+}

The toxic impact of NiO NPs on the yeast *S. cerevisiae* was evaluated using the classical growth inhibition assay in liquid medium. To clarify the role of the solubilisation of NiO NPs, yeast cells were also exposed to Ni^{2+}. NiO NPs up to 100 mg/L were not able to inhibit yeast cell growth in YEP broth (Fig 3.3A). Yeast cells in the presence or absence of 100 mg/L NiO NPs had the same growth pattern in YEP broth (data not shown). In contrast, Ni^{2+} inhibited yeast growth (Fig 3.3A), even at a very low concentration (24 h-EC_{10} = 6.6 mg/L Ni), displaying a 24 h-EC_{50} of 18.3 mg/L (Table 3.3); at 100 mg/L Ni^{2+}, yeast growth was practically arrested (Fig 3.3A).

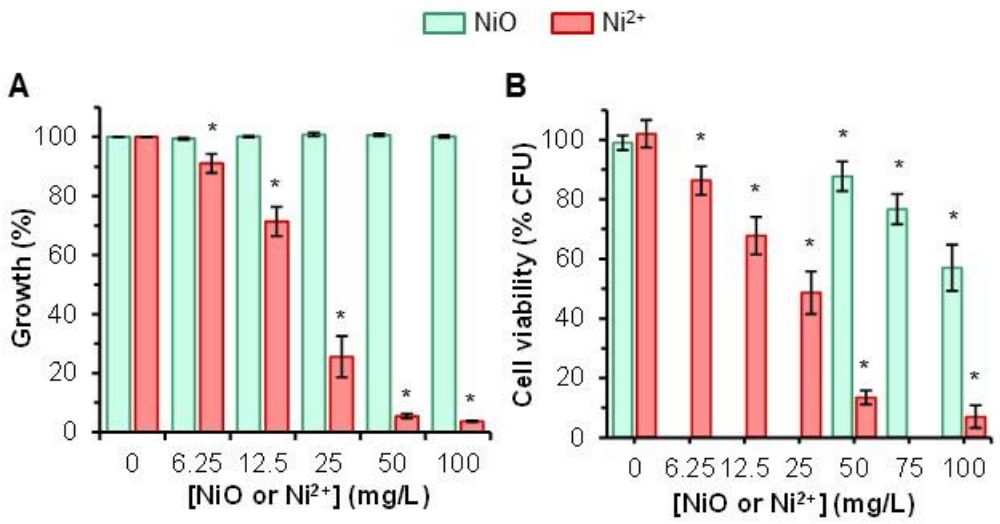

Figure 3.3. Effect of NiO NPs or Ni^{2+} on the yeast *S. cerevisiae* BY4741. Cells were exposed to NiO or Ni^{2+} in YEP broth (A) or in 10 mmol/L MES buffer, with 20 g/L glucose (B), and the growth or the viability were determined after 24 h or 6 h, respectively. The data are presented as mean values from at least three independent experiments performed in duplicate ($n \geq 6$); standard deviations are presented (vertical error bars). Mean values are significantly different: * $P < 0.05$ in comparison with untreated cells (control); unpaired t test.

The complex nature of the YEP broth can mitigate the toxic effects of the NiO NPs. To test this possibility, yeast cells were exposed to NiO NPs in a simpler solution composed of 10 mmol/L MES buffer containing 20 g/L glucose. The toxic effect was evaluated through the inhibition of cell proliferation capacity on YEP agar (viability assay). NiO NPs induced loss of cell viability in a dose-dependent way; exposure of yeast cells to 100 mg/L NiO NPs generated a reduction of viability of ~40% of the cell population (Fig 3.3B). Ni^{2+} also induced loss of cell viability in a dose-dependent manner, similar to the growth inhibition observed in liquid YEP (Fig 3.3 and Table 3.3).

Table 3.3. Effect of Ni^{2+} on the yeast *S. cerevisiae*.

		EC[a] (mg/L)				
Medium	**Time (h)**	10	25	50	75	90
YEP	24	6.6 ± 0.2	11.3 ± 0.3	18.3 ± 0.3	26 ± 1	44 ± 1
MES	6	3.9 ± 0.6	10 ± 1	24 ± 1	41 ± 1	69 ± 4

[a] EC – effect concentration. EC_{10}, EC_{25}, EC_{50}, EC_{75} and EC_{90} values represent the concentration of Ni^{2+}, which reduced cell viability (cell viability assay) after exposure to the toxicant in 10 mmol/L MES buffer (containing 20 g/L glucose) or inhibited the growth of yeast cells in YEP broth (growth inhibition assay) by 10, 25, 50, 75 or 90%, respectively.
The data reported are the mean values ± standard deviation of three independent experiments performed in duplicate (n=6).

3.3.3. Impact of NiO NPs and Ni^{2+} on metabolic activity and intracellular ROS accumulation

To obtain further insights related to the toxic action of the NiO NPs, a kinetic approach was carried out using the highest concentration of NiO NPs and Ni^{2+} previously tested in MES buffer. This approach led us to observe that the exposure of yeast cells to 100 mg/L NiO NPs generated a progressive loss of cell viability (Fig 3.4); after 2 h, ~90% of the cell population was able to form colonies on agar medium; this value declined to ~60% after 6 h of yeast cell contact with NPs (Fig 3.4). The exposure to 100 mg/L Ni^{2+} induced a higher and faster effect: after 2 h, the percentage survival assessed by CFU counts declined to ~10% (Fig 3.4).

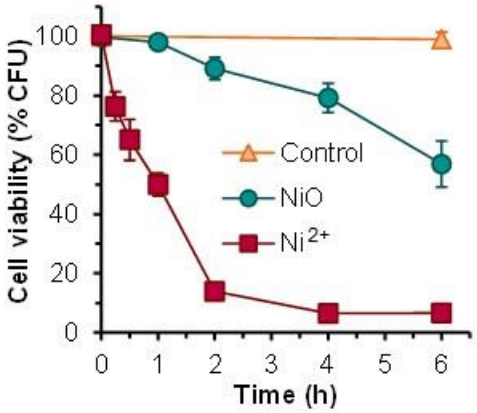

Figure 3.4. Effect of NiO NPs and Ni^{2+} on the cell viability of *S. cerevisiae* BY4741. Cells were exposed to 100 mg/L NiO or Ni^{2+} in 10 mmol/L MES buffer, with 20 g/L glucose. Control: cells incubated in MES buffer in the same conditions of the assays with toxicants. Cell viability was evaluated by colony forming units (CFU) counting. Each point represents the mean of at least three independent experiments, performed in duplicate (n>6). Standard deviations (SD) are presented (vertical error bars); where no error bars are shown, SD are within the points. All means presented are significantly different from the control ($P < 0.05$; unpaired t test), except NiO NPs for 1 h.

The impact of NiO NPs on the metabolic activity of yeast cells was evaluated through the processing of FUN-1 probe and esterase activity. Cells that are metabolically active (FUN-1 positive cells) are able to process the probe FUN-1 and present cylindrical intravacuolar structure (CIVS) (Millard et al., 1997) (Fig 3.5A, control). The exposure of yeast cells to NiO NPs generated a reduction of the percentage of FUN-1 positive cells. A deeper and faster effect was observed with yeast cells exposed to Ni^{2+} (Fig 3.5B). Metabolically active cells (FDA positive cells) display green fluorescence (Fig 3.5C, control) while metabolically inactive cells remain unstained (Breeuwer et al., 1995). Yeast cells exposed to 100 mg/L NiO NPs or Ni^{2+} remained ~100% or ~90% FDA positive, respectively (Fig 3.5D). However, the microscopic observation of NiO treated cells showed that these yeast cells were less green than non-treated cells (Fig 3.5C, 100 mg/L NiO NPs), which suggests some loss of esterase activity. To confirm this observation, the quantification of fluorescence exhibited by yeast cells treated for 6 h with 100

mg/L NiO NPs or Ni^{2+} was carried out. Cells exposed to NPs or Ni^{2+} displayed a significant decrease of fluorescence compared to the control (Fig 3.5E); these results suggest that NiO NPs and Ni^{2+} decreased the esterase activity of yeast cells, confirming the loss of metabolic activity observed with FUN-1 probe.

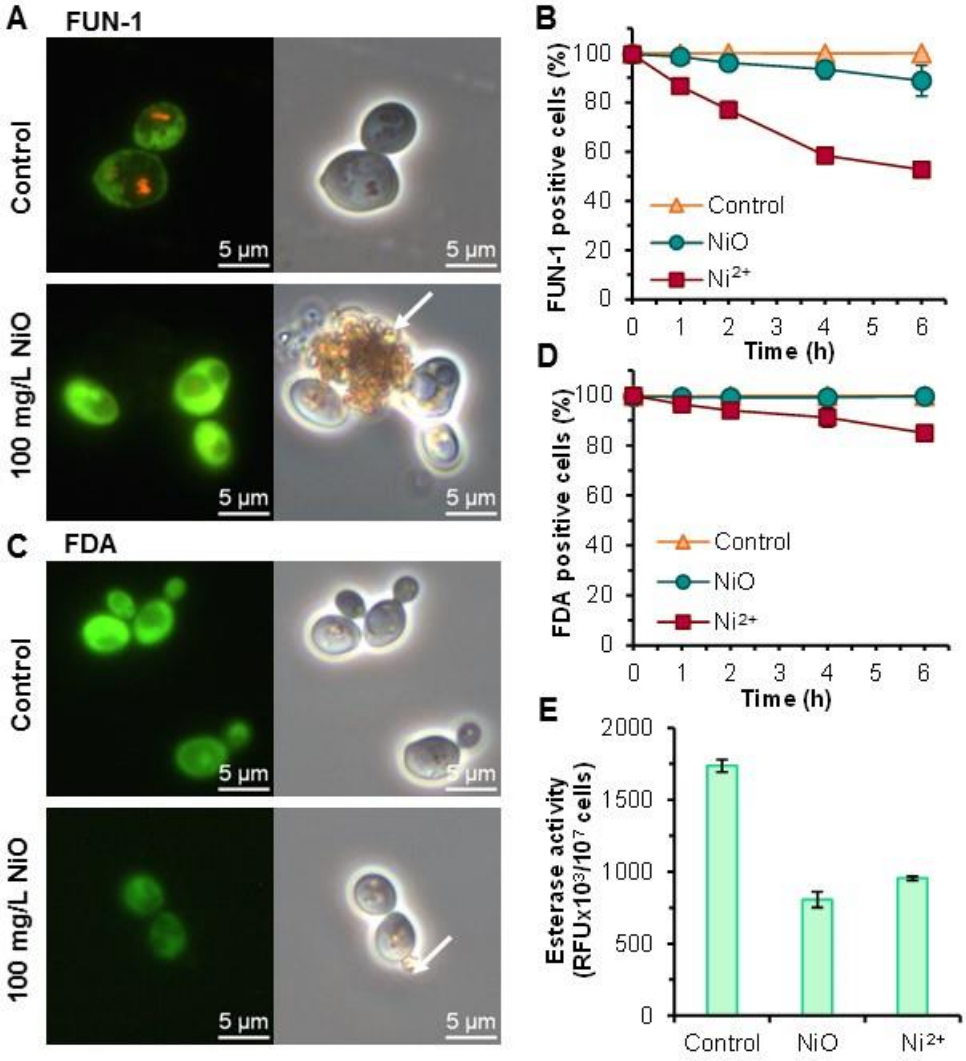

Figure 3.5. Effect of NiO NPs and Ni^{2+} on the metabolic activity of *S. cerevisiae* BY4741. A and C – Microphotographs illustrative of untreated cells (control) or cells exposed to 100 mg/L NiO NPs for 6 h and subsequently stained with FUN-1 or FDA (left side) and respective phase contrast images (right side). Cells exposed to NiO NPs and stained with FDA were shot with 2× shutter time used in the control. Arrows: NiO NPs in contact with yeast cells. B and D – Quantification by fluorescence microscopy of the percentage of metabolically active yeast cells exposed to 100 mg/L NiO or Ni^{2+} and subsequently stained with FUN-1 or FDA, respectively. Each point represents the mean of at least three independent experiments, performed in duplicate ($n \geq 6$). Standard deviations (SD) are presented (vertical error bars); where no error bars are shown, SD are within the points. E – Assessment of esterase activity, by the hydrolysis of FDA, of cells exposed to 100 mg/L NiO or Ni^{2+} for 6 h. This is a typical example of an experiment performed at least three times. Each bar represents the mean of four fluorescent readings (n=4); standard deviations are presented (vertical error bars). All means presented are significantly different from the control ($P<0.05$; unpaired t test), except for NiO in D.

The incubation of yeast cells with the general redox sensor H_2DCFDA (Tarpey et al., 2004) and subsequent exposure to NPs or Ni^{2+} for 6h revealed that NiO NPs and Ni^{2+} induced the intracellular accumulation of reactive oxygen species (ROS) (Fig 3.6).

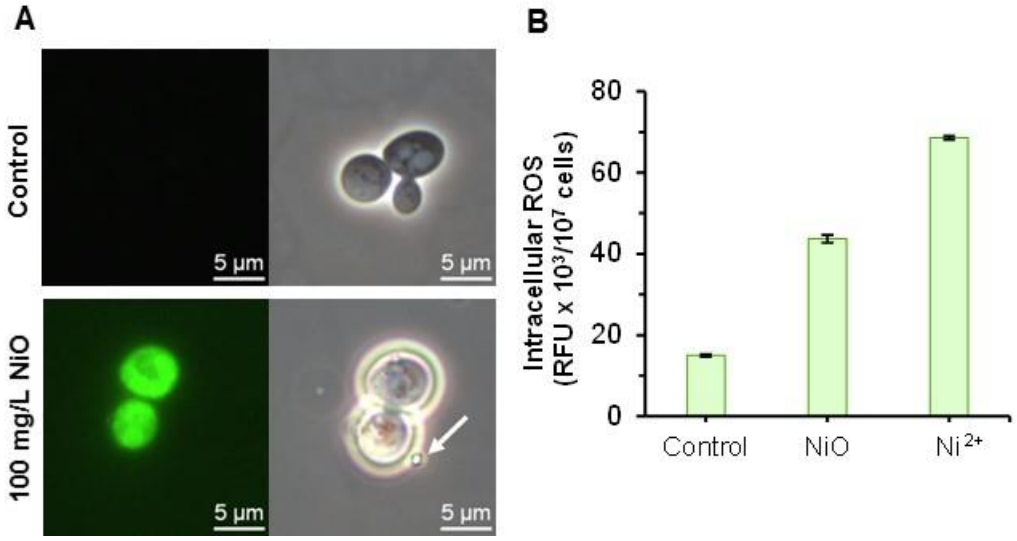

Figure 3.6. Effect of NiO NPs and Ni^{2+} on the reactive oxygen species (ROS) production by *S. cerevisiae* BY4741. A – Visualization of control (cells incubated in the absence of the toxicant, without ROS) and cells exposed for 6 h to 100 mg/L NiO NPs showing intracellular ROS (green fluorescence) (left side) and respective phase contrast images (right side). Arrow: NiO NPs in contact with yeast cells. B – Assessment of intracellular ROS in cells exposed for 6h to 100 mg/L NiO or Ni^{2+} and compared with control. This is a typical example of an experiment performed at least three times. Each bar represents the mean of four fluorescent readings (n=4). Standard deviations (SD) are presented (vertical error bars); where no error bars are shown, SD are within the points. The means are significantly different from the control ($P < 0.05$; unpaired t test).

3.3.4. Contribution of the nickel released by NPs to the observed toxicity

To test the contribution of the nickel dissolved from the NPs to the toxicity of NiO NPs, yeast cells were exposed to 5.2 mg/L Ni^{2+}. This concentration corresponds to the dissolved nickel in the MES buffer when yeast cells were incubate with 100 mg/L NiO NPs during 6 h (Fig 3.2B), and is similar to the amount of nickel released by NPs in the used MES buffer (abiotic conditions) described above (Fig 3.2A, B). Yeast cells exposed to 5.2 mg/L Ni^{2+} displayed viability $\geq$ 90% (Fig 3.7A) practically without ROS accumulation (Fig 3.7B). Similar results were observed when yeast cells were exposed to the supernatant of 100 mg/L NiO NPs (NiO NPs supernatant) (insert of Fig 3.7A; Fig 3.7B). These results were considerably different from those observed when yeast cells were exposed to 100 mg/L NiO NPs: viability of ~60% (Fig 3.3B and Fig 3.4) and a substantial accumulation of intracellular ROS (Fig 3.6A, B) were observed. Together, these results suggest that the toxic effects observed for 100 mg/L NiO should not be attributed mainly (or only) to the nickel released from the NPs.

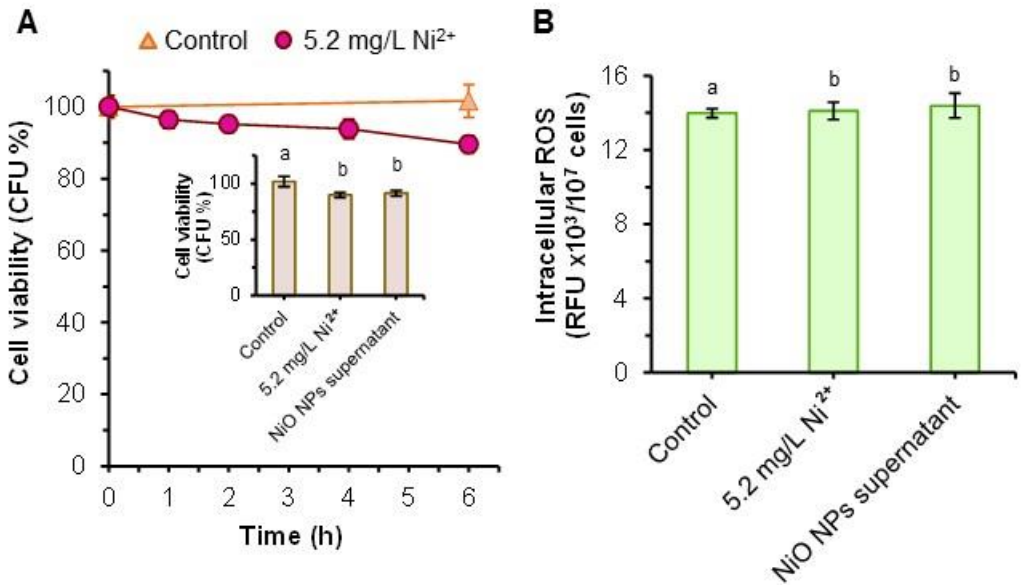

Figure 3.7. Effect of the dissolution of NiO NPs on cell viability and intracellular ROS accumulation. Cells were not exposed (control) or exposed to 5.2 mg/L Ni^{2+} in MES buffer. A – Evaluation of viability of cells exposed to 5.2 mg/L Ni^{2+}. The data reported are presented as mean values from at least three independent experiments performed in duplicate ($n \geq 6$). Standard deviations (SD) are presented (vertical error bars); where no error bars are shown, SD are within the points. Insert: comparison of the viability among non-treated cells (control) and cells exposed for 6 h to 5.2 mg/L Ni^{2+} or 100 mg/L NiO NPs supernatant. B – Levels of intracellular ROS of cells exposed for 6 h to 5.2 mg/L Ni^{2+} or 100 mg/L NiO NPs supernatant. This is a typical example of an experiment performed at least three times. Each bar represents the mean of four fluorescent readings (n=4). Standard deviations are presented (vertical error bars). The means with different letters are significantly different ($P < 0.05$; ANOVA).

3.3.5 NiO NPs adhere to cell wall but are not internalized in yeast cells

The observation, by optical microscopy, of yeast cells exposed to NiO NPs allowed visualizing the presence of agglomerated NPs adhered to the cells (Fig 3.5A, C and Fig 3.6A). The subsequent analysis of yeast cells exposed to NPS, using a more powerful observation technique (TEM), detected the presence of agglomerates, electron-dense, in contact with cell wall (Fig 3.8A). A more detailed examination of these cells revealed that the electron-dense structures are in tight contact with the yeast cell wall (right panel of Fig 3.8A). Taken together, these observations strongly suggest that NiO NPs agglomerates adhere to yeast cell wall.

To obtain further insights about the possible mechanisms of toxicity of NiO NPs, it was investigated whether the NPs enter into *S. cerevisiae* cells. Fig 3.8A, B show typical TEM images of yeast cells incubated with NiO NPs or without (control), respectively. A careful observation of the cytoplasm of yeast cells exposed to NiO NPs, using TEM, did not detect any electron-dense structures containing nickel (Fig 3.8A), which suggests that NiO NPs should not be able to cross the cell wall and plasma membrane of yeast cells.

To evaluate the effect of cell wall porosity on the susceptibility of yeast cells to NiO NPs, two isogenic mutants (*cwp1*Δ and *cwp2*Δ) which were affected in cell wall mannoproteins were used. Literature describes that the wall of yeasts with deletion of the *CWP1* or *CWP2* genes display increased permeability and sensitivity to genotoxic agents (Zhang et al., 2008). As it can be observed in Fig 3.8C, the susceptibility of *cwp1*Δ and *cwp2*Δ strains was not significantly different from that of the WT strain, which suggests that an increase of yeast cell wall porosity did not enhance the susceptibility of *S. cerevisiae* cells to NiO NPs. These results confirm the sieve effect of this cell structure.

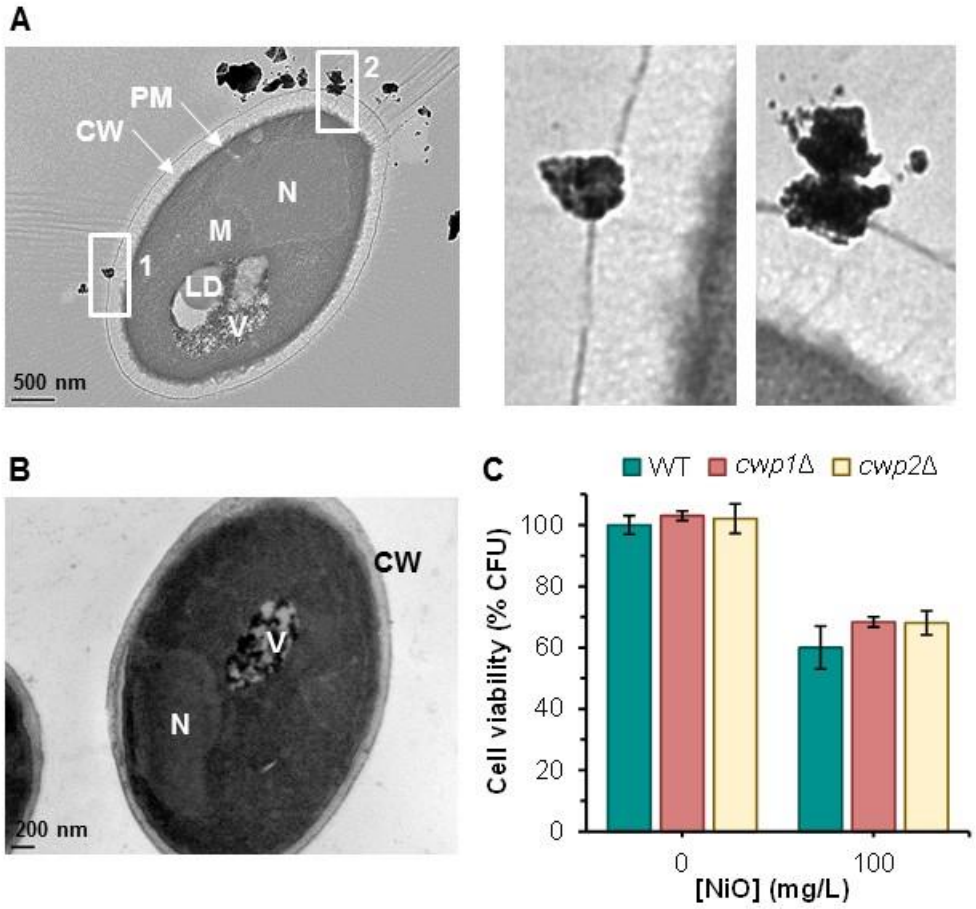

Figure 3.8. NiO NPs adhere to cell wall of the yeast *S. cerevisiae* BY4741 but are not internalized. A and B – Representative transmission electron microscopy (TEM) images of cells incubated with 100 mg/L NiO NPs or without NPs (control) for 6 h, in MES buffer, respectively. Boxes 1 and 2: electron dense particles adhered to yeast cell wall. Right panel of A – high magnification images of boxes 1 and 2, respectively. CW - cell wall; LD - lipid droplet; M – mitochondria; N – nucleus; PM – plasma membrane; V – vacuole. C – Effect of wall porosity on the susceptibility of *S. cerevisiae* to NiO NPs. Wild type strain (WT) and the isogenic mutants *cwp1*Δ and *cwp2*Δ were exposed to NiO NPs for 6 h. Each bar represents the mean of at least three independent experiments performed in duplicate ($n \geq 6$); standard deviations (SD) are presented (vertical error bars). The means are not significantly different ($P < 0.05$; ANOVA).

3.4. Discussion

The characterization of NiO NPs in both media showed that the NPs tended to agglomerate in aqueous medium (Table 3.2), which is in agreement with observations of other authors (Karlsson et al., 2014; Latvala et al., 2016; Siddiqui et al., 2012). This agglomeration is particularly notorious in MES buffer (Fig 3.1B) and, for both NP concentrations tested, NiO NPs agglomerate with time, displaying a hydrodynamic diameter distributed over a range of ~1000 to 5000 nm. In fresh YEP medium, NiO NPs displayed a hydrodynamic diameter distributed over a range of ~300 to 400 nm during the first 3 h, which is similar to that of other reports (Duan et al., 2015; Faisal et al., 2013). Zeta potential is usually seen as a key indicator of the stability of NPs. In suspensions with low zeta potential (-4 to – 8 mV), as was observed in MES buffer (Table 3.2), attractive forces exceeded the repulsive forces; thus, the NPs were poorly stabilized and tended to agglomerate. In YEP medium, NiO NPs displayed a higher value of zeta potential (-21 to – 17 mV) and were more stable in comparison with suspensions in MES buffer. Hence, the agglomeration of NiO NPs determined by DLS is in agreement with the zeta potential observed in both media. A similar value to the one observed in YEP medium was reported for NiO NPs suspended in Holtfreter's medium at pH 7.0 (-23.1±2.0 mV) (Lin et al., 2013).

Due to NiO NPs agglomeration in MES buffer, lower toxicity was expected in this medium compared to YEP. However, the opposite effect was observed: NiO NPs up to 100 mg/L did not inhibit yeast growth in liquid YEP while yeast cells exposed for 6 h to NiO NPs in MES buffer and subsequently plated on YEP agar lost their cell viability in a dose dependent manner (Fig 3.2). The difference of toxicity in these two media (YEP broth and MES buffer) can be attributed to the coating of the NiO NPs by peptides from the YEP medium. The formation of protein-coated NPs (Cedervall et al., 2007) reduces NPs bioavailability and consequently decreases their toxicity, as was suggested in the case of antibacterial activity of silver NPs complexed with albumin (Lok et al., 2007). In addition, the nickel released from the NPs was, most likely, complexed by medium components (Hausinger, 1993; Protheroe et al., 1989), which reduces its bioavailability and hinders their toxicity.

It was observed that NiO NPs were very insoluble in the tested media; the nickel released from NPs in fresh YEP broth or MES buffer being equal to or below 6.6%. Karlson et al. (2014) reported a similar percentage (5%) of dissolved Ni for NiO NPs suspended in MES buffer.

One of the main hypotheses explaining NP toxicity is associated with their tendency to induce the formation of ROS (Nel et al., 2006; von Moos and Slaveykova, 2014). Consistent with this possibility, an enhancement of intracellular ROS generation in yeast cells exposed to 100 mg/L NiO NPs was observed (Fig 3.6). Our results are in agreement with those described in the literature reporting ROS

production in different mammalian cells exposed to NiO NPs (Ahamed et al., 2013; Horie et al., 2011; 2016; Siddiqui et al., 2012).

NiO-induced reduction of metabolic activity was observed through the assessment of esterase activity and FUN-1 processing (Fig 3.5). Although yeast cells exposed to NiO NPs remained esterase positive (Fig 3.5D), a sharp reduction (compared to the control) of the ability to hydrolyse FDA was observed (Fig 3.5C, E). Similarly, in NiO NP treated cells, a reduction of the ability to process the probe dye FUN-1 was observed (Fig 3.5B). Together, the induction of intracellular ROS accumulation and the reduction of metabolic activity can contribute to the reduction of viability of yeast cells exposed to NPs (Fig 3.3B and 3.4).

The comparison of the toxic effect due to the exposure of yeast cells to 100 mg/L NiO NPs (a loss of viability of ~40% and an increase of approximately 300% of intracellular ROS) (Fig 3.4 and 3.6B) with the effect caused by 5.2 mg/L Ni^{2+} (a loss of viability <10% and an increase of 1% of the intracellular ROS) (Fig 3.7), which is the amount of nickel released by 100 mg/L NiO NPs (Fig 3.2B), suggests that nickel released from NPs, by itself, cannot be the main contributor to the toxicity observed. This possibility was confirmed by the exposure of yeast cells to the supernatant of 100 mg/L NiO NPs; under this condition, a similar effect to that of exposure to 5.2 mg/L Ni^{2+} was observed (insert of Fig 3.7A and Fig 3.7B). Together, these results strongly indicate that nickel released from NiO NPs can contribute to but does not explain all (or most) of the toxicity observed due to NiO NPs. A similar observation was described when *Photobacterium phosphoreum* was exposed to NiO NPs (Wang et al., 2016).

NiO NPs can exert their toxic effect on *S. cerevisiae* cells by a direct mechanism: the passage of NiO NPs through the yeast cell wall and subsequent internalization by endocytosis. Miao et al. (2010) reported that the internalization of silver NPs was a mechanism through which algal growth was substantially reduced. The cell wall of *S. cerevisiae* is a porous matrix composed of an external layer constituted predominantly of mannoproteins and an internal layer consisting of glucans and chitin (Klis et al., 2002; 2006). The yeast *S. cerevisiae* displays cell wall pores of approximately 200 nm, and they can increase up to 400 nm under stress conditions (de Souza Pereira and Geibel, 1999). However, passage of NiO NPs, which have an average hydrodynamic size of ~1000-5000 nm in MES buffer, through the cell wall seems to be unlikely. TEM observations of yeast cells exposed to 100 mg/L NiO NPs confirmed that no NPs were internalized by the yeast cells (Fig 3.8A). Similarly, other authors did not find CuO or ZnO NPs inside yeast cells of *S. cerevisiae* (Bao et al., 2015; Zhang et al., 2016). In the present work, it was also observed that isogenic strains with increased cell wall porosity (*cwp1*Δ and

*cwp2*Δ) were not significantly more susceptible to NiO NPs than the WT strain (Fig 3.8c). Together, these results ruled out the possibility that the toxic effects could be attributed to a direct action of NiO NPs.

As an alternative possibility, NPs can exert their toxic effect by an indirect mechanism: NiO NPs adsorb to the yeast cell wall and release nickel in the vicinity of the cell and thus enhance the toxic effect. A similar mechanism was proposed for the antibacterial activity of silver NPs (Lok et al., 2007) and for the toxic effects observed with CuO NPs in yeast cells (Bao et al., 2015; Kasemets et al., 2013). Compatible with this possibility, it was observed by optical microscopy (Figs 3.5A, C and Fig 3.6A) and transmission electron microscopy (Fig 3.8A) the adsorption of the NPs onto the surface of yeast cells. It was suggested that the metal ions released from metal oxide NPs can be adsorbed onto the NP surface, concentrating the amount of nickel at the NP-yeast cell wall interface and thus enhancing the toxic effect (Wang et al., 2016). Consistent with this possibility, we observed that yeast cells surrounded by agglomerated of NPs were usually metabolically compromised [FUN-1 negative (Fig 3.5A) or with a low level of esterase activity (Fig 3.5C)] and displayed considerable amounts of intracellular ROS (Fig 3.6). Emphasizing this possible mechanism of toxicity, the observed patterns of loss of cell viability (Fig 3.4), metabolic activity (Fig 3.5B, D, E) and enhancement of ROS accumulation (Fig 3.6B) induced by NPs and Ni^{2+} were similar. In the case of Ni^{2+}, a faster and deeper effect occurred due to its high concentration.

3.5. Conclusions

The toxicity mechanisms of NiO NPs were studied using the yeast *S. cerevisiae* as cell model:

- Toxicity were caused by the NPs themselves, probably, by an indirect mechanism: NPs adsorb to the yeast cell wall and enhance the release of Ni^{2+} at the NP-yeast cell wall interface;
- NiO NPs induced the loss of cell viability in a dose dependent manner;
- NiO NPs reduced the metabolic activity and enhanced ROS accumulation in yeasts.

References

Ahamed M, Ali D, Alhadlaq HA, Akhtar MJ (2013) Nickel oxide nanoparticles exert cytotoxicity via oxidative stress and induce apoptotic response in human liver cells (HepG2). Chemosphere 93: 2514-2522

Ates M, Demir V, Arslan Z, Camas M, Celik F (2016) Toxicity of engineered nickel oxide and cobalt oxide nanoparticles to *Artemia salina* in seawater. Water Air Soil Poll. 227: 1-8

Baek Y-W, An Y-J (2011) Microbial toxicity of metal oxide nanoparticles (CuO, NiO, ZnO, and Sb_2O_3) to *Escherichia coli*, *Bacillus subtilis*, and *Streptococcus aureus*. Sci. Total Environ. 409: 1603-1608

Bao S, Lu Q, Fang T, Dai H, Zhang C (2015) Assessment of the toxicity of CuO nanoparticles by using *Saccharomyces cerevisiae* mutants with multiple genes deleted. Appl. Environ. Microbiol. 8: 8098-8107

Breeuwer P, Drocourt JL, Bunschoten N, Zwietering MH, Rombouts FM, Abee T (1995) Characterization of uptake and hydrolysis of fluorescein diacetate and carboxyfluorescein diacetate by intracellular esterases in *Saccharomyces cerevisiae*, which result in accumulation of fluorescent product. Appl. Environ. Microbiol. 61: 1614-1619

Capasso L, Camatini M, Gualtieri M (2014) Nickel oxide nanoparticles induce inflammation and genotoxic effect in lung epithelial cells. Toxicol. Lett. 226: 28-34

Cedervall T, Lynch I, Lindman S, Berggard T, Thulin E, Nilsson H, Dawson KA, Linse S (2007) Understanding the nanoparticle-protein corona using methods to quantify exchange rates and affinities of proteins for nanoparticles. Proc. Natl. Acad. Sci. USA 104: 2050-2055

Chusuei CC, Wu C-H, Mallavarapu S, Hou FYS, Hsu C-M, Winiarz JG, Aronstarn RS, Huang Y-W (2013) Cytotoxicity in the age of nano: the role of fourth period transition metal oxide nanoparticle physicochemical properties. Chem-Biol Interact 206: 319-326

de Souza Pereira R, Geibel J (1999) Direct observation of oxidative stress on the cell wall of *Saccharomyces cerevisiae* strains with atomic force microscopy. Mol. Cell. Biochem. 201: 17-24

dos Santos SC, Sa-Correia I (2015) Yeast toxicogenomics: lessons from a eukaryotic cell model and cell factory. Curr. Opin. Biotech. 33: 183-191

dos Santos SC, Teixeira MC, Cabrito TR, Sa-Correia I (2012) Yeast toxicogenomics: genome-wide responses to chemical stresses with impact in environmental health, pharmacology, and biotechnology. Front. Genet. 3: 1-17

Duan W-X, He M-D, Mao L, Qian F-H, Li Y-M, Pi H-F, Liu C, Chen C-H, Lu Y-H, Cao Z-W, Zhang L, Yu Z-P, Zhou Z (2015) NiO nanoparticles induce apoptosis through repressing SIRT1 in human bronchial epithelial cells. Toxicol. Appl. Pharm. 286: 80-91

Faisal M, Saquib Q, Alatar AA, Al-Khedhairy AA, Hegazy AK, Musarrat J (2013) Phytotoxic hazards of NiO-nanoparticles in tomato: a study on mechanism of cell death. J. Hazard. Mater. 250: 318-332

Gillespie PA, Kang GS, Elder A, Gelein R, Chen L, Moreira AL, Koberstein J, Tchou-Wong K-M, Gordon T, Chen LC (2010) Pulmonary response after exposure to inhaled nickel hydroxide nanoparticles: short and long-term studies in mice. Nanotoxicology 4: 106-119

Goffeau A, Barrell BG, Bussey H, Davis RW, Dujon B, Feldmann H, Galibert F, Hoheisel JD, Jacq C, Johnston M, Louis EJ, Mewes HW, Murakami Y, Philippsen P, Tettelin H, Oliver SG (1996) Life with 6000 genes. Science 274: 546-567

Gong N, Shao K, Feng W, Lin Z, Liang C, Sun Y (2011) Biotoxicity of nickel oxide nanoparticles and bio-remediation by microalgae *Chlorella vulgaris*. Chemosphere 83: 510-516

Hanaor D, Michelazzi M, Leonelli C, Sorrell CC (2012) The effects of carboxylic acids on the aqueous dispersion and electrophoretic deposition of ZrO_2. J. Eur. Ceram. Soc. 32: 235-244

Hausinger RP (1993) Microbial nickel metabolism. In: Frieden E (ed) Biochemistry of nickel vol 12. Springer Science, New York, pp 181-201

Hayat K, Gondal MA, Khaled MM, Ahmed S (2011) Effect of operational key parameters on photocatalytic degradation of phenol using nano nickel oxide synthesized by sol-gel method. J. Mol. Catal a-Chem. 336: 64-71

Horie M, Fukui H, Nishio K, Endoh S, Kato H, Fujita K, Miyauchi A, Nakamura A, Shichiri M, Ishida N, Kinugasa S, Morimoto Y, Niki E, Yoshida Y, Iwahashi H (2011) Evaluation of acute oxidative stress induced by NiO nanoparticles in vivo and in vitro. J. Occup. Health. 53: 64-74

Horie M, Yoshiura Y, Izumi H, Oyabu T, Tomonaga T, Okada T, Lee B-W, Myojo T, Kubo M, Shimada M, Morimoto Y (2016) Comparison of the pulmonary oxidative stress caused by intratracheal instillation and inhalation of NiO nanoparticles when equivalent amounts of NiO are retained in the lung. Antioxidants 5: 1-12

Jemec A, Kahru A, Potthoff A, Drobne D, Heinlaan M, Bohme S, Geppert M, Novak S, Schirmer K, Rekulapally R, Singh S, Aruoja V, Sihtmae M, Juganson K, Kakinen A, Kuhnel D (2016) An interlaboratory comparison of nanosilver characterisation and hazard identification: harmonising techniques for high quality data. Environ. Int. 87: 20-32

Karathia H, Vilaprinyo E, Sorribas A, Alves R (2011) *Saccharomyces cerevisiae* as a model organism: a comparative study. PLoS One 6: 1-10

Karlsson HL, Gliga AR, Calleja FMGR, Goncalves CSAG, Wallinder IO, Vrieling H, Fadeel B, Hendriks G (2014) Mechanism-based genotoxicity screening of metal oxide nanoparticles using the ToxTracker panel of reporter cell lines. Part Fibre Toxicol. 11: 1-14

Kasemets K, Suppi S, Kuennis-Beres K, Kahru A (2013) Toxicity of CuO nanoparticles to yeast *Saccharomyces cerevisiae* BY4741 wild-type and its nine isogenic single-gene deletion mutants. Chem. Res. Toxicol. 26: 356-367

Klaine SJ, Edgington A, Seda B (2013) Nanomaterials in the environment. In: Férard J-F, Blaise C (eds) Encyclopedia of aquatic ecotoxicology. vol 2. Springer Publishers, Dordrecht, pp 767-779

Klis FM, Mol P, Hellingwerf K, Brul S (2002) Dynamics of cell wall structure in *Saccharomyces cerevisiae*. FEMS Microbiol. Rev. 26: 239-256

Klis FM, Boorsma A, De Groot PWJ (2006) Cell wall construction in *Saccharomyces cerevisiae*. Yeast 23(3):185-202

Kovriznych JA, Sotnikova R, Zeljenkova D, Rollerova E, Szabova E (2014) Long-term (30 days) toxicity of NiO nanoparticles for adult zebrafish *Danio rerio*. Interdiscip. Toxicol. 7: 23-26

Latvala S, Hedberg J, Di Bucchianico S, Möller L, Wallinder IW, Elihn K, Karlsson HL (2016) Nickel release, ROS generation and toxicity of Ni and NiO micro- and nanoparticles. PloS One 11: 1-20

Lin S, Zhao Y, Ji Z, Ear J, Chang CH, Zhang H, Low-Kam C, Yamada K, Meng H, Wang X, Liu R, Pokhrel S, Maedler L, Damoiseaux R, Xia T, Godwin HA, Lin S, Nel AE (2013) Zebrafish high-throughput screening to study the impact of dissolvable metal oxide nanoparticles on the hatching enzyme, ZHE1. Small 9: 1776-1785

Lok C-N, Ho C-M, Chen R, He Q-Y, Yu W-Y, Sun H, Tam PK-H, Chiu J-F, Che C-M (2007) Silver nanoparticles: partial oxidation and antibacterial activities. J. Biol. Inorg. Chem. 12: 527-534

Ma HB, Wallis LK, Diamond S, Li SB, Canas-Carrell J, Parra A (2014) Impact of solar UV radiation on toxicity of ZnO nanoparticles through photocatalytic reactive oxygen species (ROS) generation and photo-induced dissolution. Environ. Pollut. 193: 165-172

Miao A-J, Luo Z, Chen C-S, Chin W-C, Santschi PH, Quigg A (2010) Intracellular uptake: a possible mechanism for silver engineered nanoparticle toxicity to a freshwater alga *Ochromonas danica*. PLoS One 5: 1-8

Millard PJ, Roth BL, Thi HPT, Yue ST, Haugland RP (1997) Development of the FUN-1 family of fluorescent probes for vacuole labeling and viability testing of yeasts. Appl. Environ. Microb. 63: 2897-2905

Nel A, Xia T, Madler L, Li N (2006) Toxic potential of materials at the nanolevel. Science 311: 622-627

Nogueira V, Lopes I, Rocha-Santos TAP, Rasteiro MG, Abrantes N, Goncalves F, Soares AMVM, Duarte AC, Pereira R (2015) Assessing the ecotoxicity of metal nano-oxides with potential for wastewater treatment. Environ. Sci. Pollut. Res. 22: 13212-13224

OECD (2011) Alga, growth inhibition test (201) OECD guideline for testing of chemicals. Organization for Economic Co-Operation and Development, Paris, France

Oukarroum A, Barhoumi L, Samadani M, Dewez D (2015) Toxic effects of nickel oxide bulk and nanoparticles on the aquatic plant *Lemna gibba* L. Biomed. Res. Int. 50: 13-26

Protheroe RG, Cumming RH, Matchett A (1989) Medium-induced inhibition of microbial adsorption to nickel and activated-charcoal. Biotechnol. Bioeng. 34: 896-901

Siddiqui MA, Ahamed M, Ahmad J, Khan MAM, Musarrat J, Al-Khedhairy AA, Alrokayan SA (2012) Nickel oxide nanoparticles induce cytotoxicity, oxidative stress and apoptosis in cultured human cells that is abrogated by the dietary antioxidant curcumin. Food Chem. Toxicol. 50: 641-647

Soares EV, Duarte APRS, Soares HMVM (2000) Study of the suitability of 2-(N-morpholino) ethanesulfonic acid pH buffer for heavy metals accumulation studies using *Saccharomyces cerevisiae*. Chem. Spec. Bioavailab. 12: 59-65

Studer AM, Limbach LK, Van Duc L, Krumeich F, Athanassiou EK, Gerber LC, Moch H, Stark WJ (2010) Nanoparticle cytotoxicity depends on intracellular solubility: comparison of stabilized copper metal and degradable copper oxide nanoparticles. Toxicol. Lett. 197: 169-174

Tarpey MM, Wink DA, Grisham MB (2004) Methods for detection of reactive metabolites of oxygen and nitrogen: in vitro and in vivo considerations. Am. J. Physiol. Regul. Integr. Comp. Physiol. 286: R431-R444

von Moos N, Slaveykova VI (2014) Oxidative stress induced by inorganic nanoparticles in bacteria and aquatic microalgae - state of the art and knowledge gaps. Nanotoxicology 8: 605-630

Wang D, Lin Z, Wang T, Yao Z, Qin M, Zheng S, Lu W (2016) Where does the toxicity of metal oxide nanoparticles come from: the nanoparticles, the ions, or a combination of both? J. Hazard. Mater. 308: 328-334

Zhang M, Liang Y, Zhang X, Xu Y, Dai H, Xiao W (2008) Deletion of yeast *CWP* genes enhances cell permeability to genotoxic agents. Toxicol. Sci. 103: 68-76

Zhang W, Bao S, Fang T (2016) The neglected nano-specific toxicity of ZnO nanoparticles in the yeast *Saccharomyces cerevisiae*. Sci. Rep. 6: 1-11

Chapter 4 - Nickel oxide (NiO) nanoparticles induce loss of cell viability in yeast mediated by oxidative stress*

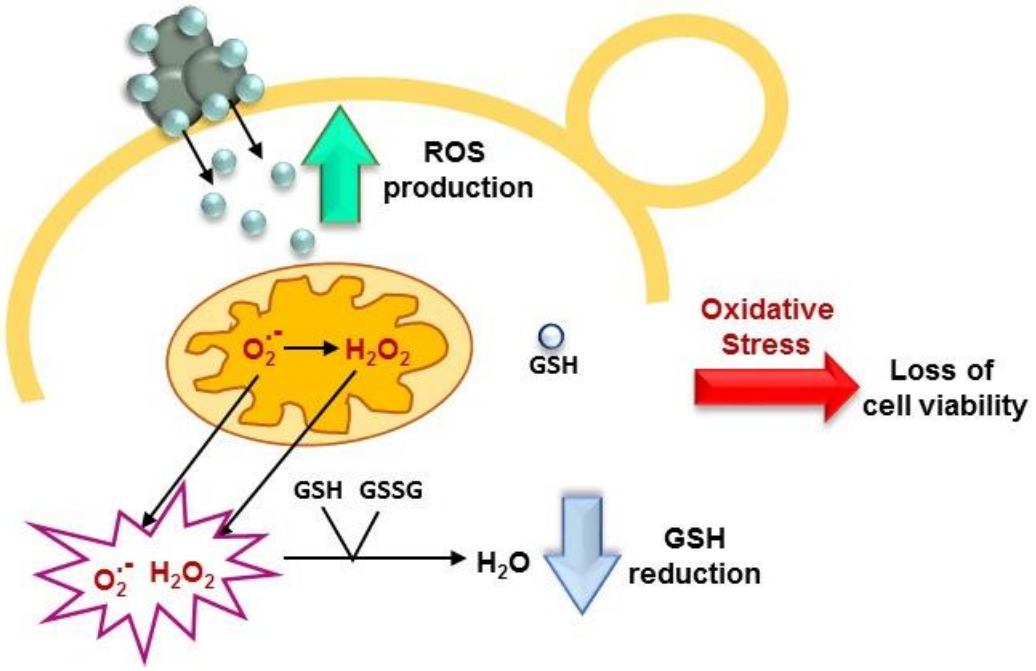

*Published in Chemical Research in Toxicology (2018) 31: 658-665 31

4.1. Introduction

Nickel oxide (NiO) nanoparticles (NPs) have been the object of a renewed interest due to their multiple applications, such as catalysts, cathode materials for alkaline batteries, diesel–fuel additives, materials for gas or temperature sensors, electronic components and pigments for ceramics and glass (EPRUI, 2017).

One of the main mechanisms associated with metal oxide NPs toxicity consists of the generation of extracellular and/or intracellular reactive oxygen species (ROS), leading to the oxidative damage of the cells (Manke et al., 2013). ROS comprises a broad category of chemical species, such as singlet oxygen ($^1O_2$), superoxide anion radical ($O_2^{\cdot -}$), hydroxyl radical ($HO^{\cdot}$), peroxyl radical ($ROO^{\cdot}$) and hydrogen peroxide (H_2O_2) (Bartosz, 2009). ROS can originate in the endoplasmic reticulum (through the formation of H_2O_2 and $O_2^{\cdot -}$ during protein folding) (Perrone et al., 2008), in peroxisomes (due to the production of H_2O_2 during fat acids oxidation) (Herrero et al., 2008) and in the mitochondria (through generation of $O_2^{\cdot -}$ and H_2O_2 in respiratory chain) (Barros et al., 2004; Guidot et al., 1993). ROS can be found in the cytosol as consequence of the escape of H_2O_2 from the endoplasmic reticulum and mitochondria (Perrone et al., 2008).

Yeast cells are equipped with an elaborate antioxidant defence mechanism to cope with oxidative stress (OS) and thus to maintain intracellular redox equilibrium. This mechanism includes antioxidant molecules, such as reduced glutathione (GSH) and enzymes (Jamieson, 1998). The yeast *S. cerevisiae* displays two superoxide dismutases (SOD) enzymes, which catalyse the dismutation of $O_2^{\cdot -}$ to H_2O_2; *SOD1* encodes a Cu/ZnSOD, which localizes to the cytosol, mitochondrial intermembrane space and nucleus; *SOD2* encodes a MnSOD present in the mitochondrial matrix. *S. cerevisiae* also displays two catalases (Cat), which reduce H_2O_2: Cat T, which localizes to the cytosol, and Cat A, which localizes to peroxisomes. In addition, yeast cells also possess peroxidases, which reduce inorganic and organic peroxides into the corresponding alcohols using cysteine thiols. Two classes of peroxidases were found: a) glutathione peroxidases, which employ GSH, such as Gpx3 (located at mitochondrial intermembrane space and peroxisomal matrix) and Grx1 (glutaredoxin, located at cytosol and nucleus); b) thioredoxin peroxidases (also called peroxiredoxins), which employ thioredoxin, such as the cytosolic Tsa1 and the mitochondrial Prx1 (Herrero et al., 2008).

When the level of ROS overcomes the defence system, the cell redox homeostasis is altered, resulting in OS, which can cause the damage of a wide range of molecules, such as unsaturated lipids via peroxidation, proteins via oxidation and DNA, leading to reduced cell viability (Avery, 2011). Oxidative

stress plays an important role in many human diseases, including diabetes, cancer and neurodegenerative diseases, such as Parkinson's and Alzheimer's disease (Farrugia and Balzan, 2012). Several studies have reported that NiO NPs induce OS in different cell models. In this context, it has been described that rats exposed to NiO NPs show pulmonary OS (Horie et al., 2012; Horie et al., 2016). Exposure to NiO NPs has been shown to induce intracellular accumulation of ROS in multiple human cell lines, such as liver (HepG2) (Ahamed et al., 2013), alveolar basal epithelial (A549) (Ahamed, 2011; Horie et al., 2011; Lu et al., 2015), airway epithelial (HEp-2) and breast cancer (MCF-7) cells (Siddiqui et al., 2012). Similarly, exposing the aquatic plant *Lemna gibba* L. (Oukarroum et al., 2015) and the barley *Hordeum vulgare* L. (Soares et al., 2016) to NiO NPs induce cellular OS.

The yeast *Saccharomyces cerevisiae* has been used as cell model in toxicological evaluations of chemicals. Yeast-based functional genomics and proteomics technologies, which include the use of the yeast deletion strain collection, are important tools for the elucidation of toxicity mechanisms (Dos Santos et al., 2012). The easy manipulation of mitochondrial respiration, namely, by the loss of mitochondrial DNA (Altmann et al., 2007), makes this simple cell model particularly attractive for investigating the role of mitochondria in ROS generation. A previous study showed that the exposure of the yeast *S. cerevisiae* to NiO NPs inhibited proliferation capacity, reduced metabolic activity and enhanced accumulation of ROS (please see Chapter 3).

The present Chapter aimed to further elucidate the role of ROS generation in the toxic effects of NiO NPs on the yeast *S. cerevisiae*. Additionally, we sought to determine the mechanism through which NiO NPs generate ROS in yeast cells. This was achieved by investigating the link between ROS production and the loss of cell viability induced by NiO NPs. OS was assessed by measuring both exogenous (acellular, abiotic, cell free) and intracellular ROS generated NPs induced. The different types of ROS produced by exposure to NiO were characterized using fluorescent probes. The involvement of mitochondria as a source of ROS was examined. The role of non-enzymatic (GSH) and enzymatic defences (using yeast deletion strain collection) in the fight against OS induced by NiO NPs was also investigated.

4.2. Materials and Methods

4.2.1. Preparation of nickel oxide nanoparticles stock suspensions

The NiO NPs preparation and characterization were previously described in Chapter 3.

4.2.2. Yeast strains, media and growth conditions

The *Saccharomyces cerevisiae* strains used in this study are listed in Table 4.1. Wild type (BY4741) and single gene deletion strains were purchased from EUROSCARF collection (Frankfurt, Germany). The isogenic derivative ρ^0 strain (BY4741- ρ^0) was obtained as previously described (Sousa and Soares, 2014).

The strains were maintained at 4 °C on YEP agar slants [5 g/L yeast extract (Difco-BD), 5 g/L peptone (Difco-BD), 10 g/L glucose (Merck) and 15 g/L agar (Merck)]. Single-gene deletion mutant strains were maintained on YEP agar with 200 mg/L Geneticin (G418 disulfate salt, Sigma-Aldrich). The pre-cultures and cultures were obtained as described in Chapter 3.

Table 4.1. List of S. cerevisiae strains used in this chapter.

Reference	Strain	Genotype	Comment
BY4741	Wild type (WT)	MAT*α*; *his3*Δ1; *leu2*Δ0; *met15*Δ0; *ura3*Δ0	control strain
Y07097	*gsh1*Δ	BY4741; *YJL101c::kanMX4*	without L-γ-glutamylcysteine synthetase
Y01740	*gsh2*Δ	BY4741; *YOL049w::kanMX4*	without glutathione synthetase
Y06913	*sod1*Δ	BY4741; *YJR104c::kanMX4*	without copper-zinc superoxide dismutase
Y06605	*sod2*Δ	BY4741; *YHR008c::kanMX4*	without manganese-superoxide dismutase
Y04718	*ctt1*Δ	BY4741; *YGR0088w::kanMX4*	without catalase T
Y03615	*cta1*Δ	BY4741; *YDR256c::kanMX4*	without catalase A
Y05972	*gpx3*Δ	BY4741; *YIR037w::kanMX4*	without glutathione peroxidase
Y06681	*grx1*Δ	BY4741; *YCL035c::kanMX4*	without glutaredoxin
Y00545	*tsa1*Δ	BY4741; *YML028w::kanMX4*	without thioredoxin peroxidase
Y03090	*prx1*Δ	BY4741; *YBL064C::kanMX4*	without peroxiredoxin
	ρ^0	MAT*α*; *his3*Δ1; *leu2*Δ0; *met15*Δ0; *ura3*Δ0; *rho*^{0}	without mtDNA

4.2.3. Treatment of yeast cells with NiO NPs

Yeast cells in exponential phase of growth were centrifuged (2.500x*g*, 5 min), washed twice and re-suspended in deionized water. Then, cells were suspended ($1x10^7$ cells/mL) in 10 mmol/L MES buffer (Sigma-Aldrich), pH 6.0 with 20 g/L glucose and incubated with 50 or 100 mg/L NiO NPs, at 30ºC, 150 rpm, for 6 h. Yeast cells were also suspended in MES buffer without NiO NPs (control).

The effect of two antioxidants, L-ascorbic acid (AA) or *N-tert*-butyl-α-phenylnitrone (PBN) on the quenching of ROS NiO NPs induced was tested. AA efficiently scavenges free radicals and other ROS produced in cell since it reacts rapidly by donating a hydrogen atom to an oxidizing radical (Arrigoni and De Tullio, 2002; Nimse and Palb, 2015). PBN is a free radical spin trapping agent, which reacts covalently with radicals and form stable adducts (Xu et al., 2012). For this purpose, yeast cells were pre-incubated with 10 mmol/L AA (Merck) or 2 mmol/L PBN (Sigma-Aldrich) 30 min before the exposure to NiO NPs.

For exposure of yeast cells to NiO NPs under nitrogen atmosphere during 6 h, yeast cells were pre-incubated in 20 mL MES buffer in wash bottles under flow of pure N_2 (less than 2 mg/L of O_2; Linde) at 100 mL/min, 30 min before the exposure to NiO NPs. During cell exposure to NiO NPs, the flow of N_2 was also maintained.

4.2.4. Cell viability assay

The toxic impact of NiO NPs on the yeast cells was evaluated by a cell viability assay. Yeast cells were incubated in MES buffer without (control) or with NiO NPs and subsequently plated on YEP agar, as described in Chapter 3. As toxicity end point, the viability was calculated considering the number of colony-forming unit (CFU)/mL at zero time as reference (100 %).

4.2.5. Determination of reactive oxygen species (ROS)

The detection of $O_2^{\cdot -}$ was carried out using dihydroethidium (DHE). This compound is a cell permeant probe that can undergo oxidation by superoxide anion radical to form the DNA-binding compound ethidium. DHE allows a specific detection of $O_2^{\cdot -}$, since this probe is minimally oxidised by H_2O_2 (Benov et al., 1998). The H_2O_2 accumulated in yeast cells was monitored using the probes 2′,7′-dichlorodihydrofluorescein diacetate (H_2DCFDA) or dihydrorhodamine 123 (DHR123). H_2DCFDA is taken up by yeast cells, being metabolized by intracellular esterases to H_2DCF; in the presence of H_2O_2, H_2DCF is oxidized to DCF (Keston and Brandt, 1965). Other ROS, such as peroxyl radical ($ROO^{\cdot}$) and peroxynitrite anion ($ONOO^-$), are capable of undergo the oxidation of H_2DCF to DCF (Crow, 1997;

Wang and Joseph, 1999). In addition, the probe DHR123, which is a structurally related analogue of H_2DCFA but lacks the diacetate and dichloro substituents of H_2DCFDA (Crow, 1997), was also used. DHR123 is a cell permeant compound that is oxidized to rhodamine 123 by oxidants such as, H_2O_2, HOCl and $ONOO^-$ (Crow, 1997). Because H_2DCFDA and DHR123 can be oxidized by different ROS, these probes can be used as general redox sensors in the assessment of cellular oxidative stress (Tarpey et al., 2004). All compounds were purchased from Sigma-Aldrich. Yeast cells were suspended in MES buffer, with 2% (w/v) glucose, at a final concentration of $1x10^7$ cells/mL, and incubated at 30ºC for 10 minutes, in the dark, with 8 µmol/L DHE or with 20 µmol/L H_2DCFDA or with 2.88 µmol/L DHR123. Subsequently, cells were treated with NiO NPs (50 or 100 mg/L) and placed in a 96-well flat microplate (Orange Scientific). As control, cells were incubated in the same conditions in the absence of NPs. Fluorescence intensity, as relative fluorescence units (RFU), was measured in a PerkinElmer (Victor3) microplate reader at a fluorescence excitation wavelength of 485/14 nm and an emission of 535/25 nm (H_2DCFDA and DHR123) or at a fluorescence excitation of 485/14 nm and an emission of 620/8 nm (DHE).

ROS production by NiO NPs or Ni^{2+} in MES buffer (abiotic ROS) was evaluated using H_2DCF. H_2DCFDA was deacetylated to H_2DCF as previously described (Aruoja et al., 2015). NiO NPs (100 mg/L) or Ni^{2+} (79 mg/L; from a 1000 mg/L $NiCl_2$ stock solution, Merck) were incubated in MES buffer in the same conditions of the assays with yeast cells. After 6h of incubation, samples of 100 µL (NiO NPs or Ni^{2+}, in MES buffer) were taken, combined with 100 µL of 52 µmol/L H_2DCF solution, placed in quadruplicate in a 96-well flat microplate and incubated at room temperature, in the dark, for 45 minutes. Blank and positive control were prepared by replacing the sample by equal volume of MES or 26 µmol/L H_2O_2 (prepared in MES buffer), respectively. Fluorescence was quantified as described above for H_2DCFDA. Abiotic ROS was expressed as the ratio of fluorescence of the assay/fluorescence of the blank.

4.2.6. Assessment of intracellular reduced glutathione

Intracellular reduced glutathione (GSH) was estimated with monochlorobimane (mBCl, Sigma-Aldrich). mBCl is a cell permeant nonfluorescent probe; once inside the cell, mBCl reacts with reduced glutathione and forms fluorescent bimane-glutathione (B-SG) adducts (Haugland, 2005). Cells were stained as previously described (Perez et al., 2013). Briefly, yeast cells were exposed to NiO NPs, as described above, for 6 h and then were harvested by centrifugation, re-suspended at $1x10^7$ cells/mL, in 0.1 mol/L phosphate buffered saline solution (PBS buffer), at pH 7.0, and incubated with 50 µmol/L

mBCl, for 2 h, at 30 ºC, in the dark. Fluorescence intensity was measured using a microplate reader at fluorescence excitation of 355/40 nm and an emission of 460/25 nm.

4.2.7. Epifluorescence microscopy

Samples were observed using a Leica DLMB epifluorescence microscope equipped with an HBO 100 mercury lamp and appropriate filter setting (A for GSH; GFP for H_2DCFDA or DHR123 and N2.1 for DHE) from Leica. The images were captured with a Leica DC 300 F camera using a 100x oil immersion N plan objective and processed using Leica IM 50-Image manager software.

4.2.8. Reproducibility of the results and statistical analysis

The data reported are presented as mean values ± standard deviations (SD) from at least three independent experiments performed in duplicate ($n \geq 6$). In fluorescence experiments, it is presented a typical example of an experiment performed at least three times; each data represents the mean (± SD) of four fluorescent readings. The means values were subjected to one-way ANOVA followed by Tukey–Kramer multiple comparison method. Alternatively, differences between control and treated cells were tested using unpaired *t* test. In all experiments, *P* values <0.05 were considered statistically significant.

4.3. Results

4.3.1. Evaluation of the possible pro-oxidant effect of NiO NPs

The previous chapter demonstrated that NiO NPs induced cytotoxicity, which was accompanied by an intracellular accumulation of ROS (see Chapter 3). To investigate whether the ROS measured had an exogenous source or whether it was generated intracellularly, we evaluated the ability of NiO NPs to induce ROS production in abiotic conditions (cell free). Therefore, an assay was conducted in MES buffer, in the same conditions of yeast exposure to NiO NPs, but without yeast cells. ROS was detected using the general redox sensor 2',7'-dichlorodihydrofluorescein diacetate (H_2DFCDA) deacetylated (H_2DCF) (Tarpey et al., 2004; von Moos et al., 2016). Since metal oxide NPs can trigger ROS production through the solubilization of the metal of the NPs, the ability of 79 mg/L Ni^{2+} to induce ROS was also tested. This Ni^{2+} concentration corresponded to the total Ni^{2+} present in 100 mg/L NiO NPs; in other words, this Ni^{2+} concentration was calculated assuming the complete dissolution of 100 mg/L NiO NPs. The functionality of the H_2DCF was tested using 26 µmol/L H_2O_2 as a positive control. As can be observed in Figure 4.1, neither 100 mg/L NiO NPs nor 79 mg/L Ni^{2+} was able to generate ROS above

background readings. These results indicate that the ROS accumulated in yeast cells exposed to NiO NPs (Fig 4.2A) were intracellularly generated.

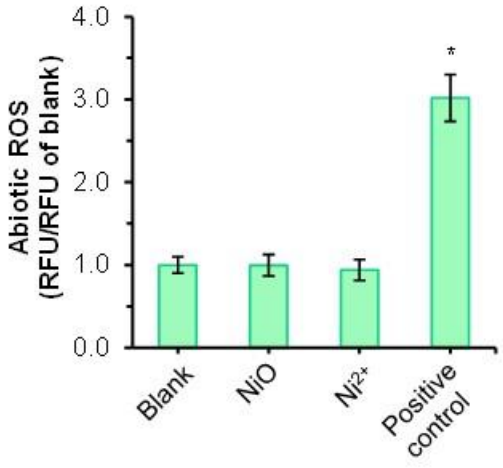

Figure 4.1. Possible pro-oxidant effect of NiO NPs and Ni^{2+}. NiO at 100 mg/L and Ni^{2+} at 79 mg/L were incubated with H_2DFC in MES buffer, for 6 h, in the dark. Blank and positive control were obtained by incubating the H_2DCF probe in MES buffer or with 26 µmol/L H_2O_2, respectively. This is a typical example of an experiment performed three times; the data represent the mean (± SD) of four fluorescent readings. Mean value with asterisk is significantly different: *P<0.05 in comparison with control; unpaired t test.

4.3.2. Antioxidants prevent the toxicity induced by NiO NPs

To determine whether there is a link between the induction of oxidative stress (OS) and the loss of cell viability, yeast cells were exposed to NiO NPs in the absence or the presence of a natural (L-ascorbic acid, AA) or a synthetic (*N-tert*-butyl-α-phenylnitrone, PBN) antioxidant (Arrigoni and De Tullio, 2002; Nimse and Palb, 2015; Xu et al., 2012). For the concentrations used in this Chapter, AA and PBN were not toxic to the cells (Fig 4.2B). It was found that the co-exposure of yeast cells to 100 mg/L NiO NPs and AA or PBN at 10 or 2 mmol/L, respectively, prevented the intracellular accumulation of ROS induced by NiO (Fig 4.2A). In addition, the presence of AA or PBN significantly restored the survival of yeast cells exposed to 100 mg/L NiO NPs (Fig 4.2B). These results support the hypothesis that the increase of intracellular ROS levels is the main cause of decreased yeast viability following treatment with NiO NPs.

4.3.3. Characterization and monitoring of intracellular ROS accumulation

Intracellular ROS induced by NPs were characterized using the following ROS sensitive probes: dihydroethidium (DHE), 2′,7′-dichlorodihydrofluorescein diacetate (H_2DCFDA) and dihydrorhodamine

123 (DHR123). DHE was used to detect superoxide anion radicals since this probe is oxidized by $O_2^{\cdot-}$ with high specificity (Benov et al., 1998). Cells exposed to NiO NPs exhibited a red fluorescence, which reflected the intracellular accumulation of $O_2^{\cdot-}$ (Fig 4.3A). Although H_2DCFDA and DHR123 can be used to monitor a broad range of ROS, they are mostly used to detect H_2O_2 (Tarpey et al., 2004). As seen in Figure 4.3A, cells incubated with NPs and stained with H_2DCFDA or DHR123 displayed a green fluorescence, which indicates the intracellular accumulation of H_2O_2.

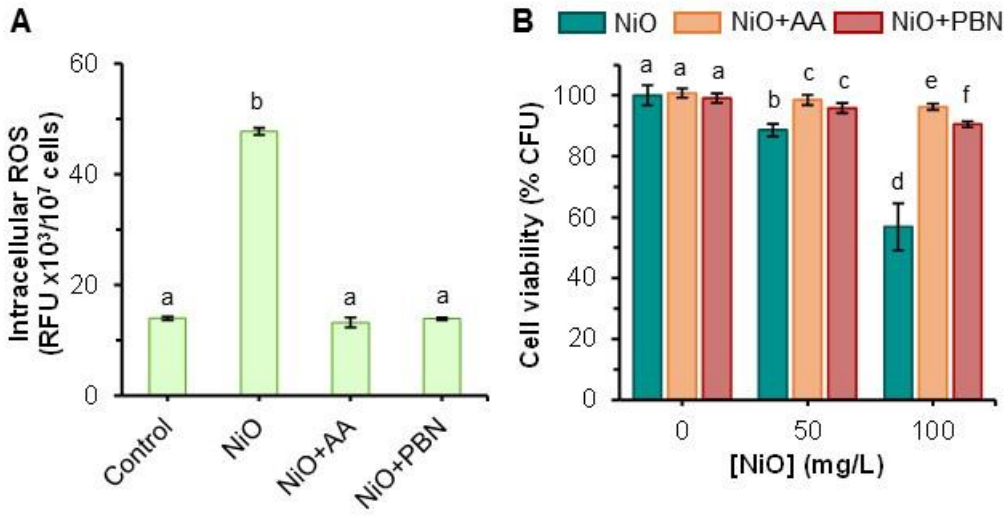

Figure 4.2. Impact of antioxidants on the yeast *S. cerevisiae* exposed to NiO NPs. Cells were exposed up to 100 mg/L NiO in MES buffer, with 20 g/L glucose, for 6 h, in the absence of an antioxidant (NiO) or co-exposed to 10 mmol/L L-ascorbic acid (NiO+AA) or 2 mmol/L N-tert-butyl-α-phenylnitrone (NiO+PBN). A – Levels of intracellular ROS quantified using H_2DCFDA. NiO concentration: 100 mg/L; control: cells incubated in MES buffer in the absence of antioxidants and NiO NPs. This is a typical example of an experiment performed three times; each bar represents the mean of four fluorescent readings. B – Cell viability assessed by colony-forming units (CFU) counting on YEP agar. The data represent the mean (± SD) of three independent experiments. Standard deviations (SD) are presented (vertical error bars). Means with different letters are significantly different ($P<0.05$; ANOVA).

Using a kinetic approach with the fluorescent probes described above, it was possible to monitor the evolution of ROS generated in yeast cells, induced by NiO NPs. As seen in Figure 4.3B, a significant increase of $O_2^{\cdot-}$ and H_2O_2 was observed in yeast cells after 2 h of incubation with NiO NPs, compared to control (non-treated cells). After 6 h of exposure to NiO NPs, a significant increase of both red and green fluorescence signal in cells treated with NiO NPs was observed, indicating high levels of $O_2^{\cdot-}$ and H_2O_2 compared to untreated cells (Fig 4.3B). The intracellular $O_2^{\cdot-}$ and H_2O_2 levels in cells exposed to NiO NPs, increased with time in a concentration dependent manner, but not linearly (Fig 4.3B).

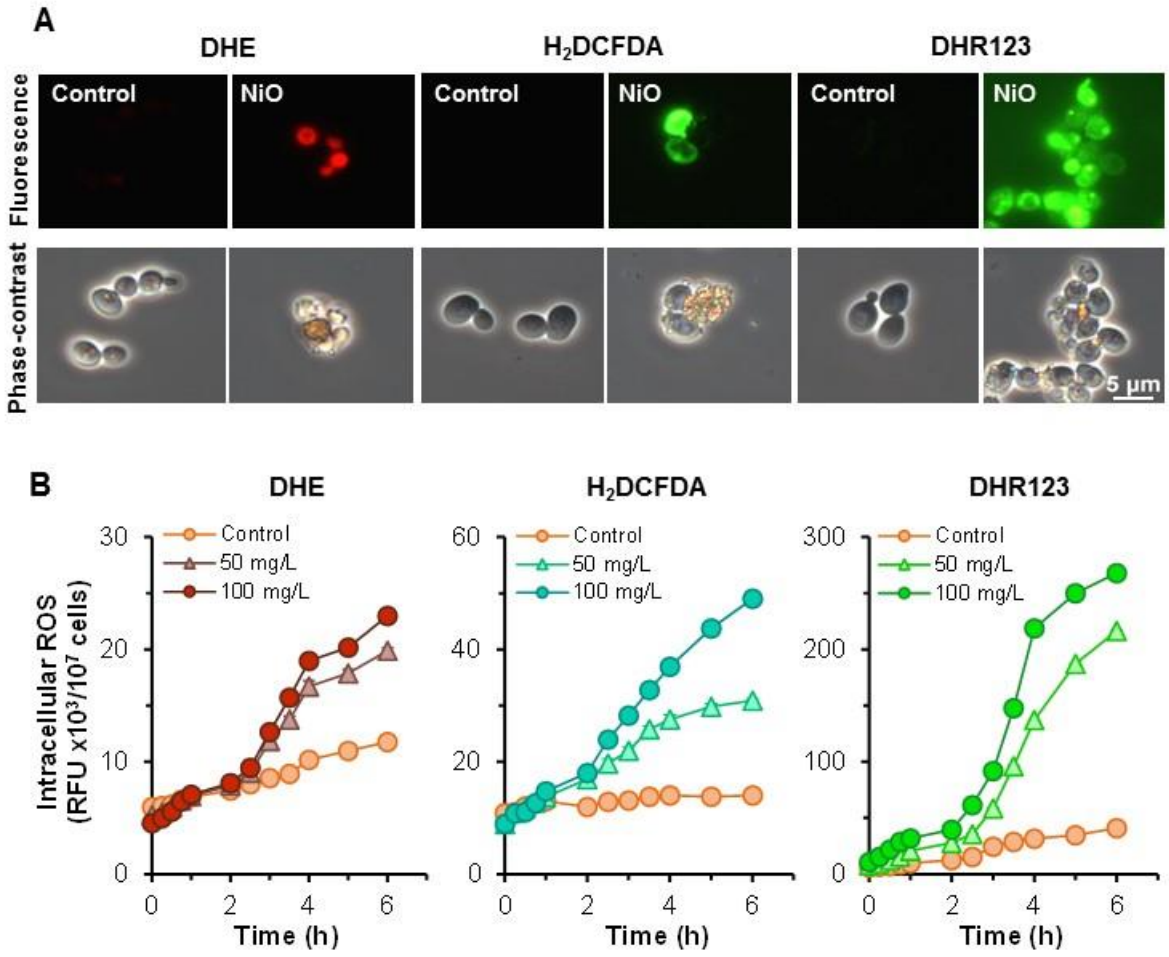

Figure 4.3. NiO NPs induce high intracellular $O_2^{\cdot-}$ and H_2O_2 levels in *S. cerevisiae*. A – Visualization by fluorescence microscopy of intracellular accumulation of $O_2^{\cdot-}$ (using DHE probe) or H_2O_2 (using H_2DCFDA and DHR123 probes). Yeast cells were incubated for 6h in the absence (control) or presence of 100 mg/L NiO NPs. B – Kinetics of intracellular ROS generation evaluated using DHE, H_2DCFDA and DHR123, respectively. This is a typical example of an experiment performed at least three times. The data represent the mean of four fluorescent readings. Standard deviations (SD) are presented (vertical error bars); where no error bars are shown, SD are within the points.

4.3.4. The isogenic derivative ρ^0 strain displays reduced levels of ROS

The results described above prompted us to investigate the origin of intracellular ROS in yeast cells exposed to NiO NPs. In normal cells, 1-2% of the electrons from the electron respiratory chain "leak" from this pathway and originate $O_2^{\cdot-}$ during respiration (Eruslanov and Kusmartsev, 2010). Considering that in the yeast *S. cerevisiae*, the respiration can be completely abolished through the loss of mtDNA (Evans, 1983), a WT isogenic derivative ρ^0 strain was used to unveil unknown aspects about the role of mitochondria in the intracellular accumulation of ROS induced by NiO. As seen in Figure 4.4A, the ρ^0 strain was exposed for 6 h to up to 100 mg/L of NiO NPs, but no intracellular accumulation of $O_2^{\cdot-}$ (evaluated using DHE) was detected. This result suggests that mitochondria are an important source

of $O_2^{\cdot -}$. It is likely that the $O_2^{\cdot -}$ formed in the WT strain exposed to NPs was dismuted by the superoxide dismutase (MnSOD), present in the mitochondrial lumen, generating H_2O_2, which then accumulated in the mitochondria or diffused into the cytosol. Thus, the $O_2^{\cdot -}$ could be an important source of H_2O_2. Accordingly, it is expected that the reduction of $O_2^{\cdot -}$ levels will lead to a decrease in H_2O_2 amount. Consistent with this possibility, a very low level of H_2O_2 in the ρ^0 strain (without detectable levels of $O_2^{\cdot -}$) was detected compared to the WT strain (Fig 4.4B and C).

Cell viability was enhanced in the ρ^0 strain compared to the WT strain (Fig 4.4D), which reinforces the role of ROS in the toxicity induced by NiO NPs.

4.3.5. Anoxic atmosphere protects against the toxicity of NiO NPs

To further confirm the mitochondrial origin of OS, the intracellular levels of ROS were compared in yeast cells incubated with NiO NPs in normal atmosphere (21% O_2) and in the absence of oxygen (N_2 atmosphere). The levels of intracellular ROS in yeast cells incubated with 100 mg/L NiO NPs in N_2 atmosphere were not significantly different from control (cells not exposed to NiO NPs) (Fig 4.4E). This indicates that the atmosphere of pure N_2 protected the yeast cells from OS. This protection was confirmed by an increase in viability in cells incubated with 100 mg/L NiO NPs and in N_2 atmosphere compared to cells exposed to NPs in normal (O_2) atmosphere (Fig 4.4F). These data all together confirm that mitochondria are an important origin of OS induced by NiO NPs.

4.3.6. NiO NPs decrease intracellular levels of GSH

Reduced glutathione (GSH) is the major intracellular redox buffer, acting as the first line of cellular defence against oxidative injury (Winther and Jakob, 2013). To obtain further insights into the role of OS in NiO NP toxicity, the intracellular levels of GSH were compared in cells incubated in the absence (control) or the presence of NPs. Staining yeast cells with monochlorobimane, which exhibits a high sensitivity to GSH (Perez et al., 2013), showed that nontreated cells displayed a typical blue fluorescence due to the formation of bimane-glutathione adducts. Cells incubated with NiO NPs displayed a faint fluorescence (Fig 4.5A). These observations suggest a reduction of intracellular levels of GSH in yeast cells exposed to NiO NPs. The quantification of fluorescence signal showed a significant decrease in cells treated with NiO NPs compared to the control (Fig 4.5B), which confirms the microscopic observations.

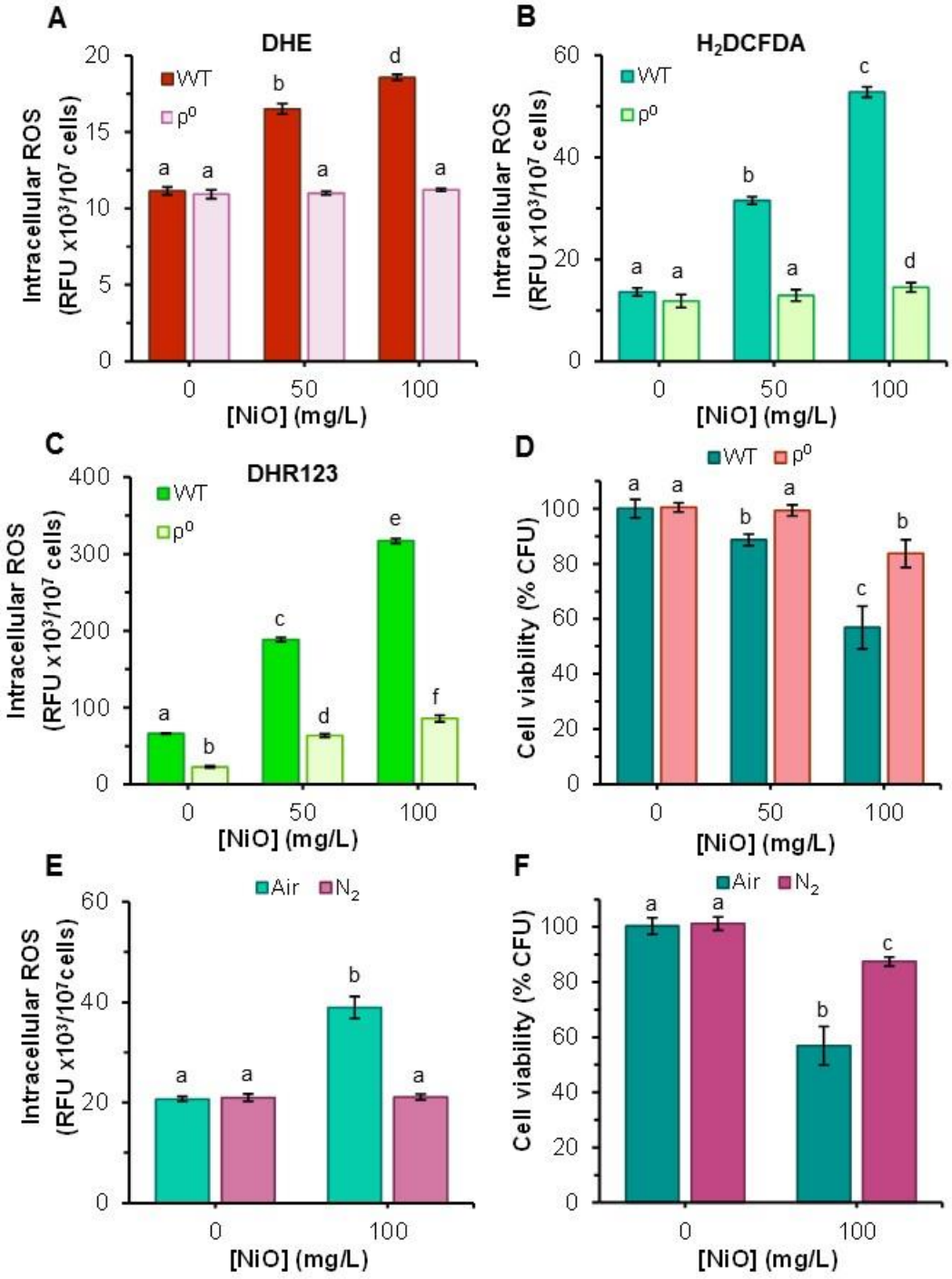

Figure 4.4. Role of mitochondria in the production of ROS induced by NiO NPs. A-D - Comparison of the effects caused by NiO NPs on *S. cerevisiae* BY4741 wild-type (WT) and the respective isogenic ρ^0 mutant. A – Levels of $O_2^{\cdot-}$ detected using DHE. B, C – Levels of H_2O_2 detected with H_2DCFDA and DHR123, respectively. D – Cell viability, evaluated by CFU counting on YEP agar. E and F – Influence of the atmosphere on WT cells exposed to NiO NPs. WT cells were incubated under normal (air) or nitrogen (N_2) atmosphere. E – Levels of ROS detected with H_2DCFDA. F – Cell viability, evaluated by CFU counting on YEP agar. A, B, C and E are typical examples of an experiment performed three times. The data represent the mean of four fluorescent readings. D, F – represent the mean of three independent experiments. Standard deviations (SD) are presented (vertical error bars). Means with different letters are significantly different ($P<0.05$; ANOVA).

4.3.7. Glutathione-deficient mutants display increased susceptibility to NiO NPs

The role of GSH in NiO NPs-induced OS was also examined using the knockout mutants *gsh1*Δ and *gsh2*Δ, which lack either *GSH1* or *GSH2*, the genes responsible for the enzymes L-γ-glutamylcysteine synthetase and γ-glutamylcysteine, respectively (Grant, 2001). The *gsh1*Δ and *gsh2*Δ strains, without and with a reduced level of GSH, respectively, displayed an increased sensitivity to NiO NPs (Fig 4.5C) compared to WT. These results led us to verify if these mutants underlie augmented OS.

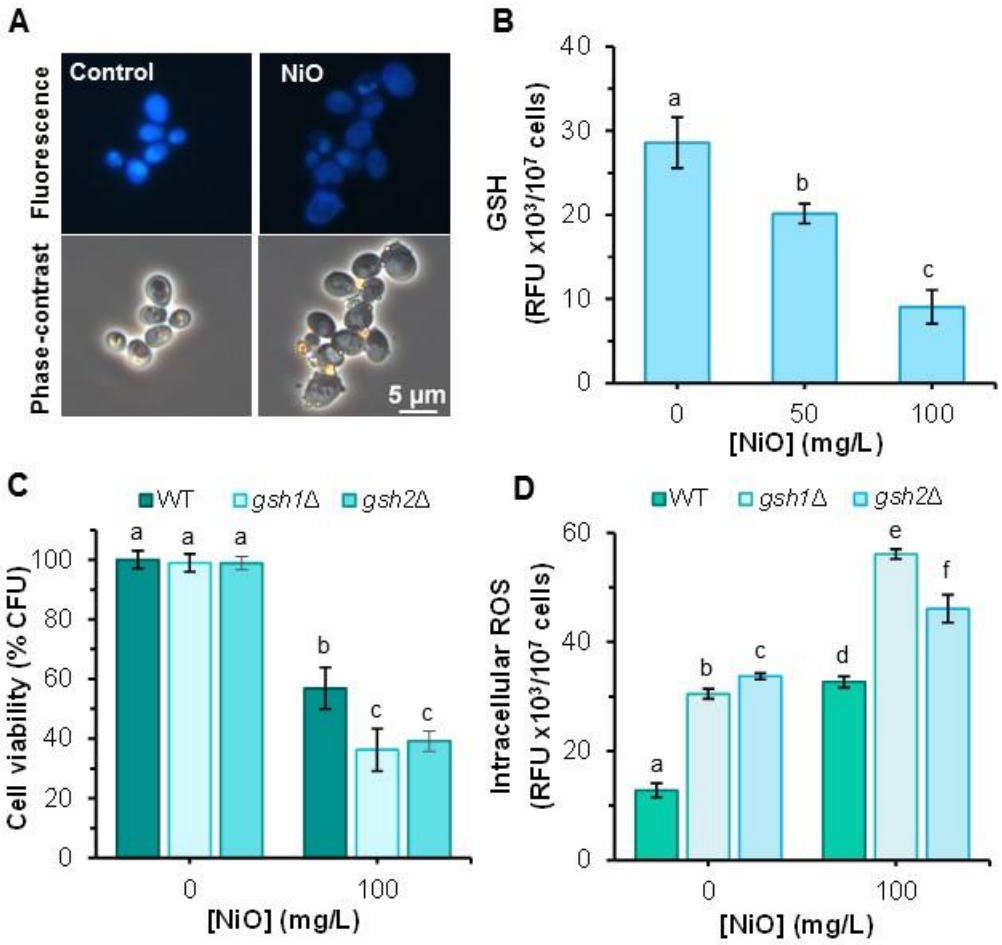

Figure 4.5. Involvement of the reduced glutathione (GSH) in the protection against the toxicity of NiO NPs. Yeast strains, in the absence (control) or presence of NiO NPs, were incubated in MES buffer for 6h. A – Photomicrographs obtained by fluorescence and phase-contrast microscopy of *S. cerevisiae* BY4741 cells incubated in the absence or presence of 100 mg/L NiO NPs. After incubation, cells were stained with mBCl. Cells non-exposed to NiO exhibited blue fluorescence (formation of bimane-glutathione conjugates), which was absent in cells exposed to NiO NPs. B – Intracellular level of GSH in *S. cerevisiae* BY4741, estimated by measuring the fluorescence signal after staining with mBCl. C – Cell viability of *S. cerevisiae* BY4741 wild-type (WT) and the isogenic GSH-deficient mutant strains *gsh1*Δ and *gsh2*Δ. Cell viability was evaluated by CFU counting on YEP agar. The data represent the mean (± SD) of three independent experiments. D – Intracellular levels of ROS detected with H_2DCFDA. Experiments of fluorescence measurements (B and D) are typical examples of an experiment performed three times. The data represent the mean (± SD) of four fluorescent readings. Means with different letters are significantly different ($P<0.05$; ANOVA).

As seen in Figure 4.5D, the *gsh1*Δ and *gsh2*Δ strains displayed an increased level of ROS compared to WT strain, even in the absence of the NPs. Both the *gsh1*Δ and *gsh2*Δ strains presented a significant increase in ROS generation when exposed to NiO NPs, compared to the WT strain (Fig 4.5D). This may explain the reduction in cell viability observed in these mutants (Fig 4.5C).

4.3.8. Single-gene mutants devoid in enzymatic defences do not display increased susceptibility to NiO NPs

To evaluate the role of different antioxidant enzymes, single-gene mutants deficient in the main enzymes associated with the defence against OS (Sod1p, Sod2p, Ctt1p, Cta1p, Gpx3p, Grx1p, Tsa1p and Pprx1p) were exposed to 100 mg/L NiO for 6 h. Surprisingly, the single-gene mutants *sod1*Δ, *sod2*Δ and *ctt1*Δ were more resistant to 100 mg/L NiO NPs than the WT strain (Fig 4.6). The susceptibility of the mutants *cta1*Δ, *gpx3*Δ, *grx1*Δ, *tsa1*Δ and *prx1*Δ to 100 mg/L NiO NPs were not significantly different from the WT strain (Fig 4.6).

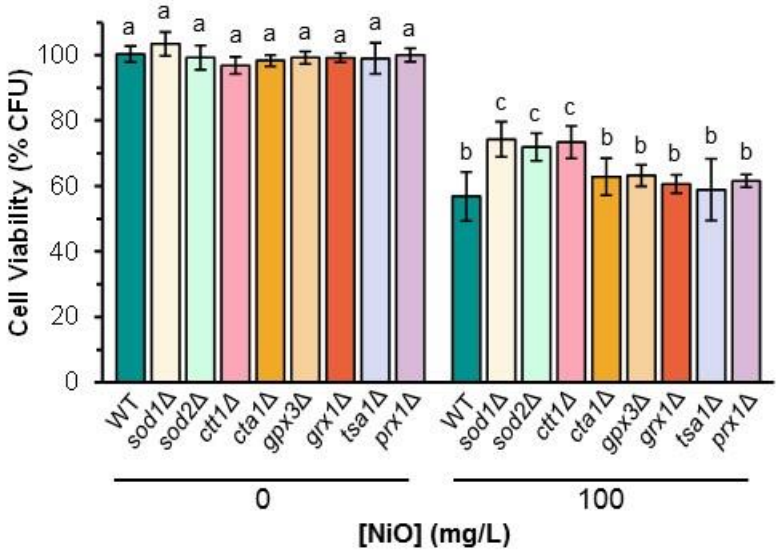

Figure 4.6. Susceptibility of *S. cerevisiae* BY4741 and the isogenic mutant strains lacking enzymatic defences against oxidative stress to NiO NPs. Cell viability of *S. cerevisiae* BY4741 wild-type (WT), and mutants was evaluated by CFU counting on YEP agar. The data represent the mean (± SD) of three independent experiments. Means with different letters are significantly different ($P<0.05$; ANOVA).

4.4. Discussion

NiO NPs are almost insoluble in MES buffer, being only a low amount of Ni^{2+} released by the NPs (see Chapter 3). In the previous Chapter, it was proposed that the toxic effects induced by NiO NPs are

mainly produced by the NPs themselves, by an indirect mechanism: NPs adsorb to the yeast cell wall and enhance the release of Ni^{2+} at the NP-yeast cell wall interface, leading to an activation of toxic responses.

OS constitutes one of the main mechanisms of the toxicity of metal oxide nanoparticles (Nel et al., 2006). Nevertheless, the underlying mechanisms associated with OS induced by NiO NPs are not understood. The present study shows that neither NiO NPs nor Ni^{2+} is able to induce abiotic extracellular ROS (Fig 4.1); these findings are compatible with the fact that Ni^{2+} is not considered a catalyst of the Haber-Weiss reaction since it is a redox-inactive metal (Avery, 2001). These results also indicate that the ROS accumulated in yeast cells upon exposure to NiO NPs were intracellularly generated (Fig 4.2A). Our results confirm the ability of NiO NPs to induce intracellular ROS production, as described in works with different cell lines such as A549, Hep-2, MCF-7and HepG2 (Ahamed et al., 2013; Horie et al., 2011; Siddiqui et al., 2012). This result is consistent with our previous studies (please see Chapter 3), in which we found that NiO NPs exert a toxic effect on *S. cerevisiae* by an indirect mechanism. The impact of NiO NPs on the redox status of yeast cells was characterized using three oxidant-sensitive fluorescent probes: DHE, H_2DCFDA and DHR123. Using these probes, it was possible to identify the presence of $O_2^{\cdot -}$ and H_2O_2 in yeast cells exposed to NiO NPs (Fig 4.3). It was also shown that the use of AA (a scavenger of free radicals) or PBN (a spin trapping agent) abrogates intracellular ROS accumulation induced by NiO NPs and significantly restored yeast viability (Fig 4.2B). Taking together, these results strongly suggest that the loss of cell viability induced by NiO NPs can be likely attributed to ROS generation.

We also show here that yeast cells without components of the respiratory chain (ρ^0 strain) did not accumulated detectable levels of $O_2^{\cdot -}$ and possessed low levels of H_2O_2, compared to the WT strain (4.4A, B and C). Although $O_2^{\cdot -}$ itself is not very reactive to biomolecules (Dawes, 2004), it can be the source of the generation of more powerful ROS, such as H_2O_2. We hypothesize that during respiration, the leakage of electrons from the mitochondrial respiratory chain is the primary source of $O_2^{\cdot -}$ and, in turn, $O_2^{\cdot -}$ are most likely the main origin of H_2O_2. Consistent with this possibility, we found that the treatment of yeast cells with a free radical spin trapping agent (PBN) strongly reduces the level of H_2O_2 (Fig 4.2B). On the other hand, yeast cells exposed to NiO NPs in nitrogen atmosphere displayed low levels of ROS and an enhanced viability compared to the same cells incubated in normal atmosphere (Fig 4.4E and F). Together, these results strongly indicate that NiO induces the production of $O_2^{\cdot -}$ at the mitochondrial level, which seems to be an important source of the intracellular ROS observed. It has been shown that Ni^{2+} can interfere with iron homeostasis, displacing iron in redox-

active molecules (Arita et al., 2009; Hausinger, 1993; Ruotolo et al., 2008). *Complex I* and *III* of the mitochondrial electron transport chain (molecular complexes containing iron) (Voet et al., 1999) constitute one of the main sites at which electron leakage to oxygen occurs and is one of the main sites of production of $O_2^{\cdot-}$ (Dröse and Brandt, 2012). It can be hypothesized that the Ni^{2+} released from NiO NPs can inhibit or interfere with the electron transport at mitochondria by displacing iron from the electron transport chain of the inner mitochondrial membrane. Compatible with this possibility, it was found that nickel ions were able to induce intracellular ROS (see Chapter 3). The presence of iron can also enhance ROS formation through the Fenton reaction.

Oxidative stress occurs as a consequence of an imbalance between the ROS production and the action of antioxidant defence mechanisms. Here, we show that yeast cells exposed to NiO NPs displayed reduced levels of GSH compared with cells not exposed to NPs (Fig 4.5A, B). A similar result was described when different cell lines were exposed to NiO NPs (Abudayyak et al., 2017; Horie et al., 2011; Siddiqui et al., 2012). The depletion of the GSH levels can be associated with higher production of ROS. In other words, the decrease of the GSH content can be explained by its increased consumption by scavenging free oxygen radicals induced by the NPs. The reduction of GSH levels in yeast cells exposed to NiO can also be explained by the high affinity of Ni^{2+} to thiol containing molecules, such as GSH (Hausinger, 1993). The stable bond of Ni^{2+} to the cysteine residue of GSH induces the depletion of the pool of these molecules, reducing the cellular antioxidant defences. We also observed that *gsh1*Δ and *gsh2*Δ strains, without or with a reduced level of GSH, respectively, when exposed to NiO NPs, displayed reduced viability and enhanced accumulation of ROS compared to the WT strain (Fig 4.5C, D). Cumulatively, these results highlight the importance of GSH in the defence against NiO NPs-induced OS.

A correlation between NiO NPs concentration, loss of cell viability (Fig 4.2B), ROS generation (Fig 4.3) and GSH depletion (Fig 4.5B) were observed. This is likely because the OS induced by NiO NPs resulted from a combination of an increase in ROS production in the mitochondria (as result of the perturbation of respiratory chain) and the reduction of antioxidant cellular defences (as consequence of GSH depletion). This may be a possible mechanism of NiO NPs-induced loss of cell viability, mediated through OS, in *S. cerevisiae*.

A common response of yeast cells exposed to metal stress is the activation of the OS response. It has been described that antioxidative genes, such as *CTT1*, *GRX1*, *GRX2*, *GPX1*, *GTT2*, *TRX3* and *PRX1* (Hosiner et al., 2014; Kucukgoze et al., 2013; Takumi et al., 2010) are induced in *S. cerevisiae* following exposure to Ni^{2+}. Interestingly, single-gene mutant strains deficient in the main enzymes involved in

the defence against OS, namely, *sod1*Δ, *sod2*Δ, *ctt1*Δ, *cta1*Δ, *gpx3*Δ, *grx1*Δ, *tsa1*Δ and *prx1*Δ, were not more susceptible to NiO NPs than the WT strain (Fig 4.6). These results can be attributed to the fact that some genes, such as the genes associated with the defence against OS in yeast, do not confer a specific phenotype when deleted due to gene redundancy or the existence of compensatory parallel pathways (Dawes, 2004).

4.5. Conclusions

In this chapter, the mechanisms underlying the ROS generation induced by NiO NPs were elucidated. Thus:

- Cells of *S. cerevisiae* exposed to NiO NPs displayed intracellular accumulation of $O_2^{\cdot-}$ and H_2O_2;
- Mitochondria are an important source of ROS;
- Yeast cells exposed to NiO NPs displayed decreased levels of GSH.

References

Abudayyak, M., Guzel, E., Ozhan, G., 2017. Nickel oxide nanoparticles induce oxidative DNA damage and apoptosis in kidney cell line (NRK-52E). Biol. Trace Elem. Res. 178, 98-104

Ahamed, M., 2011. Toxic response of nickel nanoparticles in human lung epithelial A549 cells. Toxicol. in Vitro 25, 930-936

Ahamed, M., Ali, D., Alhadlaq, H.A., Akhtar, M.J., 2013. Nickel oxide nanoparticles exert cytotoxicity via oxidative stress and induce apoptotic response in human liver cells (HepG2). Chemosphere 93, 2514-2522

Altmann, K., Dürr, M., Westermann, B., 2007. *Saccharomyces cerevisiae* as a model organism to study mitochondrial biology: general considerations and basic procedures. Methods Mol. Biol. 372, 81-90

Arita, A., Zhou, X., Ellen, T.P., Liu, X., Bai, J., Rooney, J.P., Kurtz, A., Klein, C.B., Dai, W., Begley, T.J., Costa, M., 2009. A genome-wide deletion mutant screen identifies pathways affected by nickel sulfate in *Saccharomyces cerevisiae*. BMC Genomics 10, 1-33

Arrigoni, O., De Tullio, M.C., 2002. Ascorbic acid: much more than just an antioxidant. Biochim. Biophys. Acta 1569, 1-9

Aruoja, V., Pokhrel, S., Sihtmae, M., Mortimer, M., Madler, L., Kahru, A., 2015. Toxicity of 12 metal-based nanoparticles to algae, bacteria and protozoa. Environ. Sci. Nano 2, 630-644

Avery, S.V., 2001. Metal toxicity in yeasts and the role of oxidative stress. Adv. Appl. Microbiol. 49, 111-142.

Avery, S.V., 2011. Molecular targets of oxidative stress. Biochem. J. 434, 201-210

Barros, M.H., Bandy, B., Tahara, E.B., Kowaltowski, A.J., 2004. Higher respiratory activity decreases mitochondrial reactive oxygen release and increases life span in *Saccharomyces cerevisiae*. J. Biol. Chem. 279, 49883-49888

Bartosz, G., 2009. Reactive oxygen species: destroyers or messengers? Biochem. Pharmacol. 77, 1303-1315.

Benov, L., Sztejnberg, L., Fridovich, I., 1998. Critical evaluation of the use of hydroethidine as a measure of superoxide anion radical. Free Radic. Biol. Med. 25, 826-831

Crow, J.P., 1997. Dichlorodihydrofluorescein and dihydrorhodamine 123 are sensitive indicators of peroxynitrite in vitro: Implications for intracellular measurement of reactive nitrogen and oxygen species. Nitric Oxide-Biol. Ch. 1, 145-157

Dawes, I.W., 2004. Stress responses, in: Dickinson, J.R., Scweizer, M. (Eds.), The metabolism and moelcular physiology of *Saccharomyces cerevisiae*, 2nd Ed ed. Taylor and Francis, Ltd, London, pp. 376-439

Dos Santos, S.C., Teixeira, M.C., Cabrito, T.R., Sá-Correia, I., 2012. Yeast toxicogenomics: genome-wide responses to chemical stresses with impact in environmental health, pharmacology and biotechnology. Front. Genet. 3, 1-54

Dröse, S., Brandt, U., 2012. Molecular mechanisms of superoxide production by the mitochondrial respiratory chain, in: Kadenbach, B. (Ed.), Mitochondrial oxidative phosphorylation: nuclear-encoded genes, enzyme regulation, and pathophysiology. Springer New York, pp. 145-169

EPRUI, 2017. EPRUI - nanoparticles & microspheres, Nano nickel oxide, https://www.nanoparticles-microspheres.com/Products/Nano-Nickel-Oxide.html (acessed 13 September 2017)

Eruslanov, E., Kusmartsev, S., 2010. Identification of ROS using oxidized DCFDA and flow-cytometry. Methods Mol. Biol. 594, 57-72

Evans, I.H., 1983. Molecular genetic aspects of yeast mitochondria, in: Spencer, J.F.T., Spencer, D.M., Smith, A.R.W. (Eds.), Yeast genetics: fundamental and applied aspects. Springer, New York, pp. 269-370

Farrugia, G., Balzan, R., 2012. Oxidative stress and programmed cell death in yeast. Front. Oncol. 2, 1-21

Grant, C.M., 2001. Role of the glutathione/glutaredoxin and thioredoxin systems in yeast growth and response to stress conditions. Mol. Microbiol. 39, 533-541

Guidot, D.M., McCord, J.M., Wright, R.M., Repine, J.E., 1993. Absence of electron-transport (Rho(0) state) restores growth of a manganese-superoxide dismutase-deficient *Saccharomyces cerevisiae* in hyperoxia - evidence for electron-transport as a major source of superoxide generation in vivo. . J. Biol. Chem. 268, 26699-26703

Haugland, R.P., 2005. The handbook: a guide to fluorescent probes and labeling technologies, 10th ed. Invitrogen Corp., Eugene

Hausinger, R.P., 1993. Biochemistry of nickel, in: Hausinger, R.P. (Ed.), Microbial nickel metabolism. Springer, New York, pp. 181-201

Herrero, E., Ros, J., Belli, G., Cabiscol, E., 2008. Redox control and oxidative stress in yeast cells. Biochim. Biophys. Acta 1780, 1217-1235

Horie, M., Fukui, H., Endoh, S., Maru, J., Miyauchi, A., Shichiri, M., Fujita, K., Niki, E., Hagihara, Y., Yoshida, Y., Morimoto, Y., Iwahashi, H., 2012. Comparison of acute oxidative stress on rat lung induced by nano and fine-scale, soluble and insoluble metal oxide particles: NiO and TiO2. Inhal. Toxicol. 24, 391-400

Horie, M., Fukui, H., Nishio, K., Endoh, S., Kato, H., Fujita, K., Miyauchi, A., Nakamura, A., Shichiri, M., Ishida, N., Kinugasa, S., Morimoto, Y., Niki, E., Yoshida, Y., Iwahashi, H., 2011. Evaluation of acute oxidative stress induced by NiO nanoparticles in vivo and in vitro. J. Occup. Health 53, 64-74

Horie, M., Yoshiura, Y., Izumi, H., Oyabu, T., Tomonaga, T., Okada, T., Lee, B.W., Myojo, T., Kubo, M., Shimada, M., Morimoto, Y., 2016. Comparison of the pulmonary oxidative stress caused by intratracheal instillation and inhalation of NiO nanoparticles when equivalent amounts of NiO are retained in the lung. Antioxidants 5, 1-17

Hosiner, D., Gerber, S., Lichtenberg-Frate, H., Glaser, W., Schuller, C., Klipp, E., 2014. Impact of acute metal stress in *Saccharomyces cerevisiae*. Plos One 9, 1-14

Jamieson, D.J., 1998. Oxidative stress responses of the yeast *Saccharomyces cerevisiae*. Yeast 14, 1511-1527

Keston, A.S., Brandt, R., 1965. The fluorometric analysis of ultramicro quantities of hydrogen peroxide. Anal. Biochem. , 1-5

Kucukgoze, G., Alkim, C., Yilmaz, U., Kisakesen, H.I., Gunduz, S., Akman, S., Cakar, Z.P., 2013. Evolutionary engineering and transcriptomic analysis of nickel-resistant *Saccharomyces cerevisiae*. Fems Yeast Res. 13, 731-746

Lu, S.L., Zhang, W.C., Zhang, R., Liu, P.W., Wang, Q.X., Shang, Y., Wu, M.H., Donaldson, K., Wang, Q.Y., 2015. Comparison of cellular toxicity caused by ambient ultrafine particles and engineered metal oxide nanoparticles. Part. Fibre Toxicol. 12, 1-12

Manke, A., Wang, L.Y., Rojanasakul, Y., 2013. Mechanisms of nanoparticle-induced oxidative stress and toxicity. Biomed Res. Int. 2013, 1-15

Nel, A., Xia, T., Madler, L., Li, N., 2006. Toxic potential of materials at the nanolevel. Science 311, 622-627

Nimse, S.B., Palb, D., 2015. Free radicals, natural antioxidants, and their reaction mechanisms. RSC Adv. 5, 27986-28006

Oukarroum, A., Barhoumi, L., Samadani, M., Dewez, D., 2015. Toxic effects of nickel oxide bulk and nanoparticles on the aquatic plant *Lemna gibba L*. Biomed Res. Int., 1-7

Perez, R.R., Sousa, C.A., Vankeersbilck, T., Machado, M.D., Soares, E.V., 2013. Evaluation of the role of glutathione in the lead-induced toxicity in *Saccharomyces cerevisiae*. Curr. Microbiol. 67, 300-305

Perrone, G.G., Tan, S.X., Dawes, I.W., 2008. Reactive oxygen species and yeast apoptosis. Biochim. Biophys. Acta 1783, 1354-1368

Ruotolo, R., Marchini, G., Ottonello, S., 2008. Membrane transporters and protein traffic networks differentially affecting metal tolerance: a genomic phenotyping study in yeast. Genome Biol. 9, 1-43

Siddiqui, M.A., Ahamed, M., Ahmad, J., Khan, M.A.M., Musarrat, J., Al-Khedhairy, A.A., Alrokayan, S.A., 2012. Nickel oxide nanoparticles induce cytotoxicity, oxidative stress and apoptosis in cultured human cells that is abrogated by the dietary antioxidant curcumin. Food Chem. Toxicol. 50, 641-647

Soares, C., Branco-Neves, S., de Sousa, A., Pereira, R., Fidalgo, F., 2016. Ecotoxicological relevance of nano-NiO and acetaminophen to *Hordeum vulgare L.*: combining standardized procedures and physiological endpoints. Chemosphere 165, 442-452

Sousa, C.A., Soares, E.V., 2014. Mitochondria are the main source and one of the targets of Pb (lead)-induced oxidative stress in the yeast *Saccharomyces cerevisiae*. Appl. Microbiol. Biotechnol. 98, 5153-5160

Takumi, S., Kimura, H., Matsusaki, H., Kawazoe, S., Tominaga, N., Arizono, K., 2010. DNA microarray analysis of genomic responses of yeast *Saccharomyces cerevisiae* to nickel chloride. J. Toxicol. Sci. 35, 125-129

Tarpey, M.M., Wink, D.A., Grisham, M.B., 2004. Methods for detection of reactive metabolites of oxygen and nitrogen: in vitro and in vivo considerations. Am. J. Physiol. Regul. Integr. Comp. Physiol. 286, R431-R444.

Voet, D., Voet, J.G., Pratt, C.W., 1999. Electron transport and oxidative phosporilation, in: Voet, D., Voet, J.G., Pratt, C.W. (Eds.), Fundamentals of biochemistry. John Wiley & Sons, Inc, New York, pp. 492-528

von Moos, N., Koman, V.B., Santschi, C., Martin, O.J.F., Maurizi, L., Jayaprakash, A., Bowen, P., Slaveykova, V.I., 2016. Pro-oxidant effects of nano-TiO2 on *Chlamydomonas reinhardtii* during short-term exposure. Rsc Adv. 6, 115271-115283

Wang, H., Joseph, J.A., 1999. Quantifying cellular oxidative stress by dichlorofluorescein assay using microplate reader. Free Radic. Biol. Med. 27, 612-616

Winther, J.R., Jakob, U., 2013. Redox control: A black hole for oxidized glutathione. Nat. Chem. Biol. 9(2), 1-5

Xu, Y., Gu, Y., Qian, S.Y., 2012. An advanced electron spin resonance (ESR) spin-trapping and LC/(ESR)/MS technique for the study of lipid peroxidation. Int. J. Mol. Sci. 13, 14648-14666

Chapter 5 - Nickel oxide (NiO) nanoparticles trigger caspase- and mitochondria-dependent apoptosis in yeast *Saccharomyces cerevisiae**

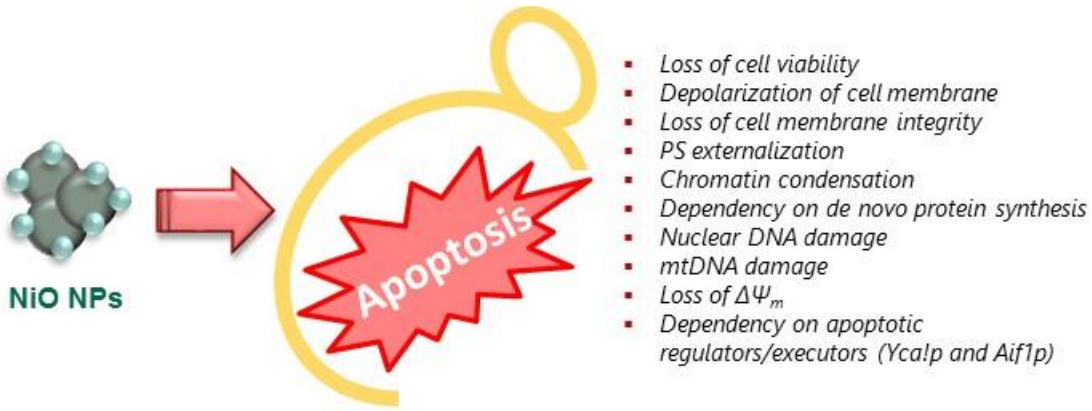

*Published in Chemical Research in Toxicology (2019) 32: 245-254

5.1. Introduction

Due to their unique physiochemical properties and reactivity, the metal oxide nanoparticles (NPs) are increasingly manufactured in the last decade. Nickel oxide (NiO) NPs are used for multiple applications, such as catalysts, memory cells, electrode materials in multilayer ceramic capacitors, diesel-fuel additives and pigments for ceramics and glasses (EPRUI, 2017). As the nanotechnology industry expands, the exposure to NiO NPs emerges as a significant occupational hazard. In addition, a deeper understanding of the potential impact of NiO NPs on the environment and human health is required.

Adverse effects as consequence of the exposure to NiO NPs, such as, cytotoxicity, inflammation and genotoxicity in human pulmonary cells, has been reported (Capasso et al., 2014; Cho et al., 2010; Horie et al., 2009; Magaye and Zhao, 2012). The International Agency for Research on Cancer classed nickel compounds as group 1 (carcinogenic to humans) and metallic nickel was classed as group 2B (possible carcinogenic to humans) (IARC, 1990).

Cell death can be classified into a not programed "accidental cell death" (ACD) and "regulated cell death" (RCD). The first subtype of cell death (ACD) occurs as a consequence of the exposure of cells to severe physical, chemical or mechanical stimuli; cells demise in an uncontrollable manner as a result of their immediate loss of structural integrity. RCD involves a genetically encoded machinery and can result from multiple signalling pathways, including apoptosis. The designation "programed cell death" (PCD) is used to refer RCD that is executed in specific physiological scenarios (Galluzzi et al., 2015; Galluzzi et al., 2018). Many human diseases, such as several neurological disorders (for example, Huntington's, Parkinson's and Alzheimer's disease) and cancer are associated with the dysregulation of cell death pathways (Munoz et al., 2012). In this context, it has been shown that the exposure to NiO NPs induce apoptosis in different cell lines, such as in human bronchial epithelial (BEAS-2B) (Duan et al., 2015), lung epithelial (NCIH460) (Pietruska et al., 2011), liver (HepG2) (Ahamed et al., 2013; Saquib et al., 2018) and neuronal cells (SH-SY5Y) (Abudayyak et al., 2017).

The yeast *S. cerevisiae* is a relevant eukaryotic cell model in different fields, such as biochemistry, molecular and cellular biology. In the last decade, this unicellular microorganism has been used in the study of RCD (Mirisola et al., 2014; Wloch-Salamon and Bem, 2013). This yeast displays some similarities (orthologues) with mammalian (including human) cells, which makes it an effective cell model to human diseases (Karathia et al., 2011). In Chapter 3, it was found that the exposure of yeast cells of *S. cerevisiae* to NiO NPs induced the loss of metabolic activity and cell viability in a dose-dependent manner. In Chapter 4, it was observed that the loss of cell viability induced by NiO could

be attributed to the intracellular generation of reactive oxygen species (ROS) and glutathione depletion. It is described that oxidative stress is a common denominator of RCD initiation (Strich, 2015). The present Chapter aimed to characterize the cell death observed in *S. cerevisiae* upon exposure to NiO NPs. For this purpose, yeast cell death induced by NiO NPs was assessed by monitoring the loss of plasma membrane integrity and cell viability. Subsequently, the presence of typical morphological and biochemical features of apoptotic cell death was examined in yeast cells exposed to a cytotoxic concentration of NiO NPs. In addition, the dependence of known apoptotic regulators/executors (Yca1p and Aif1p) in the RCD NiO NPs-induced was evaluated.

5.2. Materials and Methods

5.2.1. Preparation of nickel oxide nanoparticles stock suspensions

The NiO NPs preparation and characterization were previously described in Chapter 3.

5.2.2. Strains, media, growth conditions and treatments

Experiments were carried out using the yeast *Saccharomyces cerevisiae* BY4741 (MAT*α*; *his3*Δ1; *leu2*Δ0; *met15*Δ0; *ura3*Δ0) as a wild-type strain (WT); in addition, the respective knockout mutants in the *AIF1* or *YCA1* genes were also used. Strains were obtained from European *Saccharomyces cerevisiae* Archive for Functional Analysis (EUROSCARF).

S. cerevisiae BY4741 strain was maintained at 4 °C on YPD agar containing 5 g/L yeast extract (Difco-BD), 5 g/L peptone (Difco-BD), 10 g/L glucose (Merck) and 15 g/L agar (VWR Chemicals). The knockout strains were maintained on YPD agar with 0.2 g/L Geneticin (G418 disulfate salt, Sigma-Aldrich). The assessment of respiratory-deficient (RD) mutants (see below) was carried out using YPGly agar medium. YPGly agar is similar to YPD agar, replacing glucose by 2 % (v/v) of glycerol (Merck). In the canavanine assay (see below), the synthetic dextrose (SD) minimal agar medium (Amberg et al., 2005), containing 6.7 g/L yeast nitrogen base without amino acids (Difco-BD), 20 g/L glucose, 15 g/L agar, 0.02 g/L uracil (Sigma-Aldrich), 0.02 g/L L-methionine (Sigma-Aldrich), 0.1 g/L L-leucine (Sigma-Aldrich), 0.02 g/L L-histidine HCl (Sigma-Aldrich) without or with 60 mg/L canavanine (Sigma-Aldrich) (SD_{+can}), was used.

All strains were grown in YPD broth to exponential phase by incubating the cells overnight, to an OD_{600} of ~1.0, with continuous shaking (150 rpm) at 30ºC.

After growth, cells were harvested by centrifugation (2.500x*g*, 5 min), washed twice with water, resuspended at 1 x 10^7 cells/mL in 10 mM MES buffer (Sigma-Aldrich), pH 6.0, with 20 g/L glucose, and incubated without (control) or with 100 mg/L NiO NPs, at 30ºC, 150 rpm, up to 48 h.

The effect of 25 mg/L cycloheximide (Sigma-Aldrich) on the toxicity induced by NiO NPs was assessed by pre-incubation with this compound for 30 min before the exposure to NiO NPs. Control experiments have shown that, at the concentration used, cycloheximide was not toxic to yeast cells.

5.2.3. Survival assay

The effect of NiO NPs on yeast cells was assessed by a cell viability assay (clonogenic test), as previously described in Chapter 3. Cell viability was calculated considering the number of colony-forming unit (CFU)/mL at zero time as reference (100 %).

5.2.4. Evaluation of plasma membrane integrity

Plasma membrane permeability was accessed using the non-permeant propidium iodide (PI) probe. Yeast cells (1 x 10^7 cells/mL) were incubated with 4.5 µmol/L PI (Sigma), for 10 min, at room temperature in the dark.

Plasma membrane potential was monitored by staining the cells with bis 1,3-dibutylbarbituric acid trimethine oxonol ($DiBAC_4(3)$), known as Oxonol (Oxo) (Molecular Probes, Invitrogen) (Epps et al., 1994). Yeast cells (1 x 10^7 cells/mL) were incubated with 1.94 µmol/L Oxo (final concentration), for 10 min, at 30°C, in the dark. In double staining protocol (Oxo/PI), cells were first stained with Oxo and, subsequently, with PI, as described above.

As a positive control (cells with depolarized and permeabilized membrane), yeasts were heated at 65°C, for 1 h.

The percentage of PI or Oxo negative cells was determined by fluorescence microscopy (Leica DLMB, equipped with a HBO-100 mercury lamp and a filter set I3 [excitation filter (band pass filter, BP) BP 450– 490, dichromatic mirror 510 and suppression filter (long pass filter, LP) LP 515] from Leica. Yeast cells double stained (Oxo/PI) were observed using the filter set I3, GFP (excitation filter BP 450-490, dichromatic mirror 500 and suppression filter BP 500-550) or N2.1 (excitation filter BP 515–560, dichromatic mirror 580 and suppression filter LP 590) from Leica. In each experiment, two samples of at least 200 cells (total ≥ 400 cells) were counted in randomly selected microscope fields.

Images were acquired with a Leica DC 300 F camera and processed using Leica IM 50-Image Manager software.

5.2.5. Annexin V staining

Annexin V (fluorescein isothiocyanate, FITC-conjugated), a protein that specifically binds to phosphatidylserine (PS) residues was used to detect the externalization of PS (Vermes et al., 1995). After treatment, yeast cells were collected, washed two times with 40 mmol/L phosphate buffered saline (PBS) (pH 6.8) and resuspended at 1 x 10^7 cells/mL, in sorbitol buffer (1.2 mol/L sorbitol, 0.5 mmol/L $MgCl_2$, 35 mmol/L K_2HPO_4, pH 6.8). Cell walls were digested by incubation, with 90 U/mL lyticase (Sigma-Aldrich), in sorbitol buffer, for 45 min at 28ºC. Then, cell suspensions (1 mL) were centrifuged (250 x *g*, 5 min), resuspended in 60 µL of incubation buffer (containing Annexin-V-FLUOS labelling solution and propidium iodide) (Roche) and incubated for 10 min at 25ºC. Cells were observed in a fluorescence microscope using a filter set I3. In each experiment, two samples containing at least 100 cells (total ≥ 200 cells) were counted in randomly selected microscope fields. Images were acquired and processed as described above.

5.2.6. Assessment of mitochondrial membrane potential

The evaluation of mitochondrial membrane potential ($\Delta\Psi_m$) was carried out using the probe 3,3'dihexyloxacarbocyanine iodide ($DiOC_6(3)$) (Sigma-Aldrich) (Pozarowski et al., 2003; Rottenberg and Wu, 1998). Yeast cells (1 x 10^7 cells/mL) were collected and incubated with 30 nmol/L $DiOC_6(3)$ for 20 min at 30ºC, in the dark. Then, the cells were dispensed (200 µL per well), in quintuplicate, in a 96-well flat microplate (Orange Scientific). Fluorescence intensity (in relative fluorescence units, RFUs) was measured in a Perkin Elmer (Victor3) microplate reader at a fluorescence excitation wavelength of 485/14 nm and an emission wavelength of 535/25 nm. $\Delta\Psi_m$ was expressed as the ratio between the fluorescence in the assay and the fluorescence in the control (non-treated cells).

Cells were also double stained with $DiOC_6(3)$ and PI. After $DiOC_6(3)$ staining, cells were incubated with PI, as described above. Stained cells were observed in an epifluorescence microscope, equipped with a filter set GFP ($DiOC_6(3)$) or N2.1 (PI). Images were acquired and processed as described above.

5.2.7. Evaluation of nuclear alterations

After treatment with NiO NPs, cells were fixed with 3.5 % (w/v) formaldehyde, stained with 3 µmol/L diaminophenylindole (DAPI; Sigma-Aldrich) for 15 min, at room temperature, in the dark, and mounted with ProLong Gold antifade reagent (Molecular Probes, Invitrogen), as previously described (Bussche and Soares, 2011). Cells were observed in an epifluorescence microscope equipped with a

filter set A (excitation filter BP 340–380, dichromatic mirror 400 and suppression LP 425), from Leica. In each experiment, two samples containing at least 200 cells (total ≥ 400 cells) were evaluated in randomly selected microscope fields. Images were acquired and processed as described above.

5.2.8. Mitochondrial mutation assay

The quantification of respiratory-deficient (RD) mutants induced by NiO NPs was assessed through the complete lack of growth of these mutants on non-fermentable media (YPGly) (Eki, 2018; Gomes et al., 2008). Appropriate dilutions of cell suspensions were plated on YPD and YPGly. The percentage of RD cells was calculated as previously described (Sousa and Soares, 2014).

5.2.9. Nuclear DNA mutation rate detection (canavanine assay)

The rate of mutation induced by NiO NPs was determined by the selection of inactivation of the permease *CAN1* gene (canavanine assay) (Madia et al., 2009). Cell suspensions ($1x10^7$ cells/mL) were appropriately diluted and plated on a medium lacking arginine and containing 60 mg/L L-canavanine (Sigma-Aldrich) (SD_{+can}). In parallel, convenient dilutions of the cell suspensions were plated on the same medium (SD) without canavanine. The plates were incubated for 5-7 days at 30ºC. The frequency of mutation was calculated considering the number of UFC/mL on SD_{+can} plates (Can^R cells) and the number of UFC/mL on SD plates (total viable cells).

5.2.10. Reproducibility of the results and statistical analysis

All experiments were performed at least three times in duplicate. The data are presented as mean values ± standard deviations (SD); where no error bars are shown, SD are within the points. In the experiment where fluorescence was quantified, a typical example of an experiment repeated at least three times is presented; each data represents the mean (± SD) of five fluorescent readings.

Statistical differences between control and treated cells were tested using unpaired *t* test. *P* values <0.05 were considered statistically significant.

5.3. Results

5.3.1. Impact of NiO NPs on cell viability and plasma membrane integrity

Cell viability was evaluated by quantification of the reduction of the number of colony-forming units, after different periods of contact time of yeasts with NiO NPs. The exposure to NiO NPs induced an abrupt loss of cell cultivability. Cell viability dropped to ~60 % in the first 8h (Fig 5.1A); later exposure to NiO NPs induced a slower reduction of cell viability: ~33 % of viable cells at 48 h (Fig 5.1A).

To define a lethal scenario in yeast cells exposed to NiO NPs, a kinetic assessment of cell membrane integrity was carried out through the monitoring of propidium iodide (PI) uptake. It is assumed that viable cells exclude PI (PI negative cells) (Fig 5.1D - control). As it can be observed in Fig 5.1B, a small proportion of the cell population (2 %) stayed permeable to PI after 8h of contact with NiO NPs.

The uptake of PI requires a significant damage of the cell membrane. This means that the permeability to PI represents an irreparable damage of plasma membrane (permanent loss of the barrier function) (Davey and Hexley, 2011) and cell death (Carmona-Gutierrez et al., 2018; Galluzzi et al., 2015). On the other hand, it has also been reported that the uptake of the lipophilic anionic probe $DiBAC_4(3)$, known as Oxonol (Oxo), occurs in less damaged cells (Davey et al., 2004) with reduced membrane potential (depolarized cell membrane) (Epps et al., 1994; Novo et al., 2000). Non-stressed cells displayed a polarized membrane remaining unstained (Oxo negative cells) (Fig 5.1D - control). To obtain further information about the impact of NiO on yeast plasma membrane, after exposure to NPs, cells were stained with Oxo. The exposure of yeasts to NiO NPs up to 8h did not have any impact on the plasma membrane potential, as cells remained Oxo (-) (Fig 5.1C). After this time, the cells became permeable to Oxo. Thus, after 24 and 48 h of exposure to NPs, ~20 and 50 % of cell population was Oxo (+), respectively (Fig 5.1C). After the same time of exposure to NPs, the yeast cells PI (+) were ~8 and 15 %, respectively (Fig 5.1B). The comparative analysis of the cells stained with Oxo and PI revealed that there was a fraction of cells, which membrane presented a reduced potential, becoming Oxo (+), although they maintained the impermeability to PI (Fig 5.1B, C). These results indicate that under NiO stress, the de-energization precedes the permeabilization of cell membrane. This possibility was confirmed by fluorescence microscopic observation of the yeast cells exposed to NPs and double stained with Oxo and PI, where it was possible to detect PI(-)/Oxo (+) cells (Fig 5.1D). However, all cells PI (+) presented a depolarized membrane (Oxo +) (Fig 5.1D). Taken all results together, they evidence that the loss of cultivability preceded the loss of membrane potential and the plasma membrane integrity.

After the exposure of yeasts to NiO NPs for 24 h, ~8 % of yeast cells have passed the "point of no return" (Davey, 2011) as exhibited irreversible plasma membrane permeabilization (PI positive cells) and thus can be classified as dead (Galluzzi et al., 2015). At this time (24 h), although only ~55 % of cell population displayed the ability to undergo proliferation (Fig 5.1A), ~80 % of cell population kept intact membrane (PI -/Oxo -) and, thus, can be classified as viable which suggest RCD in yeast cells exposed to NiO NPs. These results prompted us to further characterize the cell death phenotype NiO NPs-induced through the assessment of different morphological and biochemical features.

5.3.2. NiO NPs induce cell death with typical apoptotic hallmarks

In Chapter 4, yeast cells exposed to NiO NPs presented an intracellular overload of reactive oxygen species (ROS), which can mediates yeast cell death by apoptosis. To confirm this possibility, yeast cells exposed to NiO NPs were double stained with Annexin V-FITC/PI to detect the externalization of phosphatidylserine (PS). The exposure of PS at the outer leaflet of the plasma membrane (loss of membrane asymmetry) is considered an early sign of apoptosis and one of the most reliable apoptosis markers (Eisenberg et al., 2010). Cells Annexin V (+)/PI (-) (Fig 5.2A) are considered apoptotic (Mirisola et al., 2014). As it can be seen in Fig 5.2B, after 6 h of exposure to NiO NPs, the percentage of yeast cells Annexin V (+)/PI (-) was significantly different from the control; after this time, an increase of the apoptotic cells was observed.

Another feature of apoptosis is the requirement of *de novo* protein synthesis (Acosta-Zaldivar et al., 2016; Kitagaki et al., 2007; Ludovico et al., 2002; Ludovico et al., 2001; Madeo et al., 1999). To test this possibility, the effect of cycloheximide (cyh), a protein synthesis inhibitor in eukaryotes (Smith, 2000), on RCD NPs-induced was investigated. Yeast cells were incubated for 6 or 24 h with NiO in the presence or absence of 25 mg/L cyh and CFUs were counted. NiO- and cyh-treated cells displayed a higher % of CFUs compared to the NiO-treated cells in the absence of cyh (Fig 5.2C). This result suggests that the loss of cell viability in response to NPs stress requires the participation of cellular machinery, namely *de novo* protein synthesis, which is consistent with an apoptotic program.

Apoptotic cells present chromatin condensed and modification of the shape of the nucleus as a consequence of the proteolysis of key nuclear proteins (Martelli et al., 2001). In order to evaluate if NiO NPs induces chromatin condensation and modification of nucleus morphology, non-treated (control) and NiO-treated yeast cells were stained with the DNA-binding dye DAPI. Fluorescence microscopy observations revealed that NiO-treated yeast cells displayed ring and kidney-shaped condensed chromatin, characteristic of apoptotic cells (Fig 5.2D).

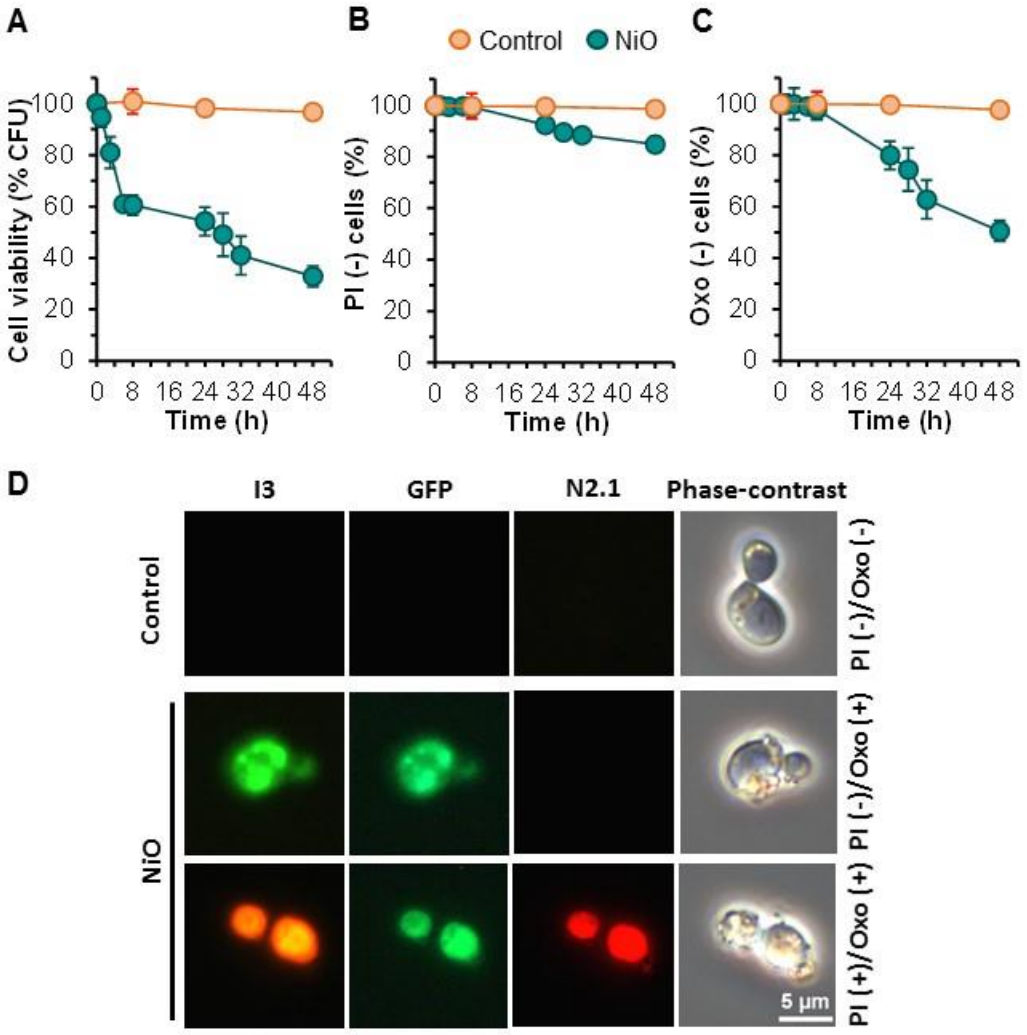

Figure 5.1. Cell viability and plasma membrane integrity in yeast cells of *S. cerevisiae* BY4741 exposed to NiO NPs. Cells were suspended in MES buffer in the absence (control) or presence of 100 mg/L NiO NPs. A – Cell viability evaluated by colony forming units (CFU) counting. B – Membrane permeability assessed by propidium iodide (PI) exclusion. C – Membrane polarization monitored by Oxonol (Oxo) exclusion. D – Photomicrographs of cells not exposed (control) or exposed to 100 mg/L NiO for 24 h and then double stained with PI and Oxo. Cells were visualized by florescence, using the filter set I3 (green and orange-red fluorescence), GFP (green fluorescence) or N2.1 (orange-red fluorescence), or by phase-contrast microscopy. The data represent the mean (± SD) of at least three independent experiments.

Control cells displayed a homogenous round-shaped nuclei (Fig 5.2D). Yeast population exposed for 8 h to NiO NPs presented a % of cells with an apoptotic nuclei significantly different from the control (cells not exposed to NiO); the % of cells with an apoptotic nuclei increased with the exposure time to NPs (Fig 5.2E).

Taken together all results presented above, they indicate that NiO NPs induced an apoptotic phenotype in yeast cells.

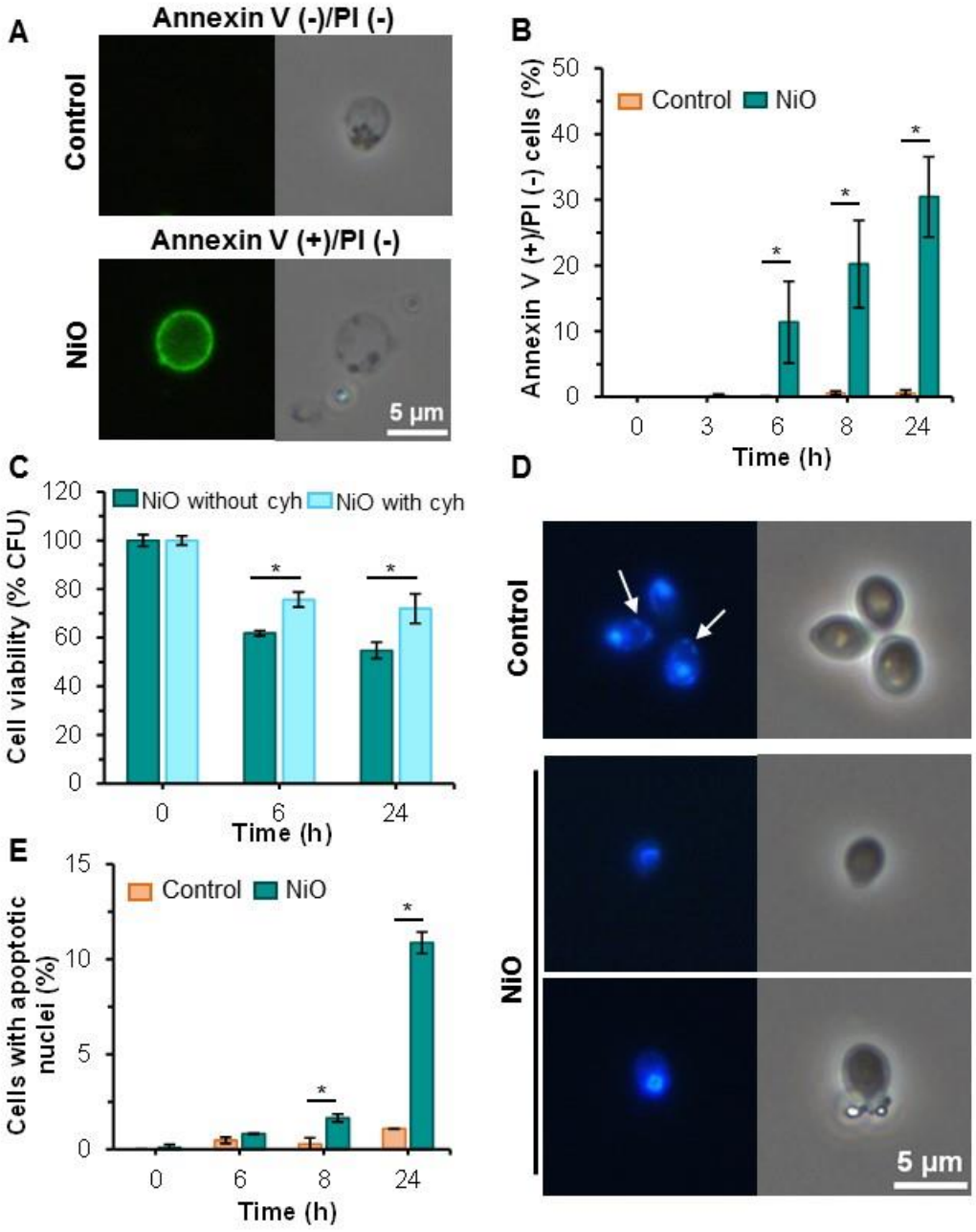

Figure 5.2. Yeast cells of *S. cerevisiae* BY4741 exposed to NiO NPs exhibited typical apoptotic hallmarks. Cells were suspended in MES buffer in the absence (control) or presence of 100 mg/L NiO NPs. A – Visualization of cells double stained with Annexin V-FITC/PI; fluorescence microscopy and respective phase contrast images (right side). B – Evolution of the percentage of apoptotic cells (Annexin +/PI-). C – Cell viability, in the absence (NiO without cyh) or the presence (NiO with cyh) of the protein synthesis inhibitor cycloheximide (cyh), evaluated by CFU counting. D – Photomicrographs of cells stained with DAPI; fluorescence microscopy and respective phase contrast images (right side). Control cells presented homogeneous round nucleus and mitochondria (arrows). Mitochondria appeared as small dots predominantly located at the periphery of the cells. Cells treated with NiO NPs for 24 h displayed kidney (middle panel) or ring (bottom panel) shape nucleus, characteristic of apoptotic cells; in these cells, it was not possible to visualize mtDNA. E – Determination of cells exhibiting chromatin condensation (apoptotic nuclei) monitored by fluorescence microscopy after DAPI staining. The data represent the mean (± SD) of at least three independent experiments. Mean values are significantly different: **P*<0.05 in comparison with untreated cells (control); unpaired t test.

5.3.3. NiO NPs induce mitochondrial membrane depolarization

It has been shown that mitochondria play a central role during the execution of RCD by apoptosis in yeast cells (Guaragnella et al., 2012; Ligr et al., 1998; Madeo et al., 1999; Manon et al., 1997; Pereira et al., 2008). Modification of the mitochondrial membrane potential ($\Delta\Psi_m$) lead to the disruption of mitochondrial function. In the present work, $\Delta\Psi_m$ was assessed by quantification of the fluorescence of cells stained with the membrane potential-sensitive probe $DiOC_6(3)$. This probe accumulates in the negatively-charged mitochondrial matrix and the extent of their uptake, as measured by the intensity of cellular fluorescence, reflects the $\Delta\Psi_m$ (Perry et al., 2011; Rottenberg and Wu, 1998). Observation of the control cells, by fluorescence microscopy, allowed the visualization of the typical mitochondrial networks as a result of the polarization of the inner mitochondrial membrane (Fig 5.3A). Fluorescence quantification revealed that after 1h of exposure to NiO NPs, yeast cells presented a progressive reduction of fluorescence (up to 6-8 h), comparatively to control cells (Fig 5.3B). These results indicate that NiO NPs induce the depolarization of the mitochondrial membrane. Microscopic observation of cells exposed to NPs for 8 h confirmed the presence of yeasts with decreased green fluorescence and even the presence of yeasts that failed to accumulate $DiOC_6(3)$ (Fig 5.3A) probably as a consequence of the dissipation of the mitochondrial membrane potential. Yeast cells exposed to NiO NPs for 24 h presented a higher fluorescence comparatively to cells exposed for 6-8h (Fig 5.3B).

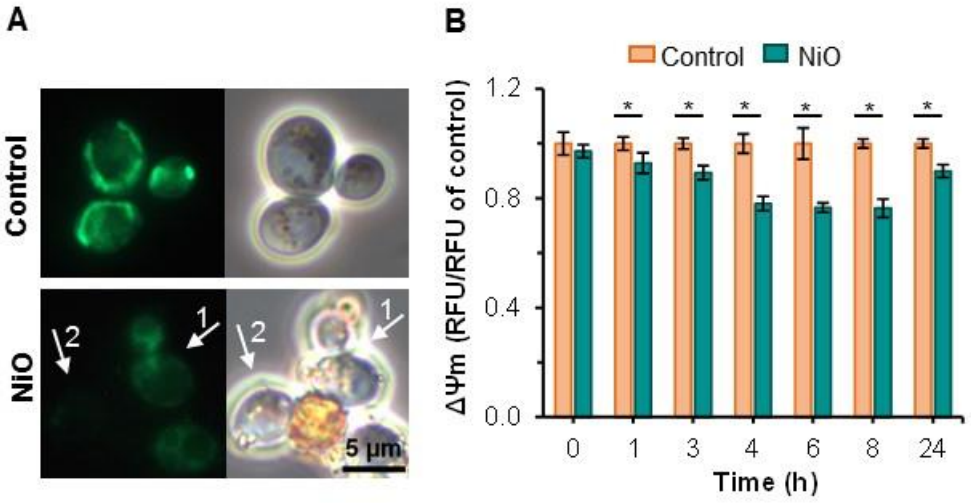

Figure 5.3. NiO NPs induces depolarization of the mitochondrial membrane (ΔΨm) in *S. cerevisiae* BY4741. Cells were exposed for 24 h in the absence (control) or presence of 100 mg/L NiO NPs and, subsequently, stained with $DiOC_6(3)$. A – Visualization of yeast cells. Arrow 1: cells with decreased green fluorescence; arrow 2: cell that failed to accumulate $DiOC_6(3)$. Fluorescence microscopy (left side) and respective phase contrast images (right side). B – ΔΨm monitored with the probe $DiOC_6(3)$. This is a typical example of an experiment performed at least three times. The data represent the mean (± SD) of five fluorescent readings. Mean values marked with * are significantly different ($P<0.05$).

However, this increase of fluorescence can be explained by the presence of some cells exhibiting a strong green fluorescence, all over the cells, as result of the accumulation of $DiOC_6(3)$ in the cytosol and not due to the repolarization of mitochondrial membrane. The double staining of these cells with $DiOC_6(3)$ and PI confirmed that the cells strongly fluorescent presented a permeabilized plasma membrane (PI+ cells) (Fig 5.4).

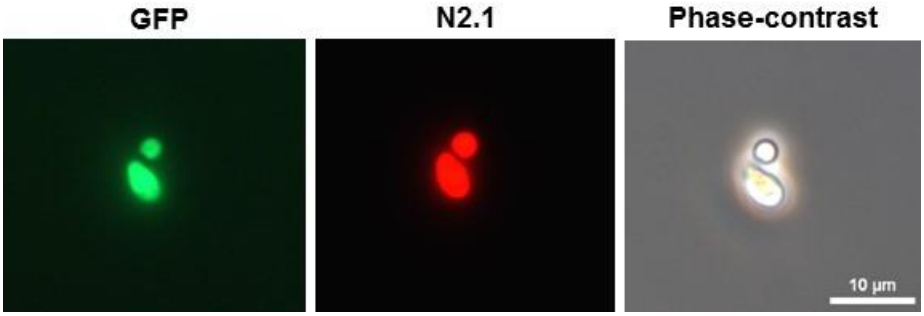

Figure 5.4. Double staining [$DiOC_6(3)$ and propidium iodide] of *S. cerevisiae* BY4741 exposed to NiO. Yeast cells were exposed to 100 mg/L NiO NPs for 24 h in MES buffer and, subsequently, stained as described in Material and methods. Cells were visualized by florescence, using the filter set GFP (green emission) or N2.1 (orange-read emission), or by phase-contrast microscopy.

5.3.4. NiO NPs induce apoptosis Yca1p and Aif1p-dependent

In order to better characterize the RCD, the effect of NiO NPs on the cell viability of knockout mutant strains *yca1*Δ and *aif1*Δ, devoid in protein known to be involved in apoptotic cell death, was evaluated. The proteases known as caspases are usually activated in the early stages of apoptosis and play a pivotal role in the yeast cell death execution (Carmona-Gutierrez et al., 2010; Mazzoni and Falcone, 2008). Yeast cells bear the metacaspase Yca1p, which is an ortholog of mammalian caspases (Madeo et al., 2002). The disruption of *YCA1* gene (*yca1*Δ strain) render cells significantly more resistant to the toxic effect of the NPs (Fig 5.5), which suggest that NiO-induced cell death is caspase-dependent.

The apoptosis-inducing factor (Aif1p), is a flavoprotein with NADH oxidase activity localized in the mitochondrial intermembrane space of healthy cells; yeast Aif1p undergoes a translocation to the nucleus upon apoptosis induction (Wissing et al., 2004). As it can be seen in Figure 5.5, the *aif1*Δ strain presented an enhanced survival in response to NiO NPs comparatively to WT strain; this fact suggests the involvement of this mitochondrial apoptotic regulator in the RCD NiO NPs-induced.

Altogether, the results presented above argue in favour of the involvement of the metacaspase Yca1p and the mitochondrial apoptotic factor Aif1p in the execution of apoptosis induced by NiO NPs.

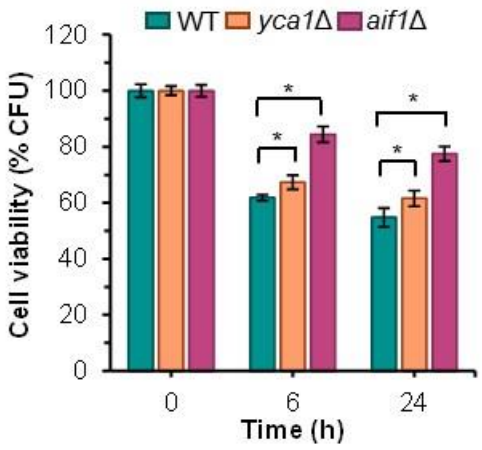

Figure 5.5. NiO NPs induces cell death Yca1p and Aif1p-dependent in *S. cerevisiae* BY4741. Viability evaluated by CFU counting of wild-type (WT), *yca1*Δ and *aif1*Δ exposed to 100 mg/L NiO NPs. The data represent the mean (± SD) of at least three independent experiments. Mean values are significantly different: **P*<0.05 in comparison with untreated cells (control); unpaired t test.

5.3.5. NiO NPs induce mitochondrial and nuclear DNA damage

Mitochondrial DNA (mtDNA) encodes several subunits of the electron respiratory chain (de Zamaroczy and Bernardi, 1985; Evans, 1983). The damage of mtDNA leads to the abolishment of respiration (formation of respiratory-deficient (RD) cells, also known as *petite* mutants). RD cells are unable to growth on non-fermentable carbon sources, such as glycerol (Yazgan and Krebs, 2012). In Chapter 3, it was found that mitochondria is the main source of intracellular ROS NiO NPs-induced. Since mtDNA is very susceptible to oxidative injury (Richter et al., 1988), the possibility of mitochondrial genome to be damaged upon exposure to NiO was evaluated by determining the percentage of RD cells. As it can be seen in Figure 5.6A, the percentage of RD cells increased over the time of NiO NPs exposure. Consistent with this result, the presence of cells lacking mtDNA (as revealed by DAPI staining) in the population exposed to NPs for 24 h (Fig 5.2D, NiO treated cells) was observed. In control cells, the percentage of RD cells remained approximately constant (2 %), which correspond to the values usually described for the spontaneous formation of these mutants (Clark-Walker et al., 1981). The results obtained indicate the damage of mtDNA, which means that mitochondrial genome is one of the targets of the ROS generated in the mitochondria.

Canavanine assay was used to evaluate the possible damage of nuclear DNA due to intracellular ROS accumulation in yeast cells exposed to NiO. This assay is based on the mutation in the plasma membrane arginine permease (coded by *CAN1* gene), which originate cells (can^R mutants) resistant to L-canavanine (an analogue of L-arginine) (Hu et al., 2013). It was possible to observe an increase of the number of Can^R colonies (among the population of viable cells) in cells exposed to NiO NPs

comparatively to the control. The mutation frequency NiO NPs-induced increased over time of exposure: after 6 and 24 h of exposure to NiO NPs, the frequency of Can^R mutations was approximately 7- and 12-fold higher compared with cells not exposed to NiO NPs (Fig 5.6B). These results demonstrate the damage of nuclear DNA by NiO NPs. In control, the frequency of Can^R mutations was similar after 6 and 24 h (7 per 10^7 viable cells), which is similar to the rate described in the literature (10-20 per 10^7 viable cells) (Letavayová et al., 2008).

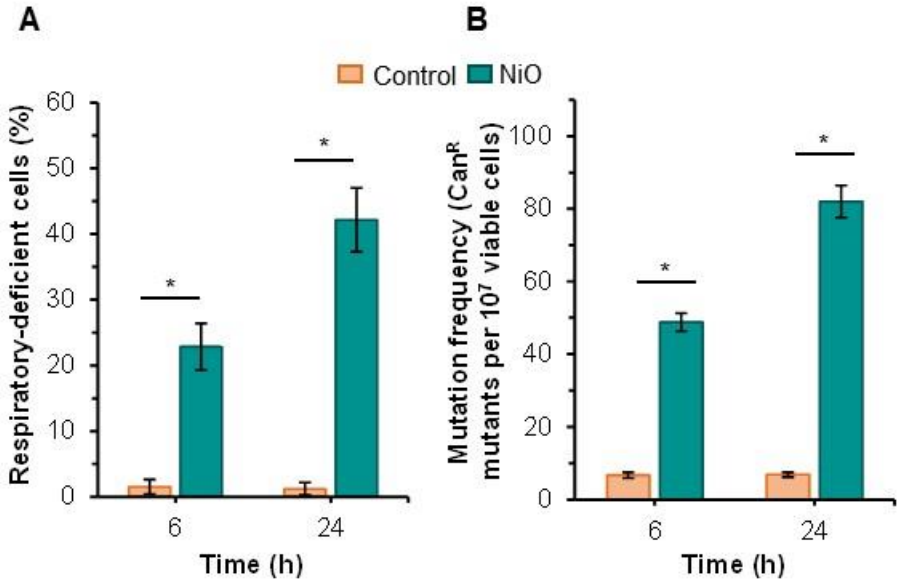

Figure 5.6. NiO NPs induces mitochondrial and nuclear DNA damage in *S. cerevisiae* BY4741. Cells were suspended in MES buffer in the absence (control) or presence of 100 mg/L NiO NPs. A – Mitochondrial DNA damage assessed through the formation of respiratory-deficient cells mutants (cells without capacity to growth on non-fermentable carbon source - YPGly). B – Nuclear DNA damage evaluated through the formation of canavanine resistant (Can^R) mutants. The data represent the mean (± SD) of at least three independent experiments. Mean values are significantly different: $*P<0.05$ in comparison with untreated cells (control); unpaired t test.

5.4. Discussion

The manufacturing and use of metal oxide NPs, such as NiO NPs, increased greatly in the last decade and, inevitably, raised concerns and uncertainties about the possible adverse effects of NPs to the environment and the human health. In Chapter 3, it was proposed that NiO NPs exert their toxic effect over yeast cells by an indirect mechanism: NiO NPs adsorb to the cell wall and releases nickel at the NP-cell wall interface originating a toxic response. Up to now, little is known about the mechanisms underlying the loss of yeast cell viability NiO NPs-induced. In order to understand deeply the toxicity mechanism induced by NiO NPs, the well-known apoptotic model *S. cerevisiae* was used.

It was shown that the exposure of yeast cells to NiO NPs up to 24 h induced a loss of cell proliferation (cell viability) without disruption of cell membrane integrity (Fig 5.1). However, extending the exposure of yeast cells to NiO originated the cell death (plasma membrane breakdown, accessed through PI staining) (Fig 5.1). It was also found that yeast cells exposed to NPs lost the plasma membrane asymmetry (PS exposure to the outer membrane leaflet) (Fig 5.2). The loss of cell viability induced by NiO required the involvement of the metacaspase Yca1p (Fig 5.5) and was attenuated by the presence of a protein synthesis inhibitor (cycloheximide) (Fig 5.2C). All these features are typical hallmarks of RCD by apoptosis in yeast cells (Carmona-Gutierrez et al., 2018; Carmona-Gutierrez et al., 2010; Ludovico et al., 2001). Our results are in agreement with those which described the PS externalization (Abudayyak et al., 2017; Duan et al., 2015) and the involvement of caspase-3 in apoptosis induced by NiO NPs in mammalian cell lines (Ahamed et al., 2013; Duan et al., 2015; Pietruska et al., 2011; Siddiqui et al., 2012). These results also suggest that *S. cerevisiae* and mammalian cell lines, exposed to NiO NPs, shares some common apoptotic features.

In Chapter 4, it was observed that antioxidants [L-ascorbic acid (an efficient scavenger of free radicals) (Arrigoni and De Tullio, 2002; Nimse and Pal, 2015) and N-tertbutyl- α -phenylnitrone, known as PBN (a free radical spin trapping agent) (Xu et al., 2012)] prevented ROS overload and abolished almost fully the loss of cell viability NiO NPs-induced; these results strongly suggest that oxidative damage plays a central role in the yeast cell death. The increased level of ROS, previously observed, was most likely in the origin of the damage of the nuclear DNA (observed through the increase of $Can1^R$ mutants) (Fig 5.6B). Our results are in agreement with those describing DNA damage in human cell lines exposed to NiO NPs (Abudayyak et al., 2017; Ahamed et al., 2013; Capasso et al., 2014; Siddiqui et al., 2012). In addition, in the present Chapter, the induction of RD mutants in yeast cells exposed to NPs was shown (Fig 5.6A), which can also be attributed to the increased ROS levels in these cells. The loss of part or all of the mtDNA was further confirmed through the observation, by fluorescence microscopy, of yeast cells stained with DAPI; in the cells exposed to NiO for 24 h, it was not possible to visualize mtDNA (Fig 5.2D, NiO treated cells).

The involvement of mitochondria in yeast apoptosis upon exposure to different stimuli have been described (Guaragnella et al., 2012; Ludovico et al., 2002; Pereira et al., 2008). Consistent with the possibility of NiO NPs to induce a mitochondria-dependent apoptosis, in Chapter 4, it was shown that mitochondria is the main contributor for the increase of ROS production. Here, it is described mitochondrial membrane depolarization (Fig 5.3), most likely, as consequence of the permeabilization of the membrane. $\Delta\Psi_m$ dissipation and the preservation of cell membrane integrity (Fig 5.1A, B) are

usually characteristic of early apoptotic cells (Cottet-Rousselle et al., 2011). The induction of formation of mutants with a *petite* phenotype, as it was described above (Fig 5.6A), together with our previous results, which have shown that cells from a derivative ρ^0 mutant (without mitochondrial DNA) presented reduced levels of ROS and increased resistance to NiO NPs (please see Chapter 4), reinforce the possibility of an active role of mitochondria in the execution of an apoptotic program in response to the exposure to NiO NPs.

Literature describes the requirement of the apoptosis inducing factor (Aif1p) in RCD induced by several stimuli (Pereira et al., 2008; Strich, 2015). Yeast cells without the mitochondrial pro-apoptotic factor Aif1p (*aif1*Δ strain) presented a higher resistance to NiO NPs (Fig 5.5), which suggests the participation of the Aif1p in the execution of RCD by apoptosis. This result also supports the role of mitochondria in the apoptosis induced by NiO NPs. It is also described that in response to apoptotic stimuli, Aif1p is released from mitochondria and translocated to the nucleus, where chromatin condensation and DNA fragmentation is carried out and, thus, cellular demise is provoked (Wissing et al., 2004). Modifications of the nucleus morphology (including the increase of cells with ring and kidney-shaped condensed chromatin) was observed in yeast cells treated with NPs (Fig 5.2D); these facts are compatible with the possibility of Aif1 participation as executioner of the RCD NiO-induced.

In resume, it was shown that the exposure of yeast cells to NiO NPs induce its cell death, which exhibits several typical features of RCD by apoptosis: (i) loss of proliferation capacity dependent of the participation of cellular machinery, namely *de novo* protein synthesis and the activation of the metacaspase Yca1p; (ii) externalization of phosphatidylserine at the surface of the cytoplasmic membrane in cells retaining membrane integrity and (iii) modification of nucleus morphology. Other further insights were also obtained, namely mitochondrial membrane potential dissipation, induction of petite mutants and the participation of the Aif1p; these facts support the mitochondrial involvement in the RCD NiO NP-induced. An overview of the sequence of detrimental effects associated with NiO NPs-induced in the yeast *S. cerevisiae* is presented in Figure 5.7.

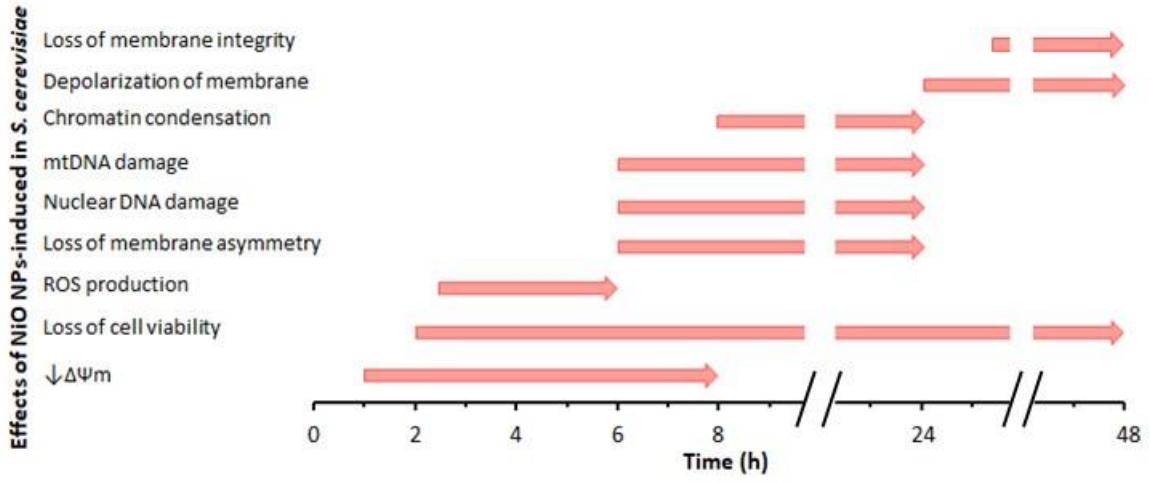

Figure 5.7. Sequence of events associated with NiO NPs-induced cell death in the yeast *S. cerevisiae*. Proposal based on the results obtained in the present and previous Chapters 3 and 4.

5.5. Conclusions

Yeast cell death process induced by NiO NPs was characterized in this Chapter:

- NiO NPs induced typical phenotypic apoptotic markers;
- Results support that yeast cell death is Yca1p metacaspase-dependent;
- Yeast cell death can be mediated by a mitochondria-dependent apoptotic pathway.

References

Abudayyak, M., Guzel, E., Ozhan, G., 2017. Nickel oxide nanoparticles are highly toxic to SH-SY5Y neuronal cells. Neurochem. Int. 108, 7-14.

Acosta-Zaldivar, M., Andres, M.T., Rego, A., Pereira, C.S., Fierro, J.F., Corte-Real, M., 2016. Human lactoferrin triggers a mitochondrial- and caspase-dependent regulated cell death in *Saccharomyces cerevisiae*. Apoptosis 21, 163-173.

Ahamed, M., Ali, D., Alhadlaq, H.A., Akhtar, M.J., 2013. Nickel oxide nanoparticles exert cytotoxicity via oxidative stress and induce apoptotic response in human liver cells (HepG2). Chemosphere 93, 2514-2522.

Amberg, D.C., Burke, D.J., Strathern, J.N., 2005. Methods in yeast genetics: a cold Spring Harbor Laboratory Course Manual, New York, USA.

Arrigoni, O., De Tullio, M.C., 2002. Ascorbic acid: much more than just an antioxidant. Biochim. Biophys. Acta 1569, 1-9.

Bussche, J.V., Soares, E.V., 2011. Lead induces oxidative stress and phenotypic markers of apoptosis in *Saccharomyces cerevisiae*. Appl. Microbiol. Biotechnol. 90, 679-687.

Capasso, L., Camatini, M., Gualtieri, M., 2014. Nickel oxide nanoparticles induce inflammation and genotoxic effect in lung epithelial cells. Toxicol. Lett. 226, 28-34.

Carmona-Gutierrez, D., Bauer, M.A., Zimmermann, A., Aguilera, A., Austriaco, N., Ayscough, K., Balzan, R., Bar-Nun, S., Barrientos, A., Belenky, P., Blondel, M., Braun, R.J., Breitenbach, M., Burhans, W.C., Buttner, S., Cavalieri, D., Chang, M., Cooper, K.F., Corte-Real, M., Costa, V., Cullin, C., Dawes, I., Dengjel, J., Dickman, M.B., Eisenberg, T., Fahrenkrog, B., Fasel, N., Frohlich, K.U., Gargouri, A., Giannattasio, S., Goffrini, P., Gourlay, C.W., Grant, C.M., Greenwood, M.T., Guaragnella, N., Heger, T., Heinisch, J., Herker, E., Herrmann, J.M., Hofer, S., Jimenez-Ruiz, A., Jungwirth, H., Kainz, K., Kontoyiannis, D.P., Ludovico, P., Manon, S., Martegani, E., Mazzoni, C., Megeney, L.A., Meisinger, C., Nielsen, J., Nystrom, T., Osiewacz, H.D., Outeiro, T.F., Park, H.O., Pendl, T., Petranovic, D., Picot, S., Polcic, P., Powers, T., Ramsdale, M., Rinnerthaler, M., Rockenfeller, P., Ruckenstuhl, C., Schaffrath, R., Segovia, M., Severin, F.F., Sharon, A., Sigrist, S.J., Sommer-Ruck, C., Sousa, M.J., Thevelein, J.M., Thevissen, K., Titorenko, V., Toledano, M.B., Tuite, M., Vogtle, F.N., Westermann, B., Winderickx, J., Wissing, S., Wolfl, S., Zhang, Z.J.J., Zhao, R.Y., Zhou, B., Galluzzi, L., Kroemer, G., Madeo, F., 2018. Guidelines and recommendations on yeast cell death nomenclature. Microb. Cell 5, 4-31.

Carmona-Gutierrez, D., Eisenberg, T., Buttner, S., Meisinger, C., Kroemer, G., Madeo, F., 2010. Apoptosis in yeast: triggers, pathways, subroutines. Cell Death Differ. 17, 763-773.

Cho, W.-S., Duffin, R., Poland, C.A., Howie, S.E.M., MacNee, W., Bradley, M., Megson, I.L., Donaldson, K., 2010. Metal oxide nanoparticles induce unique inflammatory foot prints in the lung: important implications for nanoparticles testing. Environ. Health Perspect. 118, 1699-1706.

Clark-Walker, G.D., McArthur, C.R., Daley, D.J., 1981. Does mitochondrial DNA length influence the frequency of spontaneous petite mutants in yeasts? Curr. Genet. 4, 7-12.

Cottet-Rousselle, C., Ronot, X., Leverve, X., Mayol, J.F., 2011. Cytometric assessment of mitochondria using fluorescent probes. Cytometry A 79A, 405-425.

Davey, H.M., 2011. Life, death, and in-between: meanings and methods in microbiology. Appl. Environ. Microbiol. 77, 5571-5576.

Davey, H.M., Hexley, P., 2011. Red but not dead? Membranes of stressed *Saccharomyces cerevisiae* are permeable to propidium iodide. Environ. Microbiol. 13, 163-171.

Davey, H.M., Kell, D.B., Weichart, D.H., Kaprelyants, A.S., 2004. Estimation of microbial viability using flow cytometry. Curr. Protoc. Cytom. Chapter 11, Unit 11.13-Unit 11.13.

de Zamaroczy, M., Bernardi, G., 1985. Sequence organization of the mitochondrial genome of yeast - a review. Gene 37, 1-17.

Duan, W.X., He, M.D., Mao, L., Qian, F.H., Li, Y.M., Pi, H.F., Liu, C., Chen, C.H., Lu, Y.H., Cao, Z.W., Zhang, L., Yu, Z.P., Zhou, Z., 2015. NiO nanoparticles induce apoptosis through repressing SIRT1 in human bronchial epithelial cells. Toxicol. Appl. Pharmacol. 286, 80-91.

Eisenberg, T., Carmona-Gutierrez, D., Buettner, S., Tavernarakis, N., Madeo, F., 2010. Necrosis in yeast. Apoptosis 15, 257-268.

Eki, T., 2018. Yeast-based genotoxicity tests for assessing DNA alterations and DNA stress responses: a 40-year overview. Appl. Microbiol. Biotechnol. 102, 2493-2507.

Epps, D.E., Wolfe, M.L., Groppi, V., 1994. Characterization of the steady-state and dynamic fluorescence properties of the potential-sensitive dye bis-(1,3-dibutylbarbituric acid) trimethine oxonol ($DiBAC_4(3)$) in model systems and cells. Chem. Phys. Lipids 69, 137-150.

EPRUI, 2017. Nanoparticles & microspheres, Nano nickel oxide, https://www.nanoparticles-microspheres.com/Products/Nano-Nickel-Oxide.html (Acessed October 30 2017).

Evans, I.H., 1983. Molecular genetic aspects of yeast mitochondria, in: Spencer, J.F.T., Spencer, D.M., Smith, A.R.W. (Eds.), Yeast genetics: fundamental and applied aspects. Springer, New York, USA, pp. 269–370.

Galluzzi, L., Bravo-San Pedro, J.M., Vitale, I., Aaronson, S.A., Abrams, J.M., Adam, D., Alnemri, E.S., Altucci, L., Andrews, D., Annicchiarico-Petruzzelli, M., Baehrecke, E.H., Bazan, N.G., Bertrand, M.J., Bianchi, K., Blagosklonny, M.V., Blomgren, K., Borner, C., Bredesen, D.E., Brenner, C., Campanella, M., Candi, E., Cecconi, F., Chan, F.K., Chandel, N.S., Cheng, E.H., Chipuk, J.E., Cidlowski, J.A., Ciechanover, A., Dawson, T.M., Dawson, V.L., De Laurenzi, V., De Maria, R., Debatin, K.M., Di Daniele, N., Dixit, V.M., Dynlacht, B.D., El-Deiry, W.S., Fimia, G.M., Flavell, R.A., Fulda, S., Garrido, C., Gougeon, M.L., Green, D.R., Gronemeyer, H., Hajnoczky, G., Hardwick, J.M., Hengartner, M.O., Ichijo, H., Joseph, B., Jost, P.J., Kaufmann, T., Kepp, O., Klionsky, D.J., Knight, R.A., Kumar, S., Lemasters, J.J., Levine, B., Linkermann, A., Lipton, S.A., Lockshin, R.A., López-Otín, C., Lugli, E., Madeo, F., Malorni, W., Marine, J.C., Martin, S.J., Martinou, J.C., Medema, J.P., Meier, P., Melino, S., Mizushima, N., Moll, U., Muñoz-Pinedo, C., Nuñez, G., Oberst, A., Panaretakis, T., Penninger, J.M., Peter, M.E., Piacentini, M., Pinton, P., Prehn, J.H., Puthalakath, H., Rabinovich, G.A., Ravichandran, K.S., Rizzuto, R., Rodrigues, C.M., Rubinsztein, D.C., Rudel, T., Shi, Y., Simon, H.U., Stockwell, B.R., Szabadkai, G., Tait, S.W., Tang, H.L., Tavernarakis, N., Tsujimoto, Y., Vanden Berghe, T., Vandenabeele, P., Villunger, A., Wagner, E.F., Walczak, H., White, E., Wood, W., Yuan, J., Zakeri, Z., Zhivotovsky, B., Melino, G., Kroemer, G., 2015. Essential versus accessory aspects of cell death: recommendations of the NCCD 2015. Cell Death Differ. 22, 58-73.

Galluzzi, L., Vitale, I., Aaronson, S.A., Abrams, J.M., Adam, D., Agostinis, P., Alnemri, E.S., Altucci, L., Amelio, I., Andrews, D.W., Annicchiarico-Petruzzelli, M., Antonov, A.V., Arama, E., Baehrecke, E.H., Barlev, N.A., Bazan, N.G., Bernassola, F., Bertrand, M.J.M., Bianchi, K., Blagosklonny, M.V., Blomgren, K., Borner, C., Boya, P., Brenner, C., Campanella, M., Candi, E., Carmona-Gutierrez, D., Cecconi, F., Chan, F.K.M., Chandel, N.S., Cheng, E.H., Chipuk, J.E., Cidlowski, J.A., Ciechanover, A., Cohen, G.M., Conrad, M., Cubillos-Ruiz, J.R., Czabotar, P.E., D'Angiolella, V., Dawson, T.M., Dawson, V.L., De Laurenzi, V., De Maria, R., Debatin, K.M., DeBerardinis, R.J., Deshmukh, M., Di Daniele, N., Di Virgilio, F., Dixit, V.M., Dixon, S.J., Duckett, C.S., Dynlacht, B.D., El-Deiry, W.S., Elrod, J.W., Fimia, G.M., Fulda, S., Garcia-Saez, A.J., Garg, A.D., Garrido, C., Gavathiotis, E., Golstein, P., Gottlieb, E., Green, D.R., Greene, L.A., Gronemeyer, H., Gross, A., Hajnoczky, G., Hardwick, J.M., Harris, I.S., Hengartner, M.O.,

Hetz, C., Ichijo, H., Jaattela, M., Joseph, B., Jost, P.J., Juin, P.P., Kaiser, W.J., Karin, M., Kaufmann, T., Kepp, O., Kimchi, A., Kitsis, R.N., Klionsky, D.J., Knight, R.A., Kumar, S., Lee, S.W., Lemasters, J.J., Levine, B., Linkermann, A., Lipton, S.A., Lockshin, R.A., Lopez-Otin, C., Lowe, S.W., Luedde, T., Lugli, E., MacFarlane, M., Madeo, F., Malewicz, M., Malorni, W., Manic, G., Marine, J.C., Martin, S.J., Martinou, J.C., Medema, J.P., Mehlen, P., Meier, P., Melino, S., Miao, E.A., Molkentin, J.D., Moll, U.M., Munoz-Pinedo, C., Nagata, S., Nunez, G., Oberst, A., Oren, M., Overholtzer, M., Pagano, M., Panaretakis, T., Pasparakis, M., Penninger, J.M., Pereira, D.M., Pervaiz, S., Peter, M.E., Piacentini, M., Pinton, P., Prehn, J.H.M., Puthalakath, H., Rabinovich, G.A., Rehm, M., Rizzuto, R., Rodrigues, C.M.P., Rubinsztein, D.C., Rudel, T., Ryan, K.M., Sayan, E., Scorrano, L., Shao, F., Shi, Y.F., Silke, J., Simon, H.U., Sistigu, A., Stockwell, B.R., Strasser, A., Szabadkai, G., Tait, S.W.G., Tang, D.L., Tavernarakis, N., Thorburn, A., Tsujimoto, Y., Turk, B., Vanden Berghe, T., Vandenabeele, P., Heiden, M.G.V., Villunger, A., Virgin, H.W., Vousden, K.H., Vucic, D., Wagner, E.F., Walczak, H., Wallach, D., Wang, Y., Wells, J.A., Wood, W., Yuan, J.Y., Zakeri, Z., Zhivotovsky, B., Zitvogel, L., Melino, G., Kroemer, G., 2018. Molecular mechanisms of cell death: recommendations of the Nomenclature Committee on Cell Death 2018. Cell Death Differ. 25, 486-541.

Gomes, D.S., Pereira, M.D., Panek, A.D., Andrade, L.R., Araujo Eleutherio, E.C., 2008. Apoptosis as a mechanism for removal of mutated cells of *Saccharomyces cerevisiae*: the role of Grx2 under cadmium exposure. Biochim. Biophys. Acta 1780, 160-166.

Guaragnella, N., Zdralević, M., Antonacci, L., Passarella, S., Marra, E., Giannattasio, S., 2012. The role of mitochondria in yeast programmed cell death. Front. Oncol. 2, 1-8.

Horie, M., Nishio, K., Fujita, K., Kato, H., Nakamura, A., Kinugasa, S., Endoh, S., Miyauchi, A., Yamamoto, K., Murayama, H., Niki, E., Iwahashi, H., Yoshida, Y., Nakanishi, J., 2009. Ultrafine NiO particles induce cytotoxicity in vitro by cellular uptake and subsequent Ni(II) release. Chem. Res. Toxicol. 22, 1415-1426.

Hu, J., Wei, M., Mirisola, M.G., Longo, V.D., 2013. Assessing chronological aging in *Saccharomyces cerevisiae*. Methods Mol. Biol. 965, 463-472.

IARC, 1990. IARC monography on the evolution of carcinogenic risks to humans. International Agency for Research on Cancer, Lyon, France.

Karathia, H., Vilaprinyo, E., Sorribas, A., Alves, R., 2011. *Saccharomyces cerevisiae* as a model organism: a comparative study. PloS One 6, 1-10.

Kitagaki, H., Araki, Y., Funato, K., Shimoi, H., 2007. Ethanol-induced death in yeast exhibits features of apoptosis mediated by mitochondrial fission pathway. FEBS Lett. 581, 2935-2942.

Letavayová, L., Vlasáková, D., Spallholz, J.E., Brozmanová, J., Chovanec, M., 2008. Toxicity and mutagenicity of selenium compounds in *Saccharomyces cerevisiae*. Mutat. Res. 638, 1-10.

Ligr, M., Madeo, F., Frohlich, E., Hilt, W., Frohlich, K.U., Wolf, D.H., 1998. Mammalian Bax triggers apoptotic changes in yeast. FEBS Lett. 438, 61-65.

Ludovico, P., Rodrigues, F., Almeida, A., Silva, M.T., Barrientos, A., Corte-Real, M., 2002. Cytochrome c release and mitochondria involvement in programmed cell death induced by acetic acid in *Saccharomyces cerevisiae*. Mol. Biol. Cell 13, 2598-2606.

Ludovico, P., Sousa, M.J., Silva, M.T., Leão, C., Côrte-Real, M., 2001. *Saccharomyces cerevisiae* commits to a programmed cell death process in response to acetic acid. Microbiology 147, 2409-2415.

Madeo, F., Frohlich, E., Ligr, M., Grey, M., Sigrist, S.J., Wolf, D.H., Frohlich, K.U., 1999. Oxygen stress: a regulator of apoptosis in yeast. J. Cell Biol. 145, 757-767.

Madeo, F., Herker, E., Maldener, C., Wissing, S., Lachelt, S., Herian, M., Fehr, M., Lauber, K., Sigrist, S.J., Wesselborg, S., Frohlich, K.U., 2002. A caspase-related protease regulates apoptosis in yeast. Mol. Cell 9, 911-917.

Madia, F., Wei, M., Yuan, V., Hu, J., Gattazzo, C., Pham, P., Goodman, M.F., Longo, V.D., 2009. Oncogene homologue Sch9 promotes age-dependent mutations by a superoxide and Rev1/Pol zeta-dependent mechanism. J. Cell Biol. 186, 509-523.

Magaye, R., Zhao, J., 2012. Recent progress in studies of metallic nickel and nickel-based nanoparticles' genotoxicity and carcinogenicity. Environ. Toxicol. Pharmacol. 34, 644-650.

Manon, S., Chaudhuri, B., Guérin, M., 1997. Release of cytochrome c and decrease of cytochrome c oxidase in Bax-expressing yeast cells, and prevention of these effects by coexpression of Bcl-xL. FEBS Lett. 415, 29-32.

Martelli, A.M., Zweyer, M., Ochs, R.L., Tazzari, P.L., Tabellini, G., Narducci, P., Bortul, R., 2001. Nuclear apoptotic changes: an overview. J. Cell. Biochem. 82, 634-646.

Mazzoni, C., Falcone, C., 2008. Caspase-dependent apoptosis in yeast. Biochim. Biophys. Acta 1783, 1320-1327.

Mirisola, M.G., Braun, R.J., Petranovic, D., 2014. Approaches to study yeast cell aging and death. FEMS Yeast Res. 14, 109-118.

Munoz, A.J., Wanichthanarak, K., Meza, E., Petranovic, D., 2012. Systems biology of yeast cell death. Fems Yeast Res. 12, 249-265.

Nimse, S.B., Pal, D., 2015. Free radicals, natural antioxidants, and their reaction mechanisms. RSC Adv. 5, 27986-28006.

Novo, D.J., Perlmutter, N.G., Hunt, R.H., Shapiro, H.M., 2000. Multiparameter flow cytometric analysis of antibiotic effects on membrane potential, membrane permeability, and bacterial counts of *Staphylococcus aureus* and *Micrococcus luteus*. Antimicrob. Agents Chemother. 44, 827-834.

Pereira, C., Silva, R.D., Saraiva, L., Johansson, B., Sousa, M.J., Corte-Real, M., 2008. Mitochondria-dependent apoptosis in yeast. Biochim. Biophys. Acta 1783, 1286-1302.

Perry, S.W., Norman, J.P., Barbieri, J., Brown, E.B., Gelbard, H.A., 2011. Mitochondrial membrane potential probes and the proton gradient: a practical usage guide. Biotechniques 50, 98-115.

Pietruska, J.R., Liu, X., Smith, A., McNeil, K., Weston, P., Zhitkovich, A., Hurt, R., Kane, A.B., 2011. Bioavailability, intracellular mobilization of nickel, and HIF-1a activation in human lung epithelial cells exposed to metallic nickel and nickel oxide nanoparticles. Toxicol. Sci. 124, 138-148.

Pozarowski, P., Grabarek, J., Darzynkiewicz, Z., 2003. Flow cytometry of apoptosis. Curr. Protoc. Cytom. Chapter 7, Unit 7.19-Unit 17.19.

Richter, C., Park, J.W., Ames, B.N., 1988. Normal oxidative damage to mitochondrial and nuclear-DNA is extensive Proc. Natl. Acad. Sci. U S A 85, 6465-6467.

Rottenberg, H., Wu, S.L., 1998. Quantitative assay by flow cytometry of the mitochondrial membrane potential in intact cells. Biochim. Biophys. Acta 1404, 393-404.

Saquib, Q., Siddiqui, M.A., Ahmad, J., Ansari, S.M., Faisal, M., Wahab, R., Alatar, A.A., Al-Khedhairy, A.A., Musarrat, J., 2018. Nickel oxide nanoparticles induced transcriptomic alterations in HepG2 cells. Adv. Exp. Med. Biol. 1048, 163-174.

Siddiqui, M.A., Ahamed, M., Ahmad, J., Khan, M.A.M., Musarrat, J., Al-Khedhairy, A.A., Alrokayan, S.A., 2012. Nickel oxide nanoparticles induce cytotoxicity, oxidative stress and apoptosis in cultured human cells that is abrogated by the dietary antioxidant curcumin. Food Chem. Toxicol. 50, 641-647.

Smith, A., 2000. Oxford dictionary of biochemistry and molecular biology. Oxford University Press, Oxford, UK.

Sousa, C.A., Soares, E.V., 2014. Mitochondria are the main source and one of the targets of Pb (lead)-induced oxidative stress in the yeast *Saccharomyces cerevisiae*. Appl. Microbiol. Biotechnol. 98, 5153-5160.

loss of cell viability in yeast mediated by oxidative stress. Chem. Res. Toxicol. 31, 658-665.

Strich, R., 2015. Programmed cell death initiation and execution in budding yeast. Genetics 200, 1003-1014.

Vermes, I., Haanen, C., Steffensnakken, H., Reutelingsperger, C., 1995. A novel assay for apoptosis - flow cytometric detection of phosphatidylserine expression on early apoptotic cells using fluorescein-labeled Annexin-V. J. Immunol. Methods 184, 39-51.

Wissing, S., Ludovico, P., Herker, E., Buttner, S., Engelhardt, S.M., Decker, T., Link, A., Proksch, A., Rodrigues, F., Corte-Real, M., Frohlich, K.U., Manns, J., Cande, C., Sigrist, S.J., Kroemer, G., Madeo, F., 2004. An AIF orthologue regulates apoptosis in yeast. J. Cell Biol. 166, 969-974.

Wloch-Salamon, D.M., Bem, A.E., 2013. Types of cell death and methods of their detection in yeast *Saccharomyces cerevisiae*. J. Appl. Microbiol. 114, 287-298.

Xu, Y., Gu, Y., Qian, S.Y., 2012. An advanced electron spin resonance (ESR) spin-trapping and LC/(ESR)/MS technique for the study of lipid peroxidation. Int. J. Mol. Sci. 13, 14648-14666.

Yazgan, O., Krebs, J.E., 2012. Mitochondrial and nuclear genomic integrity after oxidative damage in *Saccharomyces cerevisiae*. Front. Biosci. 17, 1079-1093.

Chapter 6 - Metal(loid) oxide (Al_2O_3, Mn_3O_4, SiO_2 and SnO_2) nanoparticles cause cytotoxicity in yeast via intracellular generation of reactive oxygen species*

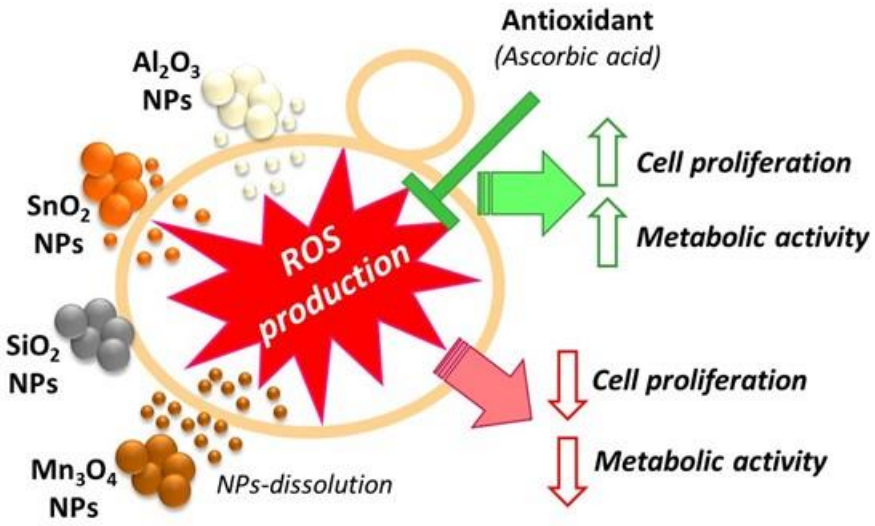

*Published in Applied Microbiology and Biotechnology (2019), DOI: 10.1007/s00253-019-09903-y

6.1. Introduction

MOx NPs constitute an important group of nanomaterials (Corr 2012; Klaine et al. 2013). The global market of MOx NPs was estimated to be between 280,000 to 1.3 million tons per year, which is led by Asian-Pacific (~34 %), North American (~30 %) and European (~30 %) market (Nanotech 2015). The analysts forecast that the global MOx NPs market is growing at a mean annual rate of 9.5 % during the period 2016-2020 (Research 2017).

MOx NPs present a wide range of applications being used in electronic devices, optic lenses, medicine (implants, cancer diagnosis, therapy and bio-imaging), personal care products, paints, coatings, water treatment, energy storage and fuel cells (Andreescu et al. 2012; Fei and Li 2010; Laurent et al. 2018; Nanotech 2015). Among the different MOx NPs, Al_2O_3, In_2O_3, Mn_3O_4, SiO_2 and SnO_2 NPs have been widely used. Al_2O_3 NPs are employed due to their chemical stability, mechanical strength and electrical insulation capacity (Nanotech 2015). In_2O_3 NPs are used in batteries as a substitute of mercury, in ceramics and electronics due to their optical and antistatic properties (AzoNano 2018; Laurent et al. 2018; Research 2018). Mn_3O_4 NPs are employed in capacitors because these nanoparticles present superior electrochemical properties (Tian et al. 2013). SiO_2 NPs present unique properties, such as mechanical, catalytic, magnetic and optical properties, which lead them to be used in paints, plastic, ceramics, batteries and cosmetics (Report 2018). Due to their semiconductor, electronic, optical and catalytic properties, SnO_2 NPs can be used in a variety of applications in industry, such as, solar cells, photo catalysis and sensors (Chavez-Calderon et al. 2016).

The increasing use of MOx NPs leads, inevitably, to an augmented concern related to its possible toxicity. Studies in soils showed that Al_2O_3, SiO_2 and SnO_2 NPs had an impact in bacterial and in fungal community (Chai et al. 2015; Chavez-Calderon et al. 2016; McGee et al. 2017). Other studies showed that Al_2O_3, Mn_3O_4 and SiO_2 NPs caused growth inhibition of bacteria (*Escherichia coli* and *Staphylococcus aureus*), alga *(Pseudokirchneriella subcapitata*) and protozoa (*Tetrahymena thermophila and Paramecium multimicronucleatum)*, and bioluminescence reduction of the bacterium *Vibrio fischeri* (Aruoja et al. 2015; Li et al. 2012). SnO_2 NPs caused a reduction of cell viability and provoked the damage of cell membrane in the bacteria *E. coli* and *Bacillus subtilis* (Chavez-Calderon et al. 2016).

To better understand the toxic modes of action of the MOx NPs, the use of a cell model is crucial. Despite the emerging commercial importance of NPs, a very limited information has been published regarding the toxicity of the NPs studied in the present Chapter. As far as we know, the toxicity of these NPs remains poorly investigated and their toxicity mechanisms are not elucidated, as well.

Taking into account these facts, the main aim of the present Chapter was to evaluate the toxic effects of five NPs (Al_2O_3, In_2O_3, Mn_3O_4, SiO_2, SnO_2) using the yeast *Saccharomyces cerevisiae* as a cell model. The impact of NPs was tested up to 100 mg/L as it is the maximum limit of concentration, advised by the Organization for Economic Co-operation and Development (OECD), for testing toxicity (OECD 2011). The NPs toxicity was evaluated under growing conditions on yeast-extract-peptone (YEP) broth (growth inhibition assay) or in a buffer medium (cell viability assay). In order to obtain a mechanistic approach of the toxic impact of NPs on yeast cells, plasma membrane integrity, metabolic activity and intracellular accumulation of reactive oxygen species (ROS) was assessed. To further evaluate the role of the oxidative stress (OS) on the cytotoxicity induced by MOx NPs, yeast cells were co-exposed to NPs and an anti-oxidant (ascorbic acid). Then, the cell viability, esterase activity and intracellular ROS accumulation was accessed and compared. Together the studies here presented allow to characterize the possible hazard of these NPs.

6.2. Materials and Methods

6.2.1. NPs characteristics and stock suspensions preparation

The main characteristics of Al_2O_3, In_2O_3, Mn_3O_4, SiO_2 and SnO_2 NPs used in the present Chapter (namely, purity, particle size and surface area) can be found in Table 6.1. The purity of NPs was determined by their digestion with aqua regia, as previously described in Chapter 3; metals (Al, In, Mn and Sn) content was determined by atomic absorption spectroscopy with flame atomization (AAS-FA) in an Analytik Jena novAA 350 spectrometer (Analytik Jena; Jena, Germany).

NPs stock suspensions at 0.5 g/L were prepared in deionized water. The suspensions were vigorously shaken, sonicated for 15 minutes in an ultrasonic bath (80 – 160 W; Bandelin, Sonorex RK 100; Berlin, Germany) and sterilized by UV light, as previously described in Chapter 3. NPs stock suspensions were stored in the dark for up to 1 month, at 4 ºC. Before use, NPs stock suspensions were shaken and sonicated as described above.

6.2.2. Characterization of NPs suspensions in different media

In the characterization of the MOx NPs, the hydrodynamic size (Z-average diameter) and the zeta potential were measured in deionized water (stock suspensions), yeast-extract-peptone (YEP) broth [5 g/L yeast extract (Difco-BD), 5 g/L peptone (Difco-BD) and 10 g/L glucose (Merck)] or in 10 mmol/L 2-(N-morpholino) ethanesulfonic acid buffer (MES, Sigma-Aldrich) with 20 g/L glucose (Merck), pH 6.0.

Table 6.1. Characteristics of the nanoparticles used in this Chapter.

NP	Molecular Mass (g/mol)	Purity (%)	Particle size (nm)	Surface area (m^2/g)	Company	Reference
Al_2O_3	101.96	99.5 ± 1.0[a]	<50 (TEM)[b]	>40[b]	Sigma-Aldrich	544833
In_2O_3	277.63	99.3 ± 1.1[a]	<100 (TEM)[b]	n.d.	Sigma-Aldrich	632317
Mn_3O_4	228.82	99.1 ± 1.0[a]	30 (TEM)[b]	65[b]	abcr GmbH	101631
SiO_2	60.08	99.5[b]	10-20 (BET)[b]	n.d.	Sigma-Aldrich	637238
SnO_2	150.71	99.6 ± 0.9[a]	<100 (TEM)[b]	47.2[c]	Sigma-Aldrich	549657

[a]Determined in this Chapter. The data correspond to the mean values and standard deviations of seven independent experiments performed in duplicate (n=14).
[b]According to the manufacturer.
[C]Source: Masuda et al. 2010.
BET: Brunauer-Emmett-Teller. n.d.: not determined or information not available. TEM: transmission electron microscopy.

MOx NPs were suspended at a final concentration of 100 mg/L and incubated in the same conditions of the assays with yeast cells, as described below. The Z-average diameter and the zeta potential were measured using a Zetasizer Nano ZS (Malvern Instruments; Malvern, UK), coupled with Zetasizer Software version 7.11, as previously described in Chapter 3.

MOx NPs agglomeration was also characterized by a sedimentation assay (Aruoja et al. 2015; Hartmann et al. 2013; OECD 2017). For this purpose, NPs were suspended in YEP or MES buffer, at a final concentration of 100 mg/L and agitated at 150 rpm for 24 h, at 30 °C, in the absence of yeast cells. For a given incubation time, the turbidity of the samples were monitored by spectrophotometric measurement of the absorbance at 600 nm, for 60 min. The percentage of initial OD_{600} after 60 min was calculated according to Eq. 6.1:

$$\% \text{ of initial } OD_{600} \text{ after 60 min} = (OD_t/OD_i) \times 100 \quad (6.1)$$

where OD_t is the OD_{600} after 60 min of settling and OD_i is the OD_{600} at zero time. The % of initial OD_{600} after 60 min calculated was plotted against the NPs incubation time.

6.2.3. Dissolution of NPs in different media

The stability of NPs was evaluated by quantifying the metal(loid)s dissolved in YEP or MES buffer. As control, the metal(loid)s dissolved in deionized water (pH 6.0) were also quantified. NPs were suspended in the different media, at 100 mg/L, and incubated in the conditions described below (please see section 6.2.5). After 24 h, samples were taken and centrifuged at 20,000 x *g*, for 30 minutes, at 25 ºC. Then, Al, In, Mn and Sn ions were determined in the supernatants by AAS-FA. Si was determined by inductively coupled plasma-optical emission spectrometry (ICP-OES) in an iCAP 7000 Series Spectrometer (Thermo Fisher Scientific, Cambridge, UK); Si standard stock solution of 1000 mg/L Si was obtained from Sigma-Aldrich.

6.2.4. Strain, medium and growth conditions

The yeast *S. cerevisiae* BY4741 was used in this Chapter. The strain was obtained from EUROSCARF collection (Frankfurt, Germany) and maintained at 4 ºC on YEP agar [YEP broth with 20 g/L agar (Merck)].

The pre–cultures and cultures were obtained as described before in Chapter 3.

6.2.5. Yeast exposure conditions

The toxic effects induced by Al_2O_3, In_2O_3, Mn_3O_4, SiO_2 or SnO_2 NPs on yeast cells were evaluated. In addition, the toxic impact caused by the respective metal ions (in the case of Al_2O_3, In_2O_3, Mn_3O_4 and SnO_2 NPs) was compared. The stock solutions of the metals used were: $Al(NO_3)_3$ (1000 mg/L, Merck), $In(NO_3)_3$ (1000 mg/L, Sigma-Aldrich), $MnCl_2$ (2000 mg/L, Merck) and $SnCl_4$ (1000 mg/L, Merck). Due to the high affinity of Si to oxygen, the chemical behavior of Si (a metalloid) is different from the metals (Hirner and Flaßbeck 2005). Thus, the dissolution of SiO_2, in water, originate the forming of orthosilicic acid, $Si(OH)_4$ (Iler 1978), which is silicon tetrahedrally co-ordinated to four hydroxyl groups (Perry et al. 2003). Therefore, experiences with Si, similar to those performed with metal ions, could not be done.

Yeast cells were exposed to chemicals in YEP broth (yeast growth inhibition assay) or in 10 mmol/L MES buffer, pH 6.0, with 20 g/L glucose (yeast viability assay). In yeast growth inhibition assay, test tubes containing 1.0 mL of double-strength YEP broth was inoculated with yeasts, in exponential

phase of growth, at $1x10^6$ cells/mL; different concentrations of each NP or the respective metals were also added: 50, 75 and 100 mg/L MOx NPs or 1.25, 3.12, 6.25, 12.5, 25 and 50 mg/L of the respective metals (toxicants final concentrations). The total volume of each assay (2.0 mL) was adjusted with sterile deionized water. Biotic (yeast cells without toxicants) and abiotic controls (NPs suspensions, at the same concentrations used in the biotic assays, in the culture medium, without yeast cells) were also prepared. Cultures and controls were incubated at 30 ºC. After 24 h, the optical density at 600 nm was measured and corrected considering the respective abiotic control. The yeast cell response (growth reduction) was evaluated as a function of the concentration of the toxic agent using as comparison the growth of non-exposed cells (biotic control). The test endpoint is the percentage of growth, expressed as cell yield, in a similar way to that proposed by the OECD for the evaluation of the toxicity of chemical substances using algae or cyanobacteria (OECD 2011); cell yield is defined as the cell concentration at 24 h minus the cell concentration at the start of the assay.

Alternatively (yeast viability assay), cells in exponential phase of growth were suspended ($1x10^7$ cells/mL) in MES buffer with glucose and incubated without (control) or with the MOx NPs (50, 75 and 100 mg/L) or the respective metals (0.125, 1.25, 3.12, 6.25, 12.5 mg/L), at 30 ºC, 150 rpm. The assay was carried out in 100-mL Erlenmeyer flasks with a final volume of 20 mL. After the exposure to toxicants for 24 h, samples were taken (two replicates), serially diluted with sterile deionized water and dispersed over YEP agar surface (from the convenient dilution) in duplicate for each replica. The cultures were incubated for 3-5 days at 30 ºC. Colony-forming units (CFU) per millilitre were determined from the number of colonies formed and the sample dilution. After this period of incubation, no further CFUs appeared. As toxicity endpoint, the cell viability was determined considering the number of colony-forming unit (CFU)/mL, at zero time, as reference (100 %).

The effect concentration (EC) values of the metals in YEP or MES buffer were determined. EC_{10}, EC_{25}, EC_{50}, EC_{75} and EC_{90} values represent the concentration of metal ions that induce the inhibition of 10, 25, 50, 75 or 90 %, respectively, of yeast growth in YEP (growth inhibition assay) or the reduction of cell viability in MES buffer (cell viability assay), after 24 h. The EC values were calculated using the linear interpolation method (TOXCALC version 5.0.32, Tidepool Scientific Software).

The toxic effects of MOx NPs supernatants were also evaluated. For this purpose, yeast cells were exposure to 100 mg/L MOx NPs in MES buffer with glucose, in 100-mL Erlenmeyer flasks. Cell suspensions were agitated at 150 rpm, at 30 ºC. After 24 h of incubation, cells were harvested by centrifugation (20,000 ×*g*, 30 min, 25 °C) and the clear supernatants carefully collected. Then, yeast cells in exponential phase of growth at $1x10^7$ cells/mL were exposed to MOx NPs supernatants, in

100-mL Erlenmeyer flasks. Cell suspensions were incubated at 30 ºC, 150 rpm, for 24 h and the viability determined as described above.

The influence of L-ascorbic acid (AA), an antioxidant, on MOx NPs toxicity was evaluated by pre-incubation of yeasts, in exponential phase of growth, at $1x10^7$ cells/mL, in MES buffer with glucose and 10 mmol/L AA (Merck) for 30 min before the exposure to MOx NPs. Cell suspensions were incubated in the same conditions described above. After 24 h of incubation, cell viability was evaluated as described above.

6.2.6. Staining procedures

Cell membrane integrity was evaluated using propidium iodide (PI, Sigma-Aldrich), as described in Chapter 4. Cells were exposed to 100 mg/L MOx NPs, for 24 h, at 30 ºC, as described above. Cells were analysed, using an epifluorescence microscope (Leica Microsystems; Wetzlar GmbH, Germany) equipped with a HBO 100 mercury lamp and the I3 filter set from Leica. In each condition tested, at least 200 cells were counted, in duplicate (total ≥400 cells) in randomly selected microscope fields.

Metabolic activity of yeast cells was assessed using the fluorescent dyes fluorescein diacetate (FDA, Sigma-Aldrich) or 2-chloro-4-(2,3-dihydro-3-methyl-(benzo-1,3-thiazol-2-yl)-methylidene)-1-phenylquinolinium iodide (FUN-1, Molecular Probes, Invitrogen), as described in Chapter 3. Cells were analysed by fluorescence microscopy, as described above, for cell membrane integrity. Hydrolyse of FDA (esterase activity) was also quantified, as described in Chapter 3. Fluorescence (in relative fluorescence units, RFU) was quantified in a microplate reader at fluorescence excitation wavelength of 485/14 nm and an emission of 535/25 nm (PerkinElmer, Victor^3).

Intracellular generation of ROS was monitored with 20 µmol/L 2´,7´-dichlorodihydrofluorescein diacetate (H_2DCFDA, Sigma-Aldrich), at 25 °C for 10 min, as described in Chapter 3. After 24 h, cells were placed in quadruplicate in 96-well flat microplate and the fluorescence was measured as described for esterase activity (hydrolysis of FDA).

For the determination of ROS in abiotic conditions, H_2DCFDA was deacetylated to H_2DCF as previously described (Aruoja et al. 2015). MOx NPs were incubated in MES buffer with glucose for 24 h, in the same conditions of the biotic assays. Then, samples (100 µL) were mixed with equal volume of 52 µmol/L H_2DCF solution, incubated for 45 min in the dark at 25 ºC and the fluorescence quantified in a microplate reader as described in Chapter 4. Blank and positive control were prepared by replacing the sample by equal volume of MES or 26 µmol/L H_2O_2, respectively. Abiotic ROS was expressed as the ratio of fluorescence of the samples/fluorescence of the blank.

6.2.7. Reproducibility of the results and statistical analysis

Z-average diameter and zeta potential measurements were determined in duplicate; in each determination, at least ten measurements were performed. All others studies were repeated at least three times, in duplicate ($n \geq 6$). The data reported are mean values ± standard deviation (SD). The mean values were subjected to unpaired *t* test or one-way ANOVA followed by Tukey-Kramer multiple comparison method; *P* values <0.05 were considered statistically significant.

6.3. Results

6.3.1. Characterization of NPs suspended in different media

The characteristics of the MOx NPs studied, namely purity, particle size (in powder), and surface area are presented in the Table 6.1. To further characterize the main physico-chemical properties of the NPs suspended in different media (MES buffer with glucose or YEP broth), the following properties were evaluated: agglomeration (Z-average diameter), surface charge (zeta potential) and solubility (quantification of the metal(loid) dissolved from the NPs). The assays were performed in the absence of yeast cells but in the same conditions of the biotic assays (with yeast cells). For comparative purposes, NPs were suspended in deionized water and the same properties were evaluated.

At zero time (immediately after the suspension in a given medium), the NPs studied, except SnO_2, presented a hydrodynamic size (Z-average diameter), in aqueous media tested, between 600 and 1400 nm (Fig 6.1A). Since the NPs tested, when in powder, presented a size <100 nm, according to the manufacturers (Table 6.1), these results suggest an immediate agglomeration of the NPs, when suspended in aqueous media. The Z-average diameter of In_2O_3, Mn_3O_4 and SiO_2 NPs were similar, in all media tested. The Z-average diameter of Al_2O_3, in MES buffer, and SnO_2 in both media (YEP or MES buffer) were higher than in deionized water (Fig 6.1A). The agglomeration of the NPs increased through the 24 h of incubation period, in both media, being particularly notorious in MES buffer (Fig. 1A). After 24 h, the agglomerates of Al_2O_3, In_2O_3, Mn_3O_4 and SnO_2 NPs could be seen with the naked eye in MES buffer (Fig 6.2). These observations were further confirmed through the measurement of NPs sedimentation profiles (Fig 6.3). In YEP, MOx NPs were more stable, which was translated by a lower sedimentation capacity over time (Fig 6.3); in this medium, the NPs agglomeration was not evident and the formation of agglomerates could not be seen with the naked eye.

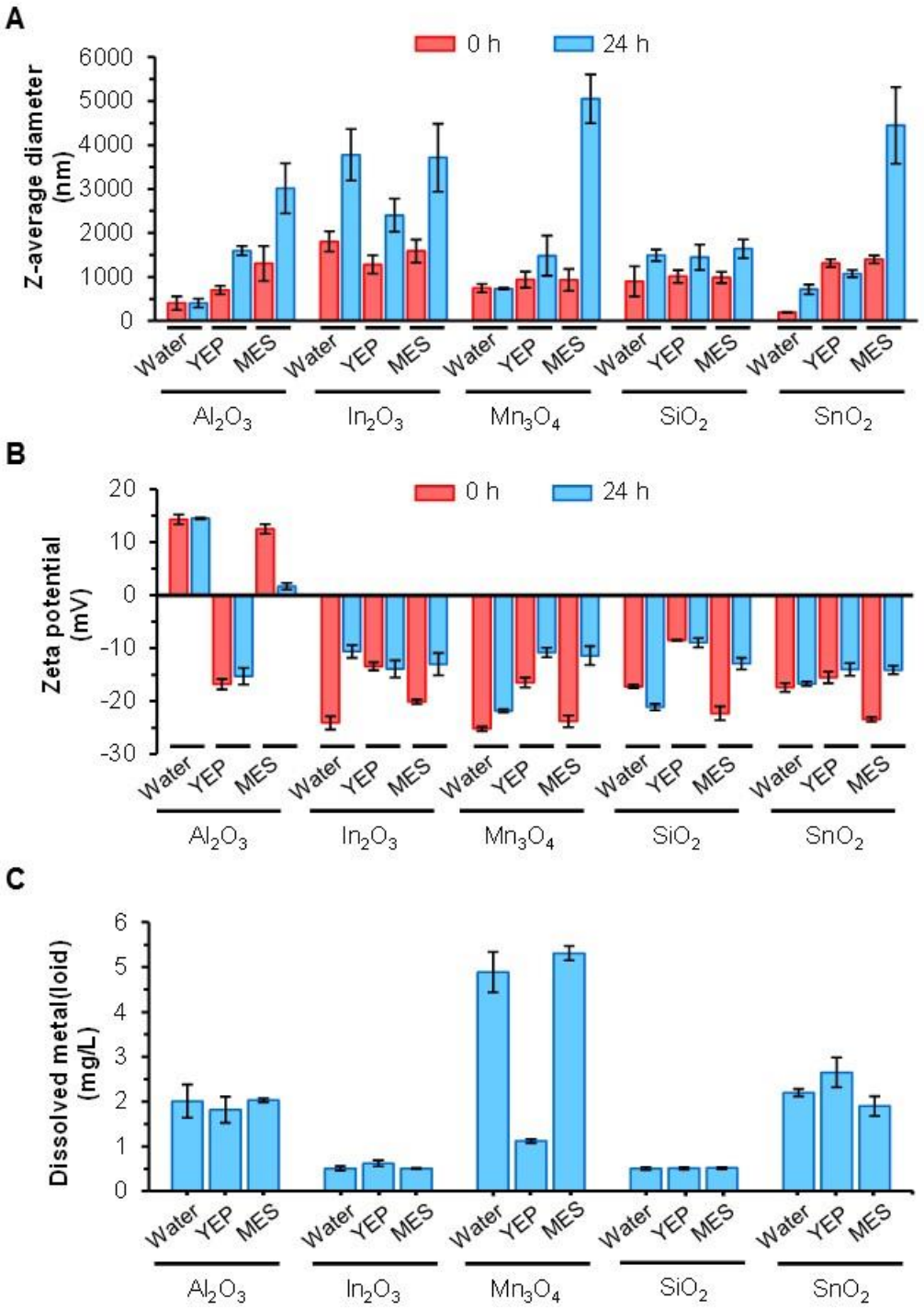

Figure 6.1. Nanoparticles properties in aqueous suspension. NPs were suspended at 100 mg/L in water, YEP or 10 mmol/L MES buffer, in the absence of yeast cells, and were incubated at 150rpm for 24 h. A – Z-average diameter. B – Zeta potential. C – Dissolved metal(loid) from the NPs after 24 h of incubation. The data represent the mean values of at least three independent experiments, performed in duplicate (n≥6); standard deviations are presented (vertical error bars).

All NPs studied presented a negative zeta potential (between – 9 and -26 mV), except Al_2O_3 in water and in MES buffer (~14 mV) (Fig 6.1B). For all NPs, the zeta potential values remained similar or become less negative after 24 h of incubation (-9 to -22 mV), except Al_2O_3 in MES buffer which become less positive (~2 mV) and SiO_2 in water which become more negative (-21 mV). These results indicate that NPs formed relatively instable suspensions, which is compatible with the observed agglomeration.

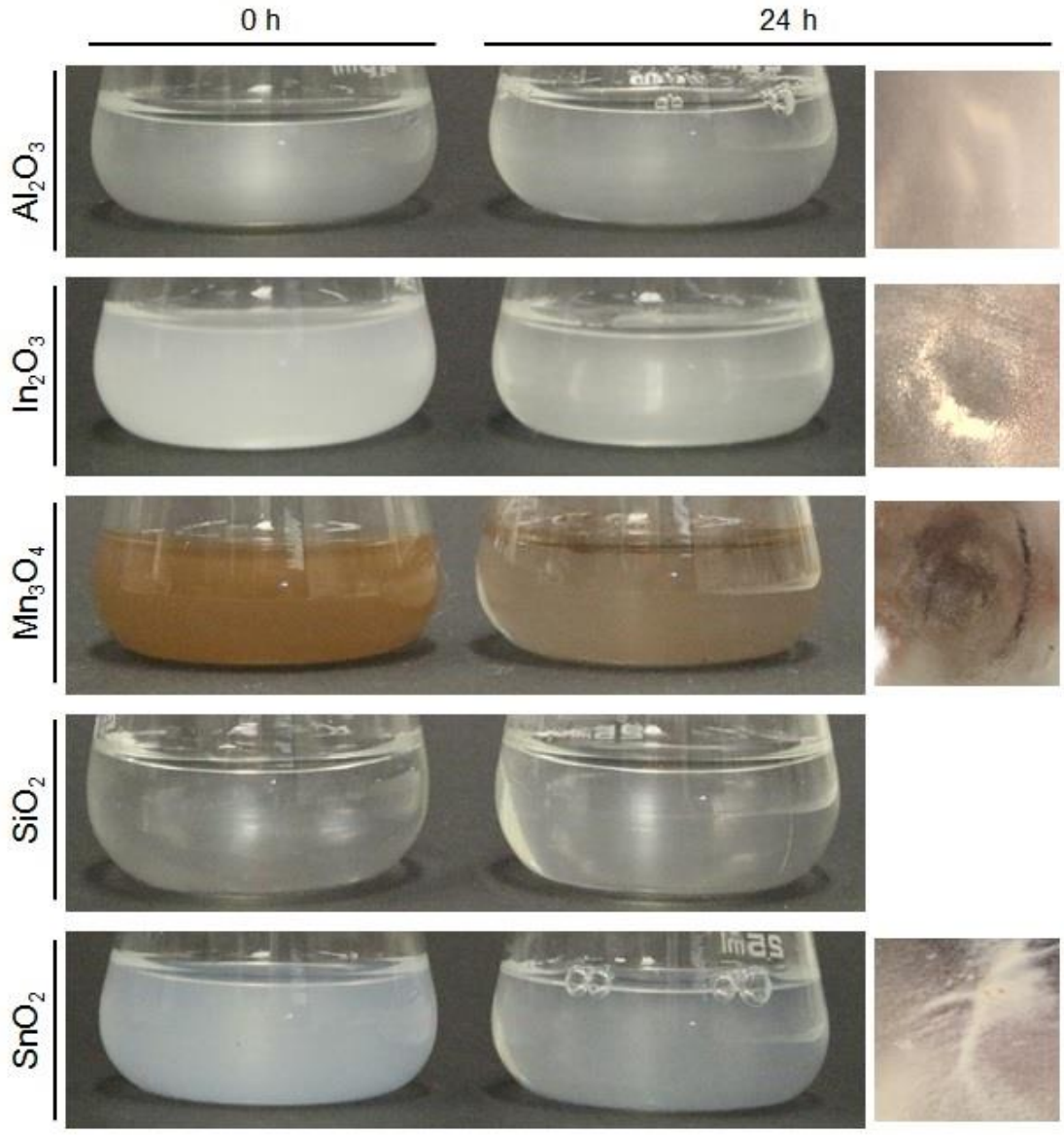

Figure 6.2. Nanoparticles suspensions in MES buffer. The NPs were suspended at a final concentration of 100 mg/L and agitated at 150 rpm for 24 h, at 30 ºC. Right-side images: bottom of the Erlenmeyer flasks after 24 h of incubation.

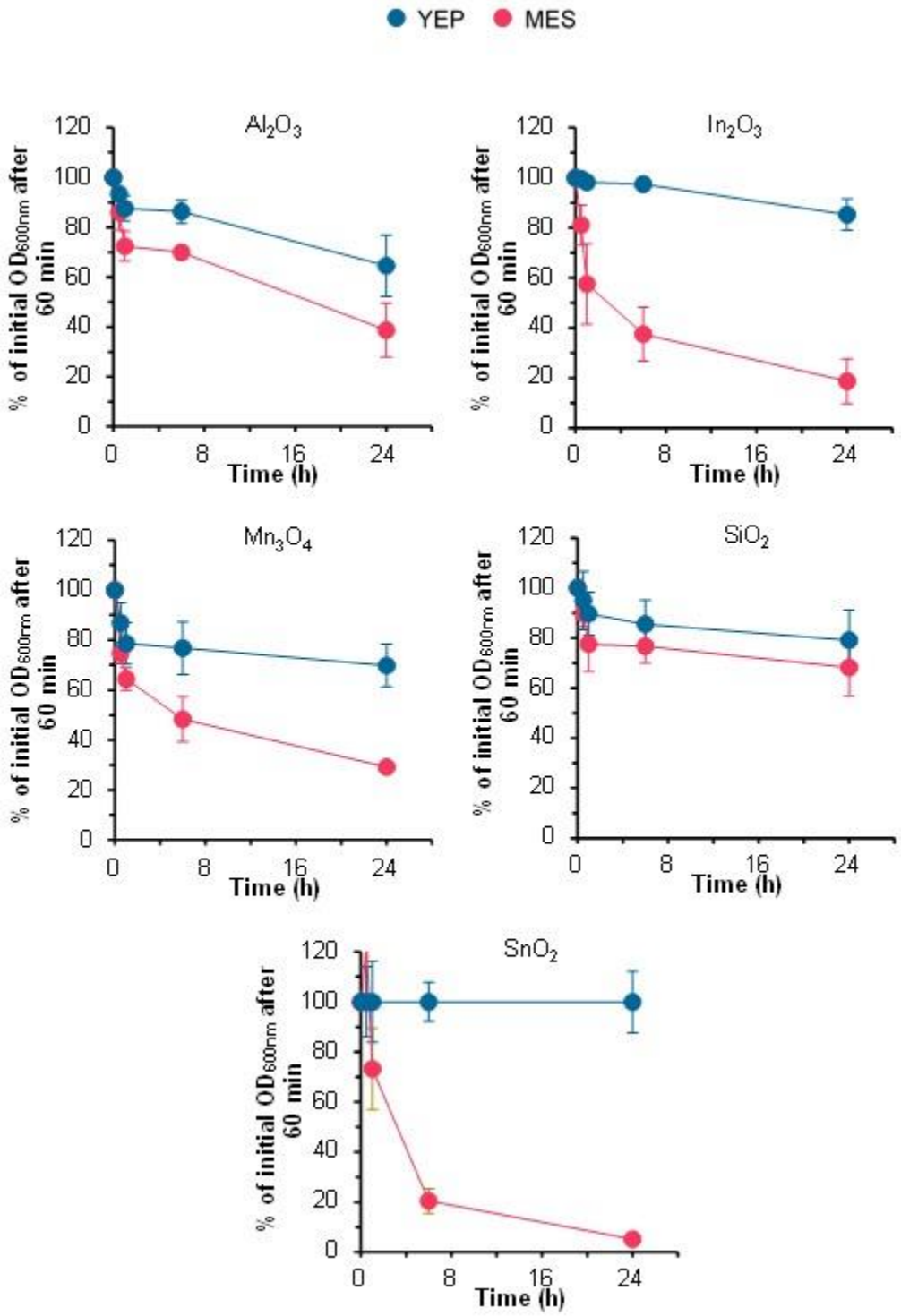

Figure 6.3. Sedimentation profiles of the nanoparticles in different media. The NPs were suspended in YEP or MES buffer, at a final concentration of 100 mg/L and agitated at 150 rpm for 24 h, at 30 °C. The data are presented as mean values from at least three independent experiments performed in duplicate (n≥6); standard deviations (SD) are presented (vertical error bars); where no error bars are shown, SD are within the points.

The amount of metal(loid) released from the NPs, in the absence of yeast cells, in the different media, was low (<6 mg/L) (Fig 6.1C). Similar results were observed, in YEP broth or MES buffer, in the presence of yeasts (Fig 6.4), which suggests that the presence of cells did not interfere with NPs dissolution. These results indicated that the NPs were poorly soluble (<8 %) in MES buffer or YEP broth (Table 6.2).

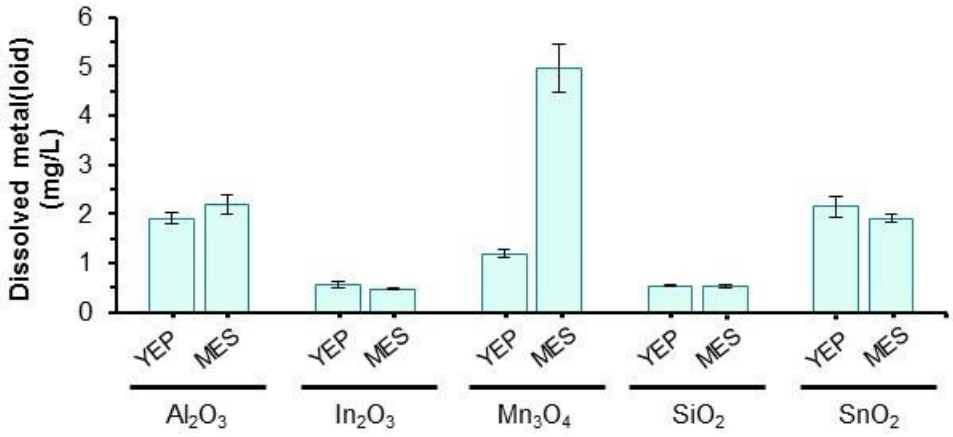

Figure 6.4. Influence of yeast cells on nanoparticles dissolution. NPs were suspended at 100 mg/L in YEP broth or 10 mmol/L MES buffer, in the presence of yeast cells, and were incubated at 150 rpm for 24 h. The data represent the mean values of at least three independent experiments, performed in duplicate (n≥6); standard deviations are presented (vertical error bars).

6.3.2. Impact of the NPs and respective ions on the growth and cell viability

As a first approach, the toxic effect of the NPs over the yeast *S. cerevisiae* was assessed through a 24 h growth inhibition assay, in rich medium (YEP). The presence of the NPs did not affect, significantly, the yeast growth (Fig 6.5A). As reported above (Fig 6.1C), Al_2O_3, In_2O_3, Mn_3O_4 and SnO_2 NPs release metal ions (NPs dissolution). Thus, for comparative purposes, the effect of the respective metal ions on yeast growth was also evaluated. Aluminium, indium and tin presented similar growth inhibition profiles (Fig 6.5B), which was translated by similar 24h-EC_{50} values (10-13 mg/L) (Table 6.3). Manganese was the less toxic (Fig 6.5B), with a 24h-EC_{50} value of 21 mg/L (Table 6.3).

Another strategy to evaluate the NPs toxicity consisted in the incubation of yeast cells with the chemicals, in a buffer (10 mmol/L MES buffer, at pH 6.0, containing 20 g/L glucose). NPs toxicity was evaluated through a clonogenic assay: determination of the ability of the NPs-exposed yeasts to form colonies on YEP agar, without toxicant. Except In_2O_3, the other MOx NPs induced a significant loss of cell viability, in a dose-dependent manner (Fig 6.5C). The exposure of yeast cells to 100 mg/L of Al_2O_3, Mn_3O_4, SiO_2 and SnO_2 NPs, for 24 h, reduced the cell viability to 50-70 % (Fig 6.5C).

Table 6.2. Percentage of nanoparticles solubilisation in YEP broth or MES buffer.

	Solubilisation (%)			
	Without yeast cells		With yeast cells	
Nanoparticle	**YEP**	**MES**	**YEP**	**MES**
Al_2O_3	7.06 ± 0.32	4.03 ± 0.09	7.14 ± 0.15	4.11 ± 0.25
In_2O_3	0.62 ± 0.07	0.64 ± 0.03	0.57 ± 0.07	0.68 ± 0.04
Mn_3O_4	1.54 ± 0.04	7.29 ± 0.13	1.63 ± 0.09	6.81 ± 0.67
SiO_2	1.09 ± 0.06	1.11 ± 0.05	1.15 ± 0.02	1.13 ± 0.04
SnO_2	3.35 ± 0.42	2.46 ± 0.29	2.71 ± 0.27	2.42 ± 0.11

The NPs were suspended in YEP broth or MES buffer at a final concentration of 100 mg/L and agitated at 150 rpm for 24 h, at 30 ºC, in the absence or the presence of yeast cells. The data correspond to the mean values and standard deviations of three independent experiments performed in duplicate (*n*=6).

The metals ions correspondent to the NPs (Al, In, Mn and Sn) induced the loss of cell viability (Fig 6.5D) and displayed 24h-EC_{50} values between 0.8 and 2.7 mg/L (Table 6.3). These values were about ten times lower that those observed in rich medium (YEP) (Table 6.3).

Table 6.3. Effect concentration (EC) values of the metals corresponding to the nanoparticles studied.

		24h-EC values (mg/L)				
Metal	**Medium**	EC_{10}	EC_{25}	EC_{50}	EC_{75}	EC_{90}
Al^{3+}	YEP	5.6 ± 0.6	8.3 ± 0.4	13 ± 1	19.4 ± 0.2	24 ± 1
In^{3+}		1.7 ± 0.1	2.7 ± 0.2	11 ± 1	19.6 ± 0.5	25 ± 1
Mn^{2+}		7.8 ± 1.0	14.0 ± 1.1	21 ± 1	34.9 ± 2.6	47 ± 1
Sn^{4+}		4.9 ± 0.2	7.1 ± 0.1	10.0 ± 0.1	14.6 ± 0.3	21.8 ± 0.2
Al^{3+}	MES	0.15 ± 0.01	0.23 ± 0.01	1.7 ± 0.1	3.2 ± 0.1	3.9 ± 0.1
In^{3+}		0.22 ± 0.01	0.38 ± 0.01	0.86 ± 0.02	1.8 ± 0.1	2.8 ± 0.1
Mn^{2+}		0.19 ± 0.01	0.34 ± 0.01	0.83 ± 0.02	1.4 ± 0.1	1.6 ± 0.1
Sn^{4+}		0.94 ± 0.2	1.7 ± 0.1	2.7 ± 0.1	4.5 ± 0.2	10 ± 1

EC_{10}, EC_{25}, EC_{50}, EC_{75} and EC_{90} values represent the metal concentration that reduced cell viability in MES buffer (cell viability assay) or inhibited the growth of yeast cells in YEP (growth inhibition assay), after 24 h, by 10, 25, 50, 75 or 90 %, respectively. The data correspond to the mean values and standard deviations of three independent experiments performed in duplicate (n=6).

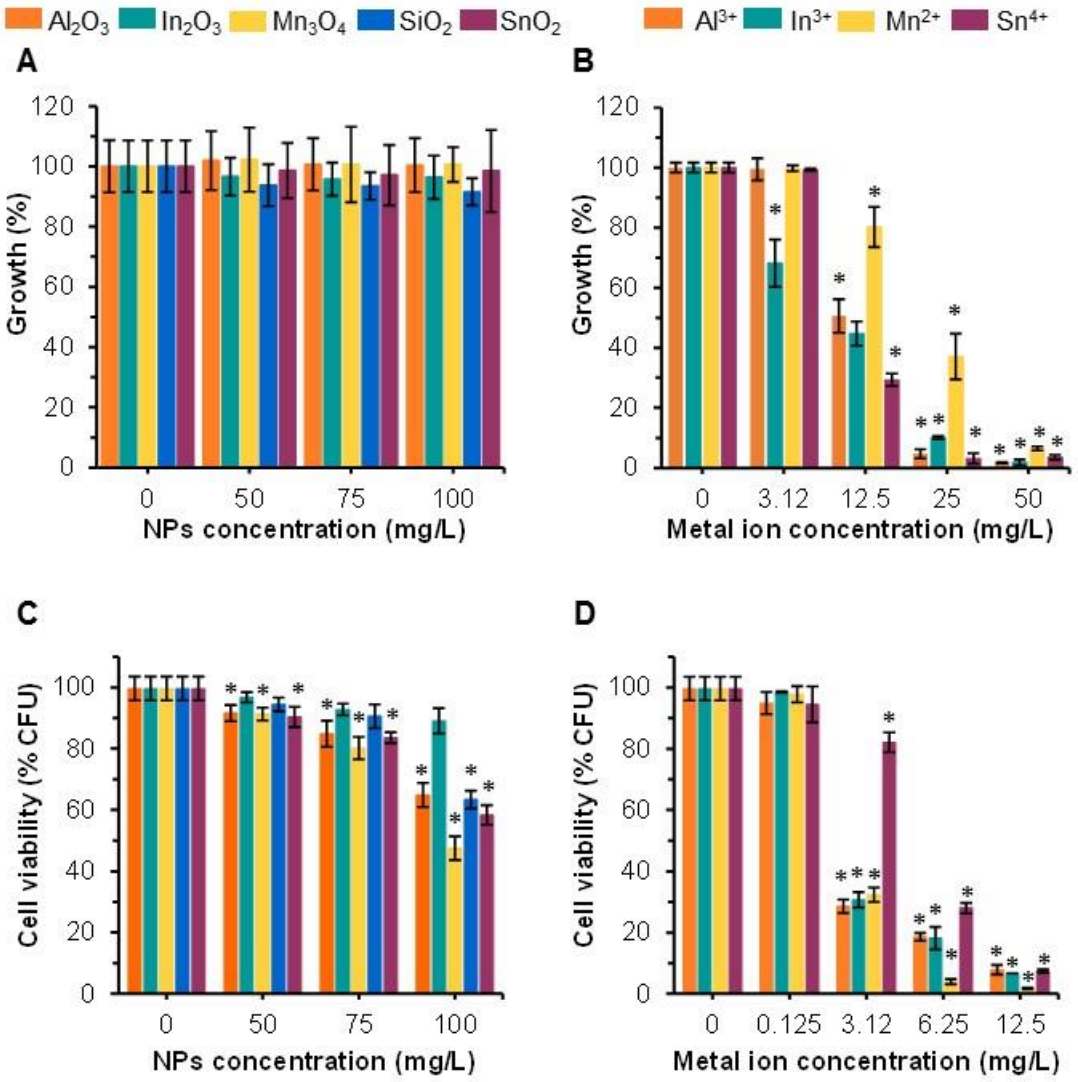

Figure 6.5. Impact of the nanoparticles and respective metal ions on yeast growth and cell viability. Yeast cells were exposed to the different toxicants in YEP broth (A and B) or in MES buffer (C and D) and the growth (growth inhibition assay) or the cell viability (colony forming units, CFU, counting) was assessed after 24 h. The data are presented as mean values from at least three independent experiments performed in duplicate (n≥6); standard deviations are presented (vertical error bars). Mean values are significantly different: *P<0.05 in comparison with untreated cells (control); unpaired t test.

6.3.2. Where does the toxicity of the NPs come from?

To investigate whether the toxicity observed was due to the nanoparticles, to the chemical species released (NPs solubilisation) or to the combination of both, the loss of cell viability induced by the NPs at 100 mg/L was compared with the toxicity associated to the respective supernatants, which contained the metal(loid)s released by the NPs. The comparative analysis revealed that the toxicity of SiO_2 NPs was mainly caused by the NPs themselves, as the supernatant had no impact on the cell

viability (Fig 6.6). For both Al_2O_3 and SnO_2 NPs, the toxicity was higher than the corresponding supernatants (Fig 6.6), which indicated that the NPs contributed, partially, to the observed toxicity. Thus, for Al_2O_3 and SnO_2 NPs, the loss of yeast cell viability could be attributed to both the NPs and the respective released ions from the NPs. Mn_3O_4 NPs supernatant had a higher toxicity effect than the NPs, which suggested that the toxicity of the NPs can be mainly caused by the released Mn ions while the contribution of the Mn_3O_4 NPs to the loss of cell viability could be, practically, neglected (Fig 6.6). The assessment of the impact of the ionic metals, corresponding to the amount of metal dissolved from 100 mg/L NPs, showed a similar toxic effect to the one observed for the respective NPs supernatant (Fig 6.6), which confirmed that the impact of the NPs supernatant was related to the release of the ions by the NPs.

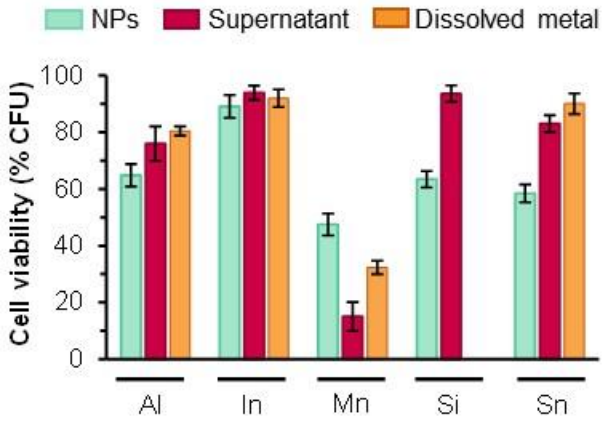

Figure 6.6. Comparison of the effect of the nanoparticles, the respective supernatants or by the dissolved metal on yeast cells. Yeasts were exposed for 24 h to the different NPs (100 mg/L), in MES buffer, or to the respective supernatants or to the respective dissolved metal. Cell viability was evaluated by colony forming units (CFU) counting. The data are presented as mean values from at least three independent experiments performed in duplicate (n≥6); standard deviations are presented (vertical error bars).

6.3.3. Possible cellular targets of NPs

To evaluate the possible cytotoxic effects of the NPs, the cell membrane integrity and the metabolic activity of yeast cells exposed for 24 h to NPs, in MES buffer, were assessed.

Membrane integrity was evaluated using a dye (PI) exclusion assay: cells with an intact plasma membrane are not able to accumulate PI; they were PI negative cells (Hewitt and Nebe-Von-Caron 2001). All NPs studied, up to 100 mg/L, did not provoke a significant modification of plasma membrane integrity, as ~100 % of cells remained PI negative (Fig 6.7A).

Metabolic health of yeast cells was assessed using a FUN-1 dye processing assay (Millard et al. 1997) and a fluorescein diacetate (FDA)-based cell esterase activity assay (Breeuwer et al. 1995).

Metabolically active cells are able to process FUN-1 dye, forming cylindrical intravacuolar structures, CIVs (orange-red structures), as showed before in Chapter 3. With the exception of In_2O_3, the NPs studied induced a small but significant reduction of the % of cells with the ability to process the FUN-1 dye (Fig 6.7B). Metabolic active cells were able to hydrolyse FDA (FDA+ cells). The exposure of yeast cells to MOx NPs caused a reduction of the percentage of FDA positive cells, except for In_2O_3 (Fig 6.7C). The nonfluorescent FDA substrate is hydrolysed, by the action of nonspecific intracellular esterases, into a fluorescent product (fluorescein) and two acetate molecules (Breeuwer et al. 1995). The decrease of the green fluorescence can be used as an indicator of the reduction of esterase activity. The quantification of green fluorescence exhibited by yeast cells loaded with FDA and exposed to MOx NPs revealed that Al_2O_3 and Mn_3O_4 induced the higher reduction of esterase activity, followed by SnO_2 and SiO_2 (Fig 6.7D). All together, these results indicate that the exposure to all NPs studied, except In_2O_3, induce a reduction of the metabolic activity in yeasts, in the absence of loss of membrane integrity.

6.3.4. Relationship between the ROS generation and the NPs cytotoxicity

The ability of NPs and/or their respective metal ions to generate ROS in abiotic conditions (cell free) was evaluated. For this end, a test was performed in which the NPs at 100 mg/L were incubated in MES buffer, for 24 h. ROS generation was evaluated using the general redox sensor H_2DCFDA, deacetylated (H_2DCF) (Tarpey et al. 2004; von Moos et al. 2016). The evaluated NPs were not able to generate ROS under abiotic conditions (Fig 6.8A).

Yeast cells exposed to all NPs (except In_2O_3), for 24 h, presented a significant accumulation of intracellular ROS (Fig 6.8B).

To test whether ROS accumulation was the main cause of cytotoxicity induced by the NPs, yeast cells were exposed to NPs in the presence of L-ascorbic acid (AA), a known free radicals scavenger agent (Arrigoni and De Tullio 2002; Nimse and Pal 2015). Subsequently, the levels of intracellular ROS, metabolic activity and cell viability were assessed. Yeast cells co-exposed to NPs and AA presented a significant reduction of the intracellular level of ROS (Fig 6.8B). For all NPs, except SiO_2, the intracellular levels of ROS of the yeasts co-exposed to the NPs and AA, were not significantly different from the control (Fig 6.8B). The co-exposure to AA practically restored the survival (Fig 6.8C) and the metabolic activity (Fig 6.8D) of yeast cells incubated with NPs. Together, these results strongly support the possibility that the toxicity exerted by the MOx studied, on yeast cells, can be attributed, mainly, to the induction of intracellular accumulation of ROS.

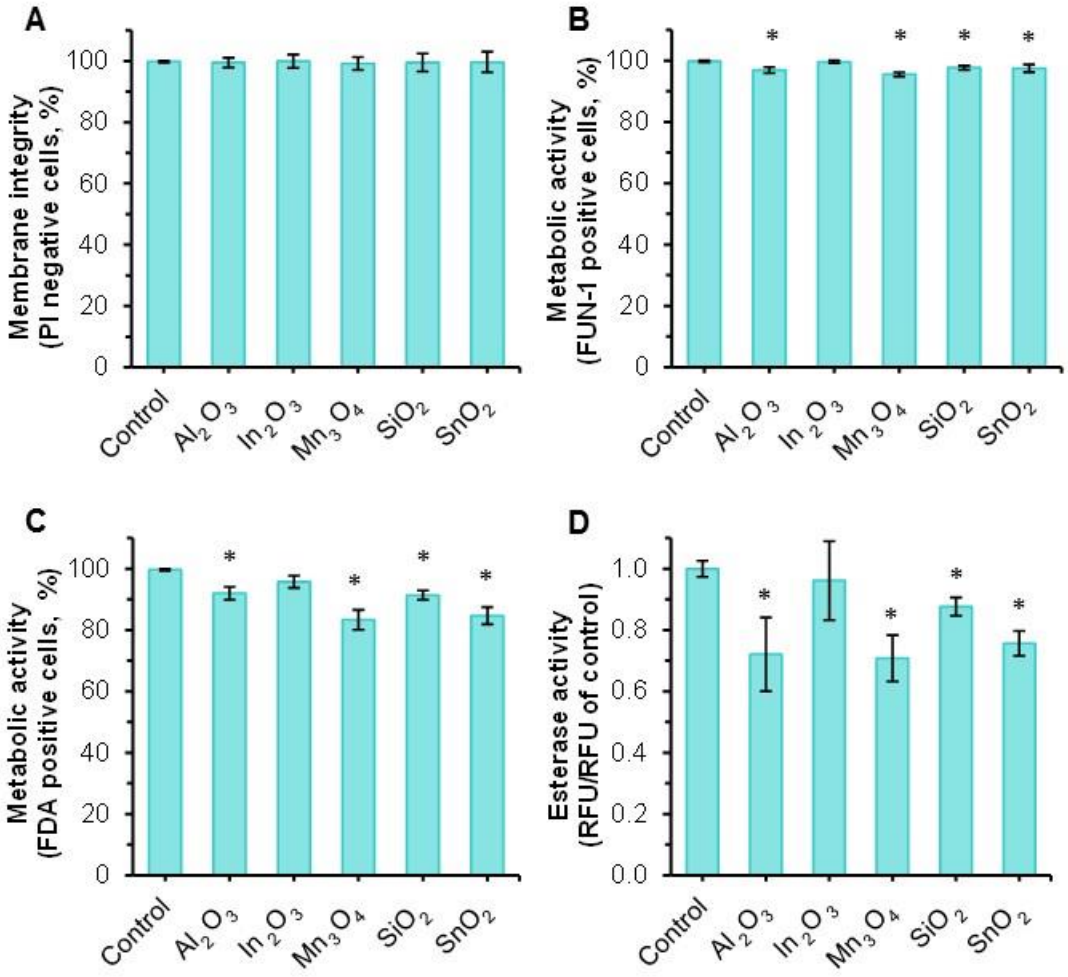

Figure 6.7. Influence of the nanoparticles on membrane integrity and metabolic activity of yeast cells. Yeasts were exposed for 24 h to 100 mg/L of the different NPs in MES buffer; control: cells incubated in MES buffer in the absence of NPs. A – Membrane integrity assessed by propidium iodide (PI) exclusion assay. B and C - Quantification of the percentage of metabolically active cells; yeasts were stained with FUN-1 or FDA, respectively. D - Assessment of esterase activity by the hydrolysis of FDA. The data are presented as mean values from at least three independent experiments performed in duplicate (n≥6); standard deviations are presented (vertical error bars). Mean values are significantly different: **P*<0.05 in comparison with untreated cells (control); unpaired t test.

6.4. Discussion

MOx NPs accounted for the largest share of the total NPs market. In the last decade, an exponential use of this type of nanomaterials, in the most varied daily products, was observed (Corr 2012). However, the increased use of MOx NPs have also raised concerns about the possible toxic impacts of these nanomaterials.

Physico-chemical characterization of the NPs is essential to understand their behavior and toxicity. In both media tested (MES buffer and YEP broth), the hydrodynamic size increased over time (Fig 6.1A) while a reduction of the zeta potential values was observed (Fig 6.1B).

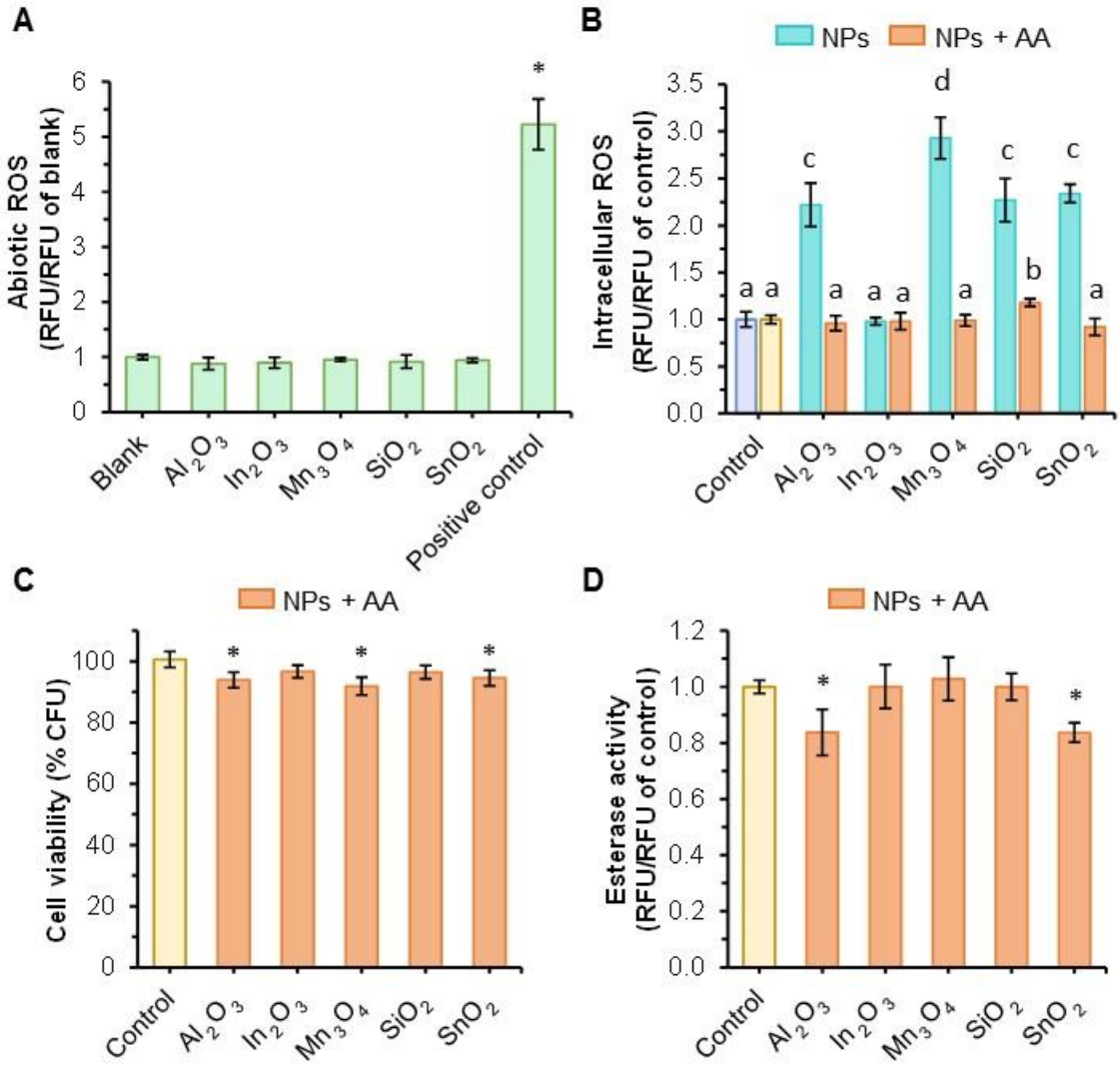

Figure 6.8. L-ascorbic acid reverts the toxic effects induced by the nanoparticles on yeast cells. A – Assessment of the possible pro-oxidant effect of MOx NPs. NPs at 100 mg/L were incubated with H_2DFC in MES buffer, for 24 h. Blank and positive control were obtained by incubating the H_2DCF probe in MES buffer or with 26 µmol/L H_2O_2, respectively. B – Evaluation of the oxidative stress induced by MOx NPs. Yeast cells were incubated with 100 mg/L NPs, in MES buffer for 24 h, without (NPs) or with 10 mmol/L L-ascorbic acid (NPs+AA); control: cells incubated in MES buffer in the absence of NPs, without (light blue) or with AA (light orange). Levels of intracellular ROS were quantified using H_2DCFDA. C and D – yeast cells co-exposed to 100 mg/L MOx NPs and 10 mmol/L AA, in MES buffer, for 24 h; control: cells incubated in MES buffer, with AA, in the absence of NPs. C – Evaluation of cell viability by colony forming units (CFU) counting. D – Metabolic activity assessed through the hydrolysis of FDA. The data are presented as mean values from at least three independent experiments performed in duplicate (n≥6); standard deviations are presented (vertical error bars). A, C and D - mean values are significantly different: **P*<0.05 in comparison with untreated cells (control); unpaired t test. B - means with different letters are significantly different (*P*<0.05); one-way ANOVA followed by Tukey-Kramer multiple comparison method.

These low zeta potential values indicated that the NPs were instable in aqueous suspension, having tendency to form agglomerates (Hanaor et al. 2012). This effect was particularly evident in MES buffer where the agglomeration of the NPs could be observed, with the naked eye, in the Erlenmeyer flasks (Fig 6.2). The properties of these MOx NPs in different aqueous media, such as Dulbecco's Modified Eagle medium, OECD algae medium and Luria-Bertani medium, was described in the literature. Similar zeta potential values to those here presented for In_2O_3 (Ahamed et al. 2017), Mn_3O_4 and SiO_2 (Ivask et al. 2015), as well as similar Z-average diameter for Al_2O_3 (Park et al. 2016), Mn_3O_4 (Ivask et al. 2015), SiO_2 (Bondarenko et al. 2016) and SnO_2 NPs (Chavez-Calderon et al. 2016) were reported. The MOx NPs studied presented a low solubility (<8 %) in YEP or MES buffer (Table 6.2). This poor solubility is in agreement with the data described in the literature. In fact, the amount of metal(loid)s released from the NPs, here presented, is of the same order of magnitude of the values reported for In_2O_3 (Bomhard 2018; Jeong et al. 2016), Mn_3O_4 (Ivask et al. 2015), SiO_2 (Van Hoecke et al. 2008) and SnO_2 NPs (Chavez-Calderon et al. 2016).

All NPs studied did not provoke yeast growth inhibition, up to 100 mg/L, when incubated in a protein rich medium (YEP) (Fig 6.5A). It is described that proteins form complexes with NPs, leading to a protein "corona" that defines the biological properties of the NPs (Cedervall et al. 2007; Kharazian et al. 2016). Probably, the formation of protein-coated NPs leads to the reduction of their toxicity, as it was described with other MOx NPs and cell models (Nguyen and Lee 2017). In addition, the metals released by the NPs (Fig 6.1C) should be, most likely, complexed by YEP components, which reduce their bioavailability and consequently their toxicity. Consistent with this possibility, it was found that 24h-EC_{50} values of metals in YEP were about ten times higher than those observed in MES buffer (Table 6.3), where no metals complexation occurs (Ferreira et al. 2015).

Except for In_2O_3, where no toxic effects on yeast cells were observed, all other NPs studied induced a loss of cell viability in a dose-dependent manner (Fig 6.5C). Regarding the causes that may induce NPs toxicity, the analysis of the effect of NPs and the respective supernatants (Fig 6.6) raises different possibilities. In the case of SiO_2, the toxicity over yeast cells was most likely mainly caused by the NPs themselves, since the supernatant had no impact on cell viability (Fig 6.6). A similar observation was reported when the *Photobacterium phosphoreum* was exposed to Fe_2O_3, Co_3O_4, Cr_2O_3 and NiO NPs (Wang et al. 2016). The toxicity of Al_2O_3 and SnO_2 NPs could be attributed to both the NPs and the respective released ions (Fig 6.6). A similar result was described when the bacterium *E. coli* was exposed to Al_2O_3 NPs (Simon-Deckers et al. 2009). The loss of yeast cell viability induced by Mn_3O_4 NPs could be mainly caused by the released Mn ions, since the contribution of the Mn_3O_4 NPs to the

toxicity could be, practically, neglected (Fig 6.6). A similar effect was described when human lung epithelial cells were exposed to Mn_3O_4 NPs (Ivask et al. 2015).

All NPs studied did not have any pro-oxidant effect (ROS generation in abiotic conditions) (Fig 6.8A). These results are compatible with the fact that Al_2O_3 and SnO_2 are considered redox-inactive (Chemicals 2018a; Chemicals 2018b). In the case of Mn_3O_4 NPs, although considered redox-active (Urner et al. 2014), in the concentration tested, these NPs were unable to oxidized H_2DCF. In the present work, it was observed that Al_2O_3, Mn_3O_4, SiO_2 and SnO_2 NPs induced a significant intracellular accumulation of ROS in yeasts (Fig 6.8B). Due to the absence of a pro-oxidant effect of the NPs, it can be deduced that the ROS presented by yeast cells were intracellularly generated. The triggering of OS on yeast cells by the MOx NPs studied (except by In_2O_3) is in agreement with the literature, which describe the ability of these NPs to induce OS in different cell models. Thus, it was reported that Al_2O_3 caused OS in plant wheat roots (*Triticum aestivum*) (Yanik and Vardar 2018) and in human lymphocytes (Rajiv et al. 2016). Mn_3O_4 NPs induced elevated ROS levels in rat alveolar macrophages (Urner et al. 2014) and alveolar epithelial cells (Frick et al. 2011) and SiO_2 NPs provoked the generation of ROS in different cell lines: lymphocyte (Azimipour et al. 2018), intestinal cells (Setyawati et al. 2015), lung and bronchial epithelial cells (Eom and Jinhee Cho 2011; Manke et al. 2013).

Main targets of ROS include membrane lipids, nucleic acids and ROS-susceptible proteins (Avery 2011). The levels of intracellular ROS in yeast cells exposed for 24 h to all NPs studied were not enough to induce the loss of cell membrane integrity (Fig 6.7A). Similarly, it was described that SiO_2 did not have any impact on membrane integrity of algal cells *Scenedesmus obliquus* (Liu et al. 2018). Although, it was reported the disruption of cell membrane in yeasts exposed to Al_2O_3 NPs (Garcia-Saucedo et al. 2011) or Mn_2O_3 (Otero-Gonzalez et al. 2013), both results were observed in the presence of 1 g/L NPs, which corresponded to a concentration ten times higher than the one used in the present study. The incubation of yeast cells with Al_2O_3, Mn_3O_4, SiO_2 or SnO_2 induced a small, but significant, loss of the metabolic activity (Fig 6.7B, C and D). A decrease of the metabolic activity due to the exposure to Mn_3O_4 NPs was observed in different animal cells (Titma et al. 2016). The reduction of the hydrolytic activity of the esterases could be due to the oxidation of this enzyme as consequence of the intracellular ROS accumulation. It was reported that protein oxidation can occur by different modes, which includes cleavage of peptide bonds and oxidation of sensitive amino acid residues, such as those containing aromatic side chain or sulfhydryl groups (Cecarini et al. 2007). Compatible with the possibility that OS may have been responsible for the reduction of yeast hydrolytic activity, it was observed that the simultaneous incubation of the cells with NPs and AA, almost (SiO_2) or completely

abrogated (Al_2O_3, Mn_3O_4 and SnO_2) the OS (Fig 6.8B) and restored the esterase activity (Mn_3O_4 and SiO_2) of yeast cells (Fig 6.8D). In addition, yeast survival was completely (SiO_2) or almost completely restored (Al_2O_3, Mn_3O_4 and SnO_2) (Fig 6.8C) when the cells were co-exposed to NPs and AA. The reversibility of the toxic effects, induced by the MOx NPs, due to the presence of AA, strongly indicates that OS is, most likely, the main contributor of the cytotoxicity observed in yeast cells.

6.5 Conclusions

The present work contributes to the characterization of the mechanisms of toxicity associated with MOx NPs:

- The MOx NPs displayed a tendency to agglomerate and were insoluble (dissolution <8 %);
- Al_2O_3, Mn_3O_4, SiO_2 and SnO_2 NPs induced the loss of yeast cell viability, caused by the NPs themselves (SiO_2), both NPs and respective released ions (Al_2O_3 and SnO_2) or only by released ions (Mn_3O_4).
- These NPs also induced the loss of metabolic activity and intracellular ROS accumulation;
- The intracellular accumulation of ROS constitutes the main cause of the cytotoxicity in yeasts treated with Al_2O_3, Mn_3O_4, SiO_2 and SnO_2 NPs.

References

Ahamed M, Akhtar MJ, Khan MAM, Alhadlaq HA, Aldalbahi A (2017) Nanocubes of indium oxide induce cytotoxicity and apoptosis through oxidative stress in human lung epithelial cells. Colloids Surf. B Biointerfaces 156:157-164

Andreescu S, Ornatska M, Erlichman JS, Estevez A, Leiter JC (2012) Biomedical applications of metal oxide nanoparticles. In: Matijević E (ed) Fine particles in medicine and pharmacy. Springer, Boston, MA, pp 57-100

Arrigoni O, De Tullio MC (2002) Ascorbic acid: much more than just an antioxidant. Biochim. Biophys. Acta 1569(1-3):1-9

Aruoja V, Pokhrel S, Sihtmae M, Mortimer M, Madler L, Kahru A (2015) Toxicity of 12 metal-based nanoparticles to algae, bacteria and protozoa. Environ. Sci. Nano 2(6):630-644

Avery SV (2011) Molecular targets of oxidative stress. Biochem. J. 434:201-210

Azimipour S, Ghaedi S, Mehrabi Z, Ghasemzadeh SA, Heshmati M, Barikrow N, Attar F, Falahati M (2018) Heme degradation and iron release of hemoglobin and oxidative stress of lymphocyte cells in the presence of silica nanoparticles. Int. J. Biol. Macromol. 118:800-807

AzoNano (2018) Indium oxide (In_2O_3) nanoparticles - properties, applications. https://www.azonano.com/article.aspx?ArticleID=3331. Acessed 15 October 2018

Bomhard EM (2018) The toxicology of indium oxide. Environ. Toxicol. Pharmacol. 58:250-258

Bondarenko OM, Heinlaan M, Sihtmae M, Ivask A, Kurvet I, Joonas E, Jemec A, Mannerstrom M, Heinonen T, Rekulapelly R, Singh S, Zou J, Pyykko I, Drobne D, Kahru A (2016) Multilaboratory evaluation of 15 bioassays for (eco)toxicity screening and hazard ranking of engineered nanomaterials: FP7 project NANOVALID. Nanotoxicology 10(9):1229-1242

Breeuwer P, Drocourt JL, Bunschoten N, Zwietering MH, Rombouts FM, Abee T (1995) Characterization of uptake and hydrolysis of fluorescein diacetate and carboxyfluorescein diacetate by intracellular esterases in *Saccharomyces cerevisiae*, which result in accumulation of fluorescent product. Appl. Environ. Microbiol. 61(4):1614-1619

Cecarini V, Gee J, Fioretti E, Amici M, Angeletti M, Eleuteri AM, Keller JN (2007) Protein oxidation and cellular homeostasis: emphasis on metabolism. Biochim. Biophys. Acta 1773(2):93-104

Cedervall T, Lynch I, Lindman S, Berggard T, Thulin E, Nilsson H, Dawson KA, Linse S (2007) Understanding the nanoparticle-protein corona using methods to quantify exchange rates and affinities of proteins for nanoparticles. Proc. Natl. Acad. Sci. USA 104(7):2050-2055

Chai HK, Yao J, Sun JJ, Zhang C, Liu WJ, Zhu MJ, Ceccanti B (2015) The effect of metal oxide nanoparticles on functional bacteria and metabolic profiles in agricultural soil. Bull. Environ. Contam. Toxicol. 94(4):490-495

Chavez-Calderon A, Paraguay-Delgado F, Orrantia-Borunda E, Luna-Velasco A (2016) Size effect of SnO_2 nanoparticles on bacteria toxicity and their membrane damage. Chemosphere 165:33-40

Chemicals (2018a) Aluminium oxide. https://cameochemicals.noaa.gov/chemical/16127. Acessed 6 August 2018

Chemicals (2018b) Tin (IV) oxide. https://cameochemicals.noaa.gov/chemical/25077. Acessed 6 August 2018

Corr SA (2012) Metal oxide nanoparticles. In: O'Brien P (ed) Nanoscience: volume 1: nanostructures through chemistry. The Royal Society of Chemistry, London, UK, pp 180-207

dos Santos SC, Teixeira MC, Cabrito TR, Sa-Correia I (2012) Yeast toxicogenomics: genome-wide responses to chemical stresses with impact in environmental health, pharmacology, and biotechnology. Front. Genet. 3(63):1-17

Eom H-J, Jinhee Cho J (2011) SiO_2 nanoparticles induced cytotoxicity by oxidative stress in human bronchial epithelial cell, Beas-2B. Environ. Health Toxicol. 26:1-7

Fei J, Li J (2010) Metal oxide nanomaterials for water treatment. In: Kumar CSSR (ed) Nanotechnologies for the life sciences: nanostructured oxides. vol 2. Wiley-VCH Verlag GmbH & Co. KGaA, Weinheim, pp 287-315

Ferreira CMH, Pinto ISS, Soares EV, Soares H (2015) (Un)suitability of the use of pH buffers in biological, biochemical and environmental studies and their interaction with metal ions - a review. Rsc Adv. 5(39):30989-31003

Frick R, Müller-Edenborn B, Schlicker A, Rothen-Rutishauser B, Raemy DO, Günther D, Hattendorf B, Stark W, Beck-Schimmer B (2011) Comparison of manganese oxide nanoparticles and manganese sulfate with regard to oxidative stress, uptake and apoptosis in alveolar epithelial cells. Toxicol. Lett. 205(2):163-172

Garcia-Saucedo C, Field JA, Otero-Gonzalez L, Sierra-Alvarez R (2011) Low toxicity of HfO_2, SiO_2, Al_2O_3 and CeO_2 nanoparticles to the yeast, *Saccharomyces cerevisiae*. J. Hazard Mater. 192(3):1572-1579

Goffeau A, Barrell BG, Bussey H, Davis RW, Dujon B, Feldmann H, Galibert F, Hoheisel JD, Jacq C, Johnston M, Louis EJ, Mewes HW, Murakami Y, Philippsen P, Tettelin H, Oliver SG (1996) Life with 6000 genes. Science 274(5287):546-567

Hanaor D, Michelazzi M, Leonelli C, Sorrell CC (2012) The effects of carboxylic acids on the aqueous dispersion and electrophoretic deposition of ZrO_2. J. Eur. Ceram. Soc. 32(1):235-244

Hartmann NB, Engelbrekt C, Zhang JD, Ulstrup J, Kusk KO, Baun A (2013) The challenges of testing metal and metal oxide nanoparticles in algal bioassays: titanium dioxide and gold nanoparticles as case studies. Nanotoxicology 7(6):1082-1094

Hewitt CJ, Nebe-Von-Caron G (2001) An industrial application of multiparameter flow cytometry: assessment of cell physiological state and its application to the study of microbial fermentations. Cytometry 44(3):179-187

Hirner AV, Flaßbeck D (2005) Speciation of silicon. In: Cornelis R, Crews H, Caruso J, Heumann KG (eds) Handbook of elemental speciation II – species in the environment, food, medicine and occupational health. John Wiley & Sons, Ltd, Chichester, UK, pp 366-377

Iler RK (1978) The occurrence, dissolution, and deposition of silica. In: Iler RK (ed) The chemistry of silica: solubility, polymerization, colloid and surface properties, and biochemistry. John Wiley & Sons, Ltd, New York, USA, pp 3-115

Ivask A, Titma T, Visnapuu M, Vija H, Kakinen A, Sihtmae M, Pokhrel S, Madler L, Heinlaan M, Kisand V, Shimmo R, Kahru A (2015) Toxicity of 11 metal oxide nanoparticles to three mammalian cell types in vitro. Curr. Top. Med. Chem. 15(18):1914-1929

Jeong J, Kim J, Seok SH, Cho WS (2016) Indium oxide (In_2O_3) nanoparticles induce progressive lung injury distinct from lung injuries by copper oxide (CuO) and nickel oxide (NiO) nanoparticles. Arch. Toxicol. 90(4):817-828

Karathia H, Vilaprinyo E, Sorribas A, Alves R (2011) *Saccharomyces cerevisiae* as a model organism: a comparative study. PLoS One 6(2):1-10

Kharazian B, Hadipour NL, Ejtehadi MR (2016) Understanding the nanoparticle-protein corona complexes using computational and experimental methods. Int. J. Biochem. Cell. Biol. 75:162-174

Klaine SJ, Edgington A, Seda B (2013) Nanomaterials in the environment. In: Férard J-F, Blaise C (eds) Encyclopedia of Aquatic Ecotoxicology. Springer Publishers, Dordrecht, pp 767-779

Laurent S, Boutry S, Müller RN (2018) Metal oxide particles and their prospects for applications. In: Mahmoudi M, Laurent S (eds) Iron oxide nanoparticles for biomedical applications: synthesis, functionalization and application. Elsevier, Ltd, pp 3-42

Li KG, Chen Y, Zhang W, Pu ZC, Jiang L, Chen YS (2012) Surface interactions affect the toxicity of engineered metal oxide nanoparticles toward *Paramecium*. Chem. Res. Toxicol. 25(8):1675-1681

Liu YH, Wang S, Wang Z, Ye N, Fang H, Wang DG (2018) TiO_2, SiO_2 and ZrO_2 nanoparticles synergistically provoke cellular oxidative damage in freshwater microalgae. Nanomaterials 8(2):1-12 doi:10.3390/nano8020095

Manke A, Wang L, Rojanasakul Y (2013) Mechanisms of nanoparticle-induced oxidative stress and toxicity. Biomed Res Int 2013:1-15

Masuda Y, Ohji T, Kato K (2010) Highly enhanced surface area of tin oxide nanocrystals. J Am Ceram Soc 93(8): 2140-2153

McGee CF, Storey S, Clipson N, Doyle E (2017) Soil microbial community responses to contamination with silver, aluminium oxide and silicon dioxide nanoparticles. Ecotoxicology 26(3):449-458

Millard PJ, Roth BL, Thi HPT, Yue ST, Haugland RP (1997) Development of the FUN-1 family of fluorescent probes for vacuole labeling and viability testing of yeasts. Appl. Environ. Microbiol. 63(7):2897-2905

Nanotech (2015) Aluminium oxide: forecast from 2010 to 2025 Nanoparticles. Future Markets Inc., Edinburgh

Nguyen VH, Lee BJ (2017) Protein corona: a new approach for nanomedicine design. Int. J. Nanomed. 12:3137-3151

Nimse SB, Pal D (2015) Free radicals, natural antioxidants, and their reaction mechanisms. Rsc Adv. 5(35):27986-28006

OECD (2011) Test Nº 201: freshwater alga and cyanobacteria, growth inhibition test. OECD guidelines for the testing of chemicals, Section 2. OECD Publishing, Paris

OECD (2017) Test nº 318: dispersion stability of nanomaterials in simulated environmental media. OECD guidelines for the testing of chemicals, Section 3. OECD Publishing, Paris

Otero-Gonzalez L, Garcia-Saucedo C, Field JA, Sierra-Alvarez R (2013) Toxicity of TiO_2, ZrO_2, Fe^0, Fe_2O_3, and Mn_2O_3 nanoparticles to the yeast, *Saccharomyces cerevisiae*. Chemosphere 93(6):1201-1206

Park EJ, Lee GH, Yoon C, Jeong U, Kim Y, Cho MH, Kim DW (2016) Biodistribution and toxicity of spherical aluminium oxide nanoparticles. J. Appl. Toxicol. 36(3):424-433

Perry CC, Belton D, Shafran K (2003) Studies of biosilicas; structural aspects, chemical principles, model studies and the future. In: Müller WEG (ed) Silicon biomineralization: biology-biochemistry-molecular biology-biotechnology. Progress in molecular and subcellular biology. Springer-Verlag, Berlin, Germany, pp 269-299

Rajiv S, Jerobin J, Saranya V, Nainawat M, Sharma A, Makwana P, Gayathri C, Bharath L, Singh M, Kumar M, Mukherjee A, Chandrasekaran N (2016) Comparative cytotoxicity and genotoxicity of cobalt (II, III) oxide, iron (III) oxide, silicon dioxide, and aluminum oxide nanoparticles on human lymphocytes in vitro. Hum. Exp. Toxicol. 35(2):170-183

Report (2018) Market research report: nanomaterials. https://www.alliedmarketresearch.com/press-release/nanomaterials-market.html. Acessed 15 October 2018.

Research (2017) Global markets for nanocomposites, nanoparticles, nanoclays, and nanotubes. http://www.bccresearch.com/market-research/nanotechnology/nanocomposites-nanoparticles-nantubes-market-report-nan021g.html. Accessed 23 January 2017

Research (2018) Indium market size by product: global industry report 2018-2025. https://www.grandviewresearch.com/industry-analysis/indium-market. Acessed 15 October 2018

Setyawati MI, Tay CY, Leong DT (2015) Mechanistic investigation of the biological effects of SiO_2, TiO_2, and ZnO nanoparticles on intestinal cells. Small 11(28):3458-3468

Simon-Deckers A, Loo S, Mayne-L'Hermite M, Herlin-Boime N, Menguy N, Reynaud C, Gouget B, Carriere M (2009) Size-, composition- and shape-dependent toxicological impact of metal oxide nanoparticles and carbon nanotubes toward bacteria. Environ. Sci. Technol. 43(21):8423-8429

Tarpey MM, Wink DA, Grisham MB (2004) Methods for detection of reactive metabolites of oxygen and nitrogen: in vitro and in vivo considerations. Am. J. Physiol. Regul. Integr. Comp. Physiol. 286(3):R431-R444

Tian Z-Y, Kouotou PM, Bahlawane N, Ngamou PHT (2013) Synthesis of the catalytically active Mn_3O_4 spinel and its thermal properties. J. Phys. Chem. C 117(2):6218–6224

Titma T, Shimmo R, Siigur J, Kahru A (2016) Toxicity of antimony, copper, cobalt, manganese, titanium and zinc oxide nanoparticles for the alveolar and intestinal epithelial barrier cells in vitro. Cytotechnology 68(6):2363-2377

Urner M, Schlicker A, Z'Graggen BR, Stepuk A, Booy C, Buehler KP, Limbach L, Chmiel C, Stark WJ, Beck-Schimmer B (2014) Inflammatory response of lung macrophages and epithelial cells after exposure to redox active nanoparticles: effect of solubility and antioxidant treatment. Environ. Sci. Technol. 48(23):13960-13968

Van Hoecke K, De Schamphelaere KAC, Van der Meeren P, Lucas S, Janssen CR (2008) Ecotoxicity of silica nanoparticles to the green alga *Pseudokirchneriella subcapitata*: Importance of surface area. Environ. Toxicol. Chem. 27(9):1948-1957

von Moos N, Koman VB, Santschi C, Martin OJF, Maurizi L, Jayaprakash A, Bowen P, Slaveykova VI (2016) Pro-oxidant effects of nano-TiO_2 on *Chlamydomonas reinhardtii* during short-term exposure. Rsc Adv. 6(116):115271-115283

Wang DL, Lin ZF, Wang T, Yao ZF, Qin MN, Zheng SR, Lu W (2016) Where does the toxicity of metal oxide nanoparticles come from: the nanoparticles, the ions, or a combination of both? J. Hazard Mat. 308:328-334

Yanik F, Vardar F (2018) Oxidative stress response to aluminum oxide (Al_2O_3) nanoparticles in *Triticum aestivum*. Biologia 73(2):129-135

Chapter 7 - Toxic effects of nickel oxide (NiO) nanoparticles on the freshwater alga *Pseudokirchneriella subcapitata**

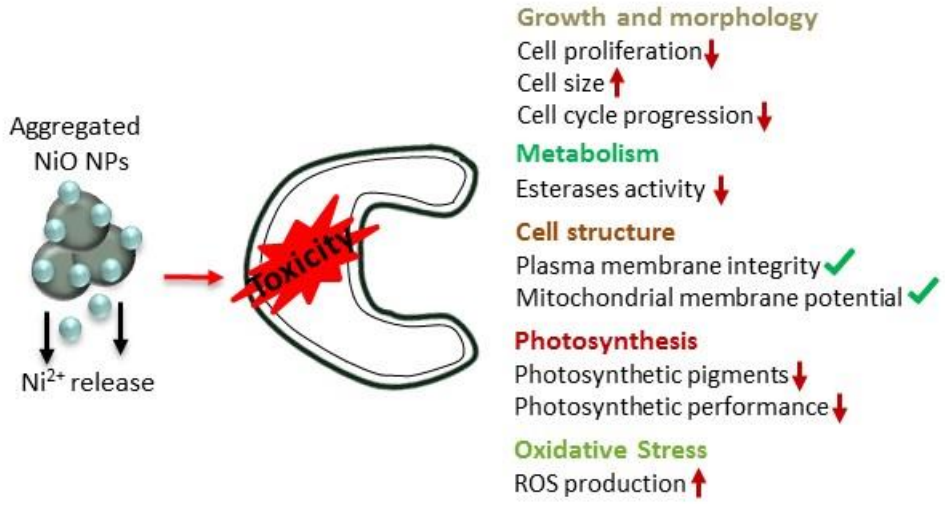

*Published in Aquatic Toxicology (2018) 204: 80-90

7.1. Introduction

Among the different nanomaterials, metal oxide NPs have been subject to significant interest due to their easy synthesis and extensive usage. Nickel oxide (NiO), is used in ceramic materials, chemical catalysts, printing inks, electronic components, biosensors and water purification methods (Ravindhranath and Ramamoorty, 2017; Srivastava et al., 2014; Zhou et al., 2017; Zhu et al., 2012).

The widespread use of NPs has inevitably increased their unintended introduction into aquatic and terrestrial environments. Thus, concerns have been raised regarding the potential adverse effects of NPs on biota and human health (Batley et al., 2013; Beaudrie et al., 2013). In fact, the characteristics that give NPs their exceptional chemical properties can also provide them with intrinsic toxicity. Various negative impacts of NiO NPs on aquatic organisms have been described, including bioluminescence inhibition in the bacterium *Vibrio fischeri* (Nogueira et al., 2015), growth inhibition in the algae *Chlorella vulgaris* and *Pseudokirchneriella subcapitata* (Gong et al., 2011; Nogueira et al., 2015; Oukarroum et al., 2017), toxicity to zebrafish (*Danio rerio*) (Kovriznych et al., 2014), and oxidative stress in the crustacean *Artemia salina* (Ates et al., 2016) and the aquatic plant *Lemna gibba* (Oukarroum et al., 2015b). Nevertheless, NiO NPs did not cause a significant increase of mortality in the estuarine amphipod *Leptocheirus plumulosus* (Hanna et al., 2013).

P. subcapitata has been considered to be an important organism, being recommended by international agencies, such as the OECD and U.S. EPA (OECD, 2011; US-EPA, 2002) as a toxicity bioindicator of freshwater environments due to its ecological relevance, ubiquitous distribution and high sensitivity to a wide range of hazardous substances, including heavy metals and organic compounds (Geis et al., 2000; Rojickova-Padrtova and Marsalek, 1999).

Although there is a general consensus from the scientific community and intergovernmental organizations (such as the OECD) about the urgency and importance of knowledge related to the potential environmental adverse effects of NPs (Hunt et al., 2013), there are no safe guidelines regarding their release into fresh or salt water (Baker et al., 2014). Taking into account that aquatic environments are considered to be an important environmental sink for NPs, their environmental fate and corresponding potential toxic effects deserve further investigation. In fact, the increasing use of NPs requires an improved understanding of their potential impacts on the environment. However, the possible environmental hazards of NiO NPs have been poorly studied, and only a few studies are available on their mechanisms of action.

This chapter aimed to investigate the possible adverse effects of NiO NPs on aquatic systems using the alga *P. subcapitata* as a test organism by means of a mechanism-based approach. To achieve this

objective, the impacts of NiO NPs on algal growth, plasma membrane integrity, metabolism (esterase activity and reactive oxygen species accumulation), photosynthesis (pigment production and photosynthetic activity), and morphology and on the algal cell cycle was evaluated.

7.2. Materials and Methods

7.2.1. Preparation of the NiO NP stock suspension

Nickel oxide nanoparticles (NiO NPs) with a particle size of <50 nm and a purity of 99.8% (trace metal basis) were obtained from Sigma-Aldrich. The stock suspensions (0.5 g/L NiO NPs) were prepared in deionized water, sterilized, shaken and sonicated as described before in Chapter 3.

7.2.2. Characterization of NiO NPs in suspension

The characterization of NiO NPs in suspension was performed in OECD algal test medium under the same conditions of the assays and in the absence of algal cells. However, some experiments (Ni dissolution from the NPs and NiO agglomeration) were also performed in OECD medium in the presence of algal cells.

Hydrodynamic size was measured using dynamic light scattering (DLS) with a polystyrene cuvette (DTS0012) and zeta potential using a disposable folded capillary cell (DTS1070) at 25ºC in a Zetasizer Nano ZS (Malvern Instruments, UK) and the Zetasizer software, version 7.11. The sedimentation of NiO agglomerates in OECD medium was also monitored by spectrophotometrically measuring the absorbance at 600 nm for 30 min and determined as described before in Chapter 6.

NiO NPs dissolution in OECD medium was quantified using atomic absorption spectroscopy with flame atomization (AAS-FA) in a PerkinElmer AAnalyst 400 spectrometer. For this analysis, NiO NPs at different concentrations were incubated for up to 72 h under the same conditions as the assays. At defined times, samples were taken and centrifuged at 20.000×g for 30 min at 25ºC. Alternatively, NiO NPs were removed from the media through centrifugal ultrafiltration using a membrane with a nominal molecular weight limit of 3 kDa (Merck Millipore, Amicon Ultra-15 3K). For this purpose, the NiO NP suspensions were placed in ultrafiltration tubes and centrifuged at 3.200×g for 20 min at 25ºC, and the Ni concentration in the filtrate was determined as described above. The literature indicates that this filter rejects particles greater than 1.3 nm (Ma et al., 2014). Using this procedure, it is assumed that the filtrate predominately contains free nickel ions and soluble nickel complexes; agglomerates greater than 1.3 nm were retained on the membrane. The total nickel content in the NiO NP suspensions was digested using aqua regia (a mixture of nitric and hydrochloric acid at a

molar ratio of 1:3, respectively) for 1 h. The remaining solutions were subsequently filtered through a 0.45-µm-pore-size filter, and the Ni content was determined using AAS-FA.

7.2.3. Strain, medium, culture conditions and alga exposure to NiO NPs or Ni^{2+}

The freshwater green alga *Pseudokirchneriella subcapitata* (strain 278/4) was obtained from the Culture Collection of Algae and Protozoa (CCAP), UK. The alga was maintained in OECD medium (OECD, 2011) with 15 g/L agar (Merck) at 4ºC in the dark.

The pre-cultures were prepared weekly by inoculating 40 mL OECD medium in 100 mL Erlenmeyer flasks with algal cells. Then, the cells were incubated at 25ºC for 3 days on an orbital shaker at 100 rpm under continuous "natural white" light-emitting diodes (LEDs) with a colour temperature of 4,000-4,200 K and an intensity of 4,000 lux at the surface of the flasks. The cultures were obtained by inoculating the cells from the pre-cultures at an initial concentration of $5x10^4$ cells/mL in 100 mL OECD medium in 250 mL Erlenmeyer flasks. The cultures were incubated for 2 days under the conditions described for the pre-cultures. After incubation, the algal cells were centrifuged at 2500×*g* for 5 min and suspended in deionized water.

Dose-response curves and the effect concentration (EC) values were determined by the exposure of algal cells, in exponential-phase of growth (2 days cultures), at a final concentration of 5×10^4 cells/mL, to seven concentrations of NiO NPs or Ni (from a stock solution of 1000 mg/L $NiCl_2$, Merck), arranged in a geometric series, in 250 mL Erlenmeyer flasks containing OECD medium, at a total volume of 100 mL. As a control, algal cells were incubated in the same medium in the absence of the toxicant. Controls and assays were incubated for 72 h under the same growth conditions (temperature, agitation and light) described above. After incubation, algal cell concentrations were determined using an automated cell counter (TC10, Bio-Rad). The algal growth (yield) was calculated considering the cell concentration at the end of the assay minus the starting cell concentration. 72h-EC_{10}, EC_{25} EC_{50}, EC_{75} and EC_{90} values representative of the NiO NPs or Ni^{2+} concentration that induced the inhibition of 10, 25, 50, 75 or 90 % of algal growth, compared to control, after an exposure for 72h were calculated using a linear interpolation method (TOXCALC version 5.0.32, Tidepool Scientific Software).

In the assessment of the impact of NiO NPs or Ni^{2+} over algal cells (biological endpoints described below), cells in exponential phase of growth (2 days cultures) were inoculated in OECD medium in 250 mL Erlenmeyer flasks, at a final concentration of $5x10^4$ cells/mL, and exposed to 1.1, 1.6 or 4 mg/L NiO NPs, in the same cultural conditions described above. The final volume of the assays was 100

mL. After exposure to toxicants for 72 h, algal cells were centrifuged at 2500x*g* for 5 minutes and resuspended in OECD medium at final concentration of 3 x 10^6 cells/mL. These cellular suspensions were further used for determining the various metabolic and physiological parameters described below.

7.2.4. Cell membrane integrity

The plasma membrane integrity was monitored using the probe SYTOX Green (SG, Molecular Probes, Invitrogen). After treatment, algal cells at 1x10^6 cells/mL were stained with 0.5 µmol/L SG, for 20 min, in the dark, at room temperature, as previously described (Machado and Soares, 2012). As positive control (cells with permeabilized plasma membrane), cells were heat treated (65 ºC for 1h) in a water bath. The cells were observed using a Leica DLMB epifluorescence microscope equipped with an HBO-100 mercury lamp and the GFP filter set from Leica. In each experiment, two samples of ~200 cells were scored in randomly selected microscope fields.

7.2.5. Metabolic activity

Metabolic activity was assessed through a fluorescein diacetate-based cell esterase activity assay. After treatment, cells were diluted to 5x10^5 cells/mL, in OECD medium and subsequently stained with 20 µmol/L fluorescein diacetate (FDA, Sigma-Aldrich) for 40 min, at 25 ºC, in the dark, as previously described (Machado and Soares, 2013). Cells not exposed to NPs (metabolically active, positive control) and heat-treated (negative control) were also stained with FDA. The assays were conducted in quintuplicate in sterile 96-well flat microplates (Orange Scientific). Fluorescence intensity (in relative fluorescent units, RFUs) was measured in a Perkin-Elmer (Victor3) microplate reader at a fluorescence excitation wavelength of 485/14 nm and an emission wavelength of 535/25 nm. Fluorescence was corrected by subtracting cell, culture medium and dye autofluorescence and normalised considering the cell concentration. The effect of NPs on esterase activity was expressed as the ratio of fluorescence in the cells exposed to NiO relatively to the fluorescence in the control (non-treated cells).

7.2.6. Mitochondrial membrane potential

The mitochondrial membrane potential (ΔΨm) was determined using 3,3′-dihexyloxacarbocyanine iodide ($DiOC_6$, Sigma-Aldrich). Cells, at a final concentration of $1x10^6$ cells/mL resuspended in OECD medium were incubated with 2.5 µmol/L $DiOC_6$, during 10 minutes, at room temperature, in the dark. As negative control, algal cells (after grown in the absence of toxicant) were treated with 50 µmol/L of the H^+ ionophore carbonyl cyanide *m*-chlorophenyl hydrazone (CCCP, Sigma-Aldrich) for 10 min; subsequently, algae were stained with $DiOC_6$, as described above. The stock solution of CCCP (5 mmol/L) was prepared in dimethylsulfoxide (DMSO; Sigma-Aldrich); in the assay, the final concentration of DMSO was ≤1 % (v/v). Fluorescence was quantified (in quintuplicate), corrected and normalized as described above (metabolic activity). Effect of the toxicants on ΔΨm was expressed as the ratio of fluorescence in the cells exposed to NiO relatively to the fluorescence in the control (non-treated cells).

7.2.7. Reactive oxygen species (ROS) production in abiotic and biotic conditions

ROS production by NiO NPs in OECD medium, in the absence of cells (abiotic conditions) was quantitatively detected using 2′,7′-dichlorodihydrofluorescein (H_2DCF). For this purpose, 2′,7′-dichlorodihydrofluorescein diacetate (H_2DCFDA, Sigma-Aldrich) was deacetylated to H_2DCF as described in the literature (Aruoja et al., 2015). NiO NPs (4 mg/L) or Ni^{2+} (3.1 mg/L) were incubated in OECD medium in the same conditions (temperature, agitation and light) described above for the assays with algal cells. After 72h of incubation, samples of 100 µL were combined with 100 µL of 52 µmol/L H_2DCF solution, placed in a 96-well microplate and incubated at room temperature, in the dark, for 45 minutes. Blank and positive control were prepared by substituting the sample by equal volume of OECD medium or 52 µmol/L H_2O_2 (prepared in OECD medium from a stock solution of 30 %, Panreac), respectively. Fluorescence was measured, corrected and normalized as described above (metabolic activity). Abiotic ROS was expressed as the ratio of fluorescence of the assay relatively to the fluorescence of the blank. At least five replicates were prepared for each sample.

Intracellular ROS accumulation was evaluated using H_2DCFDA. Algal cells at $1x10^6$ cells/mL were stained with 10 µmol/L H_2DCFDA , placed in quintuplicate in a 96-well microplate and incubated for 90 min, at 25°C, in the dark, as previously described (Machado and Soares, 2016). Fluorescence was quantified, corrected and normalized as described above for esterase activity. Intracellular ROS accumulation was expressed as the ratio of fluorescence of the assay relatively to the fluorescence of the control (cells not exposed to NPs).

Samples were observed using an epifluorescence microscope equipped with appropriate filter settings (GFP for ROS; N2.1 for chlorophyll *a* autofluorescence) from Leica. The images were obtained with a Leica DC 300 F camera using a 100x oil immersion N plan objective and processed using Leica IM 50-Image manager software.

7.2.8. Photosynthetic pigments quantification

Algal cells were resuspended in OECD medium at final concentration of 3 x 10^6 cells/mL. The pigments were extracted by placing the algal cells in 90% acetone (VWR Chemicals) at 4 ºC for 20 h. The concentrations of chlorophyll *a* (chl *a*), chlorophyll *b* (chl *b*) and carotenoids were determined by UV/Vis spectrometry, as previously described (Clesceri et al., 1999; Strickland and Parsons, 1972) and normalized considering the algal cell concentration. Photosynthetic pigment concentrations were expressed as the ratio between the pigment content in the assay and the pigment content in the control.

7.2.9. Photosynthetic performance

The parameters related to photochemical and non-photochemical quenching of Photosystem II (PSII) of algal cells were determined by pulse amplitude modulated (PAM) fluorescence assay, using a chlorophyll fluorometer (Walz, JUNIOR-PAM, Effeltrich, Germany). After treatment, algal cells in OECD medium at a final concentration of 3 x 10^6 cells/mL were dark adapted for 30 min and the minimal fluorescence (F_0) was measured. Subsequently, the maximum fluorescence (F_m) were obtained by exposing the cells for 600 ms to a blue LED saturation pulse of 10000 µmol/m^2s light intensity and a measuring beam of 5 Hz. Fluorescence parameters were automatically calculated using the WinControl software (version 3.25), according to the equations presented in Table 7.1 and expressed as the ratio of the values in cells exposed to NiO NPs and the values in control cells.

Table 7.1. Fluorescent parameters of PSII determined by pulse amplitude modulated (PAM) fluorescence assay.

Parameter	Description	Equation	Reference
F_v	Variable fluorescence	$F_v = (F_m\text{-}F_0)$	Juneau et al., 2002
F_v/F_m	Maximum quantum yield of PSII	$F_v/F_m = (F_m - F_0)/F_m$	Kitajima and Butler, 1975
Φ_{PSII}	Quantum yield of photosystem II	$\Phi_{PSII} = (F'_m\text{-}F')/F'_m$	Genty et al., 1989
qP	Photochemical quenching	$qP = (F'_m\text{-}F')/(F'_m\text{-}F'_0)$	Schreiber et al., 1986
rETR	Relative electron transport rate	$rETR = PAR \times ETR_{factor} \times (PS_2/P_{PPS}) \times \Phi_{PSII}$	Walz, 2007
NPQ	Non-photochemical quenching	$NPQ = (F_m/F'_m)\text{-}1$	Bilger and Björkman, 1990

Where: F_0 is the minimal level of fluorescence of dark-adapted cells (keeping PSII reaction centres open); F_m is the maximum level of fluorescence obtained with a saturating light pulse (closes all PSII reaction centres); F'_m is the maximal fluorescence level when PSII reaction centres are closed by a strong light pulse; F' is the fluorescence level shortly before a strong light pulse; F'_0 is the minimum chlorophyll fluorescence level in the presence of open PSII reaction centres; PAR is the photosynthetic active radiation; ETR_{factor} is the ratio of photons absorbed by photosynthetic pigments to incident photons; PS_2/P_{PPS} are the photons absorbed via PSII, related to absorption of photons by photosynthetic pigments.

7.2.10. Cell volume determination

Photos of algal cells incubated for 72 h in OECD medium in the absence (control) or the presence of the toxicants were acquired in randomly selected fields, in phase-contrast microscopy, using a 100X objective and a digital camera. The images were processed with a Leica IM 50-Image manager software. Algal biovolume was determined as previously described (Machado and Soares, 2014a), assuming that *P. subcapitata* generally conforms to the shape of a sickle-shaped cylinder (Sun and Liu, 2003). For each experimental condition, a minimum sample of 200 cells was used and the relative frequency (i.e, the % of the number of times) of each biovolume was determined.

7.2.11. Cell-cycle stage analysis

After treatment, algal cells were resuspended in OECD medium at final concentration of 3 x 10^6 cells/mL; cell membrane was permeabilized [by treatment with 1-pentanol (70 %, v/v) for 1 h] and, subsequently, stained with SG as described in cell membrane integrity subsection. Cells were observed using an epifluorescence microscope, equipped with a filter set GFP (Leica) and images were acquired and processed as described above. *P. subcapitata* cell cycle was divided in four stages, as previously described (Machado and Soares, 2014). In each experimental condition, for the determination of the % of cells belonging to each cycle stage, at least 200 cells were considered in randomly selected fields.

7.2.12. Reproducibility of the results and statistical analysis

All studies were repeated, independently, at least three times in duplicate ($n \geq 6$), except the hydrodynamic size distribution and the zeta potential of the NiO NPs, which were performed one time in duplicate. Statistical analysis was provided using one-way ANOVA ($P < 0.05$), followed by Tukey–Kramer multiple comparison method.

7.3. Results

7.3.1. Characterization of the NiO NP suspensions in OECD medium

According to the manufacturer, the primary (nominal) size of individual NiO NPs is <50 nm. This size was confirmed by transmission electron microscopy micrographs (see Chapter 3). After suspension (zero time) in OECD medium, the NiO NPs presented a Z-average diameter (mean size), determined using DLS, of ~800 nm (Table 7.2), which indicates the almost immediate agglomeration of the NPs. The NP agglomerations increased in size over time and presented a Z-average diameter of ~3400 nm after 72 h (Table 7.2). The NP suspensions presented a polydispersity index of 1.0, which indicates that the sample had a very broad size distribution of agglomerates (Table 7.2). The surface charge of the NiO NPs was evaluated based on the measurement of zeta potential. Once suspended in algal medium, the NPs presented a negative charge of -7.6 mV, which was maintained at a similar value over time (Table 7.2). The suspension of the NPs did not affect the pH of the OECD culture medium and the growth of the algal cells caused a small increase in the pH value of the culture medium (Table 7.2).

Table 7.2. Characteristics of NiO NPs suspensions in OECD algal medium.

[NiO] (mg/L)	Time (h)	Z-average diameter (nm)	PdI	Zeta potential (mV)	pH of medium (without algal cells)	pH of medium (with algal cells)
1.6	0	772 ± 73	0.51 ± 0.05	-7.6 ± 0.8	7.51 ± 0.03	7.52 ± 0.02
	72	3389 ± 655	1.0 ± 0.1	-10.6 ± 1.4	7.39 ± 0.07	7.71 ± 0.03

The data reported for Z-average diameter and zeta potential are the mean values ± standard deviation of one experiment performed in duplicate. Where PdI is the polydispersity index. In each determination, at least ten measurements were performed.

The inspection of the Erlenmeyer flasks containing NPs indicated the presence of agglomerates that were obviously visible to the naked eye after 72 h of incubation, particularly for 10mg/L (Fig 7.1A).

The changes in the NiO NP agglomeration process were alternatively monitored by spectroscopy at 600 nm. The sedimentation of NP agglomerates in the algal medium increased with the incubation time for 4 mg/L NiO (Fig 7.1B). For the highest concentration of NPs tested (10 mg/L), the sedimentation markedly increased in the first 8 h of incubation (Fig 7.1B).

Another important characteristic of NiO NPs in suspension is their ability to solubilize and release Ni^{2+} (dissolution of NPs). It was possible to observe that, for 1.6 mg/L NiO NPs, the concentrations of soluble Ni were similar during the exposure time: 0.22 ± 0.02 mg/L Ni^{2+} (Fig 7.1C); these Ni concentrations corresponded to the dissolution of the NPs of 18% and 9%, respectively. For comparative purposes, the dissolution of 1.6 mg/L NiO NPs in deionized water was also evaluated.

After 72 h, the amount of soluble Ni in water (0.25 ± 0.03 mg/L) was similar to that found in OECD medium. Control experiments showed that when 1.6 mg/L NiO was suspended in OECD medium and the NPs were separated from nickel species through ultrafiltration after 72 h, a similar amount of dissolved Ni (0.24 ± 0.03 mg/L) was found. This means that the amount of soluble Ni is independent of the process used to separate the NPs. At the end of the incubation of the algal cells (72 h) with 1.6 mg/L NiO, the concentration of soluble Ni was also similar (0.21 mg/L) to that found under abiotic conditions (in the absence of algal cells).

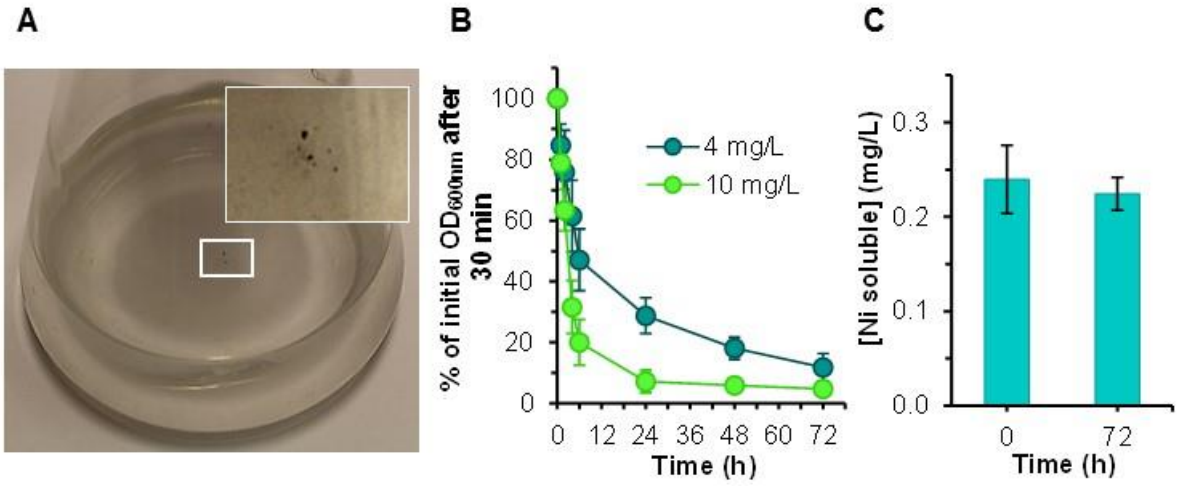

Figure 7.1. Characterization of NiO NPs suspensions in OECD medium. A - Macroscopic aspect of NiO NPs suspensions; inset: high magnification image of NPs agglomerates, limited by the white-box. B - Evolution of NiO NPs sedimentation over the time. NiO NPs were suspended in OECD medium at a final concentration of 4 or 10 mg/L. C - Ni released by NiO NPs in OECD medium. The data represent the mean values of at least three independent experiments, performed in duplicate (n≥6); standard deviations (SD) are presented (vertical error bars). Where no error bars are shown, SD are within the points.

7.3.2. Algal cells enhance NiO NP agglomeration in OECD medium

The presence of algal cells increased the agglomeration of NiO NPs in OECD medium (Fig 7.2A). Fluorescence microscopy of the large agglomerates revealed the presence of algal cells inside the agglomerates and in the surrounding media (Fig 7.2B). These hetero-agglomerates (composed of algae and NiO NPs) presented a non-compact structure and were easily dispersed by agitation (Fig 7.2C). The *P. subcapitata* cells exposed to NiO presented agglomerated NPs adsorbed onto the algal surface (Fig 7.2C).

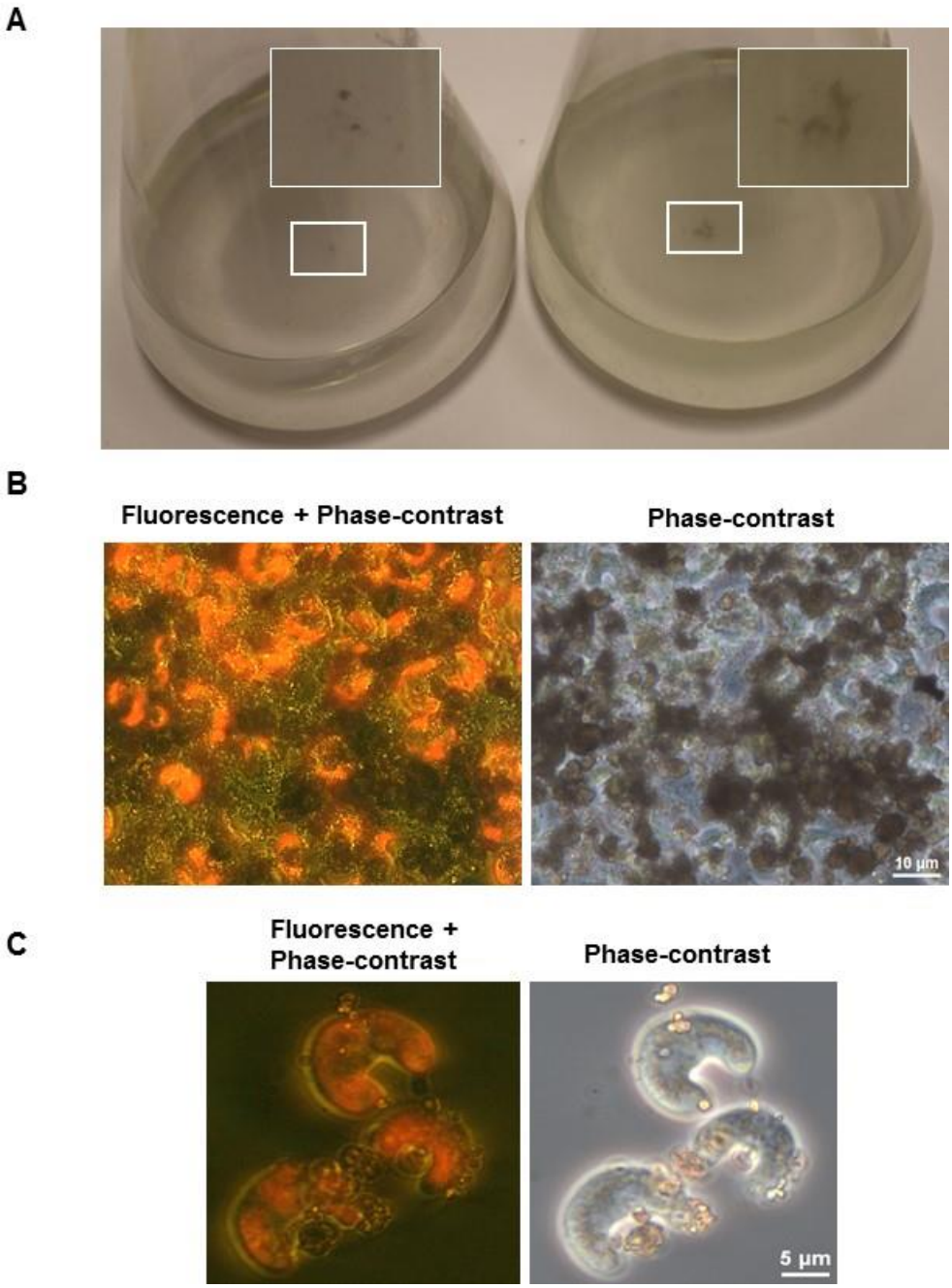

Figure 7.2. Influence of algal cells in NiO NPs agglomeration. A – NPs were suspended in OECD medium at 4 mg/L in the absence or inoculated with $5x10^4$ algal cells/mL. Suspensions were agitated for 72h at 100 rpm A – Erlenmeyer flasks without or with algal cells in the presence of 4 mg/L NiO, respectively. Inset: high magnification images of white boxes. B – Microscopy images of NiO NPs suspensions, in OECD medium, showing the interior of the agglomerates with entrapped algal cells. C – NiO NPs attached to P. subcapitata algal cells surface.

7.3.3. NiO NPs present an algistatic effect

The potential hazard presented by NiO NPs was assessed using the OECD algal growth inhibition test (OECD 2011). NiO NPs inhibit algal growth in a concentration-dependent manner. Figure 7.3 shows the dose-response curve expressed as the percentage of growth inhibition (yield) of the algal cells exposed to NiO for 72 h.

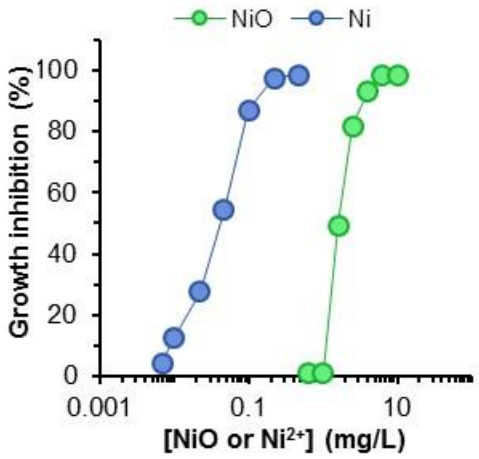

Figure 7.3. Dose-response curves of *P. subcapitata* exposure to NiO NPs or Ni^{2+} in OECD medium. The data are presented as mean values from at least three independent experiments performed in duplicate (n≥6); standard deviations (SD) are presented (vertical error bars). Where no error bars are shown, SD are within the points.

The NPs presented 72 h-EC_{10}, 72 h-EC_{50} and 72 h-EC_{90} values of 1.1, 1.6 and 3.7 mg/L, respectively (Table 7.3). For comparative purposes, the algae were exposed to Ni^{2+}, and a dose-response curve was also drawn (Fig 7.3). Ni^{2+} displayed 72 h-EC_{10}, 72 h-EC_{50} and 72 h-EC_{90} values of 8.0×10^{-3}, 4.2×10^{-2} and 13×10^{-2} mg/L, respectively. A global comparison (EC_{10}, EC_{25}, EC_{50}, EC_{75} and EC_{90} values) of NiO NP and Ni^{2+} toxicity is presented in Table 7.3.

Table 7.3. Effect of NiO NPs or Ni^{2+} on *P. subcapitata.*

	72h-EC (mg/L)				
Toxicant	10	25	50	75	90
Ni^{2+}	$0.80 \times 10^{-2} \pm 0.2 \times 10^{-2}$	$2.0 \times 10^{-2} \pm 0.3 \times 10^{-2}$	$4.2 \times 10^{-2} \pm 0.5 \times 10^{-2}$	$8.0 \times 10^{-2} \pm 0.5 \times 10^{-2}$	$13 \times 10^{-2} \pm 1.9 \times 10^{-2}$
NiO NPs	1.10 ± 0.02 (0.87 ± 0.02)[a]	1.30 ± 0.02 (1.03 ± 0.02)[a]	1.6 ± 0.1 (1.26 ± 0.08)[a]	2.30 ± 0.03 (1.82 ± 0.02)[a]	3.7 ± 0.1 (2.92 ± 0.08)[a]

72h-EC_{10}, EC_{25} EC_{50}, EC_{75} and EC_{90} values represent NiO NPs or Ni^{2+} concentration that induces the inhibition of 10, 25, 50, 75 or 90 % of alga growth, in OECD medium, after exposure to the toxicant for 72 h. Values were obtained from three independent experiences performed in duplicate (*n=6*).
[a]EC values calculated on metal basis (mg Ni^{2+}/L).

The reduction in algal biomass (yield) after 72 h could be the consequence of the disruption of plasma membrane integrity (algicidal effect) or a decrease in the algal growth (algistatic effect). To elucidate whether an algicidal or algistatic effect can be attributed to NPs, the algal cells were exposed to 1.1, 1.6 and 4 mg/L NiO, corresponding to ≈72 h-EC_{10}, 72 h-EC_{50} and 72 h-EC_{90} values, respectively. The plasma membrane integrity was assessed using the membrane-impermeant probe SYTOX green (SG) (Machado and Soares, 2012).

Cells exposed to up to 4 mg/L NiO NPs for 144 h (6 days) retained the majority of their cell membrane integrity since >85% of the cells were not able to incorporate SG [SG (-) cells] (Fig 7.4A). The exposure to NiO NPs led to a slowdown in cell division (Fig 7.4B). Algal cells exposed to 4 mg/L NiO NPs divided 6 times, with their growth being arrested after 96 h. Together, these results indicate that the NiO NPs had an algistatic effect on the *P. subcapitata* cells.

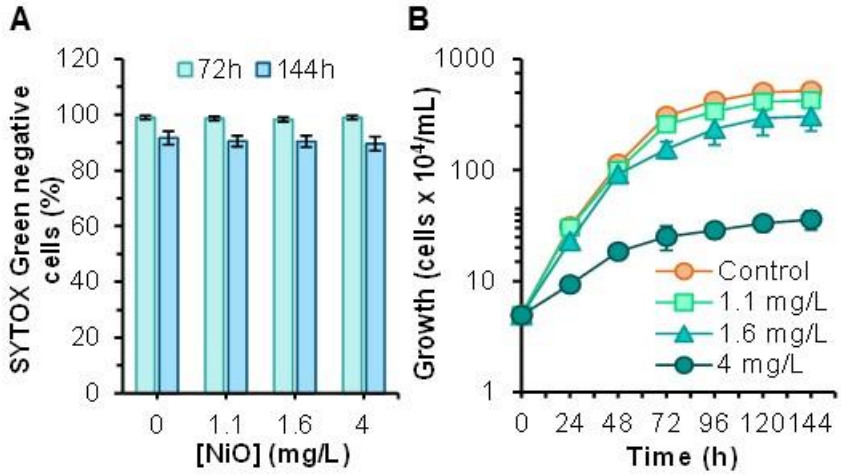

Figure 7.4. Impact of NiO NPs on the plasma membrane integrity and growth of *P. subcapitata*. Algal cells were exposed to 1.1, 1.6 and 4 mg/L NiO, which correspond or are close to 72h-EC_{10}, 72h-EC_{50} and 72h-EC_{90} values, respectively. A - Impact of NiO NPs on plasma membrane integrity. Cells were incubated without (control) or with NiO NPs for 72 h (3 days) or 144 h (6 days). Membrane integrity was assessed by SYTOX Green exclusion. B – Evolution of the growth of *P. subcapitata* in OECD medium in the absence (control) or the presence of NiO NPs. The data are presented as mean values from at least three independent experiments performed in duplicate (n≥6); standard deviations (SD) are presented (vertical error bars). Where no error bars are shown, SD are within the points. A - The means for a given incubation time are not significantly different (P<0.05) (ANOVA).

7.3.4. NiO NPs reduce metabolic activity and induce intracellular ROS accumulation

To further elucidate the causes of the algistatic effect attributed to NiO, the impact of NPs on algal metabolic activity was assessed using a fluorescein diacetate-based cell esterase activity assay; in this assay, the amount of fluorescence is related to the metabolic activity of the esterases (Machado and Soares, 2013). Algal cells exposed to 1.1-1.6 mg/L NiO NPs did not show a significant modification of esterase activity compared to the control. However, a significant decrease in esterase activity was observed for 4 mg/L NiO NPs (Fig 7.5A). These results indicate that a significant loss of metabolic activity only occurred at a NiO concentration at which algal growth was arrested.

The potential pro-oxidant activity of NiO NPs, i.e., the ability of NPs to generate extracellular reactive oxygen species (ROS), under abiotic conditions (cell free), was evaluated using the general ROS probe deacetylated H_2DCFDA (Aruoja et al., 2015; Tarpey et al., 2004). Since the mechanisms underlying ROS production by the NiO NPs could be associated with the redox properties of the nanoparticles themselves and/or the release of Ni^{2+} (dissolution of the NPs), the production of abiotic ROS by 3.1 mg/L Ni^{2+} was evaluated; this Ni^{2+} concentration corresponds to the complete dissolution of 4 mg/L NiO NPs. As can be observed in Figure 7.5B, the NiO NPs and Ni^{2+} were not able to cause the significant generation of abiotic ROS in OECD algal medium. Nevertheless, the algal cells exposed to NiO NPs for 72 h presented the intracellular accumulation of ROS (Fig 7.5C). The quantification of the ROS generated in algal cells allowed the observation that NiO NPs, even at the lowest concentration (1.1 mg/L), were able to significantly induce oxidative stress (Fig 7.5D). At the highest studied concentration of NiO NPs (4 mg/L), an increase in intracellular ROS accumulation (~1.6 times higher than the control) was observed (Fig 7.5D).

7.3.5. NiO NPs decrease pigment content and photosynthetic performance

In algal cells, ROS are normally generated in the mitochondrial respiratory chain or in chloroplast thylakoids in photosystem II (PSII) or photosystem I (PSI) (Apel and Hirt, 2004; Asada, 2006). Stress factors that affect mitochondrial or chloroplast function can increase intracellular ROS accumulation. ROS, in turn, can damage mitochondria or chloroplasts and, as a consequence, contribute to respiration or photosynthesis impairment through the consequent extra ROS generation, causing a vicious cycle. The oxidative stress experienced by algal cells exposed to NiO led us to investigate the effects of the NPs on mitochondria and chloroplasts.

The functionality of algal mitochondria can be studied though the measurement of the inner mitochondrial membrane potential ($\Delta\Psi_m$), which can be performed using lipophilic cations, such as $DiOC_6$ (Haugland, 2005). *P. subcapitata* cells exposed to NiO NPs at concentrations of up to 4 mg/L for 72 h did not display significant permeabilization of the inner mitochondrial membrane ($\Delta\Psi_m$ dissipation) compared to untreated cells (control) (Fig 7.6), which suggests that no damage to mitochondrial function occurred in algal cells within the range of NiO NPs tested.

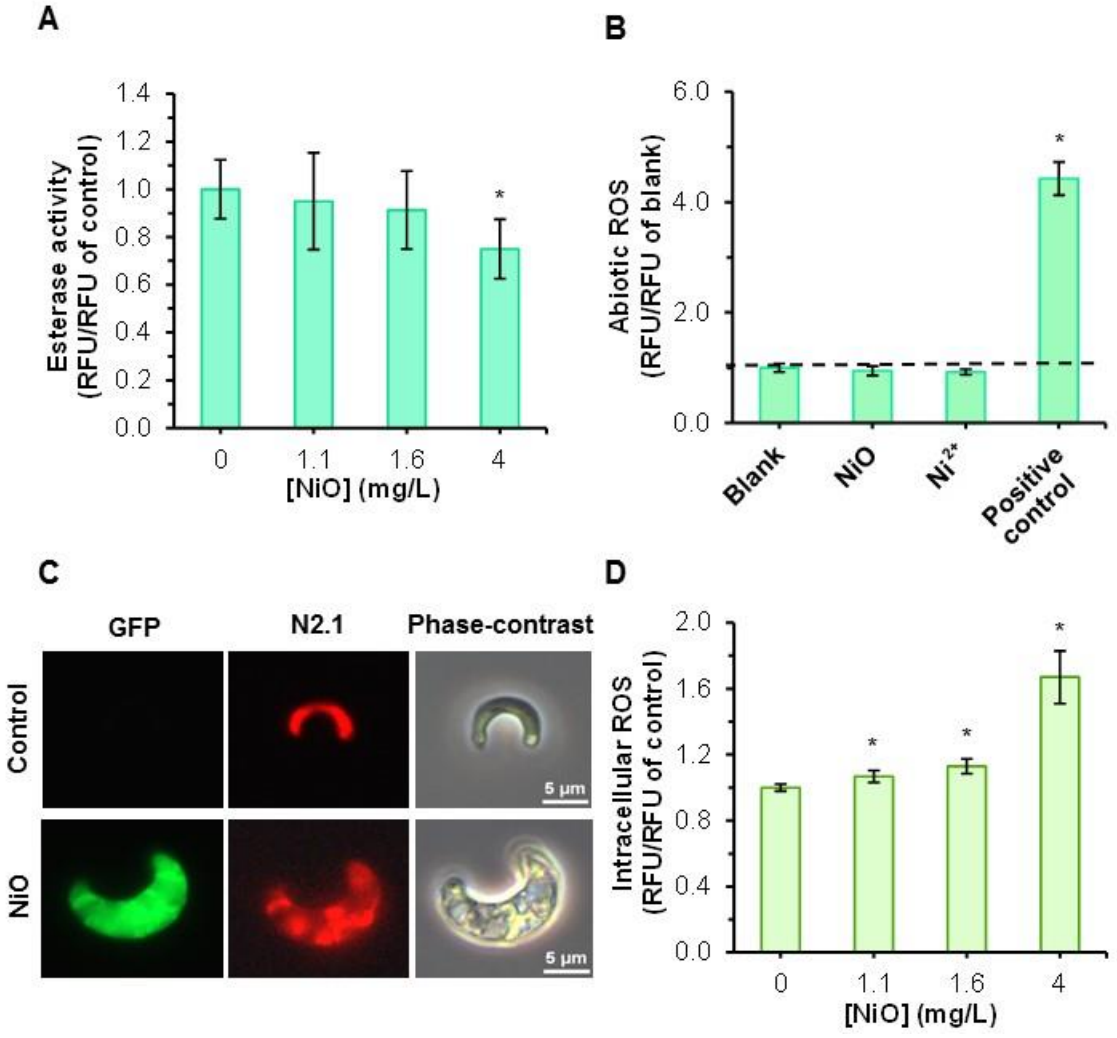

Figure 7.5. Impact of NiO NPs on the metabolism and ROS production by *P. subcapitata*. A- Metabolic activity was assessed through the hydrolysis of FDA (esterase activity assay). Algal cells were incubated in the absence or the presence of NiO NPs, in OECD medium, for 72 hours. B – Possible production of abiotic ROS by NiO NPs and Ni^{2+}. NiO at 4 mg/L or Ni^{2+} at 3.1 mg/L were incubated with H_2DFC in OECD medium, for 72 h, in the dark. Blank and positive control were obtained by incubating the H_2DCF probe in OECD medium or with 26 µM H_2O_2, respectively. C - Visualization of control (cells incubated in the absence of NiO, without ROS) and cells exposed for 72 h to 4 mg/L NiO NPs showing intracellular ROS (green fluorescence) (left side, GFP filter). Algal auto-fluorescence was observed with N.21 filter. Phase-contrast images (right side). D – Assessment of intracellular ROS in algal cells incubated for 72 h in OECD medium in the absence or in the presence of NiO NPs. The data are presented as mean values from at least three independent experiments. In each experiment, five fluorescent readings were performed ($n \geq 15$). Standard deviations are presented (vertical error bars). Statistical differences were subject to ANOVA. The results with asterisks are significantly different ($P < 0.05$).

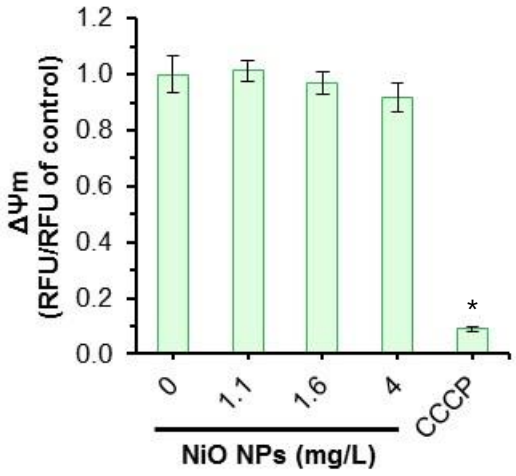

Figure 7.6. Effect of NiO NPs on the mitochondria membrane potential (ΔΨm) of *P. subcapitata*. Algal cells were incubated for 72 h in the absence or in the presence of NiO NPs; subsequently, cells were incubated with $DiOC_6$. As negative control, algal cells after grown in the absence of toxicant were treated with 50 µmol/L of carbonyl cyanide m-chlorophenyl hydrazone (CCCP) and then stained with $DiOC_6$. The data are presented as mean values from at least three independent experiments, performed in duplicate (n≥6); standard deviations are presented (vertical error bars). Statistical differences were subject to ANOVA. The result with an asterisk is significantly different (P<0.05).

In photosynthetic organisms, intracellular ROS accumulation is usually associated with photoinhibition, the bleaching of photosynthetic pigments (He and Häder, 2002) and a reduction in PSII photosynthetic efficiency (Nishiyama et al., 2006). The increased levels of ROS observed in the algal cells exposed to NiO NPs led us to determine the contents of chlorophyll *a* (Chl *a*), *b* (Chl *b*) and carotenoids. Algal cells exposed to 4 mg/L NiO presented a significant decrease in photosynthetic pigments; lower concentrations of NiO NPs did not cause a significant decrease in Chl *a*, Chl *b* or carotenoids (Fig 7.7A). A detailed analysis of photosynthesis performance was carried out using a pulse amplitude modulated (PAM) fluorescence assay. The maximum quantum yield of PSII (F_v/F_m) is a measure of the intrinsic (theoretical maximum) efficiency of PSII photochemicals (Maxwell and Johnson, 2000). The determination of this parameter revealed that photosynthetic performance significantly decreased when the algal cells were incubated with 4 mg/L NiO NPs (Fig 7.7B). The control cells presented a F_v/F_m value of 0.61 ± 0.02, which is within the values indicated for *P. subcapitata* (0.62-0.64) (Drabkova et al., 2007; van der Grinten et al., 2010), showing that the non-treated algae were photochemically efficient. The calculation of the effective photochemical quantum yield of PSII (Φ_{PSII}), which estimates the fraction of the absorbed quanta used in the PSII photochemistry (Maxwell and Johnson, 2000), allowed the detection of a reduction in light utilization efficiency in the algal cells exposed to all tested concentrations of NiO (Fig 7.7C). The coefficient of photochemical quenching (*qP*) is an index that represents the proportion of light excitation energy

trapped by the 'open' PSII reaction centres used for electron transport (Juneau et al., 2002) and reflects the redox state of the primary (quinone, Q_A) electron acceptor (Misra et al., 2012). The determination of *qP* revealed a reduction in the fraction of open PSII reaction centres in the algal cells exposed to NiO (Fig 7.7D). The calculation of the relative electron transport rate (rETR) offers an empirical estimate of the flow rate of electrons through the photosynthetic chain (Consalvey et al., 2005). The exposure of algal cells to 4 mg/L NiO was also observed to cause a significant decrease in the photosynthetic rETR (Fig 7.7E). It is likely that the change in the equilibrium between the excitation rate and the electron transfer rate caused the PSII reaction centre to enter a more reduced state. This leads the cell, as a compensatory mechanism, to dissipate more luminous energy through heat or other methods. Non-photochemical quenching (*NPQ*) represents all quenching processes of PSII not directly associated with photochemistry and can be seen as a regulatory process that quenches chlorophyll excitation (Consalvey et al., 2005; Juneau et al., 2002). Therefore, taking into account the decrease in Φ_{PSII}, the dissipation of energy via the non-regulated photochemical pathway (increase in *NPQ*) was expected; however, the opposite effect was observed (Fig 7.7F).

7.3.6. NiO NPs cause algal morphology modifications and the deterioration of cell cycle progression

The modification of the algal biovolume due to exposure to heavy metals, particularly under growth inhibition conditions, has been described in the literature (Cid et al., 1996; Franklin et al., 2001; Le Faucheur et al., 2005; Machado and Soares, 2014). In this context, the impact of NiO NPs on the morphology of *P. subcapitata* was evaluated. The cell volume of algae exposed to 1.1 or 1.6 mg/L NiO NPs for 72 h was similar to that in the control (Fig 7.8A). However, for 4 mg/L NiO NPs, an increase in the mean cell volume compared to the control was observed. For this NP concentration, a wide range of cell sizes was observed, which was reflected in the large standard deviation associated with the measurement of the mean cell volume (Fig 7.8A).

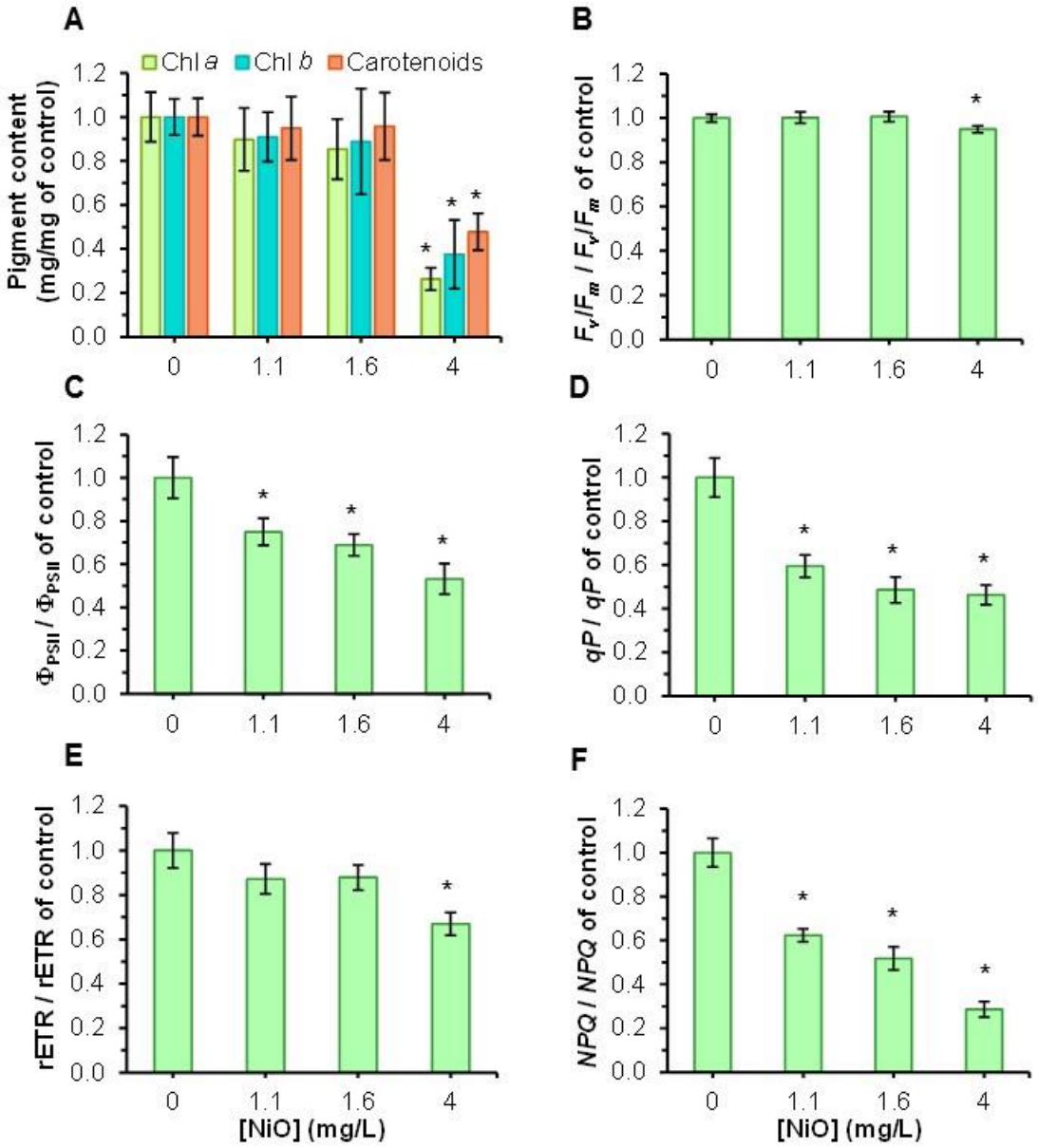

Figure 7.7. Evaluation of pigment content and photosynthetic parameters in *P. subcapitata* exposed to NiO NPs. Algal cells were incubated for 72 h in OECD medium in the absence or in the presence of NiO NPs. A - Photosynthetic pigments: chlorophyll *a* (Chl *a*), chlorophyll *b* (Chl *b*) and carotenoids. B - Maximum quantum yield of PSII (F_v/F_m). C - Effective photochemical quantum yield of PSII (Φ_{PSII}). D - Coefficient of photochemical quenching (*qP*). E – Relative electron transport rate (rETR); F -Non-photochemical quenching (*NPQ*). The data are presented as mean values from at least three independent experiments, performed in duplicate (n≥6); standard deviations are presented (vertical error bars). Statistical differences were subject to ANOVA. The results with asterisks are significantly different ($P<0.05$).

A detailed analysis of the relative frequency distribution of the two cell populations (control cells and cells exposed to 4 mg/L NiO) showed that ≈100% of the non-treated cells presented a cell volume of between 20 and 70 μm^3. The exposure of algal cells to 4 mg/L NiO triggered a shift to the right in the

algal population distribution in which ≈70% of the algal cells presented a biovolume of between 70 and 300 μm^3 (Fig 7.8B).

Considering that an increase in cell volume occurred in the algae exposed to 4 mg/L NPs, i.e., under conditions in which their growth was practically arrested (Fig 7.4B), the impact of NiO on the algal cell cycle was investigated. The green alga *P. subcapitata* reproduces asexually via autospores (van den Hoek et al., 1997). By staining the nucleus of algal cells using a fluorescent probe, it is possible to identify 4 different stages: cells released from autospores (stage 1), cell growth (stage 2), cell division 1: primary cleavage (stage 3), and cell division 2: secondary cleavage (stage 4), and the release of the four autospores (Machado and Soares, 2014b). It was observed that >90% of the algal cells exposed to 4 mg/L NiO NPs were in cell stage 2, while the untreated cells (control) were distributed across the 4 cycle stages (Fig 7.8C). These data reveal that the exposure to NiO disturbed the progression of the algal cell cycle. Algae exposed to 4 mg/L NiO divided 6 times and subsequently stopped growing (Fig 7.4B) almost synchronously (>90% of the cells remained in stage 2) prior to the first cell division and had an increased cell volume (Fig 7.8D). According to the classical model of the cell-division cycle (Smith and Fornace, 1996), the cells that remained in stage 2 were likely in the G1 phase before DNA replication (S phase). It was also possible to observe that less than 5% of the population was able to progress through the reproductive cycle (stage 4) (Fig 7.8C). Algae exposed to 4 mg/L NiO for 72 h markedly increased in size and had an aberrant shape (Fig 7.8D).

7.4. Discussion

The characterization of NiO NPs in an aqueous suspension is very important to understand their potential ecotoxicity and thus to identify their potential environmental and toxicological risks. Therefore, knowledge regarding NiO NP agglomeration, surface charge, and stability (dissolution of NPs) is essential for understanding their bioavailability and mobility (Wilkinson, 2013). The characterization of NiO in OECD medium showed that NPs are not stable (low negative zeta potential values) (Table 7.2), having a tendency to form agglomerates. NP agglomerates increase in size over time, undergo rapid sedimentation (Fig 7.1B) and can be seen with the naked eye after 72 h (Fig 7.1A). The agglomeration of NPs can be attributed to their negative surface charge (-10.6 mV) (Table 7.2) and the presence of Ni^{2+} (released from the NPs), which lead to attractive forces between particles through divalent cation bridges. NiO agglomeration has also been described by other authors when NPs are suspended in different cell culture media (Karlsson et al., 2014; Nogueira et al., 2015; Siddiqui et al., 2012).

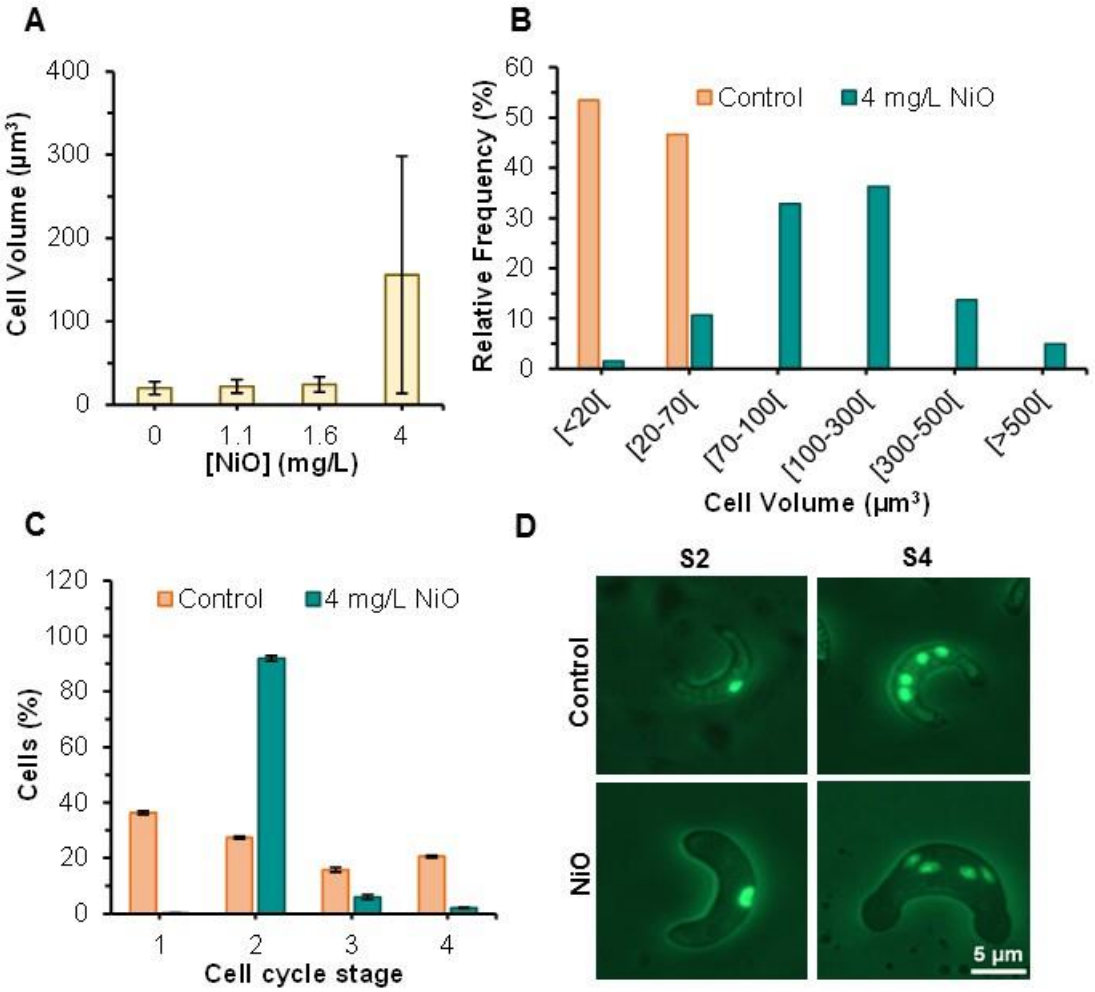

Figure 7.8. Impact of NiO NPs on *P. subcapitata* bio-volume and cell cycle. Algal cells were incubated for 72 h in OECD medium in the absence or in the presence of NiO NPs. A – Algal biovolume was determined assuming that *P. subcapitata* generally conforms to the shape of a sickle-shaped cylinder. B - Relative frequency of algae biovolume. The algae biovolumes were grouped in different classes. Relative frequency is the percentage of biovolumes falling in each class. C - Distribution of algal cells through the cell cycle. Stage 1: cell released from the autospore; stage 2: cell growth; stage 3: cell division 1; stage 4: cell division 2. D - Photomicrographs of fluorescence plus phase contrast images of algal cells at different stages, not exposed (control) or exposed to 4 mg/L NiO NPs. The data are presented as mean values from at least three independent experiments performed in duplicate (n≥6); standard deviations are presented (vertical error bars).

The presence of algal cells intensified NP agglomeration (Fig 7.3A). Microscopic analysis of the hetero-agglomerates revealed the formation of larger structures containing algal cells (Fig 7.3B). Due to the loose nature of these structures, the algae present inside the agglomerates should not be nutritionally limited as a consequence of diffusional limitations. Similar algal entrapment by Al_2O_3 was observed in *P. subcapitata* (Aruoja et al., 2015), *Scenedesmus* sp. and *Chlorella* sp. (Sadiq et al., 2011).

Algae make essential contributions to aquatic systems. *P. subcapitata* is an important model organism in freshwater environments, being frequently used in toxicity assessments of a large variety of

substances, including metals and metal-oxide NPs (Aruoja et al., 2015; Bondarenko et al., 2016; Machado et al., 2015). In the present study, the potential ecotoxicological hazards of NiO NPs were evaluated using the algal growth inhibition assay (OECD, 2011) with *P. subcapitata*. NiO NPs presented a 72 h-EC_{50} of 1.6 mg/L (Table 7.3), allowing this NP to be classified as toxic (1-10 mg/L) (Bondarenko et al., 2016). The 72 h-EC_{50} value presented here is lower but at the same order of the magnitude as the value described for the same alga (8.3 mg/L) with NiO NPs of a different size (100 nm) (Nogueira et al., 2015) and another alga, *Chlorella vulgaris*, with a 72 h-EC_{50} value of 32 mg/L and a 96 h-EC_{50} value of 14 mg/L (Gong et al., 2011; Oukarroum et al., 2017). Higher concentrations of NiO NPs were required to inhibit the growth of bacteria (24 h-EC_{50} values for *Escherichia coli*, *Bacillus subtilis* and *Staphylococcus aureus* of 160, 122 and 121 mg/L, respectively) (Baek and An, 2011) and to cause the mortality of zebrafish (*Danio rerio*) (96 h-LC_{50} value of 420 mg/L; concentration causing 50% mortality in adult zebrafish) (Kovrižnych et al., 2013), which highlights the sensitivity of algal cells, particularly *P. subcapitata***,** to toxicants.

The toxicity of NiO NPs can be attributed to the NPs themselves, the release of Ni^{2+} or both. Due to the formation of NiO NP agglomerates and the presence of the cell wall in algal cells, it would seem rather unlikely that NiO NPs are taken up by the algae. Similarly, it has been proposed that Ag NPs are not internalized by algal cells (Li et al., 2015). However, a surface effect of NPs cannot be ruled out. In fact, *P. subcapitata* cells incubated with NiO displayed agglomerated NPs adsorbed on their surface (Fig 7.2C). The adsorption of NP agglomerates on the algal surface may have a negative impact, for instance, by inhibiting the activity of extracellular enzymes, as was described for Ag NPs (Yue et al., 2017). Another possibility of how NPs can exert their toxic effects may be through their dissolution. The Ni^{2+} released from the NPs can be taken up by the alga. Indeed, the amount of Ni^{2+} leached from the NPs seems to be sufficient to explain the majority of the toxicity of NiO NPs on *P. subcapitata* algal cells, as can be deduced from the comparison of the NiO and Ni^{2+} 72 h-EC values (Table 7.3) and the amount of Ni solubilized by the NPs (Fig 7.1C).

The decreased growth observed in the algal cells exposed to NiO could result from different causes, including increased cell death, reduced metabolic activity (as a consequence of altered photosynthesis or disturbed mitochondrial function) and cell cycle deterioration. The exposure of algal cells to up to 4 mg/L NiO for 72 h caused a reduction in growth without a loss of membrane integrity (Fig 7.4). The permeability of the plasma membrane to dyes such as propidium iodide and SYTOX green represents irreparable damage to the membrane barrier function and cell death (Galluzzi et al., 2015). The results

presented here strongly suggest that NiO has an algistatic effect, i.e., growth reduction without cell death.

One of the main paradigms in nanotoxicology is the tendency of NPs to induce intracellular ROS production (Nel et al., 2006; von Moos and Slaveykova, 2014). The exposure of *P. subcapitata* cells to NiO NPs induced ROS overload, even at a low concentration (1.1 mg/L) (Fig 7.5D). It is likely that oxidative stress is a common event associated with NiO NP exposure and toxicity. In fact, intracellular ROS have been observed in cells of different species after exposure to NiO NPs: yeast (*Saccharomyces cerevisiae*) (please see Chapter 3), the alga *Chlorella vulgaris* (Oukarroum et al., 2017), the crustacean *Artemia salina* (Ates et al., 2016), the aquatic plant *Lemna gibba* (Oukarroum et al., 2015a), rats (lung cells) (Jeong et al., 2016) and humans, including liver (Ahamed et al., 2013), lung carcinoma (Horie et al., 2011), breast cancer and airway epithelial cells (Siddiqui et al., 2012).

It has been shown that the PAM fluorescence assay is a simple, fast and sensitive tool for evaluating the impacts of toxicants on the photosynthetic activity of PSII (Juneau and Popovic, 1999; Kumar et al., 2014). It is commonly accepted that PSII is the most vulnerable part of the photosynthetic apparatus, and damage to PSII is generally seen as signal of stress (Maxwell and Johnson, 2000). The maximum PSII quantum efficiency (F_v/F_m) indicates the potential capacity of photosynthetic cells to convert light energy into chemical energy (El-Berdey et al., 2000). The exposure of algal cells to concentrations of up to 1.6 mg/L NiO did not affect the F_v/F_m, which indicates that the light harvesting capacity of PSII remains undamaged at up to this concentration of NPs. Disturbance to the maximum photosynthetic capacity was only observed in algal cells exposed to 4 mg/L NiO (Fig 7.7B). However, the exposure of algal cells to all tested concentrations of NiO caused a significant reduction in the efficiency of the PSII photochemistry (Φ_{PSII}) (Fig 7.7C), which indicates an overall reduction in photosynthesis. These results are in agreement with studies in the literature that indicate that Φ_{PSII} is a sensitive indicator for assessing algal responses to toxicants (Juneau and Popovic, 1999; Kumar et al., 2014). The reduction in photochemical efficiency associated with the exposure to NPs seems to be (at least in part) related to a perturbation to the electron transport process as indicated by the reduction in the rETR (Fig 7.7E). The slowdown of PSII electron flow caused a reduction in the proportion of PSII reaction centres that were open (reduction in *qP*) (Fig 7.7D) and ultimately a reduction in the photosynthetic efficiency (Φ_{PSII}). Thus, the impairment of photosynthesis seems to be associated with damage to the reaction centres of PSII. The electrons that are no longer used in the photochemistry could be leaked and used to reduce molecular oxygen (ROS production). ROS formation can potentially damage the chloroplasts through oxidative stress. Disturbance to the

electron transport process can explain the intracellular ROS overload in algae exposed to NiO NPs (Fig 7.5D). This possibility is in agreement with the literature, which suggests that the reaction centres of PSII and PSI are the main locations of ROS production in photosynthetic organisms (Asada, 2006). Some herbicides have also been described as being able to induce ROS production in plants by blocking electron transfer, as the OS are generated in the reaction centre of PSII (Rutherford and Krieger-Liszkay, 2001). Due to the inhibition of the photochemical energy-consuming pathway (Fig 7.7C), algal cells may dissipate excess energy through non-photochemical processes in order to preserve the photosynthetic apparatus (Baker, 2008). However, a significant reduction in non-photochemical quenching (*NPQ*) in algal cells exposed to all concentrations of NiO NPs was observed (Fig 7.7F), which likely reflects the failure of the cells to protect PSII from photodamage through both regulated and unregulated (conversion of energy in the antenna complex to heat) energy dissipation pathways. A similar effect was observed when the alga *C. reinhardtii* was exposed to biocides (Almeida et al., 2017).

Chlorophytes (freshwater green algae) are able to take up heavy metals via the metal transporters and carriers used for the uptake of essential elements (Pfeiffer et al., 2017). It is likely that the Ni^{2+} released by the NPs enters the algal cells, inhibiting the synthesis of photosynthetic pigments (Fig 7.7A) and damaging the PSII reaction centre, as described above. In agreement with this possibility, it has been reported that the presence of heavy metals can bleach photosynthetic pigments by inhibiting their synthesis in parallel with the destruction of the photosynthetic apparatus (Kupper et al., 2002; Shakya et al., 2008).

The exposure of algal cells to low, sub-lethal concentrations of NPs (1.1 and 1.6 mg/L NiO, which corresponded to the ~72 h-EC_{10} and ~72 h-EC_{50} values, respectively) induced the intracellular accumulation of ROS (Fig 7.5D) and caused disturbance to the photosynthetic activity, as described above (Fig 7.7C). The algal cells exposed to a higher but also sub-lethal concentration of NPs (4 mg/L NiO, which corresponded to the ~72 h-EC_{90} value) were only able to divide in a limited way (~6 times) before their growth stopped (Fig 7.4C). It is likely that this discontinuation of growth can be attributed to the arrest of the cell cycle prior to the first cell division (cell growth stage 2) (Fig 7.8C), which in turn led to the formation of algal cells of increased size (Fig 7.8A, B) and aberrant morphology (Fig 7.8D). It can be hypothesized that this abnormal phenotype can result from the arrest of the cell cycle as a consequence of the increased levels of ROS observed in these cells (Fig 7.5D) combined with a reduction in metabolic activity (Fig 7.5A) and photosynthetic performance (Fig 7.7C).

7.5. Conclusions

The mechanisms of toxicity action of NiO NPs on *P. subcapitata* was evaluated in this Chapter:

- Using growth inhibition assay, NiO NPs can be classified as toxic;
- The toxic effects observed in *P. subcapitata* were mainly caused by the Ni^{2+} released by the NPs;
- NiO NPs reduced the photosynthetic efficiency and enhanced intracellular ROS;
- NiO NPs induced cell cycle arrest (prior the first cell division) and aberrant alga morphology.

References

Ahamed, M., Ali, D., Alhadlaq, H.A., Akhtar, M.J., 2013. Nickel oxide nanoparticles exert cytotoxicity via oxidative stress and induce apoptotic response in human liver cells (HepG2). Chemosphere 93, 2514-2522.

Almeida, A.C., Gomes, T., Langford, K., Thomas, K.V., Tollefsen, K.E., 2017. Oxidative stress in the algae *Chlamydomonas reinhardtii* exposed to biocides. Aquat. Toxicol. 189, 50-59.

Apel, K., Hirt, H., 2004. Reactive oxygen species: metabolism, oxidative stress, and signal transduction. Annu. Rev. Plant Biol. 55, 373–399.

Aruoja, V., Pokhrel, S., Sihtmae, M., Mortimer, M., Madler, L., Kahru, A., 2015. Toxicity of 12 metal-based nanoparticles to algae, bacteria and protozoa. Environ. Sci. Nano 2, 630-644.

Asada, K., 2006. Production and scavenging of reactive oxygen species in chloroplasts and their functions. Plant Physiol. 141, 391-396.

Ates, M., Demir, V., Arslan, Z., Camas, M., Celik, F., 2016. Toxicity of engineered nickel oxide and cobalt oxide nanoparticles to *Artemia salina* in seawater. Water Air Soil Pollut. 227.

Baek, Y.W., An, Y.J., 2011. Microbial toxicity of metal oxide nanoparticles (CuO, NiO, ZnO, and Sb2O3) to *Escherichia coli*, *Bacillus subtilis*, and *Streptococcus aureus*. Sci. Total Environ. 409, 1603-1608.

Baker, N.R., 2008. Chlorophyll fluorescence: a probe of photosynthesis in vivo. Annual Rev. Plant Biol. 59, 89-113.

Baker, T.J., Tyler, C.R., Galloway, T.S., 2014. Impacts of metal and metal oxide nanoparticles on marine organisms. Environ. Pollut. 186, 257-271.

Batley, G.E., Kirby, J.K., McLaughlin, M.J., 2013. Fate and risks of nanomaterials in aquatic and terrestrial environments. Acc. Chem. Res. 46, 854-862.

Beaudrie, C.E.H., Kandlikar, M., Satterfield, T., 2013. From cradle-to-grave at the nanoscale: gaps in US regulatory oversight along the nanomaterial life cycle. Environ. Sci. Technol. 47, 5524-5534.

Bondarenko, O.M., Heinlaan, M., Sihtmae, M., Ivask, A., Kurvet, I., Joonas, E., Jemec, A., Mannerstrom, M., Heinonen, T., Rekulapelly, R., Singh, S., Zou, J., Pyykko, I., Drobne, D., Kahru, A., 2016. Multilaboratory evaluation of 15 bioassays for (eco)toxicity screening and hazard ranking of engineered nanomaterials: FP7 project NANOVALID. Nanotoxicology 10, 1229-1242.

Cid, A., Fidalgo, P., Herrero, C., Abalde, J., 1996. Toxic action of copper on the membrane system of a marine diatom measured by flow cytometry. Cytometry 25, 32-36.

Clesceri, L.S., Greenberg, A.E., Eaton, A.D., 1999. Standard methods for the examination of water and wastewater, 20th ed. American Public Health Association, American Water Works Association, Water Environment Federation.

Consalvey, M., Perkins, R.G., Paterson, D.M., Underwood, G.J.C., 2005. PAM fluorescence: A beginners guide for benthic diatomists. Diatom Res. 20, 1-22.

Drabkova, M., Matthijs, H.C.P., Admiraal, W., Marsalek, B., 2007. Selective effects of H_2O_2 on cyanobacterial photosynthesis. Photosynthetica 45, 363-369.

El-Berdey, A., Juneau, P., Pirastru, L., Popovic, R., 2000. Application of the PAM fluorometric method for determination of copper toxicity to microalgae and duckweed, in: Persoone, G., Janssen, C., Wim, D.C. (Eds.), New microbiotests for routine toxicity screening and biomonitoring. Springer, Boston, pp. 135-140.

Franklin, N.M., Stauber, J.L., Lim, R.P., 2001. Development of flow cytometry-based algal bioassays for assessing toxicity of copper in natural waters. Environ. Toxicol. Chem. 20, 160-170.

Galluzzi, L., Bravo-San Pedro, J.M., Vitale, I., Aaronson, S.A., Abrams, J.M., Adam, D., Alnemri, E.S., Altucci, L., Andrews, D., Annicchiarico-Petruzzelli, M., Baehrecke, E.H., Bazan, N.G., Bertrand, M.J., Bianchi, K., Blagosklonny, M.V., Blomgren, K., Borner, C., Bredesen, D.E., Brenner, C., Campanella, M., Candi, E., Cecconi, F., Chan, F.K., Chandel, N.S., Cheng, E.H., Chipuk, J.E., Cidlowski, J.A., Ciechanover, A., Dawson, T.M., Dawson, V.L., De Laurenzi, V., De Maria, R., Debatin, K.M., Di Daniele, N., Dixit, V.M., Dynlacht, B.D., El-Deiry, W.S., Fimia, G.M., Flavell, R.A., Fulda, S., Garrido, C., Gougeon, M.L., Green, D.R., Gronemeyer, H., Hajnoczky, G., Hardwick, J.M., Hengartner, M.O., Ichijo, H., Joseph, B., Jost, P.J., Kaufmann, T., Kepp, O., Klionsky, D.J., Knight, R.A., Kumar, S., Lemasters, J.J., Levine, B., Linkermann, A., Lipton, S.A., Lockshin, R.A., Lopez-Otin, C., Lugli, E., Madeo, F., Malorni, W., Marine, J.C., Martin, S.J., Martinou, J.C., Medema, J.P., Meier, P., Melino, S., Mizushima, N., Moll, U., Munoz-Pinedo, C., Nunez, G., Oberst, A., Panaretakis, T., Penninger, J.M., Peter, M.E., Piacentini, M., Pinton, P., Prehn, J.H., Puthalakath, H., Rabinovich, G.A., Ravichandran, K.S., Rizzuto, R., Rodrigues, C.M., Rubinsztein, D.C., Rudel, T., Shi, Y., Simon, H.U., Stockwell, B.R., Szabadkai, G., Tait, S.W., Tang, H.L., Tavernarakis, N., Tsujimoto, Y., Vanden Berghe, T., Vandenabeele, P., Villunger, A., Wagner, E.F.,

Walczak, H., White, E., Wood, W.G., Yuan, J., Zakeri, Z., Zhivotovsky, B., Melino, G., Kroemer, G., 2015. Essential versus accessory aspects of cell death: recommendations of the NCCD 2015. Cell Death Differ. 22, 58-73.

Geis, S.W., Fleming, K.L., Korthals, E.T., Searle, G., Reynolds, L., Karner, D.A., 2000. Modifications to the algal growth inhibition test for use as a regulatory assay. Environ. Toxicol. Chem. 19, 36-41.

Gong, N., Shao, K., Feng, W., Lin, Z., Liang, C., Sun, Y., 2011. Biotoxicity of nickel oxide nanoparticles and bio-remediation by microalgae *Chlorella vulgaris*. Chemosphere 83, 510-516.

Hanna, S.K., Miller, R.J., Zhou, D.X., Keller, A.A., Lenihan, H.S., 2013. Accumulation and toxicity of metal oxide nanoparticles in a soft-sediment estuarine amphipod. Aquat. Toxicol. 142, 441-446.

Haugland, R.P., 2005. The handbook – a guide to fluorescent probes and labeling technologies, 10th ed. Invitrogen Corp, Eugene, OR, USA.

He, Y.Y., Häder, D.P., 2002. UV-B-induced formation of reactive oxygen species and oxidative damage of the cyanobacterium *Anabaena* sp.: protective effects of ascorbic acid and N-acetyl-L-cysteine. J. Photochem. Photobiol. B. 66, 115-124.

Horie, M., Fukui, H., Nishio, K., Endoh, S., Kato, H., Fujita, K., Miyauchi, A., Nakamura, A., Shichiri, M., Ishida, N., Kinugasa, S., Morimoto, Y., Niki, E., Yoshida, Y., Iwahashi, H., 2011. Evaluation of acute oxidative stress induced by NiO nanoparticles in vivo and in vitro. J. Occup. Health 53, 64-74.

Hunt, G., Lynch, I., Cassee, F., Handy, R.D., Fernandes, T.F., Berges, M., Kuhlbusch, T.A.J., Dusinska, M., Riediker, M., 2013. Towards a consensus view on understanding nanomaterials hazards and managing exposure: knowledge gaps and recommendations. Materials 6, 1090-1117.

Jeong, J., Kim, J., Seok, S.H., Cho, W.S., 2016. Indium oxide (In_2O_3) nanoparticles induce progressive lung injury distinct from lung injuries by copper oxide (CuO) and nickel oxide (NiO) nanoparticles. Arch. Toxicol. 90, 817-828.

Juneau, P., El Berdey, A., Popovic, R., 2002. PAM fluorometry in the determination of the sensitivity of *Chlorella vulgaris*, *Selenastrum capricornutum*, and *Chlamydomonas reinhardtii* to copper. Arch. Environ. Contam. Toxicol. 42, 155-164.

Juneau, P., Popovic, R., 1999. Evidence for the rapid phytotoxicity and environmental stress evaluation using the PAM fluorometric method: importance and future application. Ecotoxicology 8, 449-455.

Karlsson, H.L., Gliga, A.R., Calleja, F.M.G.R., Goncalves, C.S.A.G., Wallinder, I.O., Vrieling, H., Fadeel, B., Hendriks, G., 2014. Mechanism-based genotoxicity screening of metal oxide nanoparticles using the ToxTracker panel of reporter cell lines. Part. Fibre Toxicol. 11, 1-14.

Kovriznych, J.A., Sotnikova, R., Zeljenkova, D., Rollerova, E., Szabova, E., 2014. Long-term (30 days) toxicity of NiO nanoparticles for adult zebrafish *Danio rerio*. Interdiscip. Toxicol. 7, 23-26.

Kovrižnych, J.A., Sotníková, R., Zeljenková, D., Rollerová, E., Szabová, E., Wimmerová, S., 2013. Acute toxicity of 31 different nanoparticles to zebrafish (*Danio rerio*) tested in adulthood and in early life stages - comparative study. Interdiscip. Toxicol. 6, 67-73.

Kumar, K.S., Dahms, H.U., Lee, J.S., Kim, H.C., Lee, W.C., Shin, K.H., 2014. Algal photosynthetic responses to toxic metals and herbicides assessed by chlorophyll a fluorescence. Ecotoxicol. Environ. Saf. 104, 51-71.

Kupper, H., Setlik, I., Spiller, M., Kupper, F.C., Prasil, O., 2002. Heavy metal-induced inhibition of photosynthesis: targets of in vivo heavy metal chlorophyll formation. J. Phycol. 38, 429-441.

Le Faucheur, S., Behra, R., Sigg, L., 2005. Phytochelatin induction, cadmium accumulation, and algal sensitivity to free cadmium ion in *Scenedesmus vacuolatus*. Environ. Toxicol. Chem. 24, 1731-1737.

Li, X.M., Schirmer, K., Bernard, L., Sigg, L., Pillai, S., Behra, R., 2015. Silver nanoparticle toxicity and association with the alga *Euglena gracilis*. Environ. Sci. Nano 2, 594-602.

Ma, H.B., Wallis, L.K., Diamond, S., Li, S.B., Canas-Carrell, J., Parra, A., 2014. Impact of solar UV radiation on toxicity of ZnO nanoparticles through photocatalytic reactive oxygen species (ROS) generation and photo-induced dissolution. Environ. Pollut. 193, 165-172.

Machado, M.D., Lopes, A.R., Soares, E.V., 2015. Responses of the alga *Pseudokirchneriella subcapitata* to long-term exposure to metal stress. J. Hazard. Mater. 296, 82-92.

Machado, M.D., Soares, E.V., 2012. Development of a short-term assay based on the evaluation of the plasma membrane integrity of the alga *Pseudokirchneriella subcapitata*. Appl. Microbiol. Biotechnol. 95, 1035-1042.

Machado, M.D., Soares, E.V., 2013. Optimization of a microplate-based assay to assess esterase activity in the alga *Pseudokirchneriella subcapitata*. Water Air Soil Pollut. 224.

Machado, M.D., Soares, E.V., 2014. Modification of cell volume and proliferative capacity of *Pseudokirchneriella subcapitata* cells exposed to metal stress. Aquatic Toxicology 147, 1-6.
Machado, M.D., Soares, E.V., 2016. Short- and long-term exposure to heavy metals induced oxidative stress response in *Pseudokirchneriella subcapitata*. CLEAN 44, 1-6.
Maxwell, K., Johnson, G.N., 2000. Chlorophyll fluorescence - a practical guide. J. Exp. Bot. 51, 659-668.
Misra, A.N., Misra, M., Singh, R., 2012. Chlorophyll fluorescence in plant biology, in: Misra, A.N. (Ed.), Biophysics. IntechOpen, India, pp. 171-192.
Nel, A., Xia, T., Madler, L., Li, N., 2006. Toxic potential of materials at the nanolevel. Science 311, 622-627.
Nishiyama, Y., Allakhverdiev, S.I., Murata, N., 2006. Regulation by environmental conditions of the repair of photosystem II in cyanobacteria, in: Demmig-Adams, B., Adams, W.W., Mattoo, A.K. (Eds.), Photoprotection, photoinhibition, gene regulation, and environment Springer, The Netherlands, pp. 193-203.
Nogueira, V., Lopes, I., Rocha-Santos, T.A.P., Rasteiro, M.G., Abrantes, N., Goncalves, F., Soares, A.M.V.M., Duarte, A.C., Pereira, R., 2015. Assessing the ecotoxicity of metal nano-oxides with potential for wastewater treatment. Environ. Sci. Pollut. Res. 22, 13212-13224.
OECD, 2011. Alga, Growth Inhibition Test (201), OECD Guideline for Testing of Chemicals. Organization for Economic Co-Operation and Development, Paris, France.
Oukarroum, A., Barhoumi, L., Samadani, M., Dewez, D., 2015. Toxic effects of nickel oxide bulk and nanoparticles on the aquatic plant *Lemna gibba*. Biomed Res. Int. 2015, ID: 501326
Oukarroum, A., Zaidi, W., Samadani, M., Dewez, D., 2017. Toxicity of nickel oxide nanoparticles on a freshwater green algal strain of *Chlorella vulgaris*. Biomed Res. Int. 2017, ID: 9528180
Pfeiffer, T.Z., Ivna, S., Maronić, D.S., Maksimovic, I., 2017. Regulation of photosynthesis in algae under metal stress, Environment and Photosynthesis a Future Prospect. Studium Press India Pvt. Ltd, India, pp. 261-286.
Ravindhranath, K., Ramamoorty, M., 2017. Nickel based nano particles as adsorbents in water purification methods - a review. Oriental J. Chem. 33, 1603-1613.
Research, 2017. Research B. Global Markets for Nanocomposites, Nanoparticles, Nanoclays, and Nanotubes, http://www.bccresearch.com/market-research/nanotechnology/nanocomposites-nanoparticles-nantubes-market-report-nan021g.html (accessed 23 January 2017).
Rojickova-Padrtova, R., Marsalek, B., 1999. Selection and sensitivity comparisons of algal species for toxicity testing. Chemosphere 38, 3329-3338.
Rutherford, A.W., Krieger-Liszkay, A., 2001. Herbicide-induced oxidative stress in photosystem II. Trends Biochem. Sci. 26, 648-653.
Sadiq, I.M., Pakrashi, S., Chandrasekaran, N., Mukherjee, A., 2011. Studies on toxicity of aluminum oxide (Al_2O_3) nanoparticles to microalgae species: *Scenedesmus* sp and *Chlorella* sp. J. Nanopart. Res. 13, 3287-3299.
Shakya, K., Chettri, M.K., Sawidis, T., 2008. Impact of heavy metals (copper, zinc, and lead) on the chlorophyll content of some mosses. Arch. Environ. Contam. Toxicol. 54, 412-421.
Siddiqui, M.A., Ahamed, M., Ahmad, J., Khan, M.A.M., Musarrat, J., Al-Khedhairy, A.A., Alrokayan, S.A., 2012. Nickel oxide nanoparticles induce cytotoxicity, oxidative stress and apoptosis in cultured human cells that is abrogated by the dietary antioxidant curcumin. Food Chem. Toxicol. 50, 641-647.
Smith, M.L., Fornace, A.J., 1996. Mammalian DNA damage-inducible genes associated with growth arrest and apoptosis. Mutat. Res. Genet. Toxicol. Environ. Mutagen. 340, 109-124.
Srivastava, N.K., Jha, M.K., Sreekrishnan, T.R., 2014. Removal of Cr (VI) from waste water using NiO nanoparticles Int. J. Environ. Sci. Technol. 3, 395 – 402.
Strickland, J.D.H., Parsons, T.R., 1972. A Practical Handbook of Seawater Analysis. Second ed. The Alger Press Ltd, Ottawa.
Sun, J., Liu, D.Y., 2003. Geometric models for calculating cell biovolume and surface area for phytoplankton. J. Plankton Res. 25, 1331-1346.
Tarpey, M.M., Wink, D.A., Grisham, M.B., 2004. Methods for detection of reactive metabolites of oxygen and nitrogen: in vitro and in vivo considerations. Am. J. Physiol. Regul. Integr. Comp. Physiol. 286, R431-R444.
US-EPA, 2002. Short-term methods for estimating the chronic toxicity of effluents and receiving waters to freshwater organisms, 4th ed. Environmental Protection Agency, Washington, DC, pp. 1-350, EPA-821-R-302-013.
van den Hoek, C., Mann, D., Jahns, H.M., 1997. Chlorophyta: class 2. *Chlorophyceae*, Algae: an introduction to phycology. Cambridge University Press, Cambridge, UK, pp. 349-390.

van der Grinten, E., Pikkemaat, M.G., van den Brandhof, E.J., Stroomberg, G.J., Kraak, M.H.S., 2010. Comparing the sensitivity of algal, cyanobacterial and bacterial bioassays to different groups of antibiotics. Chemosphere 80, 1-6.

von Moos, N., Slaveykova, V.I., 2014. Oxidative stress induced by inorganic nanoparticles in bacteria and aquatic microalgae - state of the art and knowledge gaps. Nanotoxicology 8, 605-630.

Wilkinson, K.J., 2013. Emerging Issues in Ecotoxicology: Characterization of (Metallic) Nanoparticles in Aqueous Media, in: Férard, J.-F., Blaise, C. (Eds.), Encyclopedia of Aquatic Ecotoxicology. Springer Publishers, Dordrecht, pp. 395-405.

Yue, Y., Li, X.M., Sigg, L., Suter, M.J.F., Pillai, S., Behra, R., Schirmer, K., 2017. Interaction of silver nanoparticles with algae and fish cells: a side by side comparison. J. Nanobiotechnol. 15:16

Zhou, D., Xie, D., Xia, X.H., Wang, X.L., Gu, C.D., Tu, J.P., 2017. All-solid-state electrochromic devices based on WO3||NiO films: material developments and future applications. Sci. China Chem. 60, 3-12.

Zhu, T., Chen, J.S., Lou, X.W., 2012. Highly efficient removal of organic dyes from waste water using hierarchical NiO spheres with high surface area. J. Phys. Chem. C 116, 6873-6878.

Chapter 8 - Chronic exposure of the freshwater alga *Pseudokirchneriella subcapitata* to five oxide nanoparticles: hazard assessment and cytotoxicity mechanisms*

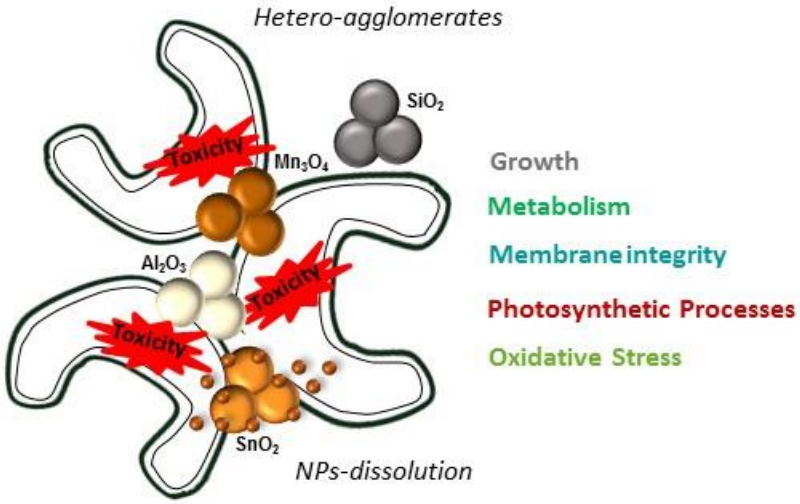

*In revision

8.1. Introduction

In the emerging field of nanotechnology, the nanoparticles (NPs) exhibit unique physical and chemical properties due to their limited size (<100 nm). Metal(loid) oxide (MOx) NPs, such as aluminium oxide (Al_2O_3), indium oxide (In_2O_3), manganese oxide (Mn_3O_4), silicon dioxide (SiO_2) and tin oxide (IV) (SnO_2) can be used in a wide range of fields, such as optics, electric and electronics, medical imaging, cosmetics, plastic production, ceramics, fuel additives and aerospace industry (Andreescu et al., 2012; Laurent et al., 2018; Nanotech, 2015; Tian et al., 2013; Vranic et al., 2019).

The safe use of nanotechnology, on an industrial scale, requires a careful evaluation of the potential environmental and human health risks that can result from the release of NPs into the environment. The increasing use of NPs inevitably intensifies their unintended introduction into the environment. Thus, the NPs toxicity data are very important for the risks evaluation in aquatic environments. Algae, as primary producers, represent the base of food chain (first trophic level). Therefore, due to their ecological importance, the alga *Pseudokirchneriella subcapitata* have been used in the assessment of toxicity (algal growth inhibition assay) (Geis et al., 2000; OECD, 2011; US-EPA, 2002).

Studies carried out in the last decade evidence that NPs, including MOx NPs can cause toxic effects. Concerning to Al_2O_3, In_2O_3, Mn_3O_4, SiO_2 and SnO_2 NPs, a very limited information about their potential toxicity over algal cells is available. In this context, it was described that Al_2O_3 NPs caused growth inhibition and reduction of chlorophyll content in the green algae *Chlorella* sp. and *Scenedesmus* sp. (Sadiq et al., 2011) and in the red alga *Porphyridium aerugineum* Geitler (Karunakaran et al., 2015). SiO_2 NPs inhibited the growth of the marine algae *Dunaliella tertiolecta* (Manzo et al., 2015); similarly, growth inhibition, reduction of chlorophyll and protein content in *P. aerugineum* Geitler exposed to SiO_2 NPs was described (Karunakaran et al., 2015). Aruoja et al. (2015) showed that Al_2O_3, Mn_3O_4 and SiO_2 NPs caused growth inhibition of the alga *P. subcapitata*. Nonetheless, Al_2O_3, In_2O_3 and SnO_2 NPs seems to be nontoxic to the marine diatom *Skeletonema costatum* (Ng et al., 2015).

Despite the commercial importance of metal(loid)-based NPs, a limited information can be found in the literature regarding the potential ecotoxicity of the NPs studied, namely: i) the hazard evaluation; ii) the understanding of the mechanisms behind NPs toxicity. In this sense, this Chapter aimed to assess the ecotoxicity (assessment and categorization of NPs hazardous) of five NPs (Al_2O_3, In_2O_3, Mn_3O_4, SiO_2 and SnO_2) by means of the environmental relevant organism *P. subcapitata*, using algal growth inhibition assay. In addition, NPs physico-chemical properties [hydrodynamic size, zeta potential, agglomeration, dissolution and abiotic production of reactive oxygen species (ROS)] were characterized in order to understand their toxic impact. With regard to shed light on the mechanisms

behind NPs toxicity, key-responses, at sub-cellular level, of the freshwater alga *P. subcapitata* were evaluated as potential markers of cytotoxicity; thus, plasma membrane integrity, intracellular accumulation of ROS, metabolic activity and photosynthetic performance was assessed in algal cells chronic exposed (72 h) to different NPs concentrations. To our knowledge, this is the first work that provides a comprehensive study of the impact of Al_2O_3, In_2O_3, Mn_3O_4, SiO_2 and SnO_2 NPs on the physiology of the microalga *P. subcapitata*. This work contributes for the systematic characterization of the potential pollutant hazards of MOx NPs in the aquatic environment.

8.2. Materials and Methods

8.2.1. Preparation of nanoparticles stock suspensions

The following NPs were used, as described in Chapter 6: Al_2O_3 (<50 nm), In_2O_3 (<100 nm); Mn_3O_4 (<30 nm), SiO_2 (<20 nm) and SnO_2 (<100 nm), with a purity ≥99.1 %.

Stock suspensions of 0.5 g/L of the different NPs (or 1 g/L in the case of In_2O_3 NPs) were prepared in deionized water; shaken, sonicated and sterilized as described in Chapter 6.

8.2.2. Characterization of NPs in aqueous suspension

The characterization of the NPs was performed in OECD algal medium or in water in the absence of algal cells, under the same conditions of the assays with algae (as described below; section 8.2.4).

The hydrodynamic size was evaluated by dynamic light scattering (DLS) and zeta potential, at 25 ºC, in a Zetasizer Nano ZS (Malvern Instruments, UK) with Zetasizer software (version 7.11), as described in Chapter 7. For this purpose, the NPs were suspended at a concentration corresponding to 72h-EC_{50} values (see section 8.2.4); In_2O_3 NPs were suspended at 100 mg/L.

The stability of the NPs was studied by measuring the metal(loid)s dissolved from the NPs. Thus, the NPs were suspended in water or OECD medium at a concentration corresponding to 72h-EC_{50} values (see section 8.2.4) or at 100 mg/L. After 72 h of incubation, samples were taken, centrifuged at 20,000 x *g*, for 30 minutes, at 25 ºC and the supernatants carefully removed. The metal(loid)s were quantified by atomic absorption spectroscopy with flame atomization (AAS-FA) (Mn), with electrothermal atomization (AAS-EA) (Al, In and Sn) or by inductively coupled plasma – optical emission spectrometry (ICP-OES) (Si) in an Analytik Jena novAA 350, a Perkin Elmer AAnalyst 600 spectrometer or a Termo Fisher iCAP 7000 series spectrometer, respectively. The total concentration of Al, In, Mn or Sn present in the NPs was evaluated by total digestion of the NPs with aqua regia as described in Chapter 3,

samples were filtered through a 0.45-µm-pore-size membrane and metals content determined by AAS-FA.

NPs agglomeration was evaluated through a sedimentation assay, as previously described in Chapter 7. Briefly, NPs were suspended in OECD medium at 100 mg/L and agitated at 150 rpm for 72 h, at 25 ºC. For a given incubation time, the settling of NPs agglomerates was monitored, spectrophotometrically (OD) at 600 nm, over a period of 60 min, and determined as described before in Chapter 6.

8.2.3. Strain, medium and culture conditions

In this study, the freshwater green alga *Pseudokirchneriella subcapitata* (strain 278/4) was used. The alga was obtained from the Culture Collection of Algae and Protozoa (CCAP), UK, and maintained in OECD agar medium (OECD, 2011).

The pre-cultures and cultures were prepared and incubated as described before in Chapter 7. After growth, algal cells were harvested by centrifugation (2,500 × *g* for 5 min) and suspended in deionized water.

8.2.4. Algal bioassays

Dose-response curves of Al_2O_3, In_2O_3, Mn_3O_4, SiO_2 or SnO_2 NPs were performed using the freshwater alga growth inhibition test (OECD, 2011). The toxicity caused by the respective metal ions (in the case of Al_2O_3, In_2O_3, Mn_3O_4 and SnO_2 NPs) was compared. Similar experiences with Si (a metalloid) could not be done, since the chemical comportment of this element is different from the metals (Hirner and Flaßbeck, 2005); the dissolution of SiO_2, in water, originate the forming of orthosilicic acid (Iler, 1978). Algal cells in exponential phase of growth (2 days), at $5x10^4$ cell/mL, were exposed (at least) to seven concentrations of toxicants, arranged in a geometric series, in OECD medium. The assays were conducted in 250 mL Erlenmeyer flasks, at a final volume of 100 mL. As control, algal cells were grown in the absence of toxicant. The metals stock solutions used were: $Al(NO_3)_3$ (1000 mg/L, Merck), $In(NO_3)_3$ (1000 mg/L, Sigma-Aldrich), $MnCl_2$ (2000 mg/L, Merck) and $SnCl_4$ (1000 mg/L, Merck). After 72 h of incubation, under the conditions described above, algal cell concentrations were determined using an automated cell counter. The test endpoint was biomass yield, defined as biomass (number of cells/mL) at the end of the exposure period (72 h) minus the biomass at the start of the exposure period (OECD, 2011). The 72h-EC_{10}, EC_{25}, EC_{50}, EC_{75} and EC_{90} values, which represent the toxicant concentration that induces an inhibition of 10, 25, 50, 75 or 90 %, respectively, of algal growth, after

72 h, when compared with control, were determined using a linear interpolation method (TOXCALC version 5.0.32, Tidepool Scientific Software).

P. subcapitata algal cells were also exposed for 72 h to three concentrations of each nanoparticle, corresponding to the 72h-EC_{10}, 72h-EC_{50}, and 72h-EC_{90} values, previously calculated. The assays were carried out as described above for the determination of dose-response curves. After exposure to NPs, algal cells were centrifuged at 2,500 x *g* for 5 min and resuspended in OECD at a final concentration of $3x10^6$ cells/mL (for photosynthetic performance assay; please see section 8.2.7) or $1x10^6$ cells/mL (for membrane integrity and ROS production assays) or $5x10^5$ cells/mL (for metabolic activity).

8.2.5. Algae entrapment assay

The dispersibility of NPs-algae hetero-agglomerates was evaluated using an algal entrapment test. A known concentration of algal cells ($1x10^5$ or $3x10^6$ cells/mL, which corresponded to the minimal and maximal cell concentrations achieved at the end of EC_{10} and EC_{90} assays, respectively) was incubated, in the same conditions of algal bioassays, with the highest NPs concentration tested; for these NPs concentrations, no algal growth was observed. After 72 h of incubation, the algal-NPs suspensions were vortexed and dispersed cell concentrations were determined using an automated cell counter. The reduction of algal cells in suspension (in percentage), which corresponded to the algae entrapped in the NPs agglomerates, was determined considering the initial algal cells concentration as reference.

8.2.6. Staining procedures

SYTOX Green (SG) staining was used to evaluate the impact of NPs on plasma membrane integrity of algal cells (Machado and Soares, 2012), as previously described in Chapter 7.

The metabolic activity of algal cells was evaluated using fluorescein diacetate (FDA) (Machado and Soares, 2013), as previously described in Chapter 7. Fluorescence was corrected by subtracting cell, culture medium and dye autofluorescence. The results were expressed as the ratio of fluorescence in the cells exposed to MOx NPs/fluorescence in the control (non-treated cells).

The intracellular accumulation of ROS was quantitatively assessed using the fluorescent probe 2',7'-dichlorodihydrofluorescein diacetate (H_2DCFDA; Sigma-Aldrich), as described in Chapter 7. Fluorescence was measured and corrected and the results expressed as described above for metabolic activity.

The production of ROS by NPs, in abiotic conditions (in the absence of cells) was also quantified by deacetylation of the probe H_2DCFDA to H_2DCF, as previously described (Aruoja et al., 2015). NPs (at

a concentration corresponding to the respective 72h-EC_{90} value) were incubated for 72 h, in OECD medium, in the same conditions described above for the assays with algal cells, as described before in Chapter 7. Briefly, 100 µL of samples were collected and incubated with 100 µL of 52 µmol/L H_2DCF, placed in quintuplicate in a 96-well microplate and incubated in the dark for 45 min at 25ºC. A blank and a positive control were prepared by replacing the sample by equal volume of OECD medium or 52 µmol/L H_2O_2, respectively, as previously described in Chapter 7. Fluorescence was measured and corrected as described above for metabolic activity. The results were presented as the ratio of fluorescence of the assay/fluorescence of the blank.

8.2.7. Algal photosynthetic performance determination

Photosynthetic performance of Photosystem II (PSII) of algal cells was evaluated trough the determination of the effective photochemical quantum yield of PS II (Φ_{PSII}) by pulse amplitude modulated (PAM) fluorescence assay, using a chlorophyll fluorometer (Walz, JUNIOR-PAM). Algal cells not exposed (control) or exposed to NPs were suspended in OECD medium at $3x10^6$/mL. After a dark adaption for 30 min the minimal fluorescence was measured. Then, the maximum fluorescence was determined by exposing the cells for 600 ms to a blue LED saturation pulse of 10,000 µmol/m^2.s light intensity and a measuring beam of 5Hz. Φ_{PSII} was automatically calculated using the WinControl software (version 3.25), as described before in Chapter 7 (Table 7.1) (Genty et al., 1989). The results were expressed as a ratio of the values in assay (cells treated with the MOx NPs) and the values in control.

8.2.8. Microphotographs

Algal cells in the presence of NPs were also microscopically observed by phase-contrast and fluorescence microscopy using an I3 filter set from Leica. All images were acquired with a Leica DC 300F camera, using a N plan ×100 objective, and were processed using Leica IM 50-Image manager software.

8.2.9. Reproducibility of the results and statistical analysis

The hydrodynamic size and zeta potential measurements were performed one time in duplicate; in each measurement, ten repetitions were considered. The others studies were repeated at least three times in duplicate ($n \geq 6$). The data are presented as mean values ± standard deviations (SD). The mean values were subject to one-way ANOVA, followed by Tukey-Kramer multiple comparison method; in some experiments, differences between control and treated cells were tested using unpaired *t* test. In all experiments, *P* values <0.05 were considered statistically significant.

8.3. Results

8.3.1. Physico-chemical characterization of NPs suspensions

The NPs suspensions were characterized in the algal (OECD) medium; for comparative purposes, the same analysis was performed in deionized water.

The hydrodynamic (Z-average) diameter of the NPs in suspension as well as the zeta potential was determined after the preparation of the suspensions (0 h). Z-average diameter of the NPs, in OECD medium, ranged between 418 and 3859 nm while in water ranged between 145 and 1785 nm (Fig 8.1A). Since all NPs, when in powder, presented a nominal size <100 nm, these results showed that the NPs agglomerated, almost instantaneously, after suspension in aqueous solution. The agglomeration of all NPs studied, increased over the time, in OECD medium, as it can be seen in the sedimentation profiles of the NPs (Fig 8.2). This effect was particularly evident for Mn_3O_4 and In_2O_3 NPs where agglomerates could be detected with the naked eye (Fig 8.3).

The zeta potential of NPs, in both media, presented negative values (between -11 and -25 mV), except for Al_2O_3 NPs in water, which presented a value of +14 mV (Fig 8.1B). In a general way, the magnitude of the zeta potential values was lower in OECD medium comparatively to water (Fig 8.1B).

The solubility of all NPs, after 72 h of incubation, at a concentration corresponding to 72h-EC_{50} values, was similar in OECD medium and deionized (Fig 8.1C).

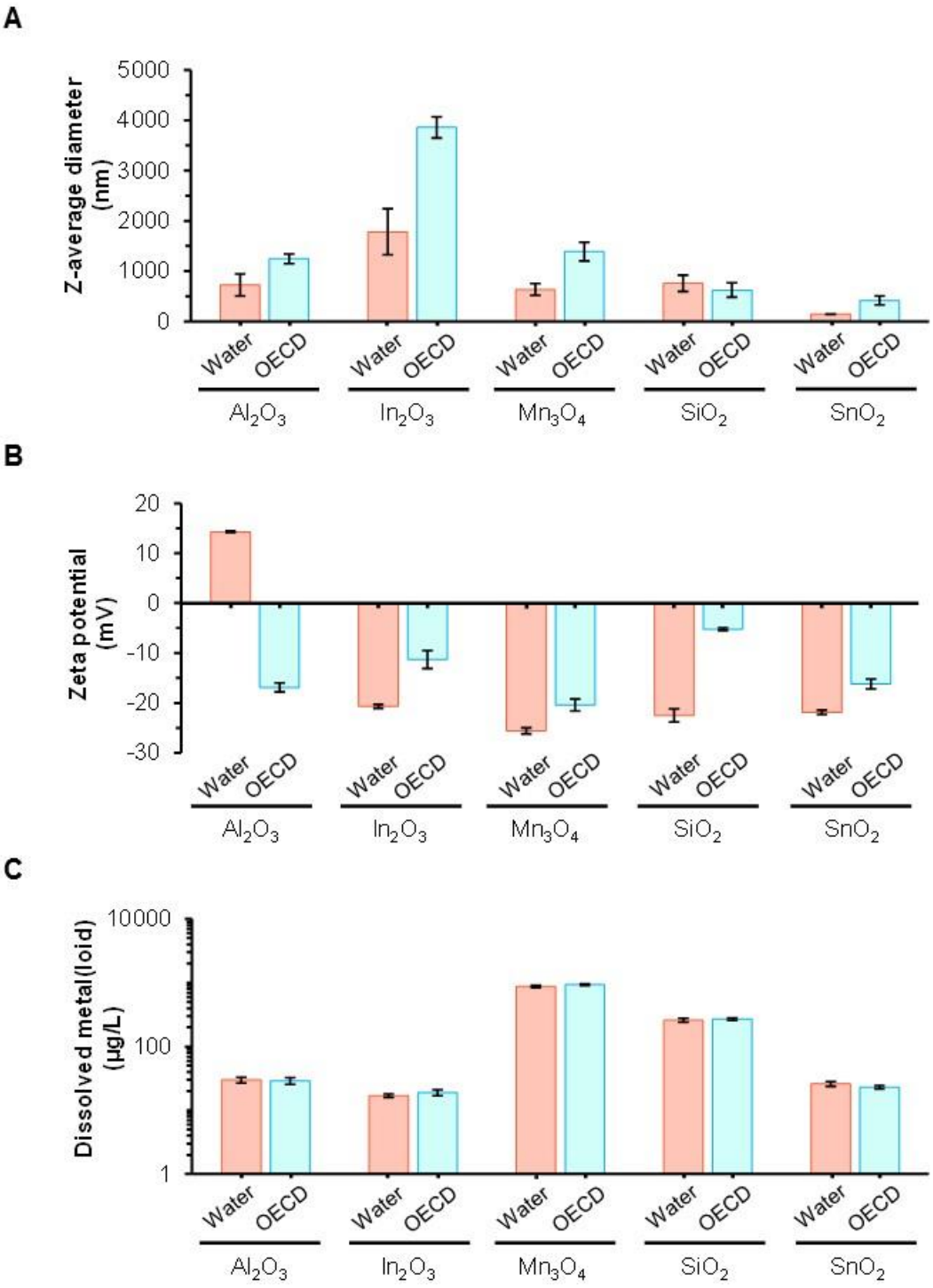

Figure 8.1. Physico-chemical characterization of the nanoparticles in water and in OECD medium. NPs were suspended in water or OECD medium, at 72h-EC_{50} values, except for In_2O_3 NPs, which were suspended at 100 mg/L. A and B – Z-average diameter and zeta potential, respectively, at 0 h (immediately after suspension of the NPs). C – Dissolved metal(loid) from the NPs at 72 h. The data represent the mean values; standard deviations are presented as vertical error bars. The hydrodynamic size and zeta potential measurements were performed one time in duplicate; in each measurement, ten repetitions were considered. NPs solubility experiences were carried out at least three times in duplicate (n≥6).

For comparative purposes, the NPs were suspended in OECD medium at 100 mg/L. Mn_3O_4 NPs were the most soluble; for these NPs, after 72 h of incubation, the amount of Mn ions released was 1000 µg/L (Fig 8.4), which corresponded to a NPs solubilisation of 4.2 %. The Si released from NPs was 452 µg/L (Fig 8.4), which corresponded to a NPs solubilisation of ~1 %. The other NPs studied displayed a much lower solubility (≤0.15 %). The suspension of NPs in OECD medium did not modify substantially the pH during the incubation period of 72 h, varying in general between 7.54 to 7.61 or 7.51 to 7.81 in the absence or presence of algae, respectively.

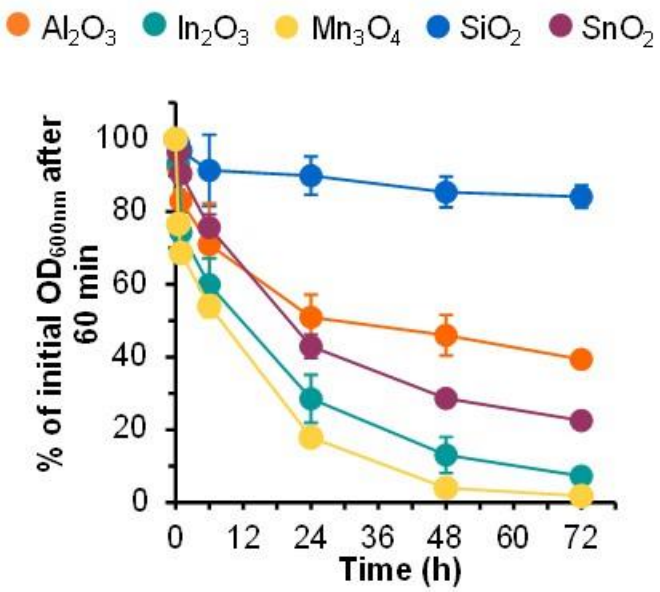

Figure 8.2. Sedimentation profile of the nanoparticles in OCED medium. NPs were suspended in OECD medium at 100 mg/L and incubated for 72 h, at 100 rpm, at 25 ºC, in the absence of algal cells. At defined times, samples were collected and the absorbance was measured spectrophotometrically at 600nm. The data are presented as mean values from at least three independent experiments performed in duplicate (n≥6); standard deviations are presented (vertical error bars).

8.3.2. Hazardous ranking of NPs

In the last decade, there has been a rapid advance of nanotechnology in terms of developing of new nanomaterials along with their commercial applications, which makes the aspect of nanosafety particularly important. In this context, the potential toxic impact of Al_2O_3, Mn_3O_4, In_2O_3, SiO_2 and SnO_2 NPs was evaluated using the microalga *P. subcapitata* through the OECD algal growth inhibition test (OECD, 2011). For comparative purposes, the toxicity of the corresponding metal ions was also studied. Hence, *P. subcapitata* cells were exposed to a series of geometric concentrations of the toxicants and the corresponding dose-response curves (expressed as % of growth inhibition) were constructed (Fig 8.5).

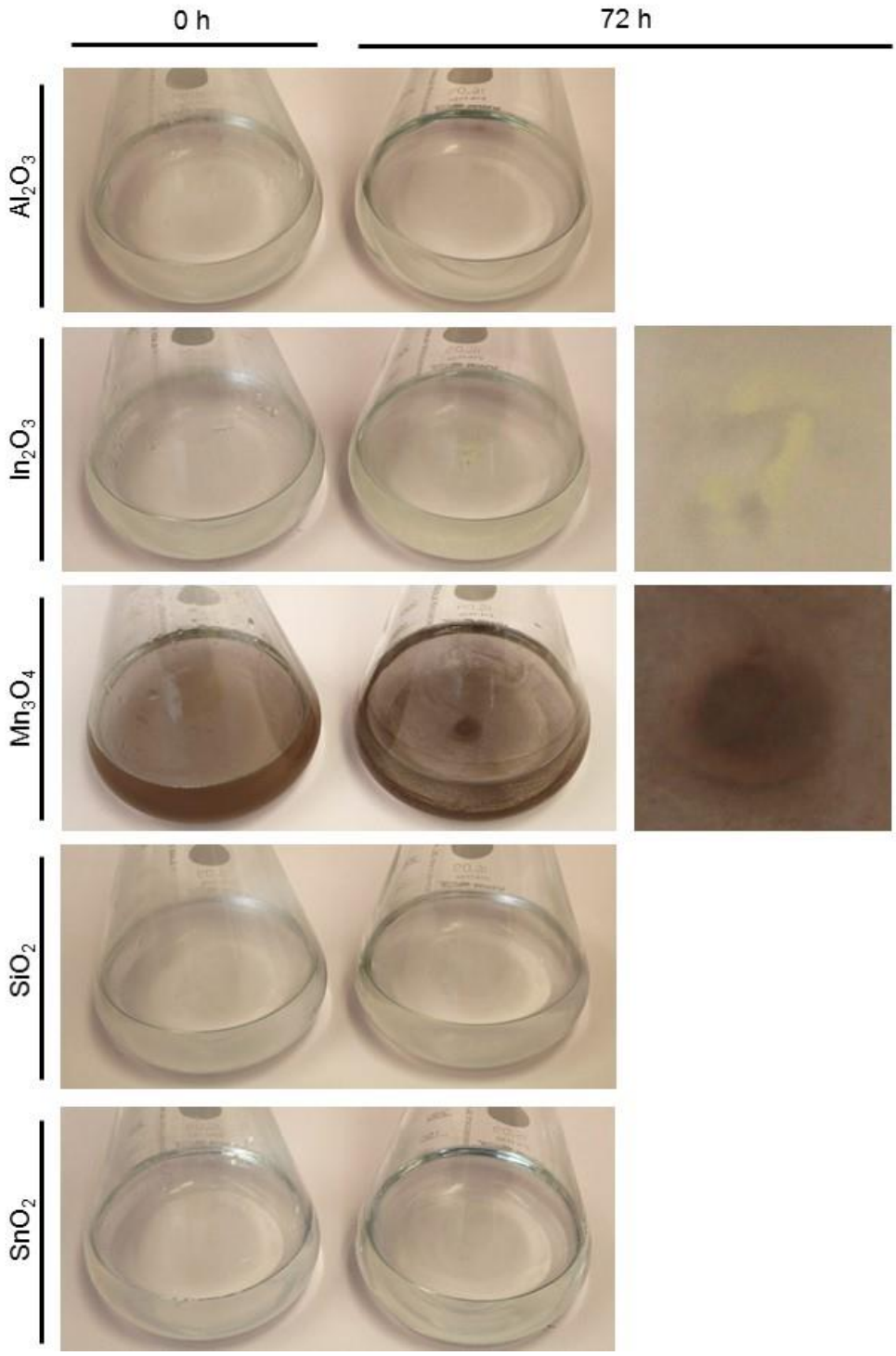

Figure 8.3. Macroscopic observations of the nanoparticles suspended in OECD medium. NPs were suspended in OCED medium at a concentration corresponding to the 72h-EC_{90} value, except for In_2O_3 NPs, which were suspended at 100 mg/L, in the absence of algal cells. Suspensions were incubated for 72 h, at 100 rpm, at 25 ºC. Right-side images: bottom of the Erlenmeyer flasks.

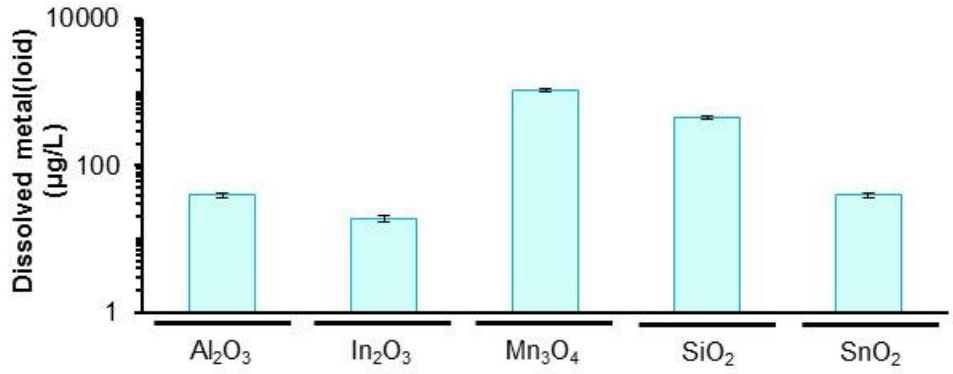

Figure 8.4. Dissolved metal(loid) from the nanoparticles. NPs were suspended in OCED medium, in the absence of algal cells, at 100 mg/L and incubated for 72 h in the same conditions described in Fig 8.3. The data are presented as mean values from at least three independent experiments performed in duplicate ($n \geq 6$); standard deviations are presented (vertical error bars).

Among the NPs studied, SnO_2 was the most toxic with a 72h-EC_{50} value of 2.1 mg/L (Table 8.1). Considering the 72h-EC_{50} values (Table 8.1), the decreasing order of toxicity of the NPs studied is: $SnO_2 > Al_2O_3 > Mn_3O_4 > SiO_2 > In_2O_3$. Relatively to the metal ions present in the NPs, the decreasing order of toxicity is: $Sn^{4+} > In^{3+} > Al^{3+} > Mn^{2+}$ (Table 8.1). A detailed comparison of the NPs hazardous, considering the respective 72h-EC_{10}, EC_{25}, EC_{50}, EC_{75} and EC_{90} values is presented in the Table 8.1.

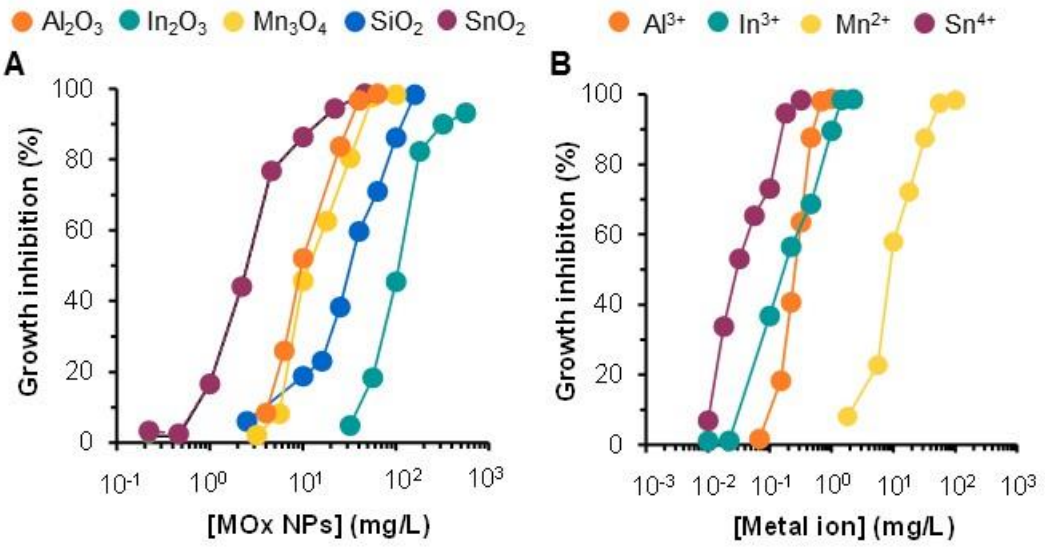

Figure 8.5. Dose-response curves of the nanoparticles or the respective metals ions. A and B – Algal cells of *P. subcapitata* exposed to NPs or to metal ions, respectively, in OECD medium, for 72 h. The data are presented as mean values from at least three independent experiments performed in duplicate (n≥6); standard deviations are presented (vertical error bars). Where no error bars are shown, SD are within the points.

Table 8.1. Toxicity of the nanoparticles studied or the respective metal ions to *P. subcapitata*.

		72h-EC values (mg/L)[a]				
	Toxicant	10	25	50	75	90
NPs[b)]	Al_2O_3	4.4 ± 0.4 (2.3 ± 0.2)	6.2 ± 0.9 (3.2 ± 0.5)	9.4 ± 0.3 (5.0 ± 0.2)	21 ± 1 (11 ± 0.5)	30 ± 1 (16 ± 0.5)
	In_2O_3	41 ± 6 (34 ± 5)	67 ± 4 (55 ± 4)	110 ± 5 (91 ± 5)	164 ± 3 (136 ± 3)	319 ± 22 (264 ± 18)
	Mn_3O_4	5.8 ± 0.5 (4.2 ± 0.4)	7.5 ± 0.2 (5.4 ± 0.1)	12 ± 1 (8.6 ± 0.7)	28 ± 1 (20 ± 1)	45 ± 1 (32 ± 1)
	SiO_2	4.8 ± 1.7 (2.2 ± 0.8)	17 ± 2 (7.9 ± 0.9)	33 ± 1 (15 ± 1)	7 ± 3 (34 ± 1)	120 ± 4 (56 ± 2)
	SnO_2	0.59 ± 0.09 (0.46 ± 0.07)	0.92 ± 0.04 (0.72 ± 0.03)	2.1 ± 0.1 (1.7 ± 0.1)	11 ± 1 (8.6 ± 0.8)	21 ± 1 (17 ± 1)
Metal ions[c)]	Al^{3+}	0.11 ± 0.03	0.17 ± 0.02	0.26 ± 0.01	0.39 ± 0.02	0.51 ± 0.01
	In^{3+}	$2.0x10^{-2}$ ± $0.5x10^{-2}$	$6.2x10^{-2}$ ± $0.8x10^{-2}$	0.18 ± 0.01	0.62 ± 0.04	1.0 ± 0.1
	Mn^{2+}	2.3 ± 0.1	5.8 ± 0.8	9.0 ± 0.5	21 ± 2	38 ± 4
	Sn^{4+}	$1.1x10^{-2}$ ± $0.3x10^{-2}$	$1.5x10^{-2}$ ± $0.1x10^{-2}$	$3.0x10^{-2}$ ± $0.4x10^{-2}$	0.11 ± 0.01	0.16 ± 0.01

[a]72h-EC_{10}, EC_{25}, EC_{50}, EC_{75} and EC_{90} values of the nanoparticles or the respective metal ions that induce the inhibition of 10, 25, 50, 75 or 90% of algal growth, compared to control, in OECD medium, after exposure to the toxicant for 72 h. Values were obtained from three independent experiences performed in duplicate (n=6); standard deviations are presented.
[b]72h-EC values were calculated based on nominal exposure concentrations (mg nanoparticle/L); values in parenthesis: 72h-EC values calculated on metal basis (mg metal/L).
[c]72h-EC values were calculated based on nominal exposure concentrations (mg metal/L).

8.3.3. How can NPs affect algal growth?

NPs can exert a toxic impact on algae by different ways, such as: sequestration of the cells by the NPs (isolating the cells from nutrients), generation of ROS in the external milieu or through the release of metal(loid)s (NPs dissolution) (Aruoja et al., 2015; Rogers et al., 2010; Wang et al., 2017).

Algal cells can be sequestered due to their co-agglomeration with NPs; in this situation, the access of algae to nutrients, present in the culture medium, can be reduced or impaired. The co-agglomeration of NPs and algal cells was observed for Al_2O_3, Mn_3O_4 and SnO_2 NPs; this effect was particularly notorious at high NPs concentrations (corresponding to 72h-EC_{90} values). These hetero-agglomerates presented a loose structure appearance (Fig 8.6A) and were easily dispersed by simple vortexing of the suspensions. After the stirring of these hetero-agglomerates, the algal cells entrapped in these structures was <7 % (Table 8.2). In these algal-NPs agglomerates, it was possible to observe cells inside and at the periphery of the structures as well as in the surrounding medium.

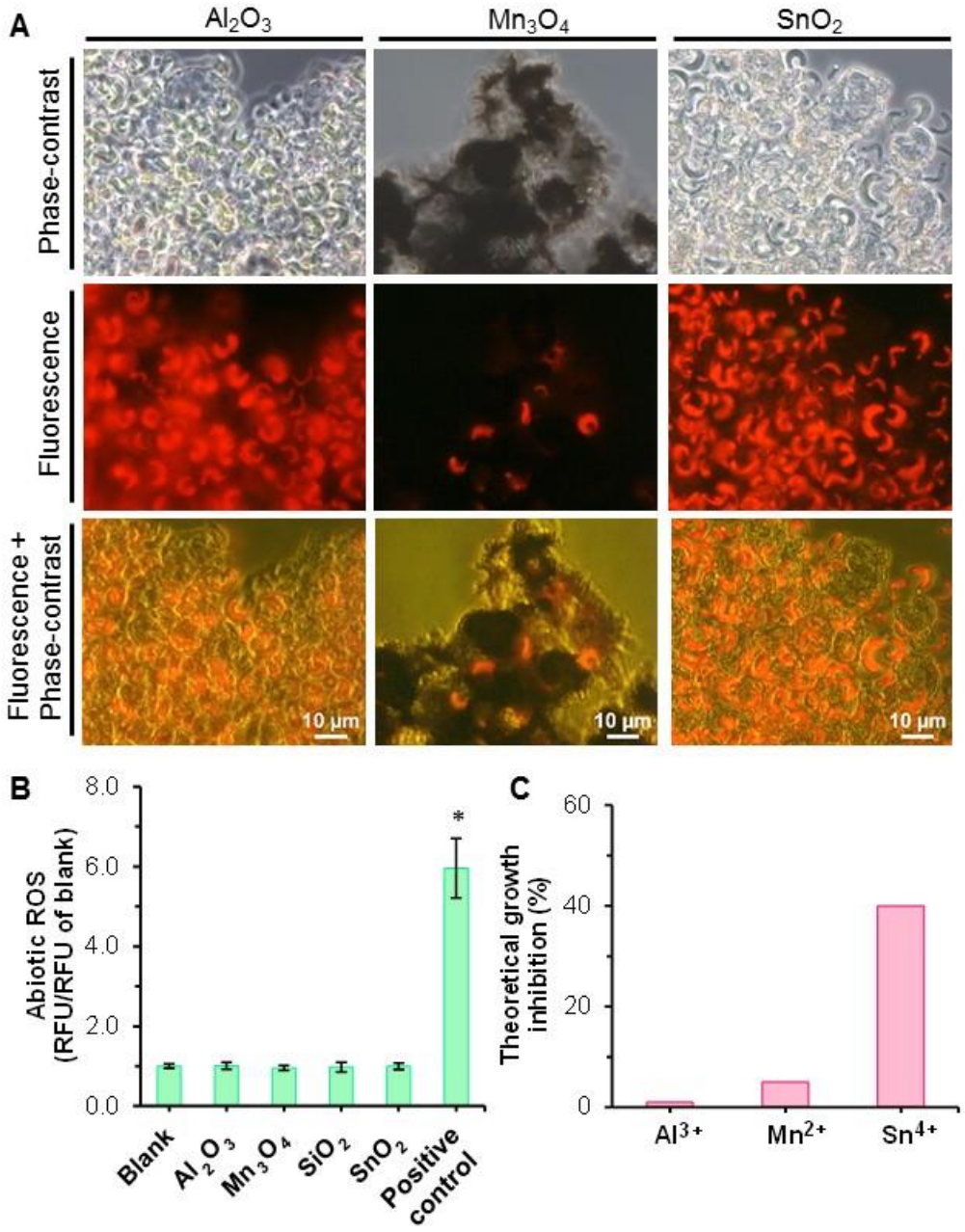

Figure 8.6. Possible toxic mechanisms of the nanoparticles. A – Microscopic visualization of algal-NPs agglomerates. Algal cells were incubated with NPs for 72 h, at a concentration corresponding to 72h-EC_{90} values. B – Evaluation of abiotic ROS production by nanoparticles. NPs were suspended in OECD medium at a concentration corresponding to 72h-EC_{50} values and incubated for 72 h in the same conditions of the biotic assays. Blank and positive control were prepared by incubating the H_2DCF probe with OECD medium or 26 µmol/L H_2O_2, respectively. The data represented the mean values from at least three independent experiments performed in duplicate ($n \geq 6$); standard deviations are presented (vertical error bars). The mean values were subject to one-way ANOVA, followed by Tukey-Kramer multiple comparison method; the result with asterisk is significantly different ($P < 0.05$). C – Theoretical algal growth inhibition. Growth inhibition was calculated considering the metal ions released from NPs, at a concentration corresponding to 72h-EC_{50} values, and dose-response curves of the metals (Fig 8.5B).

For SiO_2 and In_2O_3, only NPs homoagglomerates were observed. Together, these observations strongly indicated that the toxicity caused by NPs cannot be attributed to nutritional limitation of algae due to their entrapment by the NPs.

The potential of NPs to generate reactive oxygen species (ROS) and, thus, to induce oxidative stress and cell toxicity was assessed using the general redox probe H_2DCFDA (Tarpey et al., 2004), previously deacetylated to H_2DCF. Under the concentrations and conditions used, the NPs studied did not generate abiotic ROS (Fig 8.6B). Due to the absence of a pro-oxidant effect, it is not plausible that the toxicity observed could be attributed to the abiotic induction of OS, by the NPs, in the surrounding medium.

A common question in nanotoxicology is: what is the contribution of the metal leached from the NPs to the observed toxicity? To answer this question, the theoretical algal growth inhibition was calculated (Fig 8.6C), in percentage, taking into account the amount of metals released from the NPs, at a concentration corresponding to 72h-EC_{50} values (Fig 8.1C), and the dose-response curves of metals ions (Fig 8.5B). The comparative analysis of the observed (~50 % of algal growth inhibition) with the expected toxicity (considering the metals released from the NPs) revealed that, in the case of Al_2O_3, the toxicity can be attributed to the NPs, since the toxicity that can be attributed to the metals released should be <1 % (Fig 8.6C). For Mn_2O_3, the toxicity could be mainly attributed to the NPs, although a small inhibition (<5 %) could be due to the release of Mn ions. On the contrary, the toxicity of SnO_2 NPs can be attributed, mainly, to the release of Sn ions, once the Sn dissolved from the NPs should provoke an algal growth inhibition of 40 % (Fig 8.6C).

Table 8.2. Algal sequestration due to the nanoparticles agglomeration.

	Algal sequestration (%)[a]	
Nanoparticles	1 x 10^5 cells/mL	3 x 10^6 cells/mL
Al_2O_3	5.6 ± 0.8	4.2 ± 0.7
Mn_3O_4	6.2 ± 0.9	3.6 ± 0.7
SnO_2	4.2 ± 0.9	4.5 ± 1.0

[a]The % of sequestered cells was determined using an algae entrapment assay, described in material and methods. The assay was performed using 1x10^5 or 3x10^6 cells/mL (minimal and maximal algal cell concentrations, respectively, achieved in the ECs assays). The data are presented as mean values and the corresponding standard deviations from three independent experiments, performed in duplicate (n=6).

8.3.4. NPs toxicity: cellular targets

To further contribute for the elucidation of the modes of toxicity of the NPs, different key cell targets were assessed: cell membrane integrity, metabolic activity, intracellular accumulation of ROS and photosynthetic activity. Therefore, algal cells were exposed for 72 h to different concentrations of NPs, corresponding to 72h-EC_{10}, EC_{50} and EC_{90} values. With this strategy, algal cells were chronically exposed to a wide range of NPs concentrations: from a concentration with a little impact on algal growth (72h-EC_{10} values) to a concentration where the growth was practically arrested (72h-EC_{90} values). This study was not conduced with In_2O_3, since these NPs presented a lower toxicity: a 72h-EC_{50} value > 100 mg/L (Table 8.1).

8.3.4.1 Cell membrane integrity

Cell membrane integrity was evaluated using the fluorescent probe SG. Cells with an intact membrane are not penetrated by SG (SG negative cells) (Machado and Soares, 2012). The exposure of algal cells to high NPs concentrations (corresponding to 72h-EC_{90} values), induced growth arrest (Fig 8.7A) without disruption of cell membrane integrity (Fig 8.7B). Extending the exposure of algae to NPs up to 144 h (6 days), it was possible to observe the growth stop (Fig 8.7A), although the cells remained mostly (>85 %) with an intact cell membrane (SG negative cells) (Fig 8.7B). These results indicated that these NPs induced an algistatic effect on *P. subcapitata*.

8.3.4.2 Metabolic activity

Metabolic activity of algal cells was assessed through the quantification of the esterase activity, using fluorescein diacetate (FDA) as substrate. Esterases, present in metabolic active cells, hydrolyse the FDA, originating cells with green fluorescence. The decrease of green fluorescence has been used as an indicator of the loss of algal metabolic activity (Dorsey et al., 1989; Machado and Soares, 2013).

Algal cells exposed to Al_2O_3, Mn_3O_4 or SiO_2 NPs, at concentrations that inhibit 50 or 90 % of algal growth, displayed a reduction of the metabolic activity (Fig 8.8A-C). In the case of Al_2O_3 NPs, the reduction of esterase activity was also observed for the lowest concentration tested (4.4 mg/L). SnO_2 NPs seems not disturb algal metabolic activity, up to 21 mg/L. In fact, algal cells maintained the esterase activity even when exposed to a concentration that inhibit almost completely cell growth (72h-EC_{90}) (Fig 8.8D).

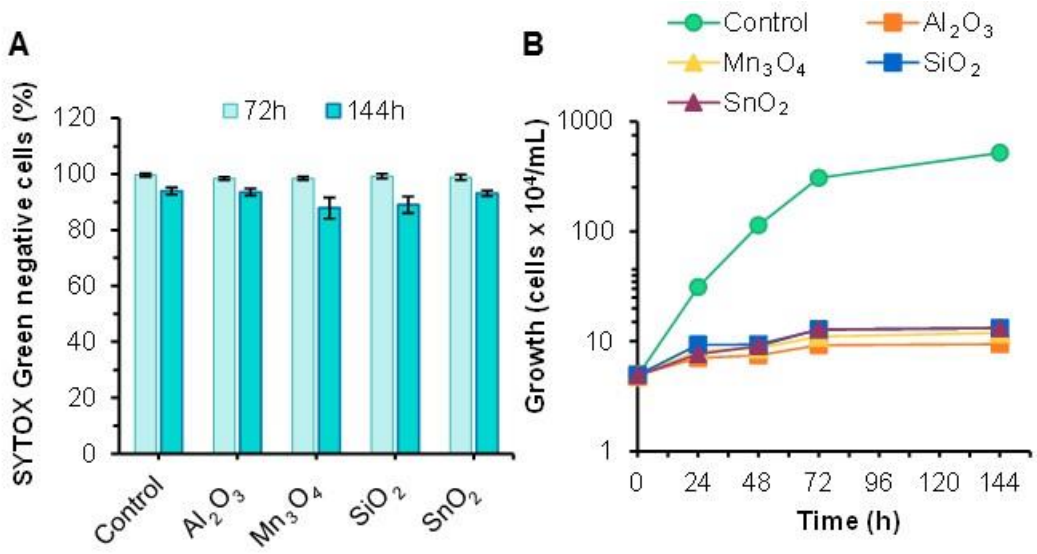

Figure 8.7. Effect of nanoparticles on cell membrane integrity and growth of *P. subcapitata*. Algal cells were incubated in OECD medium in the absence (control) or in the presence of NPs, at a concentration corresponding to 72h-EC_{90} values. A – Cell membrane integrity, evaluated by SYTOX Green exclusion assay, after the exposure of algal cells to NPs for 72 h or 144 h. B – Algal growth. The data are presented as the mean values from at least three independent experiments performed in duplicate ($n \geq 6$); standard deviations are presented (vertical error bars). A – Means for 72 h or 144 h are not significantly different ($P<0.05$; ANOVA).

8.3.4.3 Intracellular ROS accumulation

The accumulation of ROS by algal cells was monitored with the probe H_2DCFDA, which has been used to detect a broad range of ROS (Tarpey et al, 2004). Algal cells exposed to Al_2O_3, Mn_3O_4 or SiO_2 NPs accumulated ROS (Fig 8.9). Since these NPs did not generate ROS in abiotic conditions (Fig 8.6B), the levels of ROS exhibited by algal cells were, most likely, intracellularly generated. The oxidative stress experienced by algae was particularly notorious in cells exposed to high Al_2O_3 and Mn_3O_4 NPs concentrations (corresponding to 72h-EC_{90} values) (Fig 8.9). Within the NPs studied, the decreasing order of intracellular ROS accumulation was: Mn_3O_4>Al_2O_3>SiO_2. SnO_2 NPs, up to 21 mg/L, did not induce intracellular ROS accumulation (Fig 8.9).

8.3.4.4 Photosynthetic performance

The photosynthetic performance was evaluated using a PAM fluorescence assay. It was possible to observe that algal cells exposed to Al_2O_3, Mn_3O_4, SiO_2 or SnO_2 NPs presented a reduction in the light utilization efficiency of photosystem II (PSII) (reduction of photosynthetic efficiency).

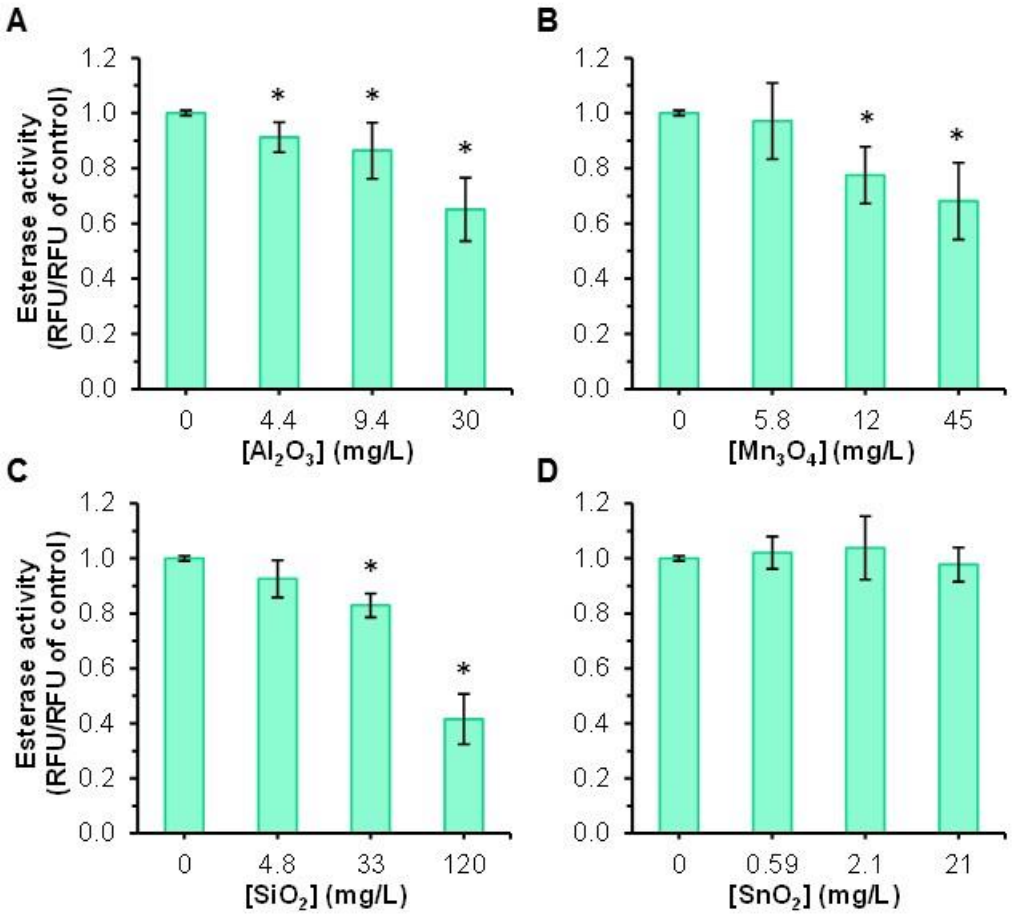

Figure 8.8. Influence of the nanoparticles in the metabolic activity of *P. subcapitata*. Algal cells were incubated in the absence or in the presence of NPs, for 72h, in OECD medium. Esterase activity was evaluated by the quantification of the hydrolysis of FDA. The data are presented as mean values from at least three independent experiments; in each experiment, five fluorescent readings were performed (n≥15). Standard deviations are presented (vertical error bars). Statistical differences were subject to ANOVA. The means with asterisks are significantly different ($P < 0.05$).

The decrease in the photochemical quantum yield of PSII (Φ_{PSII}) was particularly noticeable in algal cells exposed to high NPs concentrations (Fig 8.10). The reduction of Φ_{PSII} is generally seen as a sensitive indicator of stress (Juneau and Popovic, 1999).

8.4. Discussion

The physico-chemical characterization of NPs in aqueous suspension, namely the study of their agglomeration and the stability (solubilisation), is essential to understand their possible toxic effects (Rogers et al., 2010; Wang et al., 2017). The evaluation of the electrokinetic potential of Al_2O_3, In_2O_3, Mn_3O_4, SiO_2 and SnO_2, in OECD algal medium and deionized water, showed that these NPs presented low zeta potential values, in aqueous media (Fig 8.1B).

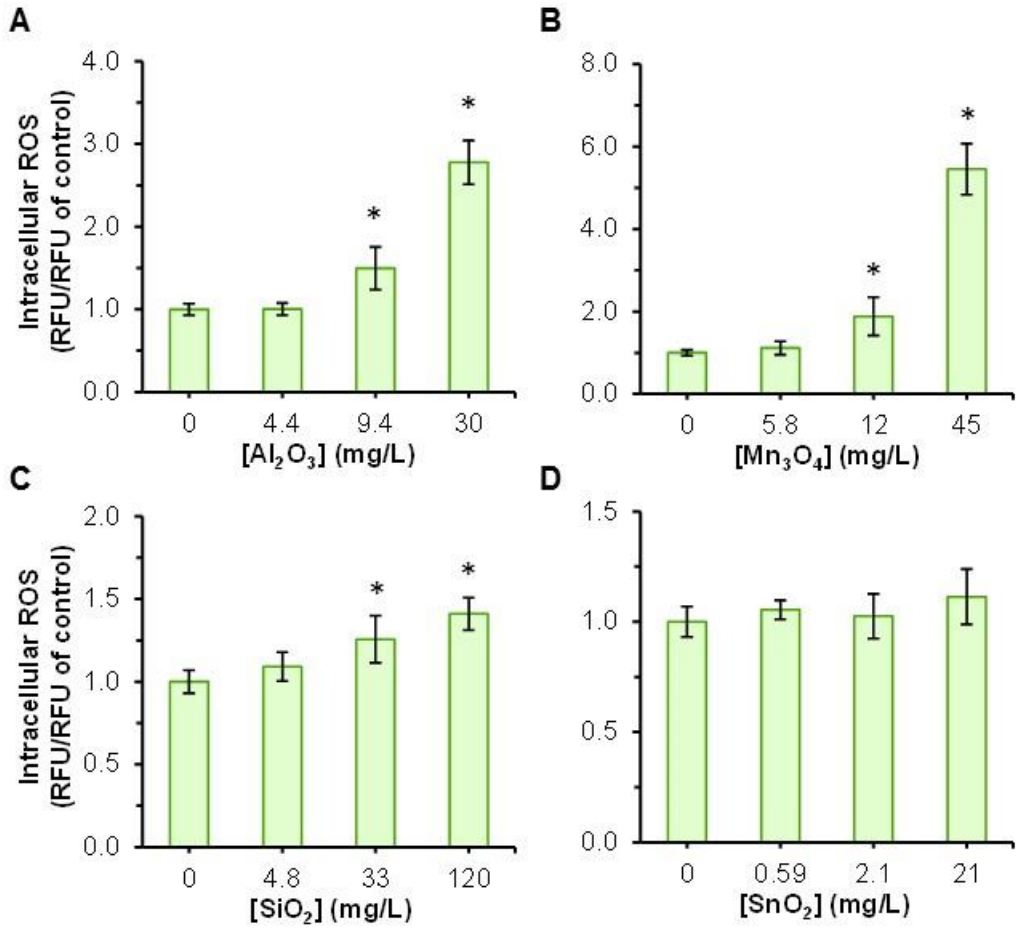

Figure 8.9. Evaluation of intracellular ROS accumulation by *P. subcapitata* exposed to nanoparticles. Algal cells were incubated in the absence or in the presence of NPs, in OECD medium, for 72h. Intracellular accumulation of ROS was detected using H_2DCFDA. The data are presented as mean values from at least three independent experiments; in each experiment, five fluorescent readings were performed (n≥15). Standard deviations are presented (vertical error bars). Statistical differences were subject to ANOVA. The means with asterisks are significantly different ($P < 0.05$).

These results indicated that these NPs are poorly stabilized as consequence of the low electrostatic repulsion between adjacent particles. Particles with low zeta potential tend to agglomerate (Hanaor et al., 2012). Consistent with these data, it was observed that the NPs studied, in aqueous media, presented a hydrodynamic size between ~150 – 4000 nm (Fig 8.1A). In addition, the sedimentability of the NPs increased over the time (Fig 8.2), and it was possible to detect NPs agglomerates even with the naked eye (In_2O_3 and Mn_3O_4) (Fig 8.3). In line with our data, zeta potential values of the same order of magnitude were described for In_2O_3 (Ahamed et al., 2017; Hasegawa et al., 2012; Jeong et al., 2016), Mn_3O_4 and SiO_2 NPs (Aruoja et al., 2015). Similarly, the agglomeration of the NPs was observed by other authors. For Al_2O_3 NPs, a hydrodynamic size between 392 and 1232 nm, in OECD medium, was described (Aruoja et al., 2015; Sadiq et al., 2011).

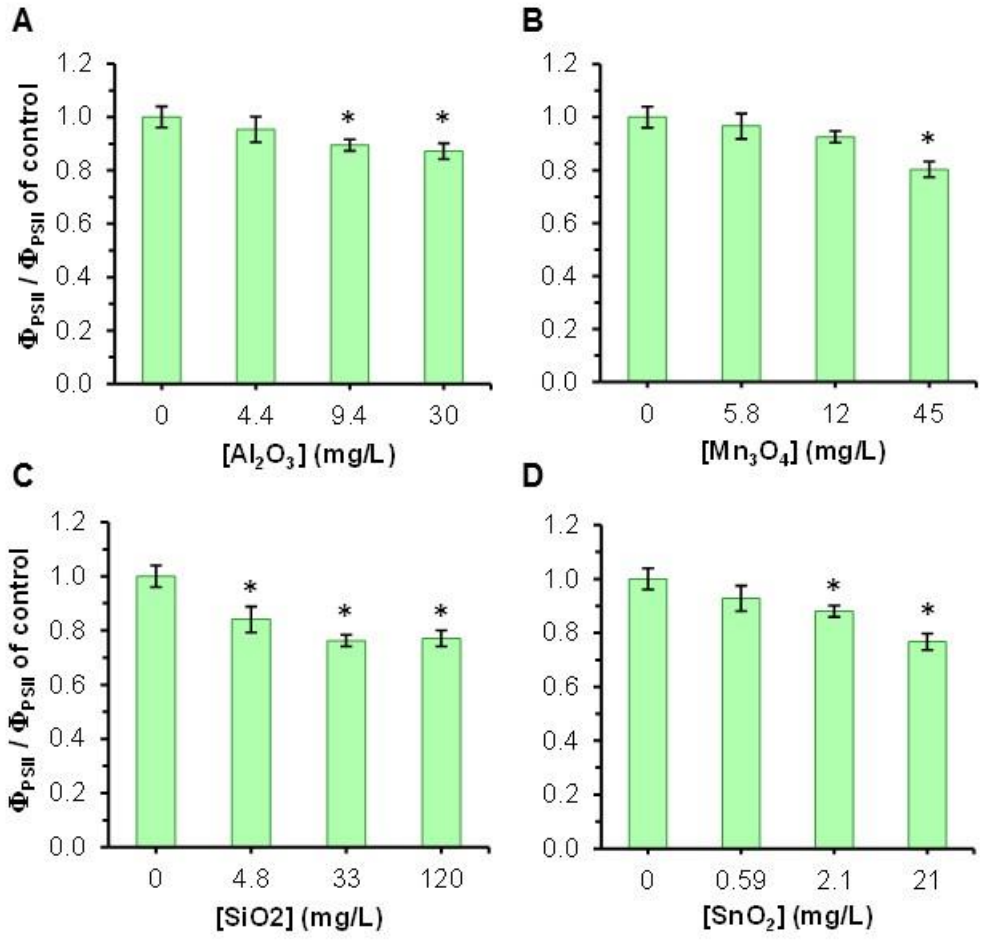

Figure 8.10. Photosynthetic performance of algal cells exposed to the nanoparticles. Algal cells were incubated in absence or the presence of NPs, in OECD medium, for 72 h. Effective photochemical quantum yield of PSII (ΦPSII) was accessed using PAM fluorescence assay. The data are presented the mean values from at least three independent experiments, performed in duplicate (n≥6); standard deviations are presented (vertical error bars). Statistical differences were subject to ANOVA. The results with asterisks are significantly different ($P < 0.05$).

In the case of Mn_3O_4 and SiO_2 NPs, Aruoja et al. (2015) described an hydrodynamic size in water of 395 and 148 nm, respectively, and in OECD medium of 920 and 154 nm, respectively.

NPs can exert a toxic impact on algae by different ways, such as: sequestration of the cells by the NPs (isolating the cells from nutrients), generation of ROS in the external milieu or through the release of metal(loid)s (NPs dissolution) (Aruoja et al., 2015; Rogers et al., 2010; Wang et al., 2017). Despite the agglomeration of NPs, it is unlikely that algae entrapment in these structures is the cause of the observed toxicity since algae-NPs hetero-agglomerates present a loose structure (Fig 8.6A). Reinforcing this possibility, it was shown that after a simple mechanical stirring of algal-NPs hetero-agglomerates only <7 % of the algae remained captured in the agglomerates (Table 8.2).

The quantification of metal(loid)s leached from the NPs (Fig 8.1C), revealed that these nanomaterials were poorly soluble in water or OCED medium. A similar solubility was described for Al_2O_3 and Mn_3O_4 NPs in OECD medium (Aruoja et al., 2015). Notwithstanding the lower solubility of SnO_2 NPs, the amount of Sn ions released seems to be the main contributor of the observed toxicity. In fact, SnO_2 NPs presented a 72h-EC_{50} value of 2.1 mg/L (Table 8.1). When suspended in OECD medium, 2.1 mg/L SnO_2 NPs released ~23 µg/L Sn^{4+} (Fig 8.1C). According to Sn^{4+} dose-response toxicity curves (Fig 8.5B), this metal concentration (~23 µg/L) should induce an inhibition of 40 % of algal growth (Fig 8.6C). In the case of Al_2O_3 and Mn_3O_4 NPs, the ions released should have a minor influence on the observed toxicity (Fig 8.6C).

The environmental risk assessment of NPs requires information about their possible adverse effects on aquatic organisms. In the present work, the ecotoxicological hazard of NPs was assessed through their impact on *P. subcapitata* using the OECD algal growth inhibition test. In the framework of EU chemical safety policy, all chemicals manufactured or imported in the EU, above 1 ton per year, their potential impact on aquatic ecosystems have to be characterized (ECHA, 2016). According to the European Commission Directive No 1272/2008, the assessment of risks in the aquatic environment can be made using algal cells and by calculating the EC_{50} values of toxicants through dose-response curves (EC, 2008). Considering this directive, the impact of pollutants on aquatic systems, based on the EC_{50} values, can be classified as: very toxic (< 1mg/L), toxic (1-10 mg/L), harmful (10-100 mg/L) and not classified/not harmful (> 100 mg/L). Therefore, the hazardous of the NPs, evaluated through the algae growth inhibition test, using *P. subc*apitata, can be ranked as follows: SnO_2 (2.1 mg/L) and Al_2O_3 (9.4 mg/L) are considered as toxic; Mn_3O_4 (12 mg/L) and SiO_2 (33 mg/L) are classified as harmful and In_2O_3 (110 mg/L) is classified as not classified/not harmful. A similar 72h-EC_{50} value (34.6 mg/L) for SiO_2 NPs with *P. subcapitata* was described (Aruoja et al., 2015); however, different EC_{50} values were described for Al_2O_3 (31 mg/L) and Mn_3O_4 (1.3 mg/L) (Aruoja et al., 2015); these differences in the EC_{50} values can be due to the use of different alga strains and/or endpoint determination (in the present work: growth yield; literature: fluorescence of algal pigment extract). Higher 72h-EC_{50} values were described for Al_2O_3 and SiO_2 NPs, evaluated with other algal cells. Thus, for Al_2O_3 NPs, 72h-EC_{50} values of 39, 45 and 100-300 mg/L for *Scenedesmus* sp., *Chlorella* sp. (Sadiq et al., 2011) and *Porphyridium aerugineum* Geitler (Karunakaran et al., 2015), respectively, were described. In the case of SiO_2 NPs, a 72h-EC_{50} value of 1000 mg/L for the green algae *P. aerugineum* Geitler was reported (Karunakaran et al., 2015). The higher sensitivity of *P. subcapitata* to NPs, comparatively with other algal genera, reinforces the significance of this alga in the ecotoxicity assessment of freshwaters.

A critical issue regarding to the NPs ecotoxicity is related with the knowledge of the toxic modes of action of these nanomaterials. Through photosynthesis, algae convert light energy into chemical energy that can be further used in cell activities. Thus, it is expected that any impact on algae photosynthesis may cause disturbance of cell functioning. The exposure of cells to Al_2O_3, Mn_3O_4, SiO_2 and SnO_2 NPs induced a reduction of Φ_{PSII} (Fig 8.10), which indicated a decrease in the light utilization efficiency of PSII of algal cells. In fact, Φ_{PSII} gives a measure of the efficiency at which light absorbed by PSII is used in photochemistry (Baker, 2008). Due to the reduction of photosynthesis efficiency, most likely, algal cells exposed to the NPs studied should present reduced levels of ATP which, in turn, can be one of the reasons (or the main reason) of algal growth inhibition. A disturbance of photosynthesis was also described in algal cells of *P. subcapitata* exposed for 72 h to CeO_2 (Rodea-Palomares et al., 2012) or NiO NPs (please see Chapter 7).

The electrons that were no longer used in the photosynthesis (due to the reduction of PSII activity) could induce the production of ROS through the reduction of molecular oxygen (Rutherford and Krieger-Liszkay, 2001). Compatible with this possibility, intracellular accumulation of ROS in algal cells exposed to 72h-EC_{50} and 72h-EC_{90} values of Al_2O_3, Mn_3O_4 or SiO_2 NPs was observed (Fig 8.9). Our results are in agreement with different authors, who reported ROS production in different model cells when exposed to Al_2O_3, Mn_3O_4 or SiO_2 NPs. Thus, it was described that Al_2O_3 NPs caused oxidative stress in the plant *Triticum aestivum* (Yanik and Vardar, 2015, 2018) and in human lymphocytes (Rajiv et al., 2016); Mn_3O_4 NPs induced ROS production in rat alveolar cells (Frick et al., 2011; Urner et al., 2014) and SiO_2 NPs provoked ROS production in lymphocytes (Azimipour et al., 2018), intestinal (Setyawati et al., 2015), lung and human bronchial epithelial cells (Eom and Jinhee Cho, 2011; Manke et al., 2013).

Two of the main intracellular ROS targets are cell membrane (via oxidation of lipids) and proteins, which can be inactivated through oxidation (Valavanidis et al., 2006). The chronic exposure (up to 6 days) of algal cells to the NPs studied, even at high concentrations, did not cause the perturbation of membrane integrity (Fig 8.7B). A similar result was observed with the alga *Scenedesmus obliquus* when exposed to SiO_2 NPs (Liu et al., 2018). In relation to protein oxidation, different mechanisms were described, which includes the oxidation of amino acid residues containing aromatic side chain or sulfhydryl groups (Cecarini et al., 2007). In agreement with this possibility, the reduction of esterase activity (metabolic activity) in algal cells exposed to Al_2O_3, Mn_3O_4 or SiO_2 NPs was observed (Fig 8.8), which corresponded to the same NPs that caused the intracellular accumulation of ROS (Fig 8.9). A

similar effect (inhibition of esterase activity) was observed in alveolar and intestinal cells exposed to Mn_3O_4 NPs (Titma et al., 2016).

8.5. Conclusions

The toxicity of five NPs (Al_2O_3, In_2O_3, Mn_3O_4, SiO_2 and SnO_2) was evaluated using the alga *P. subcapitata*:

• Considering 72h-EC_{50} values, NPs can be categorized as: toxic (Al_2O_3 and SnO_2); harmful (Mn_3O_4 and SiO_2) and non-toxic (In_2O_3);

• Al_2O_3, Mn_3O_4, SiO_2 and SnO_2 induced an algistatic effect: growth inhibition without loss of membrane integrity;

• Al_2O_3, Mn_3O_4 and SiO_2 induced reduction of photosynthetic efficiency, metabolic activity and ROS accumulation;

• SnO_2 caused algal growth inhibition probably as a consequence of the reduction of photosynthetic efficiency.

References

Ahamed, M., Akhtar, M.J., Khan, M.A.M., Alhadlaq, H.A., Aldalbahi, A., 2017. Nanocubes of indium oxide induce cytotoxicity and apoptosis through oxidative stress in human lung epithelial cells. Colloids Surf B Biointerfaces 156, 157-164.

Andreescu, S., Ornatska, M., Erlichman, J.S., Estevez, A., Leiter, J.C., 2012. Biomedical applications of metal oxide nanoparticles, in: Matijević, E. (Ed.), Fine particles in medicine and pharmacy. Springer, Boston, MA, pp. 57-100.

Aruoja, V., Pokhrel, S., Sihtmae, M., Mortimer, M., Madler, L., Kahru, A., 2015. Toxicity of 12 metal-based nanoparticles to algae, bacteria and protozoa. Environ. Sci. Nano 2, 630-644.

Azimipour, S., Ghaedi, S., Mehrabi, Z., Ghasemzadeh, S.A., Heshmati, M., Barikrow, N., Attar, F., Falahati, M., 2018. Heme degradation and iron release of hemoglobin and oxidative stress of lymphocyte cells in the presence of silica nanoparticles. Int. J. Biol. Macromol. 118, 800-807.

Baker, N.R., 2008. Chlorophyll fluorescence: a probe of photosynthesis in vivo. Annu. Rev. Plant Biol. 59, 89-113.

Cecarini, V., Gee, J., Fioretti, E., Amici, M., Angeletti, M., Eleuteri, A.M., Keller, J.N., 2007. Protein oxidation and cellular homeostasis: emphasis on metabolism. Biochim. Biophys. Acta 1773, 93-104.

Dorsey, J., Yentsch, C.M., Mayo, S., McKenna, C., 1989. Rapid analytical technique for the assessment of cell metabolic-activity in marine microalgae. Cytometry 10, 622-628.

EC, 2008. Classification, labelling and packaging of substances and mixtures, amending and repealing – Regulation (EC) nº 1272/2008 of the European Parliament and of the Council of 16 December 2008. Official Journal of the European Union, L353, 1-1355.

ECHA, 2016. Endpoint specific guidance, in: ECHA (Ed.), Guidance on information requirements and chemical safety assessment. European Chemicals Agency, Helsinki, Finland.

Eom, H.-J., Jinhee Cho, J., 2011. SiO_2 nanoparticles induced cytotoxicity by oxidative stress in human bronchial epithelial cell, Beas-2B. Environ. Health Toxicol. 26, 1-7.

Frick, R., Muller-Edenborn, B., Schlicker, A., Rothen-Rutishauser, B., Raemy, D.O., Gunther, D., Hattendorf, B., Stark, W., Beck-Schimmer, B., 2011. Comparison of manganese oxide nanoparticles and manganese sulfate with regard to oxidative stress, uptake and apoptosis in alveolar epithelial cells. Toxicol. Lett. 205, 163-172.

Geis, S.W., Fleming, K.L., Korthals, E.T., Searle, G., Reynolds, L., Karner, D.A., 2000. Modifications to the algal growth inhibition test for use as a regulatory assay. Environ. Toxicol. Chem. 19, 36-41.

Genty, B., Briantais, J.M., Baker, N.R., 1989. The relationship between the quantum yield of photosynthetic electron transport and quenching of chlorophyll fluorescence. Biochim. Biophys. Acta 990, 87-92.

Hanaor, D., Michelazzi, M., Leonelli, C., Sorrell, C.C., 2012. The effects of carboxylic acids on the aqueous dispersion and electrophoretic deposition of ZrO_2. J. Eur. Ceram. Soc. 32, 235-244.

Hasegawa, G., Shimonaka, M., Ishihara, Y., 2012. Differential genotoxicity of chemical properties and particle size of rare metal and metal oxide nanoparticles. J. Appl. Toxicol. 32, 72-80.

Hirner, A.V., Flaßbeck, D., 2005. Speciation of silicon, in: Cornelis, R., Crews, H., Caruso, J., Heumann, K.G. (Eds), Handbook of elemental speciation II – species in the environment, food, medicine and occupational health. John Wiley & Sons, Ltd, Chichester, UK, pp. 366-377.

Iler, R.K., 1978. The occurrence, dissolution, and deposition of silica, in: Iler, R.K. (Ed), The chemistry of silica: solubility, polymerization, colloid and surface properties, and biochemistry. John Wiley & Sons, Ltd, New York, USA, pp. 3-115.

Jeong, J., Kim, J., Seok, S.H., Cho, W.S., 2016. Indium oxide (In_2O_3) nanoparticles induce progressive lung injury distinct from lung injuries by copper oxide (CuO) and nickel oxide (NiO) nanoparticles. Arch. Toxicol. 90, 817-828.

Juneau, P., Popovic, R., 1999. Evidence for the rapid phytotoxicity and environmental stress evaluation using the PAM fluorometric method: importance and future application. Ecotoxicology 8, 449-455.

Karunakaran, G., Suriyaprabha, R., Rajendran, V., Kannan, N., 2015. Toxicity evaluation based on particle size, contact angle and zeta potential of SiO_2 and Al_2O_3 on the growth of green algae. Adv. Nano Res. 3, 243-255.

Laurent, S., Boutry, S., Muller, R.N., 2018. Metal oxide particles and their prospects for applications, in: Mahmoudi, M., Laurent, S. (Eds.), Iron oxide nanoparticles for biomedical applications: synthesis, functionalization and application. Elsevier, Ltd, pp. 3-42.

Liu, Y.H., Wang, S., Wang, Z., Ye, N., Fang, H., Wang, D.G., 2018. TiO_2, SiO_2 and ZrO_2 nanoparticles synergistically provoke cellular oxidative damage in freshwater microalgae. Nanomaterials 8, 1-12.

Machado, M.D., Soares, E.V., 2012. Development of a short-term assay based on the evaluation of the plasma membrane integrity of the alga *Pseudokirchneriella subcapitata*. Appl. Microbiol. Biotechnol. 95, 1035-1042.

Machado, M.D., Soares, E.V., 2013. Optimization of a microplate-based assay to assess esterase activity in the alga *Pseudokirchneriella subcapitata*. Water Air Soil Pollut. 224, 1-9.

Manke, A., Wang, L., Rojanasakul, Y., 2013. Mechanisms of nanoparticle-induced oxidative stress and toxicity. Biomed. Res. Int. 2013, 1-15.

Manzo, S., Buono, S., Rametta, G., Miglietta, M., Schiavo, S., Di Francia, G., 2015. The diverse toxic effect of SiO_2 and TiO_2 nanoparticles toward the marine microalgae *Dunaliella tertiolecta*. Environ. Sci. Pollut. Res. 22, 15941-15951.

Nanotech, 2015. Aluminium oxide: forecast from 2010 to 2025. Nanoparticles. Future Markets Inc., Edinburgh.

Ng, A.M.C., Guo, M.Y., Leung, Y.H., Chan, C.M.N., Wong, S.W.Y., Yung, M.M.N., Ma, A.P.Y., Djurisic, A.B., Leung, F.C.C., Leung, K.M.Y., Chan, W.K., Lee, H.K., 2015. Metal oxide nanoparticles with low toxicity. J. Photochem. Photobiol. B 151, 17-24.

OECD, 2011. Alga, growth inhibition test (201), OECD guideline for testing of chemicals. Organization for Economic Co-Operation and Development, Paris, France.

Rajiv, S., Jerobin, J., Saranya, V., Nainawat, M., Sharma, A., Makwana, P., Gayathri, C., Bharath, L., Singh, M., Kumar, M., Mukherjee, A., Chandrasekaran, N., 2016. Comparative cytotoxicity and genotoxicity of cobalt (II, III) oxide, iron (III) oxide, silicon dioxide, and aluminum oxide nanoparticles on human lymphocytes in vitro. Hum. Exp. Toxicol. 35, 170-183.

Report, 2018. Market Research Report: Nanomaterials. Allied Market Research Inc., https://www.alliedmarketresearch.com/press-release/nanomaterials-market.html (Acessed 15 October 2018).

Research, 2018. Indium market size by product: global industry report 2018-2025, https://www.grandviewresearch.com/industry-analysis/indium-market (Acessed 15 October 2018).

Rodea-Palomares, I., Gonzalo, S., Santiago-Morales, J., Leganes, F., Garcia-Calvo, E., Rosal, R., Fernandez-Pinas, F., 2012. An insight into the mechanisms of nanoceria toxicity in aquatic photosynthetic organisms. Aquat. Toxicol. 122, 133-143.

Rogers, N.J., Franklin, N.M., Apte, S.C., Batley, G.E., Angel, B.M., Lead, J.R., Baalousha, M., 2010. Physico-chemical behaviour and algal toxicity of nanoparticulate CeO_2 in freshwater. Environ. Chem. 7, 50-60.

Rutherford, A.W., Krieger-Liszkay, A., 2001. Herbicide-induced oxidative stress in photosystem II. Trends Biochem. Sci. 26, 648-653.

Sadiq, I.M., Pakrashi, S., Chandrasekaran, N., Mukherjee, A., 2011. Studies on toxicity of aluminum oxide (Al_2O_3) nanoparticles to microalgae species: *Scenedesmus* sp and *Chlorella* sp. J. Nanopart. Res. 13, 3287-3299.

Setyawati, M.I., Tay, C.Y., Leong, D.T., 2015. Mechanistic investigation of the biological effects of SiO_2, TiO_2, and ZnO nanoparticles on intestinal cells. Small 11, 3458-3468.

Tarpey, M.M., Wink, D.A., Grisham, M.B., 2004. Methods for detection of reactive metabolites of oxygen and nitrogen: in vitro and in vivo considerations. Am. J. Physiol. Regul. Integr. Comp. Physiol. 286, R431-R444.

Tian, Z.-Y., Kouotou, P.M., Bahlawane, N., Ngamou, P.H.T., 2013. Synthesis of the catalytically active Mn_3O_4 spinel and its thermal properties. J. Phys. Chem. C 117, 6218–6224.

Titma, T., Shimmo, R., Siigur, J., Kahru, A., 2016. Toxicity of antimony, copper, cobalt, manganese, titanium and zinc oxide nanoparticles for the alveolar and intestinal epithelial barrier cells in vitro. Cytotechnology 68, 2363-2377.

Urner, M., Schlicker, A., Z'Graggen, B.R., Stepuk, A., Booy, C., Buehler, K.P., Limbach, L., Chmiel, C., Stark, W.J., Beck-Schimmer, B., 2014. Inflammatory response of lung macrophages and epithelial cells after exposure to redox active nanoparticles: effect of solubility and antioxidant treatment. Environ. Sci. Technol. 48, 13960-13968.

US-EPA, 2002. Short-term methods for estimating the chronic toxicity of effluents and receiving waters to freshwater organisms, 4th ed. Environmental Protection Agency, Washington, DC, pp. 1-350, EPA-821-R-302-013.

Valavanidis, A., Vlahogianni, T., Dassenakis, M., Scoullos, M., 2006. Molecular biomarkers of oxidative stress in aquatic organisms in relation to toxic environmental pollutants. Ecotoxicol. Environ. Saf. 64, 178-189.

Vranic, S., Shimada, Y.,Ichihara, S., Kimata, M., Wu, W., Tanaka, T., Boland, S., Tran, L., Ichihara, G., 2019. Toxicological evaluation of SiO_2 nanoparticles by zebrafish embryo toxicity test. Int. J. Mol. Sci. 20, 1-12.

Wang, Y.L., Ding, L., Yao, C.J., Li, C.C., Xing, X.J., Huang, Y.A., Gu, T.J., Wu, M.H., 2017. Toxic effects of metal oxide nanoparticles and their underlying mechanisms. Sci. China Mat. 60, 93-108.

Yanik, F., Vardar, F., 2015. Toxic effects of aluminum oxide (Al_2O_3) nanoparticles on root growth and development in *Triticum aestivum*. Water Air Soil Pollut. 226, 1-12.

Yanik, F., Vardar, F., 2018. Oxidative stress response to aluminum oxide (Al_2O_3) nanoparticles in *Triticum aestivum*. Biologia 73, 129-135.

Chapter 9 - Effect of natural organic matter, pH and hardness on the toxicity of metal oxide nanoparticles (Al_2O_3, NiO and SnO_2) in the freshwater alga *Pseudokirchneriella subcapitata**

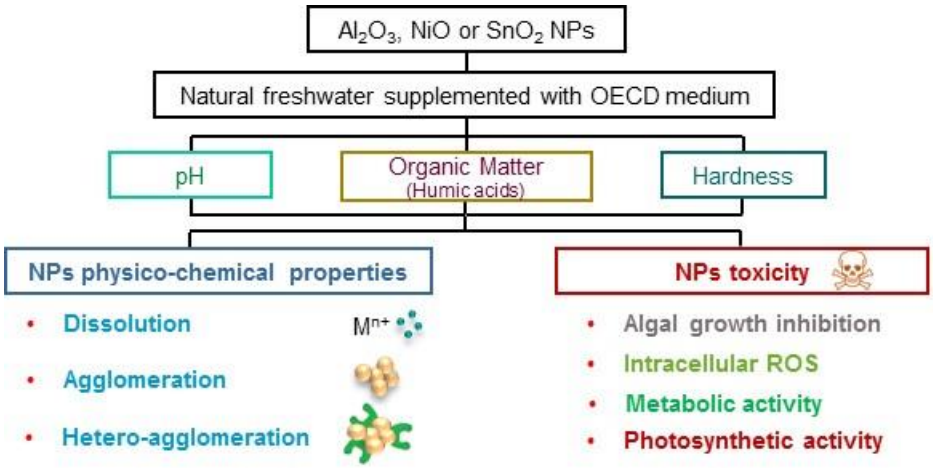

*Submitted for publication

9.1. Introduction

Due to their distinct physico-chemical characteristics (such as, electronic, magnetic and catalytic properties), high surface area and mechanical stability, nanoparticles (NPs) have been incorporated in different products in order to produce materials more strong, durable, reactive and with better electrical conduction capacity (Andreescu et al., 2012; Fernández-García and Rodriguez, 2007). Among the different metal oxide (MOx) NPs, Al_2O_3, NiO and SnO_2 are normally present in coatings, composite materials, ceramics, sensors, chemical catalysts and energy storage devices (Nanotech, 2015; Sajid et al., 2015).

The dramatic increase of NPs production and application observed in the recent years has raised concerns related with their environmental and human safety, which underlines the relevance of assessing NPs potential hazard. MOx NPs can be released directly into the environment either intentionally or accidentally: atmospheric emissions and solid or liquid effluents from production facilities. NPs can also be released from consumer products; in this case, the quantity of NPs that enter into the environment is proportional to their use (Nowack et al., 2012). Whatever the circumstances, NPs have the potential to contaminate soil, ground and surface waters and produce toxic effects in the biota (Klaine et al., 2013). In this context, some studies with Al_2O_3, NiO and SnO_2 NPs were performed, where toxic effects to aquatic organisms were described. Thus, it was reported that the exposure to Al_2O_3 NPs induced growth inhibition in green algae *Pseudokirchneriella subcapitata* (Aruoja et al., 2015), *Chlorella sp*. and *Scenedesmus sp*. and the red alga *Porphyridium aerugineum* Geitler (Karunakaran et al., 2015; Sadiq et al., 2011). NiO NPs caused bioluminescence inhibition in the bacterium *Vibrio fischeri* (Nogueira et al., 2015), growth inhibition in the algae *Chlorella vulgaris* and *P. subcapitata* (Gong et al., 2011; Nogueira et al., 2015; Oukarroum et al., 2017), toxicity to zebrafish *Danio rerio* (Kovriznych et al., 2014), and oxidative stress in the crustacean *Artemia salina* (Ates et al., 2016) and in the aquatic plant *Lemna gibba* (Oukarroum et al., 2015). Recently, using the algal growth inhibition test, with *P. subcapitata,* it was shown that Al_2O_3, NiO and SnO_2 NPs can be classified as toxic (72 h-EC_{50} values between 1-10 mg/L) (please see Chapter 8).

Natural freshwaters are characterized by different parameters, such as, pH, natural organic matter (NOM) and hardness. These parameters can interfere with the behavior (stability - dissolution) of the MOx NPs and, consequently, influence their toxic affect (Amde et al., 2017). In a general way, in freshwaters, namely surface waters (such as, rivers and lakes), pH can vary between 6.5 and 8.5, which is a range tolerable by aquatic organisms (UNEP, 2016). The pH value can interfere with the surface charge of NPs, changing their agglomeration and dissolution behavior (Guzman et al., 2006). NOM is

a highly heterogeneous mixture, constituted mainly by fulvic (FA) and humic acids (HA), resulting from biochemical modifications (biodegradation and synthesis) of plant and animal substrates and their intermediate products. In surface waters, NOM can be found as dissolved organic matter (Kosobucki and Buszewski, 2014). NOM can vary in composition and concentration, in surface waters, due to exportation of organic material from terrestrial environments with high levels of carbon or the increase of agriculture or forest harvesting; in addition, the increase of water retention time rises the amount of NOM in surface waters (such as, lakes) once waters are stagnant (Lavonen, 2015). In surface waters, NOM present dissolved organic carbon (DOC) in the range 0.1 - 332 mg/L and the median is 5.71 mg/L (Sobek et al., 2007). NOM can cause NPs agglomeration due to bridging effect among the NPs; alternatively, the organic matter can be adsorbed to NPs surface through various types of interactions, including electrostatic, hydrogen bonding, and hydrophobic interactions, and thus originating NPs steric stabilization (Navarro et al., 2008) and modify their toxic effects (Keller et al., 2010). The hardness of surface waters varies normally between 0–30 mg/L Ca^{2+} (classified as soft) and 60–150 mg/L Ca^{2+} (classified as hard) (Sawyer et al., 2003; Todd, 2007). The major natural sources of water hardness are dissolved Ca ions from calcareous soils, sedimentary rocks and seepage, causing a variation of the Ca^{2+} levels between regions (WHO, 2011). The electrolytes, namely the water hardness (as Ca^{2+}), can influence the stabilization of NPs in freshwaters. The presence of Ca^{2+} can interfere with the adsorption between NPs and NOM or metal complexation by NOM, preventing the NPs stabilization (Zhang et al., 2009).

Although the toxicity of Al_2O_3, NiO and SnO_2 NPs has been studied, the impact of abiotic factors, such as those described above, on the NPs toxicity have not been yet addressed. The present Chapter had as objective to evaluate the impact of pH, water hardness and the presence of organic matter (HA) on the stability (dissolution) of Al_2O_3, NiO and SnO_2 NPs in a fresh water supplemented with OECD medium. In addition, the impact of these abiotic factors on the NPs toxicity was also evaluated using the freshwater alga *P. subcapitata* under similar conditions. For this purpose, algal cells were exposed for 72 h to the three NPs, at a concentration corresponding to 72 h-EC_{50} values, and the influence of the abiotic factors, individually or in a combined way, was evaluated using different endpoints: algal growth, intracellular reactive oxygen species (ROS) accumulation, metabolic activity and photosynthetic efficiency. This approach will provide insight about the influence of abiotic factors on MOx NPs and will contribute to the understanding of the impact of the release of MOx NPs in aquatic systems, under real scenarios.

9.2. Materials and Methods

9.2.1. Preparation of MOx NPs stock suspensions

Three NPs were used in the present Chapter: Al_2O_3 (< 50 nm), NiO (< 50 nm) and SnO_2 (< 100 nm). NPs stock suspensions of 0.5 g/L were prepared, sonicated and sterilized as described before in Chapters 6 and 7.

9.2.2. Natural freshwater characterization

In the evaluation of NPs stability (please see below, section 2.3) and in the toxicological tests (please see below, section 2.5) a natural freshwater, marketed under the name "Água do Gerês" was used; it is a mineral water, collected in the Gerês mountain, Portugal, which corresponds to a pristine region. The freshwater was characterized by measuring the pH and quantification of metals (Al, Cd, Cr, Cu, Fe, Ni, Pb, Sn and Zn), hardness (Ca^{2+}), total organic carbon (TOC) and inorganic carbon (IC) (Table A1). The pH measurement was carried out using a combined glass electrode using a pH meter Orion, model 4210. The water hardness was determined by titration with EDTA 0.01 mol/L according to the Standard Methods (Clesceri et al., 2010). Metals quantification was carried out by atomic absorption spectroscopy with electrothermal atomization (AAS-EA), in a Perkin Elmer AAnalyst 600 spectrometer. TOC and IC were determined using a TOC-5000A analyser (Shimadzu, Japan).

9.2.3. Stability of MOx NPs

The stability of Al_2O_3, NiO and SnO_2 NPs was evaluated by measuring the metal dissolved from the NPs. The metals solubilized were separated from the non-soluble fraction of the NPs by ultrafiltration using a membrane with a nominal molecular weight limit of 3 kDa. As this membrane rejects particles greater than 1.3 nm (Ma et al., 2014), it was assumed that the metals present in filtrate corresponded, predominantly, to free metal ions and the respective soluble complexes lower that 1.3 nm, being collectively presented, in this Chapter, under the term "metals dissolved".

For this purpose, Al_2O_3, NiO and SnO_2 NPs were suspended at 9.4, 1.6 and 2.1 mg/L, respectively, in the freshwater describe above supplemented with OECD medium. NPs suspensions were incubated for 72 h, in the absence of algal cells, in the same conditions used for toxicological tests (please see below, section 9.2.5). Then, samples were submitted to a centrifugal ultrafiltration (Sartorius, Vivaspin 20 – 3K), being centrifuged at 3.200 × *g* for 40 min, at 25 ºC. The metals and the DOC in the filtrate were quantified by AAS-EA and using a TOC-5000A analyzer, respectively. These studies were performed one time in duplicate.

9.2.4. Strain and culture conditions

In this Chapter, the freshwater green alga *Pseudokirchneriella subcapitata* (strain 278/4) was used. The alga was obtained from the Culture Collection of Algae and Protozoa (CCAP), UK, and maintained in OECD agar medium (OECD, 2011).

The pre-cultures and cultures were prepared and incubated as described before in Chapter 7.

9.2.5. Exposure conditions of algal cells to toxicants

Algal cells at $5x10^4$ cell/mL, in exponential phase of growth, were exposed for 72 h to MOx NPs, in the natural freshwater described in section 2.2 supplemented with OECD medium. Al_2O_3, NiO and SnO_2 NPs were suspended at 9.4, 1.6 and 2.1 mg/L, respectively; these NPs concentrations corresponded to the respective 72h-EC_{50} values, previously determined in Chapter 7 and 8. Different conditions of pH (6.0, 7.5 or 9.0), NOM as HA (2 or 10 mg/L) and hardness (150 mg/L of Ca^{2+}) were tested. In order to fix the pH in the selected values, three buffers at a final concentration of 5 mmol/L were used: 2-(N-morpholino) ethanesulfonic acid (MES, Sigma-Aldrich), 3-(cyclohexylamino)-2-hydroxy-1-propanesulfonic acid (CAPSO, Sigma-Aldrich) and 4-(2-hydroxyethyl)-1piperazineethanesulfonic acid (HEPES, Sigma-Aldrich); the final pH value was adjusted with 2 mol/L NaOH or HCl. HA (ref 53680, Sigma-Aldrich) were dispersed in 80-160 W ultrasonic bath, for 10 min. For water hardness, Ca^{2+} was added at a final concentration of 150 mg/L from a stock solution of 40 g/L $CaCl_2$. As control, algal cells were grown in the same conditions of the assay but in the absence of toxicant.

The assays were performed in 250 mL Erlenmeyer flasks, combining 90 mL of freshwater (with the convenient modification) supplemented with 10 mL of OECD medium (ten times concentrated). After 72 h of incubation, algal cell concentrations (growth assays) were determined using an automated cell counter (TC10, Bio-Rad). Then, cells were harvested by centrifugation at 2,500 x *g* for 5 min and re-suspended in OECD medium at a final concentration of $1x10^6$ cells/mL (ROS detection assays), $5x10^5$ cells/mL (metabolic activity evaluation) or $3x10^6$ cells/mL (photosynthetic performance assays). These studies were performed one time in duplicate.

9.2.6. Intracellular ROS level evaluation

The intracellular ROS accumulation was evaluated using the fluorescent dye 2',7'-dichlorodihydrofluorescein diacetate (H_2DCFDA, Sigma), as previously described in Chapter 7. The fluorescence values were corrected (by subtracting cell, culture medium and dye autofluorescence) and normalized as the ratio of fluorescence in the cells exposed to MOx NPs/fluorescence in the control (cells non-exposed to toxic).

9.2.7. Metabolic activity estimation

Metabolic activity of algal cells was evaluated using a fluorescein diacetate (FDA)-based esterase assay, where the amount of green-fluorescence is related with the metabolic activity of algal cells (Machado and Soares, 2013) and was evaluated as described in Chapter 7. Fluorescence was measured and corrected and the results expressed as described above for intracellular ROS evaluation.

9.2.8. Photosynthetic efficiency assessment

Algal photosynthetic performance of photosystem II (PSII) was evaluated through the determination of the effective photochemical quantum yield of PS II (Φ_{PSII}), by pulse amplitude modulated (PAM) fluorescence assay, using a chlorophyll fluorometer (Walz, JUNIOR-PAM, Effeltrich, Germany), as described in Chapter 7. The Φ_{PSII} was automatically obtained using the WinControl software (version 3.25), according to the equation presented in Chapter 7 (Table 7.1).

9.2.9. Microscopy

Samples were observed by phase-contrast and/or by epifluorescence microscopy using a I3 filter from Leica. The images were acquired with a Leica DC 300F camera using 40x or 100x oil immersion N plan objectives and processed using Leica IM 50-image manager software.

9.3. Results

The characteristics of freshwaters can vary appreciably namely, pH, organic matter and water hardness. The modification of these characteristics can influence NPs properties, such as their stability (dissolution, i.e., release of metal ions) and agglomeration as well as their toxicity.

9.3.1. Repercussion of pH, hardness and organic matter on NPs stability and hetero-agglomeration

The modification of the medium pH (increase from 6.0 - 9.0), within the tolerable values for aquatic organisms (UNEP, 2016), lead to a decrease of the concentration of metals dissolved (Fig 9.1). A marked reduction of dissolved metal concentrations was observed in the presence of 10 mg/L HA (Fig 9.1); this HA concentration translated into DOC values ranging from 5.6 and 8.6 mg/L (Table A2), which correspond to the most frequent DOC values found in surface waters (Sobek et al., 2007). The addition of Ca^{2+}, at pH 9.0, even at a concentration found in hard waters (150 mg/L) (Sawyer et al., 2003; Todd, 2007) did not modify the concentration of metals dissolved (Fig 9.1). The simultaneous presence of 150 mg/L Ca^{2+} and 10 mg/L HA lead to an increase of the concentration of dissolved Al, at pH 9.0, comparatively to 10 mg/L HA, without Ca^{2+}. In the case of Ni and Sn, the addition of 150 mg/L Ca^{2+} did not influence the HA effect, since no modification of the concentrations of metals dissolved were observed with 10 mg/L HA, in the presence or absence of Ca^{2+} (Fig 9.1).

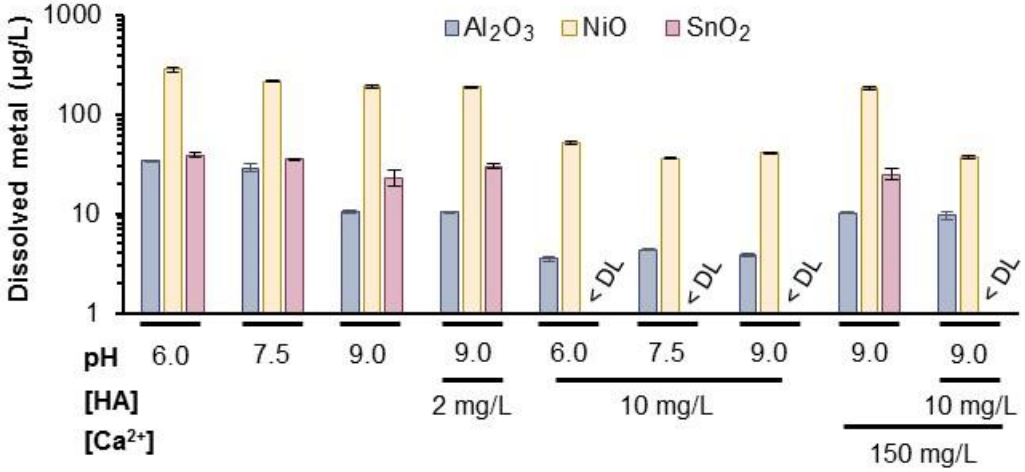

Figure 9.1. Influence of abiotic factors on the dissolution of NPs. Abiotic factors studied: pH, humic acids (HA) and Ca^{2+}. Al_2O_3, NiO and SnO_2 NPs were suspended in fresh water supplemented with OECD medium at 9.4, 1.6 and 2.1 mg/L, respectively. The suspensions were incubated for 72 h, at 100 rpm, at 25 ºC, in the absence of algal cells. DL: detection limit; DL for Sn: 7.2 µg/L.

All NPs studied formed homo-agglomerates (as result of the interaction among the same NPs) in the fresh water supplemented with OECD medium, independently of the pH, although they were not observed at the naked eye for Al_2O_3 and SnO_2 NPs (Fig A1-A3); however, the formation of homo-agglomerates for the three NPs could be seen by optical microscopy (Fig A4-A6). Green agglomerates, which were well visible to the naked eye, were observed when Al_2O_3 NPs were incubated with *P.*

subcapitata cells for 72 h (Fig A7). In contrast, no agglomeration was observed, macroscopically, when algal cells were incubated with NiO or SnO_2 NPs, in the fresh water supplemented with OECD medium, at different pH values (Fig A8 and A9). The inspection of the suspensions, by optical microscopy, revealed the formation of algae-NPs hetero-agglomerates, for Al_2O_3 (Fig A10A); when incubated with NiO or SnO_2 NPs, algal cells remained dispersed in the medium (Fig A11).

The presence of 150 mg/L Ca^{2+}, at pH 9.0, seems also not influence the agglomeration of the NPs tested; under this condition, algal cells suspensions had a similar appearance to that observed without Ca^{2+}, in the absence (Fig A1-A3) or in the presence of algal cells (Fig A7-A9).

HA, at 10 mg/L, were not completely dissolved at pH 6.0 and 7.5, in the absence (Fig A1-A3) (also evidenced by the lower DOC values registered when compared to the ones measured at pH 9.0, Table A2) or in the presence of algal cells (Fig A7-A9). An increase of HA dissolution with the increase of pH was observed in the absence of algal cells, which translated into an increase of the DOC, namely for 10 mg/L at pH 9.0 (Table A2). The observation, by optical microscopy, of the suspensions confirmed the presence of brown agglomerates, probably of HA, at pH 6.0 and 7.5 but not at pH 9.0 (Fig A4-A6). HA promoted the dispersion of Al_2O_3 NPs-algal hetero-agglomerates. This effect, although observed for 2 mg/L HA (as it can be seen through the increase of the greenness of the suspensions) was particularly evident for 10 mg/L HA, for all pH values tested (Fig A7). The microscopic observation of the suspensions confirmed the dispersive effect of HA over Al_2O_3 NPs-algal hetero-agglomerates, although for 2 mg/L HA some hetero-agglomerates still could be observed (Fig A10B). In the presence of 10 mg/L HA, algal cells were completely dispersed, although some brown agglomerates could be observed at pH 6.0 and 7.5 (Fig A12). In the case of NiO and SnO_2 NPs, dispersed algal cells were microscopically observed with 10 mg/L HA (Fig A13 and A14).

The addition of 150 mg/L Ca^{2+} to 10 mg/L HA, at pH 9.0, seems not influence the dispersive effect of HA, observed at the naked eye (Fig A7-A9) and confirmed by optical microscopy (Fig A12-A14).

9.3.2. Effect of pH on NPs toxicity

Algal cells were exposed to 9.4 mg/L Al_2O_3, 1.6 mg/L NiO and 2.1 mg/L SnO_2 NPs, corresponding to the respective 72h-EC_{50} values. The toxicity of the three NPs studied, evaluated through algal growth inhibition assay, was similar (caused ~50 % of growth inhibition), which showed that the pH of the fresh waters supplemented with OECD medium (between 6.0 – 9.0) did not modify the NPs toxicity (Fig 9.2).

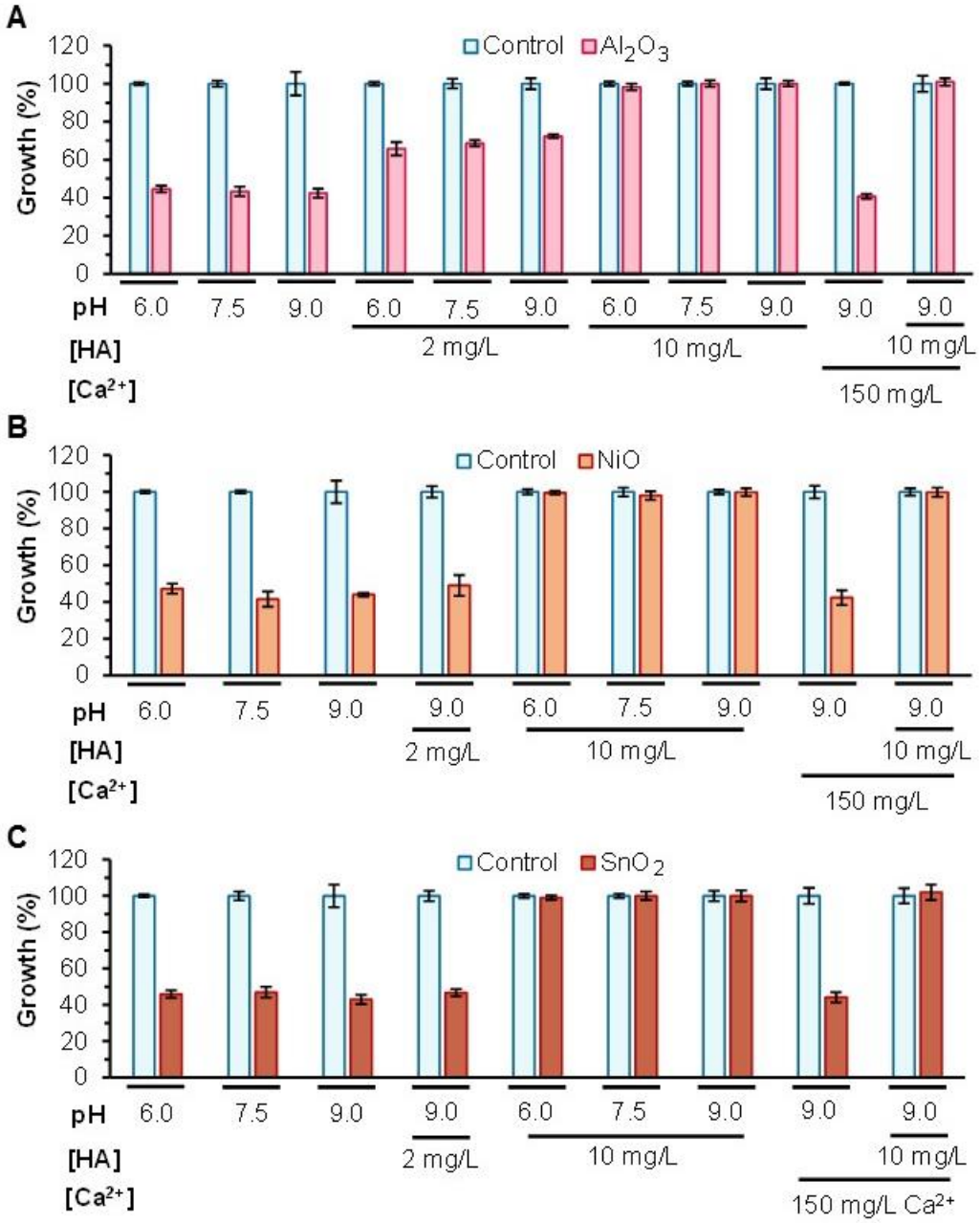

Figure 9.2. Impact of the abiotic factors plus each NP on the growth of *P. subcapitata*. Abiotic factors studied: pH, humic acids (HA) and Ca^{2+}. A - Al_2O_3. B - NiO. C - SnO_2. NPs were suspended at the concentrations reported in Fig 9.1. The suspensions were incubated for 72 h, at 100 rpm, at 25 ºC, in the same experimental conditions described in Fig 9.1.

The increase of intracellular ROS accumulation (Fig 9.3A and B) and the decrease of metabolic activity (esterase activity) (Fig 9.4A and B), induced due to the exposure to Al_2O_3 and NiO NPs, was also similar in the pH range values tested.

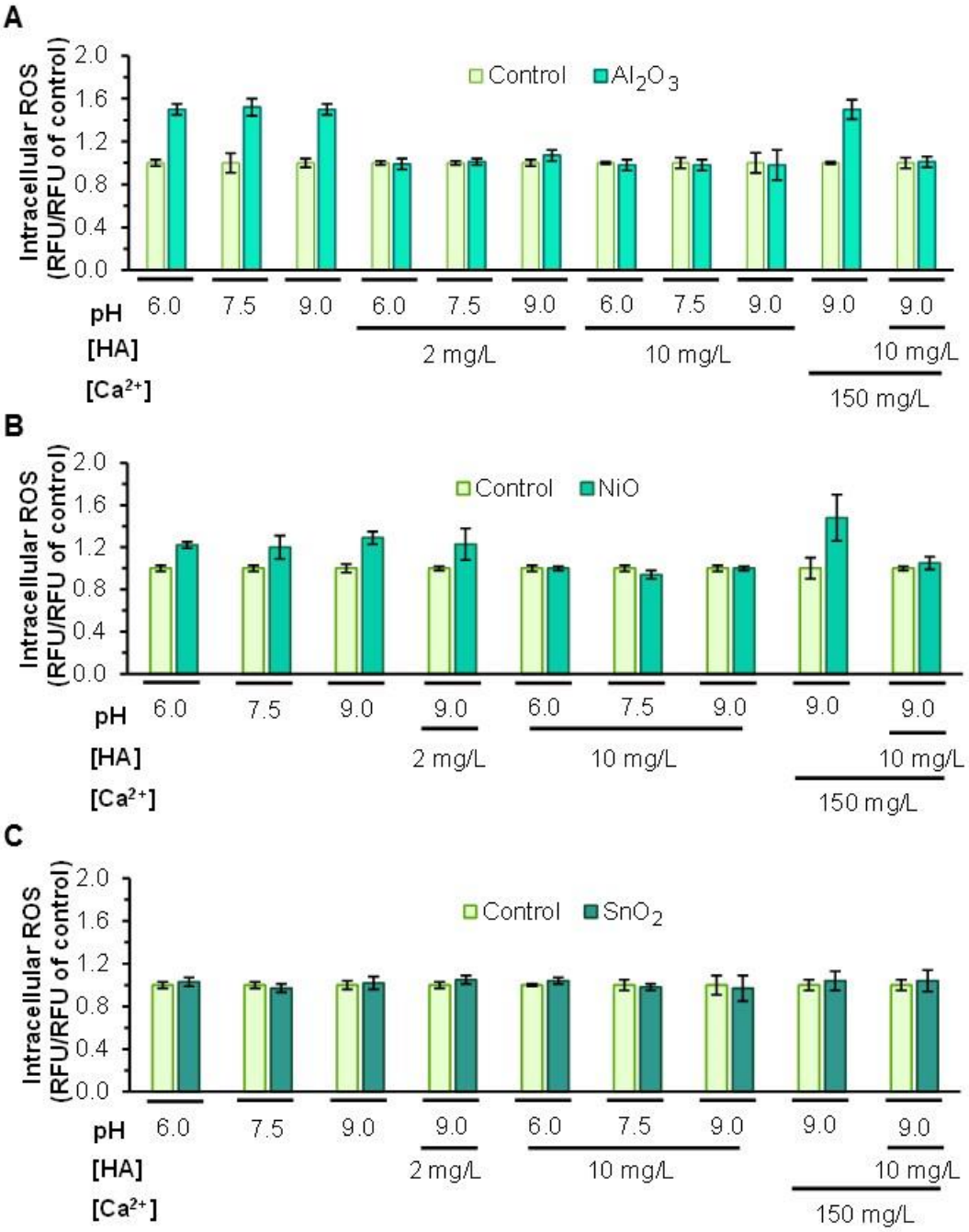

Figure 9.3. Effect of the abiotic factors plus each NP on the intracellular ROS accumulation in *P. subcapitata*. Abiotic factors studied: pH, humic acids (HA) and Ca^{2+}. A - Al_2O_3. B - NiO. C - SnO_2. NPs were suspended at the concentrations reported in Fig 9.1. The suspensions were incubated for 72 h, at 100 rpm, at 25 ºC, in the same experimental conditions described in Fig 9.1. Intracellular ROS in algal cells was assessed using H_2DCFDA.

Similarly, the reduction of effective photochemical quantum yield of PSII (Φ_{PSII}) of algal cells (photosynthetic activity) (Fig 9.5) exposed to NPs, was not affected by the pH of the freshwaters supplemented with OECD medium.

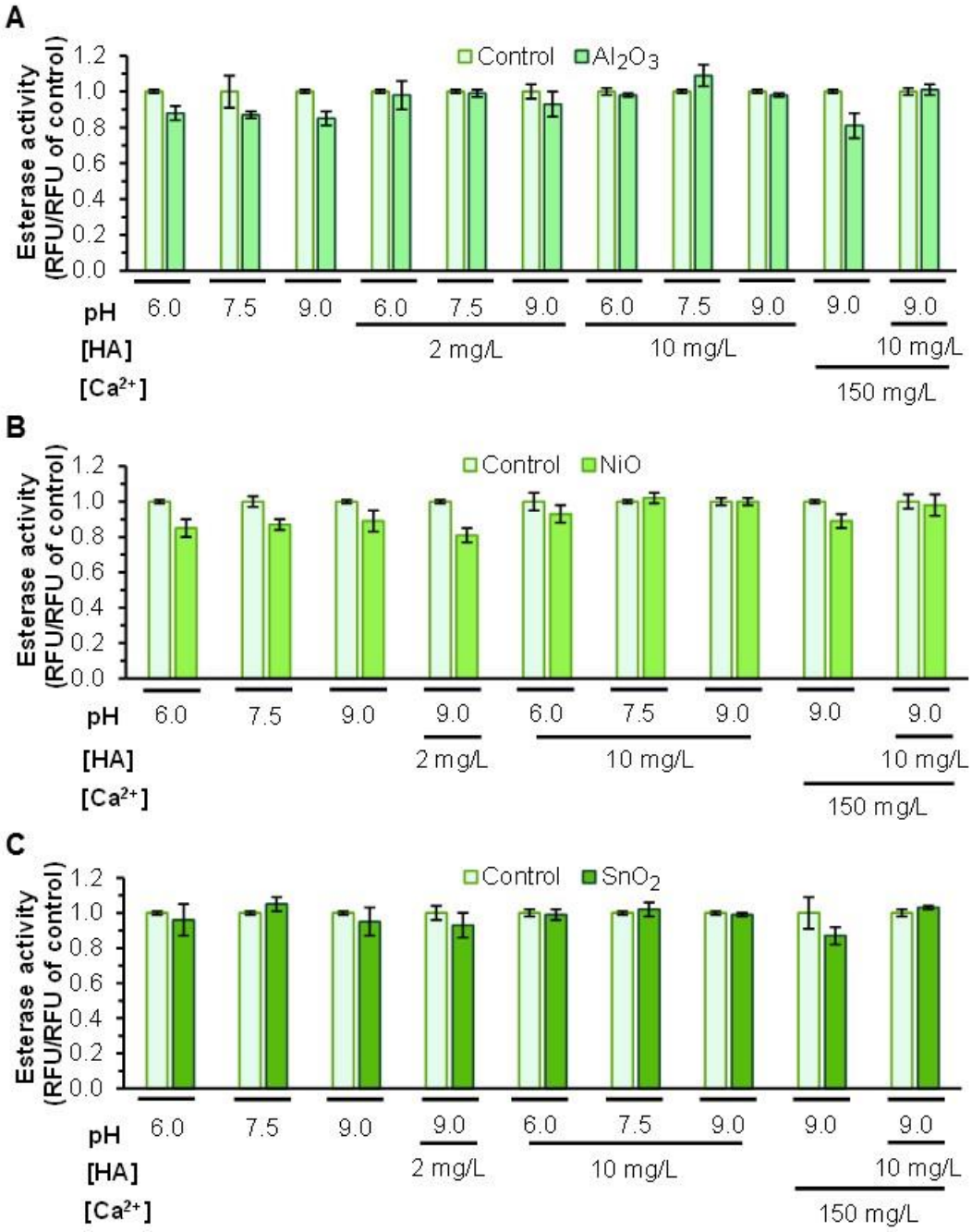

Figure 9.4. Repercussion of abiotic factors plus each NP on the metabolic activity of *P. subcapitata*. Abiotic factors studied: pH, humic acids (HA) and Ca^{2+}. A - Al_2O_3. B - NiO. C - SnO_2. NPs were suspended at the concentrations reported in Fig 9.1. The suspensions were incubated for 72 h, at 100 rpm, at 25 ºC, in the same experimental conditions described in Fig 9.1. Metabolic activity of algal cells was determined using a FDA-based esterase assay.

Taken together, these results, strongly indicate that the pH value of the culture medium (between 6.0 – 9.0) did not influence Al_2O_3, NiO and SnO_2 NPs toxicity, over algal cells, evaluated by different endpoints, at cellular or sub-cellular level.

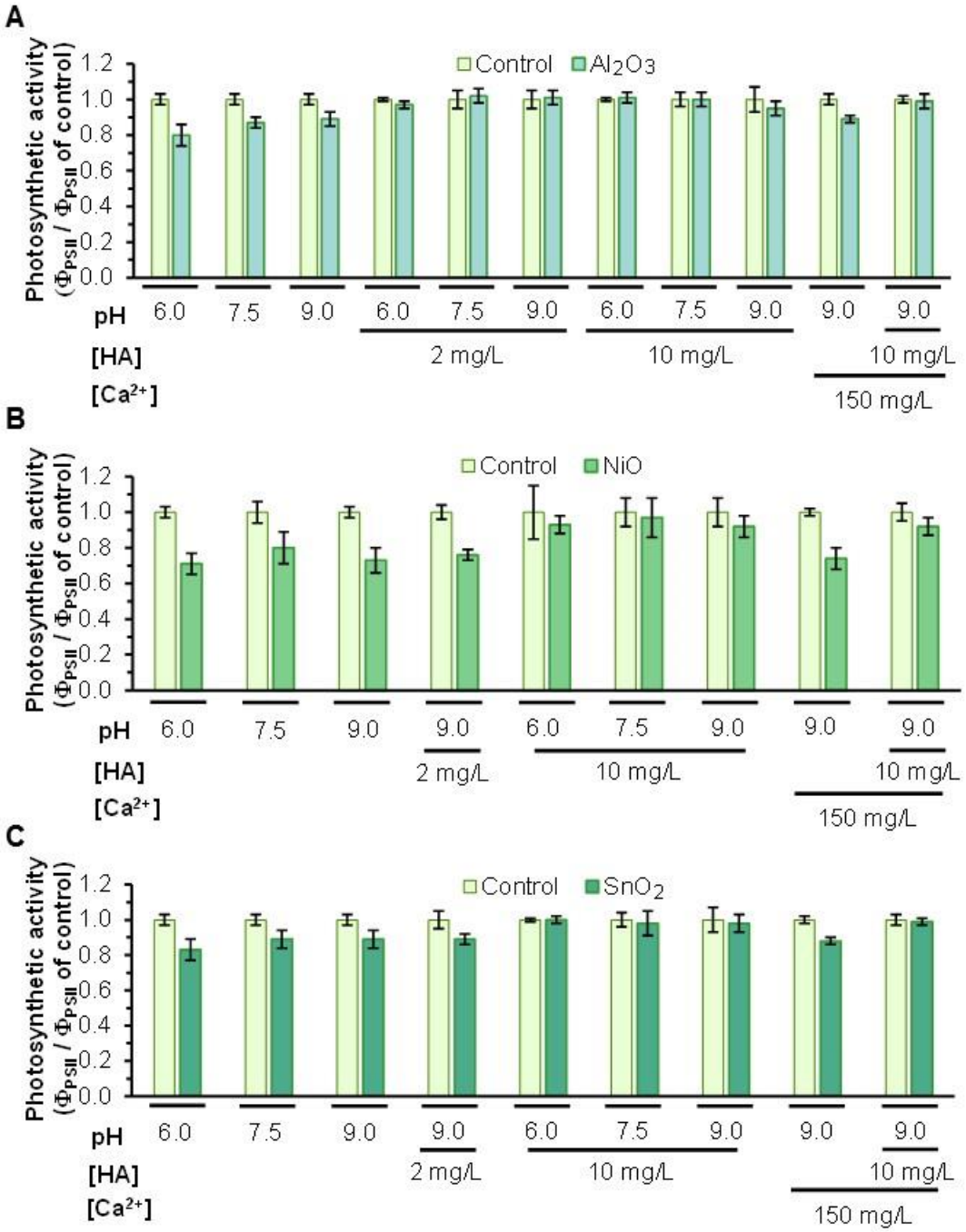

Figure 9.5. Influence of the abiotic factors plus each NP on the photosynthetic activity of *P. subcapitata*. A - Al_2O_3. B - NiO. C - SnO_2. NPs were suspended at the concentrations reported in Fig 9.1. The suspensions were incubated for 72 h, at 100 rpm, at 25 ºC, in the same experimental conditions described in Fig 9.1. Effective photochemical quantum yield of PSII (Φ_{PSII}) of algal cells was evaluated by PAM fluorescence assay.

9.3.3. Influence of water hardness on NPs toxicity

The evaluation of the impact of the water hardness, at pH 9.0, on NPs toxicity revealed that the presence of 150 mg/L Ca^{2+} did not modify Al_2O_3, NiO and SnO_2 NPs toxicity, evaluated through algal growth (Fig 9.2), intracellular ROS accumulation (Fig 9.3), metabolic (esterase) activity (Fig 9.4) and photosynthetic efficiency (Fig 9.5). Due to the results obtained, the impact of lower Ca^{2+} concentrations (corresponding to soft waters) on NPs toxicity were not tested.

9.3.4. Impact of pH and organic matter on NPs toxicity

The influence of NOM was evaluated using two HA concentrations: 2 and 10 mg/L. As the level of protonation of HA can vary with the pH of the solution (Motta et al., 2016), which can influence the interaction of HA with the MOx NPs or the respective soluble metals, the influence of the pH was simultaneously considered.

The algal growth inhibition due to the presence of Al_2O_3 NPs was attenuated when the cells were incubated in the simultaneous presence of 2 mg/L HA, independently of the pH value tested (Fig 9.2A). A marked effect (complete reversion of Al_2O_3 NPs toxicity) was observed when the algal cells were co-exposed to NPs and 10 mg/L HA, independently of the pH value tested (Fig 9.2A). The toxic effects evaluated through sub-cellular endpoints were completely reverted, even for the lowest (2 mg/L) HA concentration tested. Thus, when incubated with 2-10 mg/L HA, Al_2O_3 NPs were not able to induce intracellular ROS production (Fig 9.3A), loss of metabolic activity (Fig 9.4A) or modification of the photosynthetic efficiency (Fig 9.5A).

Within the pH range values tested, at pH 9.0, HA present the higher level of deprotonation (Motta et al., 2016). Since the mixture of 2 mg/L HA with NiO NPs, at pH 9.0, did not modify the NPs toxicity, independently of the endpoint tested (Fig 9.2B, 3B, 4B and 5B) relatively to the toxicity profile recorded at the same pH in the absence of HA, the effect of 2 mg/L HA at other pH values was not tested. However, the presence of 10 mg/L HA completely abolished the NiO NPs toxicity, for all algal endpoints evaluated, independently of the pH of the medium (Fig 9.2B, 3B, 4B and 5B).

Similarly, to what was observed with NiO NPs, 2 mg/L HA, at pH 9.0, did not hamper algal growth inhibition (Fig 9.2C) or reduction of photosynthetic activity (Fig 9.5C) due to the presence of SnO_2 NPs. Algal growth inhibition (Fig 9.2C) and reduction of photosynthetic activity (Fig 9.5C) was reverted when algal cells were incubated with SnO_2 NPs and 10 mg/L HA, independently of the pH of the medium.

Taking together, these results indicate that HA had a protective effect against the toxic impact induced by Al_2O_3, NiO and SnO_2 NPs on *P. subcapitata* algal cells.

9.3.5. Simultaneous influence of pH, hardness and organic matter on NPs toxicity

At pH 9.0, where carboxylic groups of HA are deprotonated, 150 mg/L Ca^{2+} did not hindered the protective effect of 10 mg/L HA against Al_2O_3, NiO and SnO_2 NPs toxicity, evaluated through algal growth (Fig 9.2), intracellular ROS generation (Fig 9.3), metabolic activity (Fig 9.4) or photosynthetic efficiency (Fig 9.5).

9.4. Discussion

The use of Al_2O_3, NiO and SnO_2 NPs in different products makes it likely to be released into the aquatic environment where their potential toxic effects to the organisms are largely unknown. When MOx NPs reach aquatic compartment can undergo several transformations, which includes agglomeration, sedimentation and dissolution (Amde et al., 2017). The study of agglomeration and dissolution of NPs can provide valuable information for the speciation of NPs in the environment (Topuz et al., 2015), which, in turn, is essential for the understanding of their reactivity and toxicity. MOx NPs dissolution involves the release of the respective metal ions in aqueous solution, which is dependent of several factors, such as the pH of the surrounding medium and ligand availability.

In the present work, it was observed that the increase of pH lead to a reduction of metals released from the three NPs studied (Fig 9.1). A similar result was described with ZnO NPs (Odzak et al., 2017). This behavior can be explained by the lower solubility exhibited by these MOx NPs, which is enhanced at neutral and slight alkaline pH values. Although it has been reported that the pH of the solution can affect NPs agglomeration behavior since it affects their surface charge (Amde et al., 2017; Peng et al., 2017), here, an expressive modification of NPs homo-agglomeration (Fig A1-A6) or Al_2O_3 NPs-algal hetero-agglomeration (Fig A7), with the modification of the pH, seems not to be occurred. This relative constant homo-agglomeration profile along the pH range tested reflects the decreased surface charge (and, thus, the electrostatic repulsion) evidenced by these NPs as a consequence of the lower zeta potential values recently described for similar pH value (please see Chapters 7 and 8). Similarly, an increase of the agglomeration of ZnO NPs with the pH values near the zero point of charge, accompanied by a decrease of the dissolution of the NPs, was described (Domingos et al., 2013). In addition, the toxicity of Al_2O_3, NiO or SnO_2 NPs, when evaluated through the algal growth inhibition (Fig 9.2), did not change through the pH and remained at 50% growth inhibition, as it was

expected. Moreover, a toxicity effect, when evaluated by the quantification of intracellular ROS accumulation (Fig 9.3) and the metabolic activity (Fig 9.4), which remained constant along the pH range tested, was observed for Al_2O_3 and NiO NPs. Additionally, for all NPs, the toxicity, assessed by the photosynthetic efficiency (Fig 9.5), revealed a constant inhibitory effect for all pH range tested being more pronounced in the case of NiO NPs.

The raise of water hardness (increase of Ca^{2+}) can screen the surface charge of NPs and lead to their agglomeration due to the decrease of the electrostatic repulsion (Handy et al., 2008; Topuz et al., 2015). In fact, ionic strength/Ca^{2+} concentrations in the milimolar range, as they occur in freshwaters, have shown to cause TiO_2 NPs hetero-agglomeration with microalgae cells (Sendra et al., 2017) and stronger agglomeration of Ag-NPs in waters, namely those with higher ionic strength (Odzak et al., 2017). However, in the present study, the elevation of water hardness (through the addition of 150 mg/L Ca^{2+}), at pH 9.0 did not have an appreciable impact on the NPs homo-agglomeration (Fig A1-A3) or Al_2O_3 NPs hetero-agglomeration (Fig A7). Similarly, the presence of 150 mg/L Ca^{2+}, at pH 9.0, did not modify neither the concentration of metals dissolved (Fig 9.1) nor the NPs toxicity over algal cells comparatively to the profile observed at pH 9.0 in the absence of Ca^{2+} whatever the toxicity endpoints studied (Fig 9.2-9.5).

NOM, an ever-present component of natural waters, can influence the metals bioavailability, as well as promote the change of NPs properties (Chen et al., 2010). We observed that the presence of HA induced the dispersion of Al_2O_3 NPs-algal cells hetero-agglomerates, in a dose-dependent manner (Fig A7 and A10). These results suggest that HA stabilized Al_2O_3 NPs and are in agreement with the literature that describes the adsorption of HA on Al_2O_3 NPs (Ghosh et al., 2008; Yang et al., 2009). In fact, since the point of zero charge of Al_2O_3 NPs is well above the environmental pH values and because most NOM is negatively charged in the environmental pH range values (Yu et al., 2018), it was reported that HA adsorption by oxide NPs was mostly induced by electrostatic attraction and ligand exchange between HA and NPs-surface; in the case of Al_2O_3 NPs, it was identified that the OH phenolic/aliphatic and COOH groups of HA are responsible for its ligand exchange with the NPs. Thus, it was proposed that HA coated Al_2O_3 NPs are more easily dispersed and stable in solution than the uncoated ones due to their enhanced electrostatic repulsion (Yang et al., 2009). Similarly, it was described the stabilization of CeO_2 NPs when treated with polyacrylic acid, a compound with similar properties to HA (Sehgal et al., 2005) or with natural organic matter (Quik et al., 2010); the hindering of ZnO-NPs agglomeration due the presence of 10 mg/L NOM (Zhou and Keller, 2010) or HA (Peng et al., 2017) was also described. In this study, a reduction of the metals dissolved when the NPs were

incubated in the presence of HA was observed (Fig 9.1). These results can be attributed to the formation of metal-HA complexes. The free metal ions, released by the NPs, were probably complexed by HA, which size was greater than 1.3 nm and, thus, was retained in the membrane of the ultrafiltration device, reducing the concentration of metals in the filtrate. In previous works, it was shown that NiO and SnO_2 NPs toxicity, over *P. subcapitata* algal cells, can be attributed to the release of metal ions (please see Chapters 7 and 8). Therefore, the reduction of dissolved metals concentration, due to the presence of HA, is consistent with the reduction of NiO and SnO_2 NPs toxicity, when the NPs were co-incubated with 10 mg/L HA (Fig 9.2). In the case of Al_2O_3, it was observed that the toxic effects over algal cells were mainly due to the NPs (please see Chapter 8). The reduction of Al_2O_3 toxicity, even for the lowest concentration of HA tested (2 mg/L) can be due to the coating of the NPs by HA, in a similar way of formation of protein-coated NPs (Cedervall et al., 2007; Lok et al., 2007). This possibility is aligned with the literature, which describes the stabilization of NPs by NOM; as consequence, a reduction of the NPs bioavailability and toxicity occurs (Chen et al., 2010). NPs-HA interaction can be even more complex as HA and MOx NPs can also interact with other constituents, present in aqueous solution, such as bivalent cations. In this context, it was described that the modification of the ionic composition of the aqueous solution may be enough to promote the desorption of a given chemical species; in certain circumstances, a chemical species with high affinity to the adsorbent binding sites may promote the desorption and replace the initially adsorbed substance (Nowack et al., 2012). This can be a plausible explanation for the increase of the concentration of dissolved Al, when 150 mg/L Ca^{2+} was added to a solution containing 10 mg/L HA, at pH 9.0 (Fig 9.1). In fact, Ca^{2+} may have replaced Al^{3+}, at the HA binding sites, with the consequent Al desorption, which was translated by the increase of Al dissolved, compared to the same conditions (10 mg/L HA, at pH 9.0), in the absence of Ca^{2+} (Fig 9.1). However, under the same conditions studied (10 mg/L HA, at pH 9.0), the simultaneous presence of 150 mg/L Ca^{2+} did not modify the concentration of Ni or Sn dissolved (Fig 9.1). This diverse behavior of the NPs can be due to the different affinity of Al^{3+}, Ni^{2+} and Sn^{4+} to HA binding sites. Although it was described that the addition of Ca^{2+} can revert the stabilization effect of 4 mg/L NOM on NiO NPs (Zhang et al., 2009), this effect was observed in the presence of 40-60 mmol/L Ca^{2+}, which corresponded to a Ca^{2+} concentration ~11-16 times higher than the one used in the present study. Additionally, the increasing of water hardness did not abrogate the protective effect of HA over the NPs toxicity, whatever the toxicity endpoints studied (Fig 9.2-9.5). The increase of dissolved Al (from 4 to 10 µg/L) due to the presence of 150 mg/L Ca^{2+} is not enough to induce toxicity in *P. subcapitata* algal cells (please see Chapter 8).

In previous works, it was shown that algal cells exposed to Al_2O_3, NiO or SnO_2 NPs presented a disturbance of the photosynthetic process. The exposure to Al_2O_3 or NiO NPs was also accompanied by an intracellular accumulation of ROS (probably as a consequence of the leakage of the electrons from the photosynthetic chain) and a reduction of the (esterase) metabolic activity (please see Chapters 7 and 8). As it was discussed above, the presence of 10 mg/L HA, abrogated the inhibitory growth effect induced by the three NPs studied (Fig 9.2). Interestingly, the incubation of algal cell with Al_2O_3, NiO or SnO_2 NPs and HA, restored the photosynthetic efficiency (Φ_{PSII}) (Fig 9.5); in the case of NiO or SnO_2 NPs and HA, algal cells did not accumulate ROS (Fig 9.3) and the metabolic activity was re-established (Fig 9.4). Taken together, these results confirm the mechanisms of toxicity previously proposed.

9.5. Conclusions

A generalized scheme of the influence of the abiotic factors (pH, organic matter and hardness) on the transformations of the MOx (Al_2O_3, NiO and SnO_2) NPs in freshwater and its toxicity over *P. subcapitata* can be seen in Fig 9.6. In resume:

- The rise of pH value of the natural water supplemented with OECD medium decreased the concentration of dissolved metals from the NPs;
- The presence of HA, reduced the concentration of dissolved metals and lead to the complete dispersion of Al_2O_3 NPs-algal cells hetero-agglomerates;
- HA also had a protective effect against Al_2O_3, NiO or SnO_2 NPs toxicity.

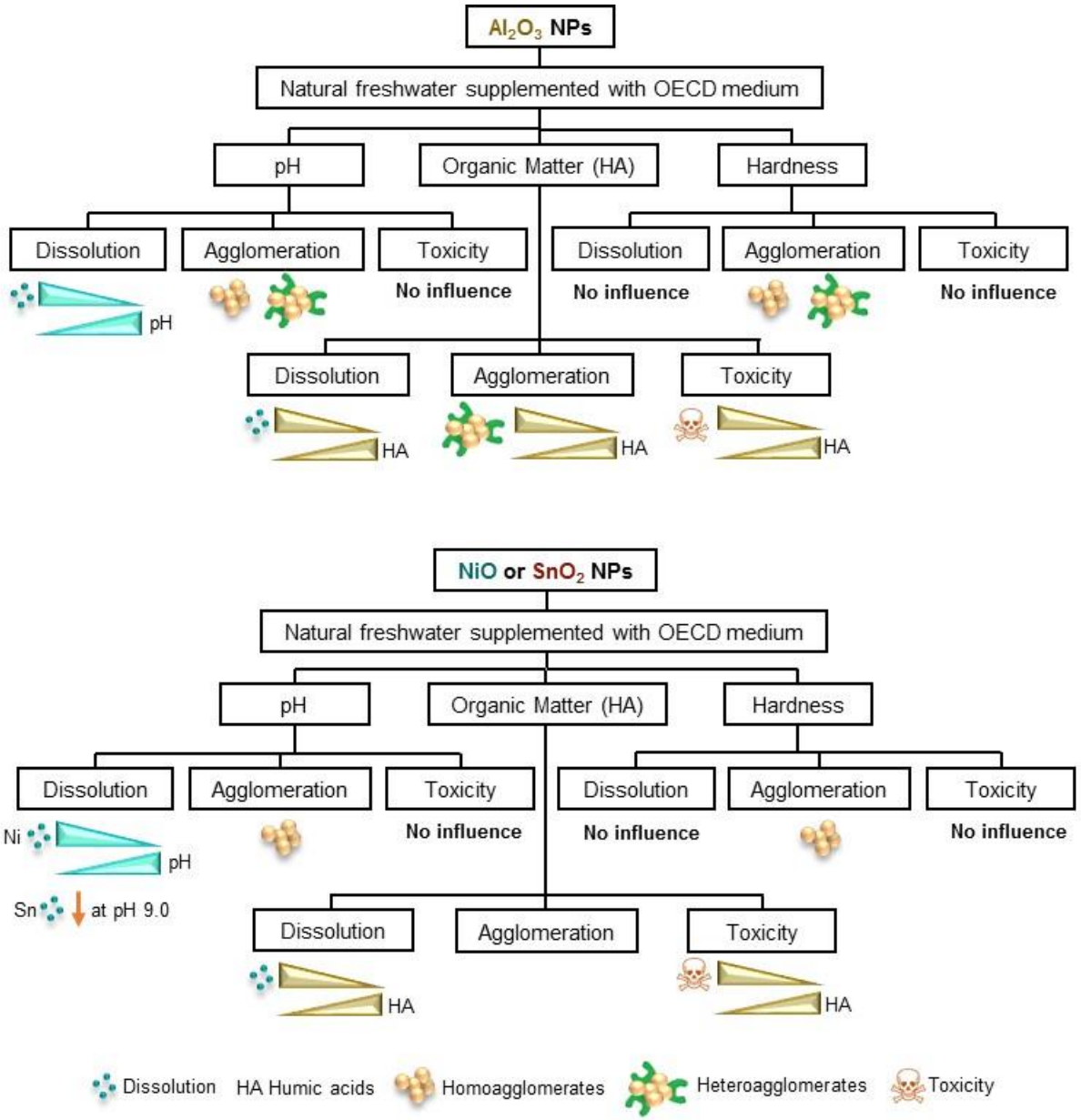

Figure 9.6. Schematic description of the main effects of the abiotic factors on the Al_2O_3, NiO and SnO_2 NPs ecotoxicity and physico-chemical proprieties [(stability (dissolution) and agglomeration)] in a freshwater (supplemented with the OECD medium).

References

Amde, M., Liu, J.F., Tan, Z.Q., Bekana, D., 2017. Transformation and bioavailability of metal oxide nanoparticles in aquatic and terrestrial environments. A review. Environ. Pollut. 230, 250-267.

Andreescu, S., Ornatska, M., Erlichman, J.S., Estevez, A., Leiter, J.C., 2012. Biomedical applications of metal oxide nanoparticles, in: Matijević, E. (Ed.), Fine particles in medicine and pharmacy. Springer, Boston, MA, pp. 57-100.

Aruoja, V., Pokhrel, S., Sihtmae, M., Mortimer, M., Madler, L., Kahru, A., 2015. Toxicity of 12 metal-based nanoparticles to algae, bacteria and protozoa. Environ. Sci. Nano 2, 630-644.

Ates, M., Demir, V., Arslan, Z., Camas, M., Celik, F., 2016. Toxicity of engineered nickel oxide and cobalt oxide nanoparticles to *Artemia salina* in seawater. Water Air Soil Pollut. 227.

Cedervall, T., Lynch, I., Lindman, S., Berggard, T., Thulin, E., Nilsson, H., Dawson, K.A., Linse, S., 2007. Understanding the nanoparticle-protein corona using methods to quantify exchange rates and affinities of proteins for nanoparticles. Proc. Natl. Acad. Sci. USA 104, 2050-2055.

Chen, K.L., Smith, B.A., Ball, W.P., Fairbrother, B.H., 2010. Assessing the colloidal properties of engineered nanoparticles in water: case studies from fullerene C_{60} nanoparticles and carbon nanotubes. Environ. Chem. 7, 10-27.

Clesceri, L.S., Greenberg, A.E., Eaton, A.D., 2010. Standard methods for the examination of water and wastewater. American Public Health Association, Washington.

Domingos, R.F., Rafiei, Z., Monteiro, C.E., Khan, M.A.K., Wilkinson, K.J., 2013. Agglomeration and dissolution of zinc oxide nanoparticles: role of pH, ionic strength and fulvic acid. Environ. Chem. 10, 306-312.

Fernández-García, M., Rodriguez, J.A., 2007. Metal oxide nanoparticles Nanomaterials: inorganic and bioinorganic perspectives. Brookhaven Science Associates, LLC New York, USA.

Genty, B., Briantais, J.M., Baker, N.R., 1989. The relationship between the quantum yield of photosynthetic electron transport and quenching of chlorophyll fluorescence. Biochim. Biophys. Acta 990, 87-92.

Ghosh, S., Mashayekhi, H., Pan, B., Bhowmik, P., Xing, B.S., 2008. Colloidal behavior of aluminum oxide nanoparticles as affected by pH and natural organic matter. Langmuir 24, 12385-12391.

Gong, N., Shao, K., Feng, W., Lin, Z., Liang, C., Sun, Y., 2011. Biotoxicity of nickel oxide nanoparticles and bio-remediation by microalgae *Chlorella vulgaris*. Chemosphere 83, 510-516.

Guzman, K.A.D., Finnegan, M.P., Banfield, J.F., 2006. Influence of surface potential on aggregation and transport of titania nanoparticles. Environ. Sci. Technol. 40, 7688-7693.

Handy, R.D., von der Kammer, F., Lead, J.R., Hassellov, M., Owen, R., Crane, M., 2008. The ecotoxicology and chemistry of manufactured nanoparticles. Ecotoxicology 17, 287-314.

Karunakaran, G., Suriyaprabha, R., Rajendran, V., Kannan, N., 2015. Toxicity evaluation based on particle size, contact angle and zeta potential of SiO_2 and Al_2O_3 on the growth of green algae. Adv. Nano Res. 3, 243-255.

Keller, A.A., Wang, H.T., Zhou, D.X., Lenihan, H.S., Cherr, G., Cardinale, B.J., Miller, R., Ji, Z.X., 2010. Stability and aggregation of metal oxide nanoparticles in natural aqueous matrices. Environ. Sci. Technol. 44, 1962-1967.

Klaine, S.J., Edgington, A., Seda, B., 2013. Nanomaterials in the environment, in: Férard, J.-F., Blaise, C. (Eds.), Encyclopedia of aquatic ecotoxicology. Springer Publishers, Dordrecht, pp. 767-779.

Kosobucki, P., Buszewski, B., 2014. Natural organic matter in ecosystems - a review Nova Biotechnol. Chim. 13, 109-128.

Kovriznych, J.A., Sotnikova, R., Zeljenkova, D., Rollerova, E., Szabova, E., 2014. Long-term (30 days) toxicity of NiO nanoparticles for adult zebrafish *Danio rerio*. Interdisciplinary toxicology 7, 23-26.

Lavonen, E., 2015. Tracking changes in dissolved natural organic matter composition, Department of Aquatic Sciences and Assessment Faculty of Natural Resources and Agricultural Sciences Uppsala, Sweden, pp. 13-21.

Lok, C.N., Ho, C.M., Chen, R., He, Q.Y., Yu, W.Y., Sun, H., Tam, P.K.H., Chiu, J.F., Che, C.M., 2007. Silver nanoparticles: partial oxidation and antibacterial activities. J. Biol. Inorg. Chem. 12, 527-534.

Ma, H.B., Wallis, L.K., Diamond, S., Li, S.B., Canas-Carrell, J., Parra, A., 2014. Impact of solar UV radiation on toxicity of ZnO nanoparticles through photocatalytic reactive oxygen species (ROS) generation and photo-induced dissolution. Environ. Pollut. 193, 165-172.

Machado, M.D., Soares, E.V., 2013. Optimization of a Microplate-Based Assay to Assess Esterase Activity in the Alga *Pseudokirchneriella subcapitata*. Water Air Soil Pollut. 224.

Maxwell, K., Johnson, G.N., 2000. Chlorophyll fluorescence - a practical guide. J. Exp. Bot. 51, 659-668.

Motta, F.L., Melo, B.A.G., Santana, M.H.A., 2016. Deprotonation and protonation of humic acids as a strategy for the technological development of pH-responsive nanoparticles with fungicidal potential. N. Biotechnol. 33, 773-780.

Nanotech, 2015. Aluminium oxide: forecast from 2010 to 2025 Nanoparticles. Future Markets Inc., Edinburgh, pp. 1-3.

Navarro, E., Baun, A., Behra, R., Hartmann, N.B., Filser, J., Miao, A.J., Quigg, A., Santschi, P.H., Sigg, L., 2008. Environmental behavior and ecotoxicity of engineered nanoparticles to algae, plants, and fungi. Ecotoxicology 17, 372-386.

Nogueira, V., Lopes, I., Rocha-Santos, T.A.P., Rasteiro, M.G., Abrantes, N., Goncalves, F., Soares, A.M.V.M., Duarte, A.C., Pereira, R., 2015. Assessing the ecotoxicity of metal nano-oxides with potential for wastewater treatment. Environmental Science and Pollution Research 22, 13212-13224.

Nowack, B., Ranville, J.F., Diamond, S., Gallego-Urrea, J.A., Metcalfe, C., Rose, J., Horne, N., Koelmans, A.A., Klaine, S.J., 2012. Potential scenarios for nanomaterial release and subsequent alteration in the environment. Environ. Toxicol. Chem. 31, 50-59.

Odzak, N., Kistler, D., Sigg, L., 2017. Influence of daylight on the fate of silver and zinc oxide nanoparticles in natural aquatic environments. Environ. Pollut. 226, 1-11.

OECD, 2011. Test Nº 201: freshwater alga and cyanobacteria, growth inhibition test. OECD guidelines for the testing of chemicals, Section 2. OECD Publishing, Paris.

Oukarroum, A., Barhoumi, L., Samadani, M., Dewez, D., 2015. Toxic effects of nickel oxide bulk and nanoparticles on the aquatic plant *Lemna gibba* L. Biomed Res. Int. 215, 1-7.

Oukarroum, A., Zaidi, W., Samadani, M., Dewez, D., 2017. Toxicity of Nickel Oxide Nanoparticles on a Freshwater Green Algal Strain of *Chlorella vulgaris*. Biomed Res. Int.

Peng, Y.H., Tsai, Y.C., Hsiung, C.E., Lin, Y.H., Shih, Y.H., 2017. Influence of water chemistry on the environmental behaviors of commercial ZnO nanoparticles in various water and wastewater samples. J. Hazard. Mater. 322, 348-356.

Quik, J.T.K., Lynch, I., Van Hoecke, K., Miermans, C.J.H., De Schamphelaere, K.A.C., Janssen, C.R., Dawson, K.A., Stuart, M.A.C., Van de Meent, D., 2010. Effect of natural organic matter on cerium dioxide nanoparticles settling in model fresh water. Chemosphere 81, 711-715.

Sadiq, I.M., Pakrashi, S., Chandrasekaran, N., Mukherjee, A., 2011. Studies on toxicity of aluminum oxide (Al_2O_3) nanoparticles to microalgae species: *Scenedesmus* sp and *Chlorella* sp. J. Nanopart. Res. 13, 3287-3299.

Sajid, M., Ilyas, M., Basheer, C., Tariq, M., Daud, M., Baig, N., Shehzad, F., 2015. Impact of nanoparticles on human and environment: review of toxicity factors, exposures, control strategies, and future prospects. Environ. Sci. Pollut. Res. 22, 4122-4143.

Sawyer, C.N., McCarty, P.L., Parkin, G.F., 2003. Chemistry for environmental engineering and science. MacGraw-Hill, Boston.

Sehgal, A., Lalatonne, Y., Berret, J.F., Morvan, M., 2005. Precipitation-redispersion of cerium oxide nanoparticles with poly(acrylic acid): toward stable dispersions. Langmuir 21, 9359-9364.

Sendra, M., Yeste, M.P., Gatica, J.M., Moreno-Garrido, I., Blasco, J., 2017. Homoagglomeration and heteroagglomeration of TiO_2, in nanoparticle and bulk form, onto freshwater and marine microalgae. Sci. Total Environ. 592, 403-411.

Sobek, S., Tranvik, L.J., Prairie, Y.T., Kortelainen, P., Cole, J.J., 2007. Patterns and regulation of dissolved organic carbon: an analysis of 7,500 widely distributed lakes. Limnol. Oceanogr. 52, 1208-1219.

Biotechnol. DOI: 10.1007/s00253-019-09903-y.

Todd, D.K., 2007. Groundwater hydrology. John Wiley, New York.

Topuz, E., Traber, J., Sigg, L., Talinli, I., 2015. Agglomeration of Ag and TiO_2 nanoparticles in surface and wastewater: role of calcium ions and of organic carbon fractions. Environ. Pollut. 204, 313-323.

UNEP, 2016. Water quality outlook, UN GEMS/Water Programme, Burlington, Canada, pp. 6-7.

WHO, 2011. Guidelines for drinking-water quality Hardness in drinking-water Washington, DC, USA, pp. 1-6.

Yang, K., Lin, D.H., Xing, B.S., 2009. Interactions of humic acid with nanosized inorganic oxides. Langmuir 25, 3571-3576.

Yu, S.J., Liu, J.F., Yin, Y.G., Shen, M.H., 2018. Interactions between engineered nanoparticles and dissolved organic matter: a review on mechanisms and environmental effects. J. Environ. Sci. China 63, 198-217.
Zhang, Y., Chen, Y.S., Westerhoff, P., Crittenden, J., 2009. Impact of natural organic matter and divalent cations on the stability of aqueous nanoparticles. Water Res. 43, 4249-4257.
Zhou, D.X., Keller, A.A., 2010. Role of morphology in the aggregation kinetics of ZnO nanoparticles. Water Res. 44, 2948-2956.

Chapter 10 - Conclusions

10.1. Conclusions

The overall aim of this thesis was to study the physico-chemical properties of six oxide NPs (Al_2O_3, In_2O_3, Mn_3O_4, NiO, SiO_2 and SnO_2) and the possible toxic mechanisms of action using two cell models, yeast as eukaryotic cell model and alga as ecologically relevant organism.

The first study contributed to the elucidation of the toxicity mechanisms of NiO NPs using the yeast *S. cerevisiae*. NiO NPs are very insoluble in aqueous solutions and form agglomerates. The quantification of nickel released from NPs and the toxic effects observed suggests that nickel released by the NiO NPs cannot explain, by itself, all (or most) of the toxicity caused by the NPs. NiO NPs adsorb to cell wall but are not internalized in yeast cells, which suggests that NiO NPs can exerts their toxicity by an indirect mechanism. NiO NPs inhibit metabolic activity and induce loss of yeast viability. NiO NPs are unable to generate abiotic ROS. However, cells of *S. cerevisiae* exposed to NiO NPs displayed intracellular accumulation of $O_2^{\cdot-}$ and H_2O_2, when incubated in normal atmosphere. Mitochondria are an important source of ROS since WT yeast cells under nitrogen atmosphere as well as cells of ρ^0 strain (lacking respiratory chain) exposed to NiO NPs displayed low levels of ROS and higher resistance to NiO NPs. It is proposed that NiO NPs induce the loss of cell viability in *S. cerevisiae* through OS, which can be the result of a combined effect of the enhancement of ROS production and the depletion of GSH. The yeast cell death induced by NiO NPs presented typical phenotypic apoptotic markers and was caspase- and mitochondrial dependent RCD.

The other five MOx NPs tested when suspended in aqueous media displayed, in a general way, a negative charge, agglomerated (except SnO_2 in YEP), were almost insoluble and were unable to generate ROS in abiotic conditions. In_2O_3 NPs did not provoke any detectable toxic effect on yeast cells up to 100 mg/L. Al_2O_3, Mn_3O_4, SiO_2 and SnO_2 NPs induced the loss of yeast cell viability. The comparative analysis of the effect of the MOx NPs and the corresponding supernatants, suggested that the SiO_2 toxicity was mainly caused by the NPs themselves, Al_2O_3 and SnO_2 toxic effects could be attributed to both the NPs and the respective released ions and Mn_3O_4 harmfulness could be mainly produced by the released ions. These NPs also induced the loss of metabolic activity and intracellular ROS accumulation. The co-incubation of yeast cells with the NPs and AA quenched intracellular ROS and reverted the NPs toxicity (nearly restored cell survival and metabolic activity), evidencing that the intracellular accumulation of ROS constitutes the main cause of the cytotoxicity experienced by yeasts treated with Al_2O_3, Mn_3O_4, SiO_2 and SnO_2 NPs.

Using the alga *P. subcapitata*, NiO NPs release Ni^{2+} in aqueous medium, which is the main contributor to the toxicity observed. NiO NPs presented a 72 h-EC_{50} of 1.6 mg/L, evaluated by the growth

inhibition assay, allowing this NP to be classified as toxic. Algal cells exposed for 72 h to 4 mg/L NiO (72 h-EC_{90}) presented a loss of metabolic activity, photosynthetic pigment bleaching and intracellular ROS accumulation but no loss of membrane integrity. At this concentration, the NiO NPs caused a reduction in the photosynthetic efficiency (Φ_{PSII}), most likely as a consequence of a decrease in the flow rate of electrons through the photosynthetic chain. The combined effects of the decreased metabolic activity, disturbance to photosynthetic performance and increased intracellular ROS accumulation may have caused the arrest of the cell cycle prior to the first cell division, which in turn may be the cause of the increased algal cell volume and aberrant morphology and ultimately the discontinuation of algal growth.

The other five MOx NPs tested were instable in OECD algal medium and presented tendency to agglomerate. However, these agglomerates were easily dispersed by simple agitation and presented a loose structure, which makes very unlikely that the toxicity of these NPs could be due to the entrapment of the algal cells in the NPs agglomerates. The NPs studied were poorly soluble in OECD medium. However, the amount of Sn^{4+} leached from the SnO_2 NPs seems to be the main contributor for the toxicity observed by this NP. Using the algal growth inhibition test, performed with the freshwater alga *P. subcapitata*, and based on the 72h-EC_{50} values obtained, the hazard of the NPs were categorized as: toxic (Al_2O_3 and SnO_2 NPs), harmful (Mn_3O_4 and SiO_2 NPs) and not classified/not toxic (In_2O_3). In the case of Al_2O_3, Mn_3O_4 and SiO_2, the algistatic effect (inhibition of algal growth in the absence of cell dead) can be attributed to the great disturbance of algal physiology: reduction of photosynthetic and metabolic activity and intracellular accumulation of ROS. The exposure of algal cells to SnO_2 NPs induced the disturbance of the functionality of PSII in the absence of intracellular ROS accumulation or loss of metabolic activity.

The influence of the abiotic factors (pH, organic matter and hardness) on the transformations of the MOx (Al_2O_3, NiO and SnO_2) NPs in freshwater and its toxicity over *P. subcapitata* was also evaluated. The rise of pH value of the natural water supplemented with OECD medium decreased the concentration of dissolved metals from the NPs. Under the conditions studied, when evaluated individually, pH value and hardness of the medium did not influence the formation of NPs homo-agglomerates or Al_2O_3 NPs-algal hetero-agglomerates, as well as, did not modify the toxicity of Al_2O_3, NiO or SnO_2 NPs over *P. subcapitata*. Conversely, the presence of HA, reduced the concentration of dissolved metals and lead to the complete dispersion of Al_2O_3 NPs-algal cells hetero-agglomerates. HA also had a protective effect against Al_2O_3, NiO or SnO_2 NPs toxicity (evaluated through algal growth inhibition assay), probably as a consequence of the reduction of the dissolved metals levels

(NiO and SnO_2 NPs) or Al_2O_3 NPs bioavailability. In the simultaneous presence of HA and each one of the three NPs under study, algal photosynthetic activity was restored. In addition, the simultaneous presence of HA and Al_2O_3 or NiO NPs impaired the intracellular accumulation of ROS. The increase of water hardness (150 mg/L Ca^{2+}), at pH 9.0, did not inhibit the dispersive effect of HA (over Al_2O_3 NPs-algal cells hetero-agglomerates) or reduced the protective effect of HA against NPs toxicity.

Considering that for 10 mg/L HA, which DOC range values are within the most frequent DOC values found in surface waters, no toxicity effects were recorded over *P. subcapitata* when suspended in the presence of Al_2O_3, NiO and SnO_2 NPs at 9.4, 1.6 and 2.1 mg/L, respectively, it seems plausible to anticipate that the release of these NPs in surface waters up to similar NPs concentrations as tested in Chapter 9 would not have significant toxicant impact. Moreover, due to the same reasons, no significant agglomeration of the NPs is expected.

The results presented herein reinforce the need to study the NPs, in an extended way, in order to provide a systematic characterization of their potential hazards in humans or aquatic environments and can be useful for regulatory purposes related to the release of MOx NPs. Also, this thesis contributes to a better understanding of the effect of abiotic factors on the behavior of Al_2O_3, NiO and SnO_2 NPs in the aquatic environment. This information can be further used to predict the impact of the release of these NPs in different natural fresh waters scenarios.

10.2. Future work

In the future, to better understand the importance of monitoring the MOx NPs usage, controlling their production and release in the environment, it will be important the usage of others relevant cell models, without cell wall, in order to compare the toxic mechanisms of action by MOx NPs and the usage of different media to compare the NPs behavior.

Also, the study of other water parameters, such as ionic strength or different electrolytes, which can influence the properties of MOx NPs and, consequently, affect their toxicity in organisms with different concentrations of MOx NPs can be performed.

Annex A – Effect of natural organic matter, pH and hardness on the toxicity of metal oxide nanoparticles (Al_2O_3, NiO and SnO_2) in the freshwater alga *Pseudokirchneriella subcapitata*

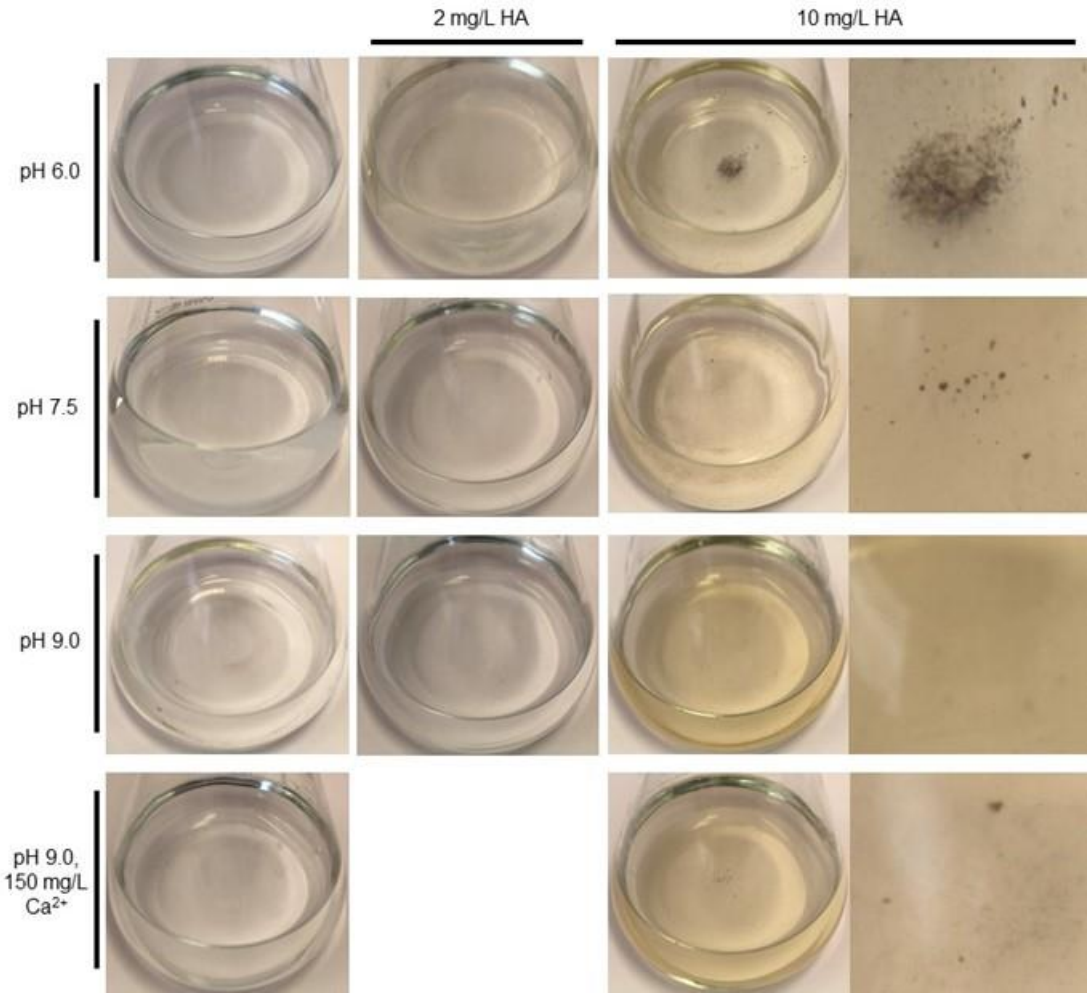

Figure A.1. Macroscopic observation of Al_2O_3 NPs, in natural freshwater supplemented with OECD medium, in the absence of algal cells, under different abiotic conditions. Al_2O_3 NPs at 9.4 mg/L were incubated for 72 h, in different abiotic conditions: pH, humic acids (HA) and water hardness (Ca^{2+}). Abiotic conditions were individually studied or in a combined way (conditions reported on top and left-side). Right-side images: bottom of the Erlenmeyer flasks.

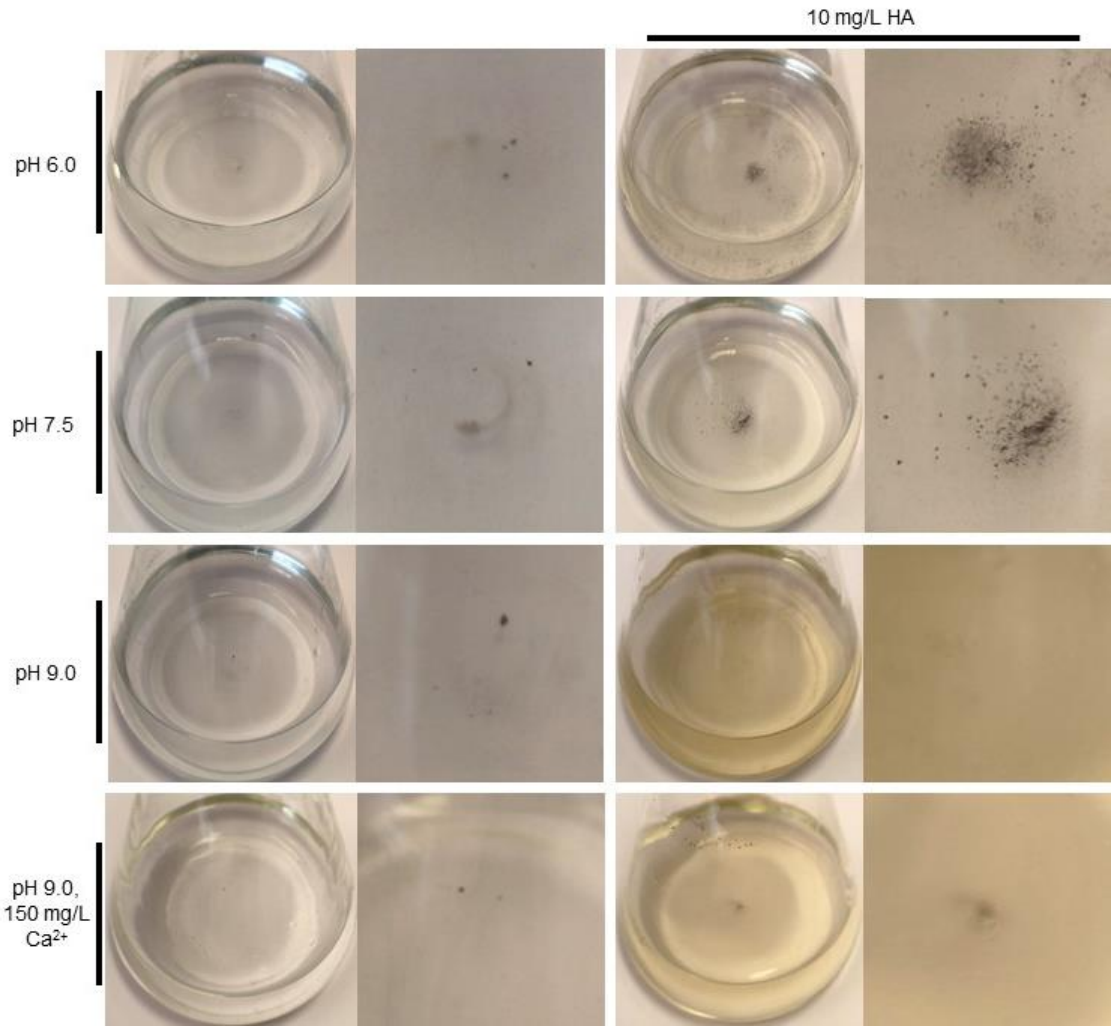

Figure A.2. Macroscopic observation of NiO NPs, in natural freshwater supplemented with OECD medium, in the absence of algal cells, under different abiotic conditions. NiO NPs at 1.6 mg/L were incubated for 72 h, in different abiotic conditions: pH, humic acids (HA) and water hardness (Ca^{2+}). Abiotic conditions were individually studied or in a combined way (conditions reported on top and left-side). Right-side images: bottom of the Erlenmeyer flasks.

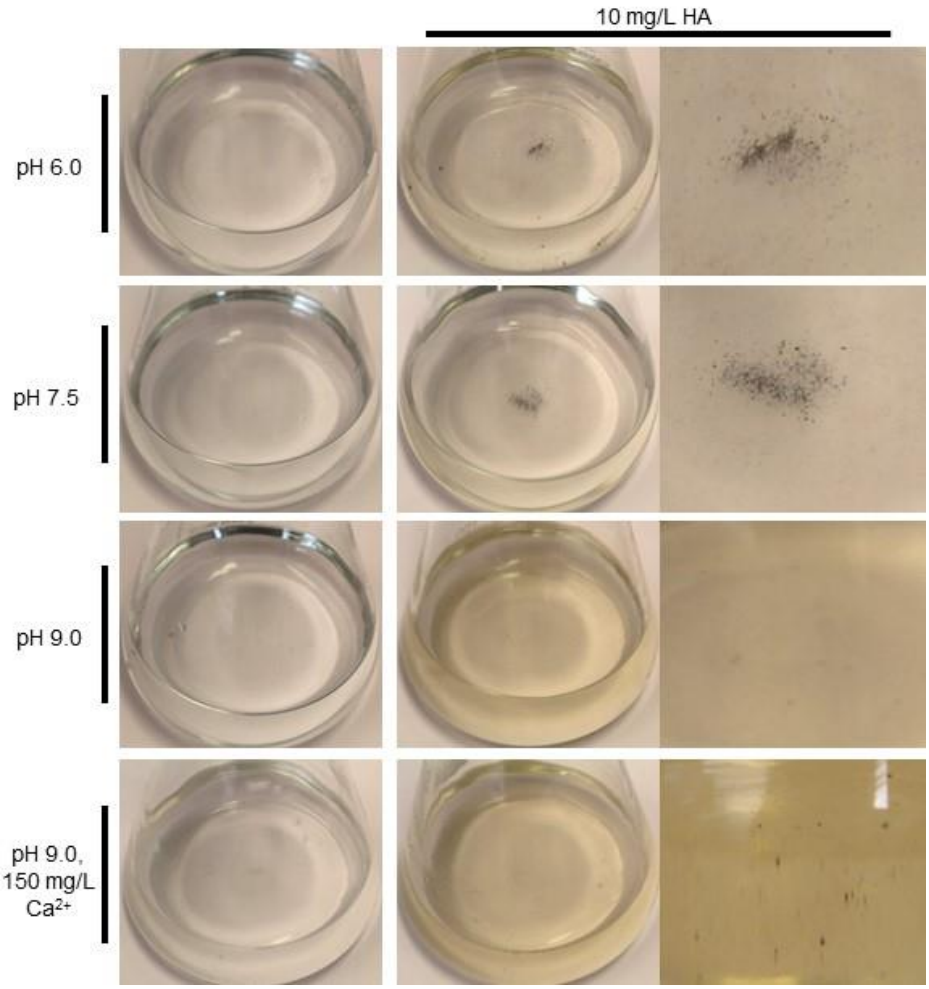

Figure A.3. Macroscopic observation of SnO_2 NPs, in natural freshwater supplemented with OECD medium, in the absence of algal cells, under different abiotic conditions. SnO_2 NPs at 2.1 mg/L were incubated for 72 h, in different abiotic conditions: pH, humic acids (HA) and water hardness (Ca^{2+}). Abiotic conditions were individually studied or in a combined way (conditions reported on top and left-side). Right-side images: bottom of the Erlenmeyer flasks.

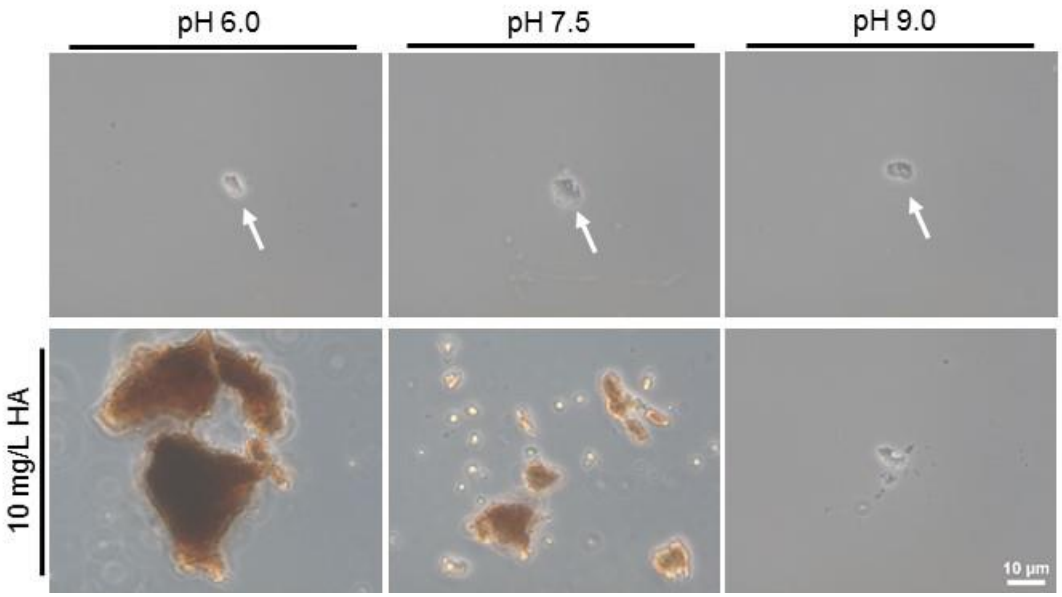

Figure A.4. Microscopic observation of Al_2O_3 NPs, in natural freshwater supplemented with OECD medium, in the absence of algal cells, under different abiotic conditions. Al_2O_3 NPs at 9.4 mg/L were incubated for 72 h at different pH values in the absence (top images) or the presence (bottom images) of humic acids (HA). Arrows: NPs homoagglomerates.

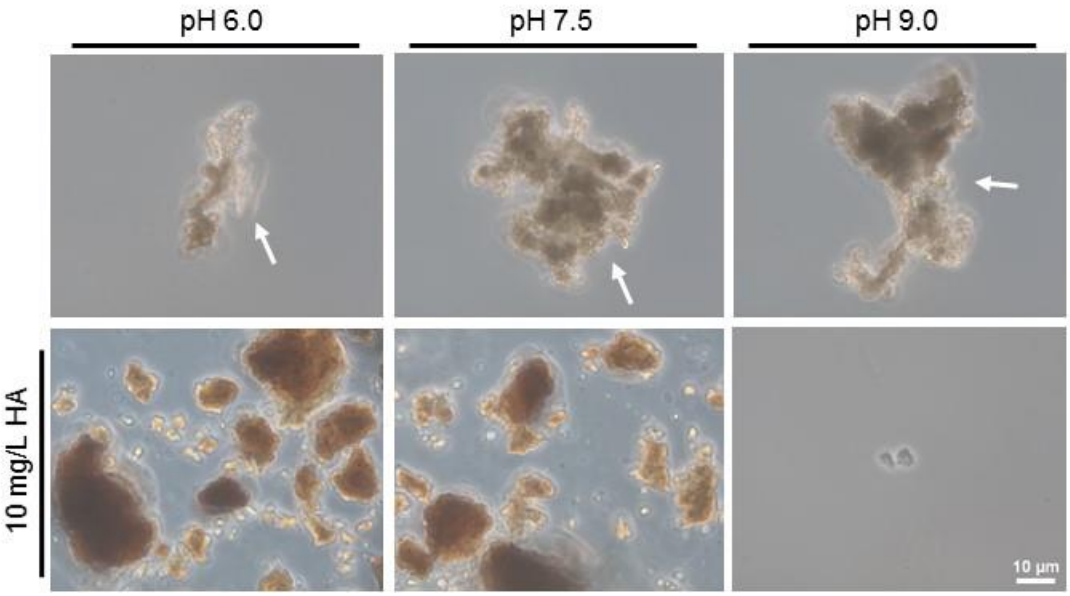

Figure A.5. Microscopic observation of NiO NPs, in natural freshwater supplemented with OECD medium, in the absence of algal cells, under different abiotic conditions. NiO NPs at 1.6 mg/L were incubated for 72 h at different pH values in the absence (top images) or the presence (bottom images) of humic acids (HA). Arrows: NPs homoagglomerates.

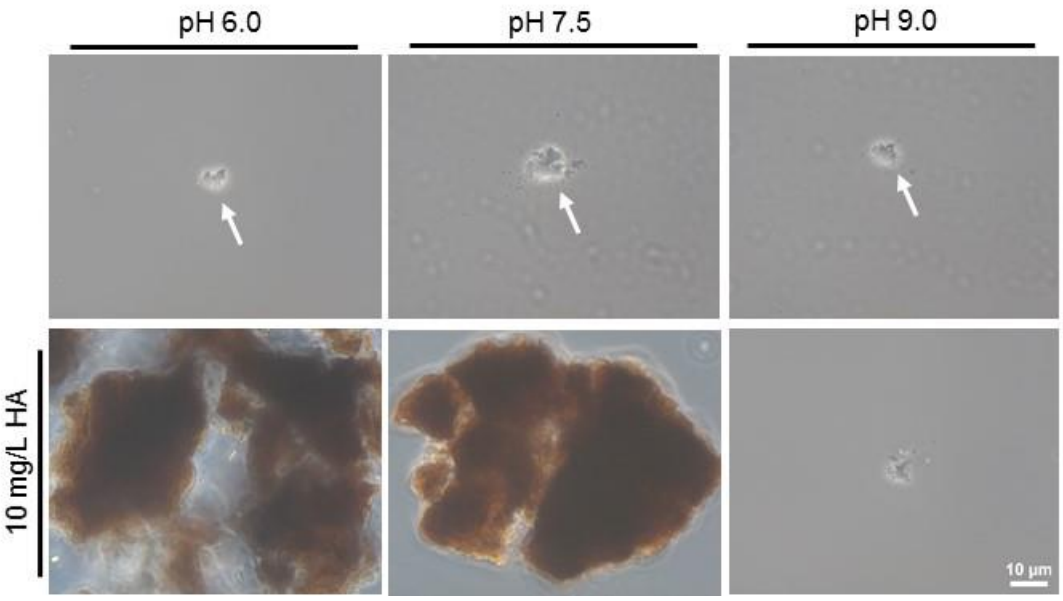

Figure A.6. Microscopic observation of SnO_2 NPs, in natural freshwater supplemented with OECD medium, in the absence of algal cells, under different abiotic conditions. SnO_2 NPs at 2.1 mg/L were incubated for 72 h at different pH values in the absence (top images) or the presence (bottom images) of humic acids (HA). Arrows: NPs homoagglomerates.

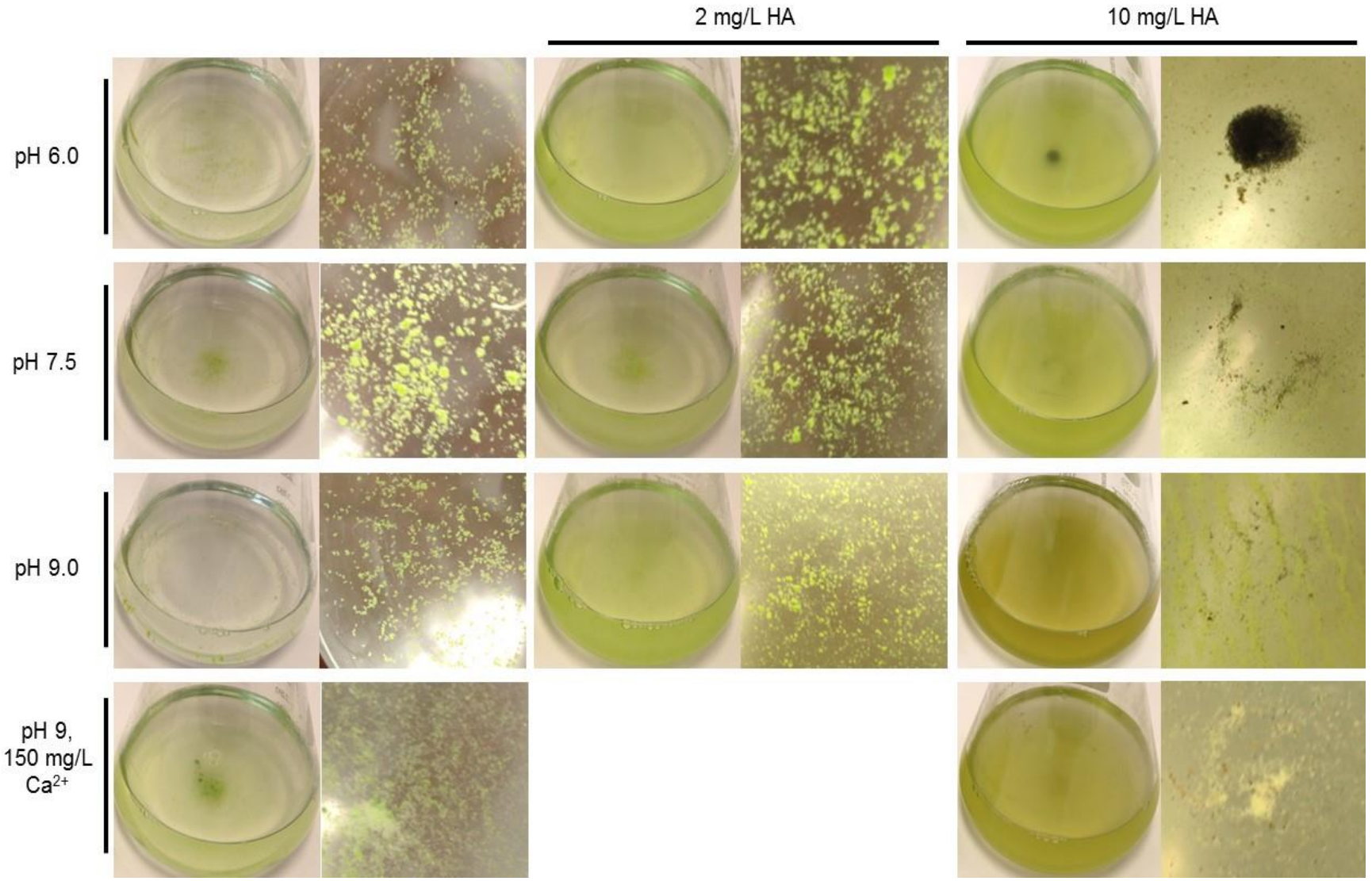

Figure A.7. Macroscopic observation of Al_2O_3 NPs, in natural freshwater supplemented with OECD medium, in the presence of algal cells, in different abiotic conditions. Al_2O_3 NPs at 9.4 mg/L were incubated with *P. subcapitata* algal cells, for 72 h, under different abiotic conditions: pH, humic acids (HA) and water hardness (Ca^{2+}). Abiotic conditions were individually studied or in a combined way (conditions reported on top and left-side). Right-side images: bottom of the Erlenmeyer flasks.

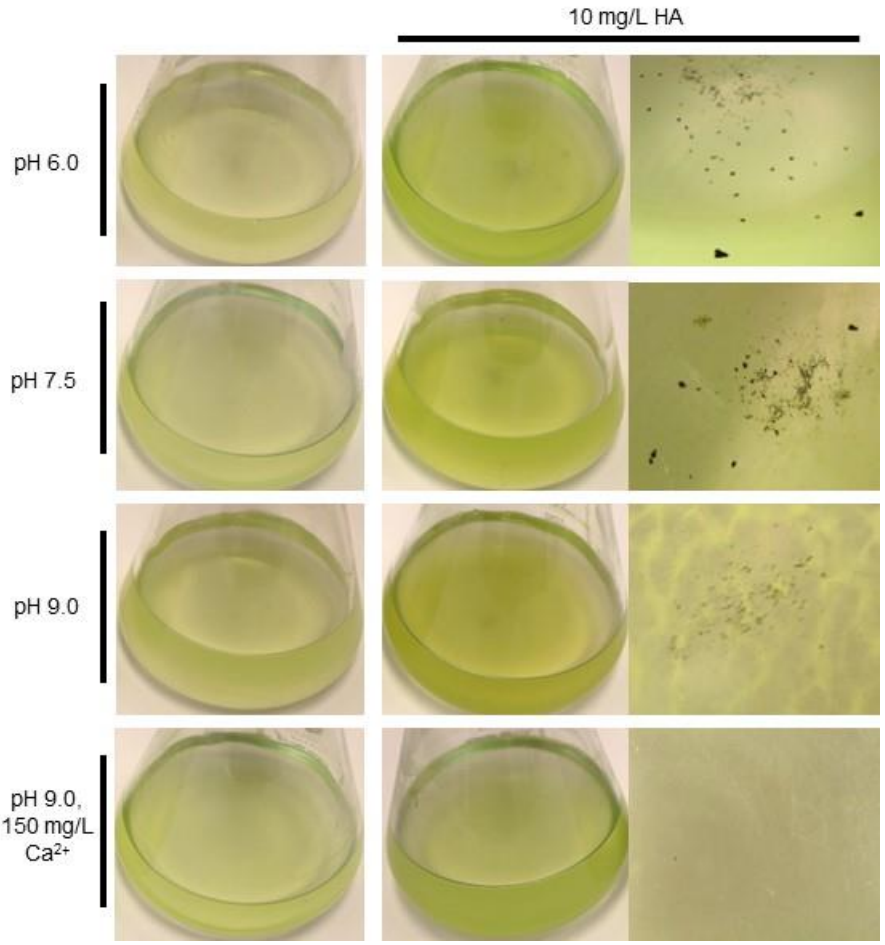

Figure A.8. Macroscopic observation of NiO NPs, in natural freshwater supplemented with OECD medium, in the presence of algal cells, under different abiotic conditions. NiO NPs at 1.6 mg/L were incubated with *P. subcapitata* algal cells, for 72 h, in different abiotic conditions: pH, humic acids (HA) and water hardness (Ca^{2+}). Abiotic conditions were individually studied or in a combined way (conditions reported on top and left-side). Right-side images: bottom of the Erlenmeyer flasks.

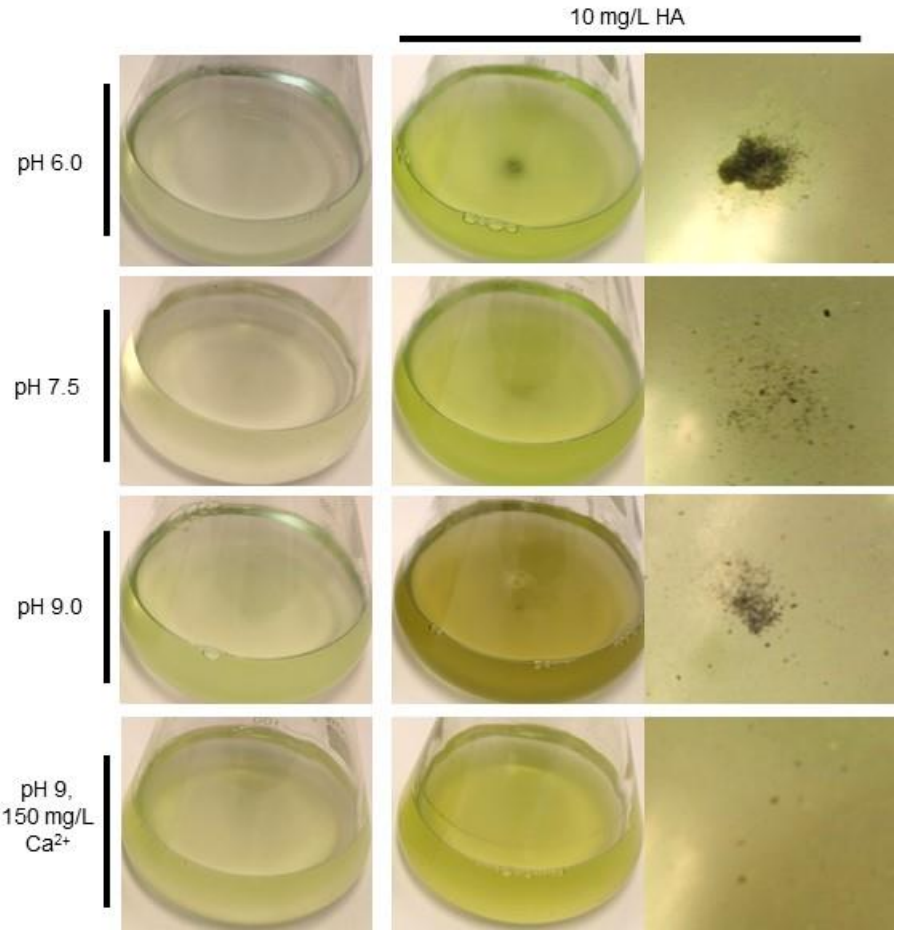

Figure A.9. Macroscopic observation of SnO_2 NPs, in natural freshwater supplemented with OECD medium, in the presence of algal cells, under different abiotic conditions. SnO_2 NPs at 2.1 mg/L were incubated with *P. subcapitata* algal cells, for 72 h, in different abiotic conditions: pH, humic acids (HA) and water hardness (Ca^{2+}). Abiotic conditions were individually studied or in a combined way (conditions reported on top and left-side). Right-side images: bottom of the Erlenmeyer flasks.

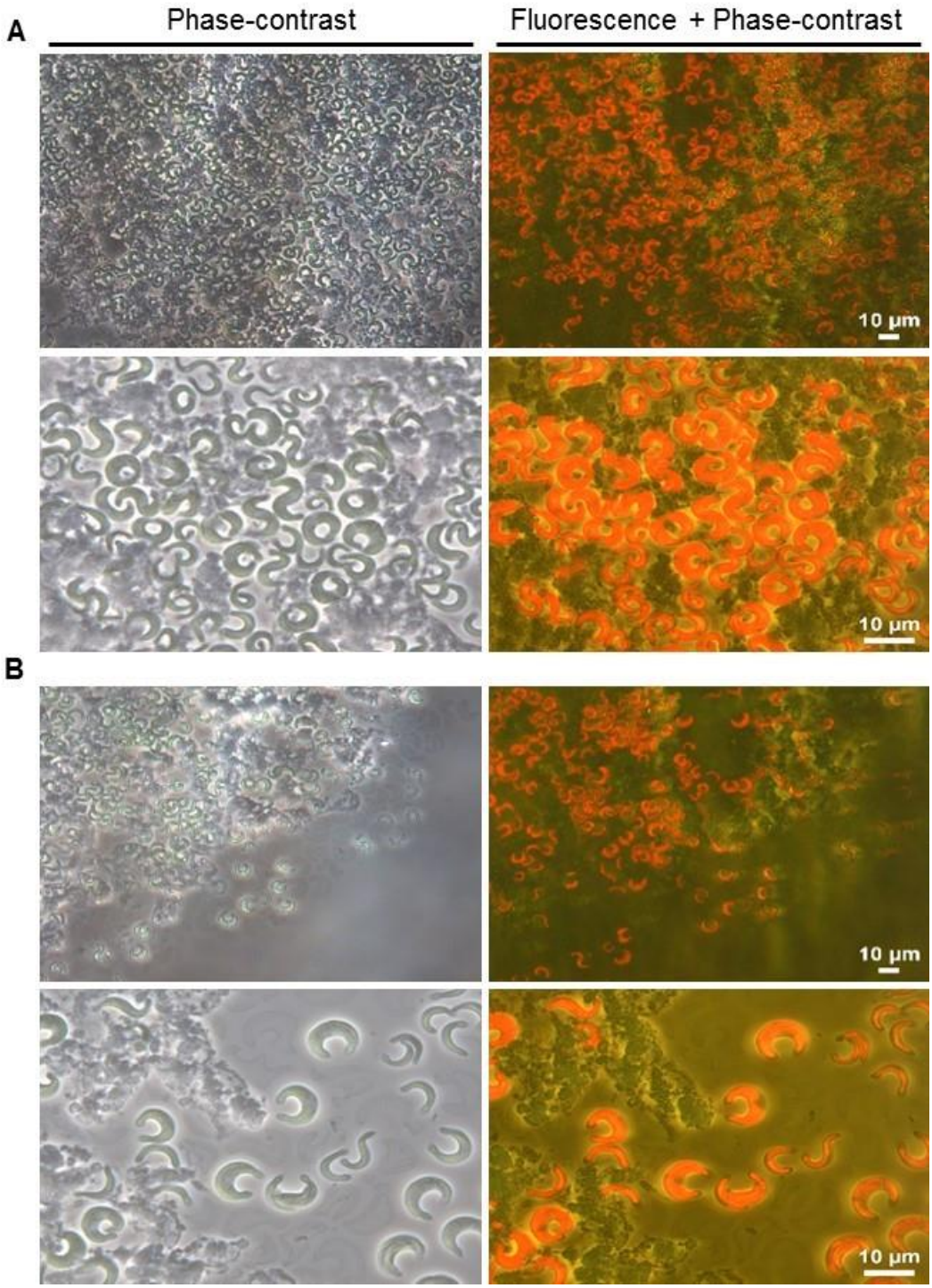

Figure A.10. Microscopic observation of Al_2O_3 NPs, at pH 9.0, in natural freshwater supplemented with OECD medium, in the presence of algal cells, without or with humic acids. Al_2O_3 NPs at 9.4 mg/L were incubated with *P. subcapitata* for 72 h, in the absence (A) or the presence of 2 mg/L humic acids (B). Algal cells can be distinguished due to orange-autofluorescence. A and B bottom images: higher amplification of NPs-algal hetero-agglomerates.

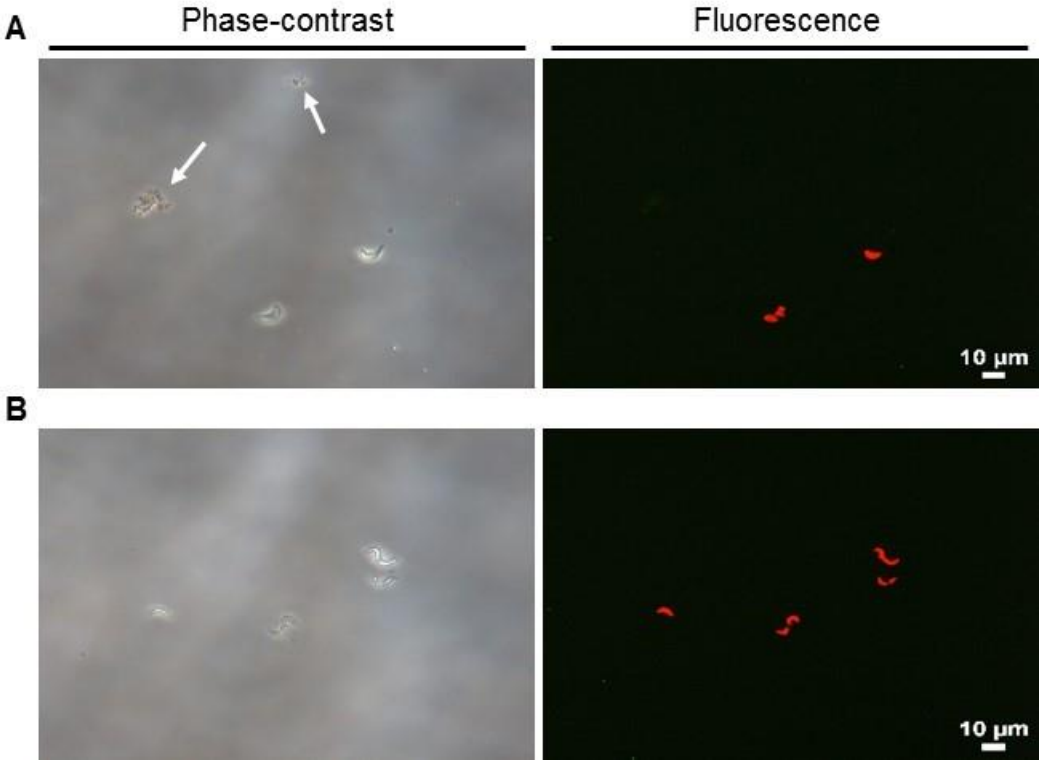

Figure A.11. Microscopic observation of NiO or SnO_2 NPs, in natural freshwater supplemented with OECD medium, in the presence of algal cells, at pH 9.0. NiO NPs at 1.6 mg/L (A) or SnO2 NPs at 2.1 mg/L were incubated with *P. subcapitata* for 72 h. Algal cells can be distinguished due to orange-autofluorescence. Arrows: NiO NPs homoagglomerates.

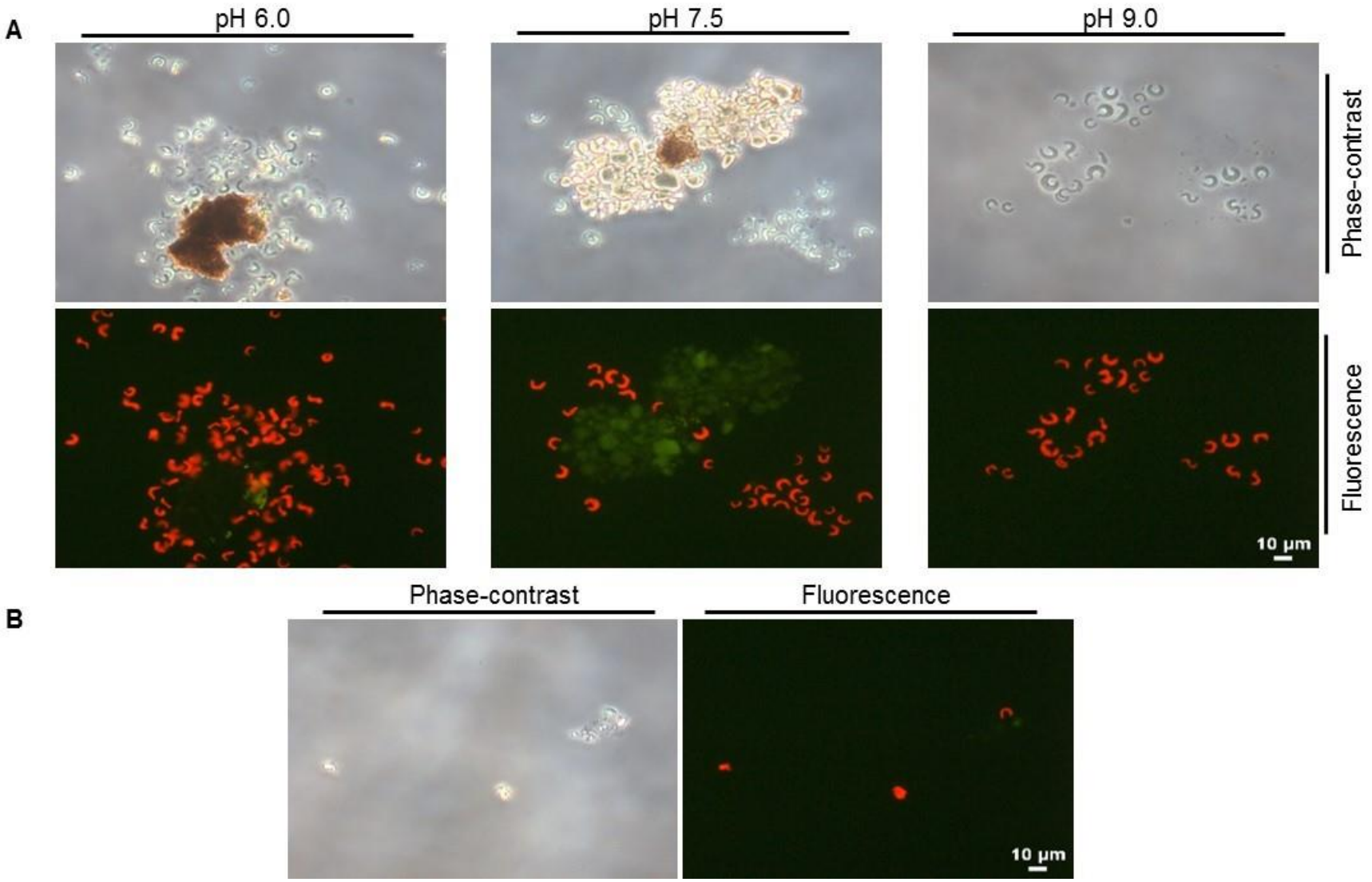

Figure A.12. Microscopic observations of Al_2O_3 NPs, in natural freshwater supplemented with OECD medium, in the presence of algal cells, under different abiotic conditions. Al_2O_3 NPs at 9.4 mg/L were incubated with *P. subcapitata* for 72 h at different pH values, in the presence of 10 mg/L humic acids (HA) (A) or at pH 9.0, in the simultaneous presence of 10 mg/L HA and 150 mg/L Ca^{2+} (B). Algal cells can be distinguished due to orange-autofluorescence.

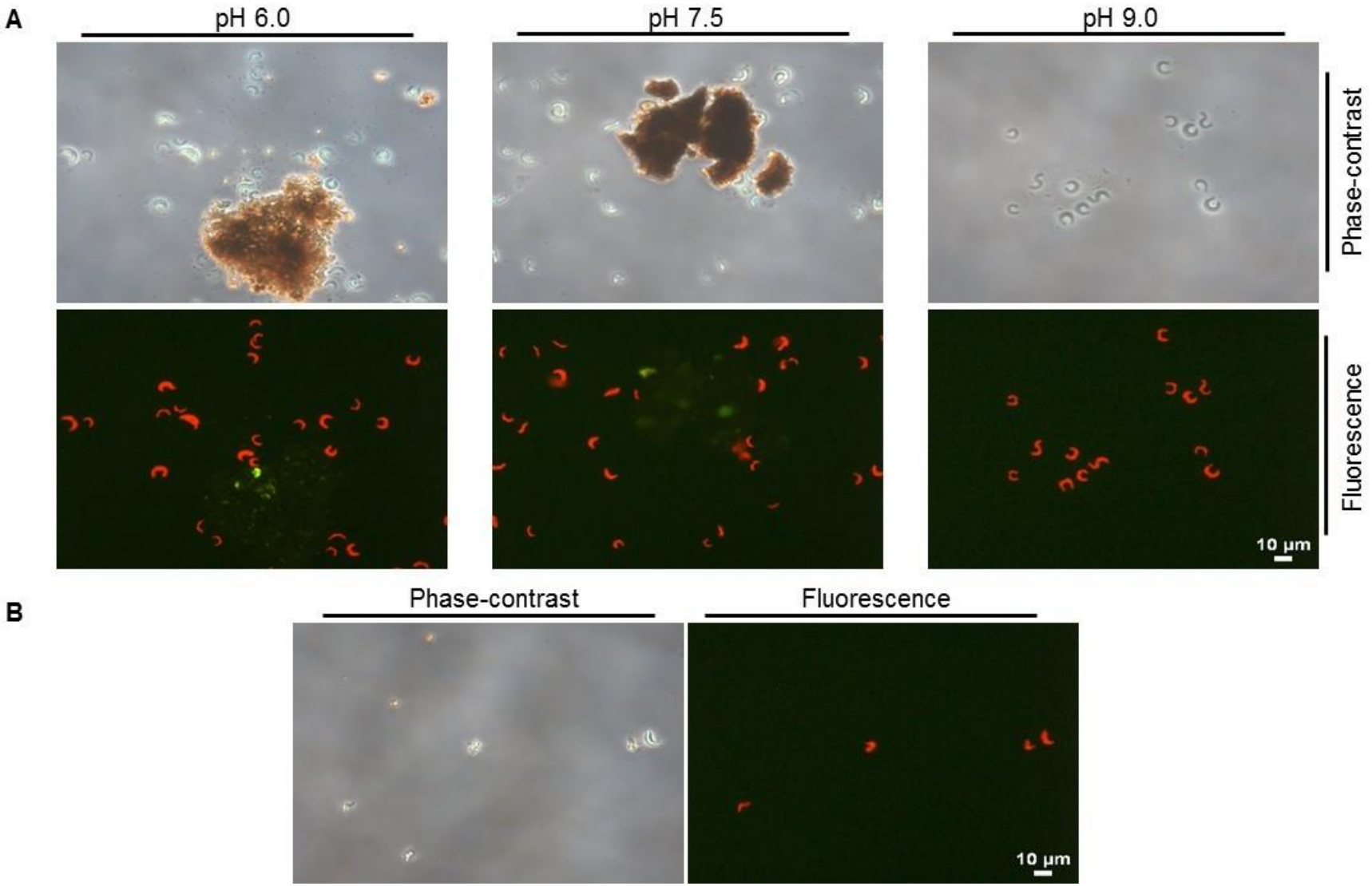

Figure A.13. Microscopic observation of NiO NPs, in natural freshwater supplemented with OECD medium, in the presence of algal cells, under different abiotic conditions. NiO NPs at 1.6 mg/L were incubated with *P. subcapitata* for 72 h, at different pH values, in the presence of 10 mg/L humic acids (HA) (A) or at pH 9.0, in the simultaneous presence of 10 mg/L HA and 150 mg/L Ca^{2+} (B). Algal cells can be distinguished due to orange-autofluorescence.

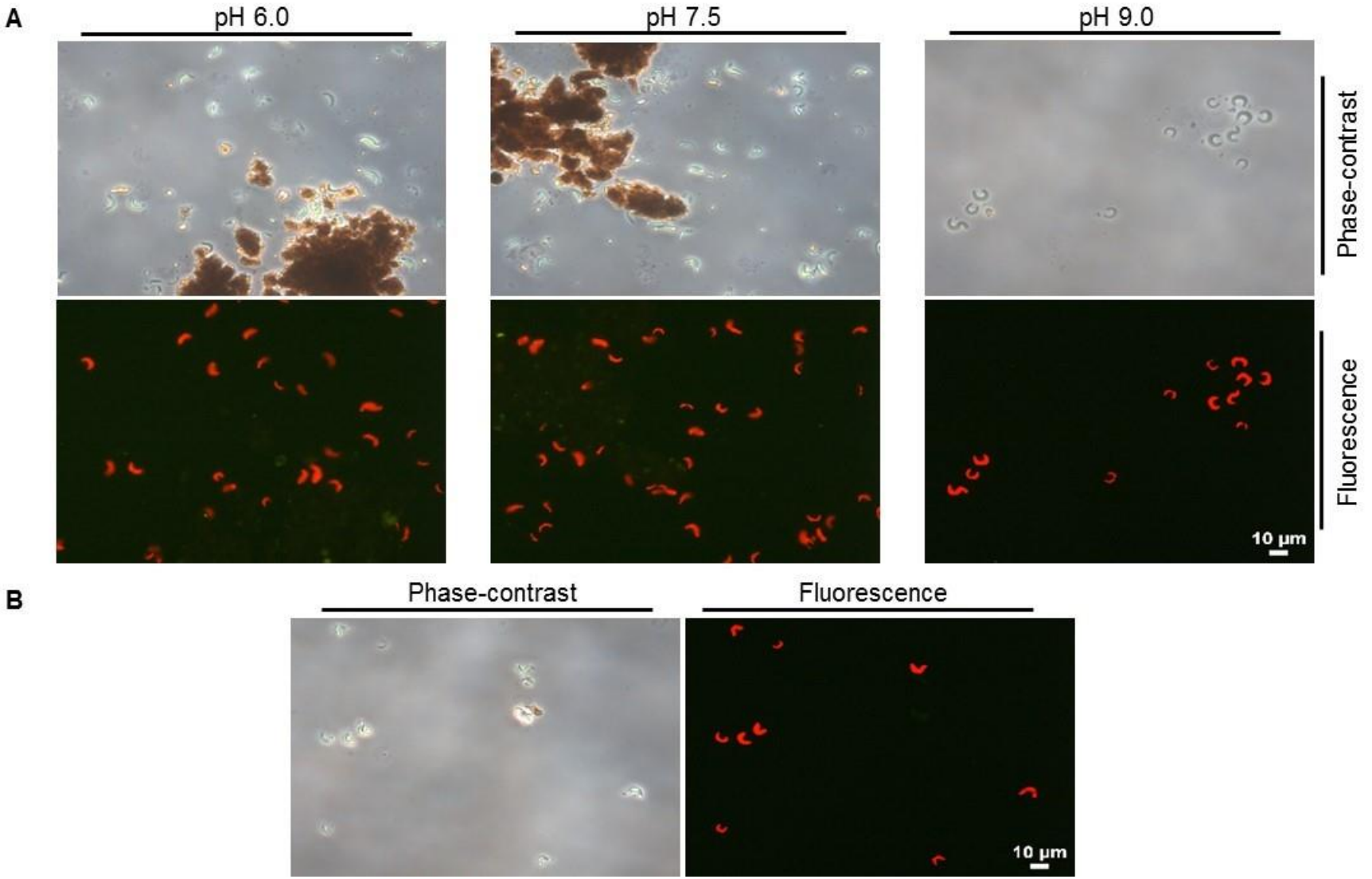

Figure A.14. Microscopic observations of SnO_2 NPs, in natural freshwater supplemented with OECD medium, in the presence of algal cells, under different abiotic conditions. SnO_2 NPs at 2.1 mg/L were incubated with *P. subcapitata* for 72 h, at different pH values, in the presence of 10 mg/L humic acids (HA) (A) or at pH 9.0, in the simultaneous presence of 10 mg/L HA and 150 mg/L Ca^{2+} (B). Algal cells can be distinguished due to orange-autofluorescence.

Table A.1. Characterization of the natural freshwater used in Chapter 9.

Analyzed parameters												
pH	Al (µg/L)	Cd (µg/L)	Cr (µg/L)	Cu (µg/L)	Fe (µg/L)	Ni (µg/L)	Pb (µg/L)	Sn (µg/L)	Zn (µg/L)	TOC[a] (mg/L)	IC[b] (mg/L)	Water hardness (Ca^{2+}, mg/L)
6.5	< 1.2[c]	< 0.14[c]	<1.5[c]	< 2.4[c]	< 0.78[c]	< 3.7[c]	< 5.2[c]	< 7.2[c]	< 1.8[c]	2.8 ± 0.3	1.9 ± 0.3	3.0 ± 0.3

[a]TOC – Total organic carbon.

[b]IC – Inorganic carbon.

[c]DL – Detection limit measured by atomic absorption spectroscopy with electrothermal atomization.

Table A.2. Determination of dissolved organic matter (DOC) in the freshwater (supplemented with OECD medium), in the absence of algal cells, under different abiotic conditions.

NPs	[HA] (mg/L)	pH	[Ca^{2+}] (mg/L)	[DOC] (mg/L)
Al_2O_3	2	6.0	-	2.2
		7.5		2.4
		9.0		2.5
	10	6.0		5.6
		7.5		6.8
		9.0		7.7
	10	9.0	150	7.5
NiO	2	9.0	-	2.2
	10	6.0		7.2
		7.5		7.1
		9.0		8.1
	10	9.0	150	8.5
SnO_2	2	9.0	-	2.5
	10	6.0		7.1
		7.5		7.3
		9.0		8.6
	10	9.0	150	8.2

Each NP at a specific concentration (9.4 mg/L Al_2O_3 or 1.6 mg/L NiO or 2.1 mg/L SnO_2) was suspended in natural freshwater supplemented with OECD medium for 72 h, under different abiotic conditions (pH, HA and Ca^{2+}). Samples were collected, filtered through a 0.45 µm-pore-size filter and DOC was measured as described in material and methods.